

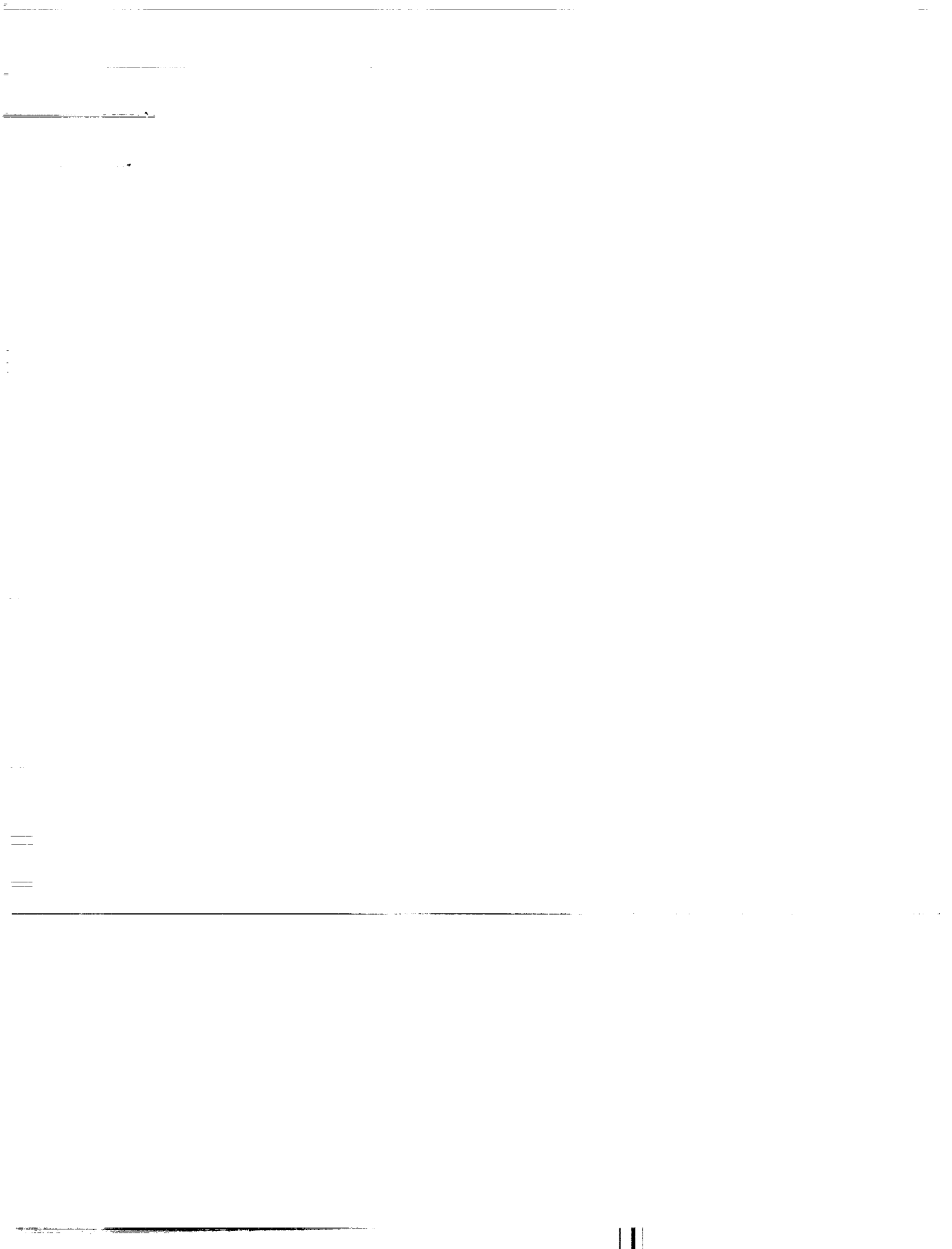
*N72-32845*  
REPORT NO. GDCA-DFM72-005  
CONTRACT NAS 8-27048

**CASE FILE  
COPY**

INVESTIGATION OF STRUCTURAL  
FACTORS OF SAFETY  
FOR THE SPACE SHUTTLE

FINAL REPORT

GENERAL DYNAMICS  
Convair Aerospace Division



REPORT NO. GDCA-DFM72-005

INVESTIGATION OF STRUCTURAL FACTORS OF SAFETY  
FOR THE SPACE SHUTTLE

26 June 1972

Prepared Under Contract NAS 8-27048 by  
CONVAIR AEROSPACE DIVISION OF GENERAL DYNAMICS  
San Diego, California

for

National Aeronautics and Space Administration  
GEORGE C. MARSHALL SPACE FLIGHT CENTER  
Huntsville, Alabama

11 11 11 11

11 11 11 11

11 11 11 11

11 11 11 11

11 11 11 11

11 11 11 11

11 11 11 11

11 11 11 11

11 11 11 11

11 11 11 11

11 11 11 11

11 11 11 11

11 11 11 11

11 11 11 11





## FOREWORD

This investigation was conducted for the NASA Marshall Space Flight Center by the Convair Aerospace Division of the General Dynamics Corporation under Contract NAS 8-27048.

The NASA technical monitor was Mr. John Key (S&E-ASTN-AAS). Mr. J. E. Jensen was the Principal Investigator for General Dynamics/Convair Aerospace, assisted by Mr. P. J. Wilson and Mr. N. E. Strandlund of the Space Structural Analysis Group, Mr. T. C. Johnson of the Economics Analysis Group, Mr. H. B. Sturtevant of the Reliability and Safety Analysis Group, and Mr. C. J. Kropp of the Materials Research Group.

The investigation was conducted from April 1971 to June 1972.

1

2

3

4

5

6

7

8

9

10

11

12

13

14

15

16

17

18

19

20

21

22

23

24

25

26

27

28

29

30

31

32

33

34

35

36

37

38

39

40

41

42

43

44

45

46

47

48

49

50

51

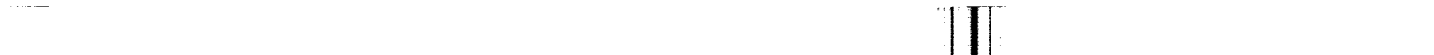


## TABLE OF CONTENTS

<u>Section</u>		<u>Page</u>
1	INTRODUCTION	1-1
1.1	DISCUSSION	1-1
1.2	MAIN STRUCTURAL SAFETY VARIABLES	1-1
1.2.1	Design Loads	1-1
1.2.2	Structural Strength	1-3
1.2.3	Factors of Safety and Reliability	1-4
1.2.4	Brittle Fracture	1-6
1.2.5	Proof Factors and Test Methods	1-7
1.2.6	Safe-Life and Fail-Safe Design Philosophy	1-9
1.3	OBJECTIVES OF STUDY	1-10
1.4	STUDY APPROACH	1-10
2	BASELINE BOOSTER DEFINITION	2-1
2.1	BOOSTER MISSION	2-1
2.1.1	Ascent	2-1
2.1.2	Separation	2-1
2.1.3	Entry	2-4
2.1.4	Abort	2-5
2.1.5	Atmospheric Flight	2-6
2.1.6	Ferry	2-6
2.2	BOOSTER STRUCTURAL CONFIGURATION	2-6
2.3	BOOSTER STRUCTURAL MATERIALS	2-21
2.4	BOOSTER WEIGHT SUMMARY	2-23
2.5	DESIGN CRITERIA	2-26
2.6	DESIGN CONDITIONS	2-28
2.7	SERVICE LOAD SPECTRA	2-39
2.7.1	Wing Load Spectra	2-39
2.7.2	Vertical Tail Load Spectra	2-39
2.7.3	Fuselage Load Spectra	2-39
2.7.4	Orbiter-To-Booster Attachment Load Spectra	2-39
2.7.5	Thrust Load Spectra	2-39
2.7.6	Propellant Tank Pressure Spectra	2-39
2.7.7	Crew Module Pressure Spectrum	2-39
3	STRUCTURAL SIZING AND SENSITIVITY OF WEIGHT TO FACTOR OF SAFETY PERTURBATIONS FOR BASELINE BOOSTER	3-1
3.1	LIQUID OXYGEN TANK	3-1
3.1.1	LO <sub>2</sub> Tank Structural Sizing	3-1

# TABLE OF CONTENTS, Contd

<u>Section</u>		<u>Page</u>
3.1.2	LO <sub>2</sub> Tank Weight Sensitivity to Factor of Safety Perturbations	3-5 3-8
3.2	LIQUID HYDROGEN TANK	3-8
3.2.1	LH <sub>2</sub> Tank Structural Sizing	
3.2.2	LH <sub>2</sub> Tank Weight Sensitivity to Factor of Safety Perturbations	3-15 3-21
3.3	AFT ORBITER SUPPORT FRAME	3-21
3.3.1	Aft Orbiter Support Frame Structural Sizing	
3.3.2	Aft Orbiter Support Frame Weight Sensitivity to Factor of Safety Perturbations	3-24 3-25
3.4	THRUST STRUCTURE	3-25
3.4.1	Thrust Structure Structural Sizing	
3.4.2	Thrust Structure Weight Sensitivity to Factor of Safety Perturbations	3-34 3-35
3.5	WING BOX	3-35
3.5.1	Wing Box Structural Sizing	
3.5.2	Wing Box Weight Sensitivity to Factor of Safety Perturbations	3-40 3-41
3.6	VERTICAL TAIL BOX	3-41
3.6.1	Vertical Tail Box Structural Sizing	
3.6.2	Vertical Tail Box Weight Sensitivity to Factor of Safety Perturbations	3-43 3-44
3.7	CREW MODULE	3-44
3.7.1	Crew Module Structural Sizing	
3.7.2	Crew Module Weight Sensitivity to Factor of Safety Perturbations	3-46 4-1
4	FATIGUE ANALYSIS	
4.1	LIQUID OXYGEN TANK	4-3
4.2	LIQUID HYDROGEN TANK	4-3
4.3	AFT ORBITER SUPPORT FRAME	4-3
4.4	THRUST STRUCTURE	4-12
4.5	WING BOX	4-12
4.6	VERTICAL TAIL BOX	4-12
4.7	CREW MODULE	4-13
5	SAFE-LIFE ANALYSIS	5-1
5.1	CYCLIC AND SUSTAINED FLAW GROWTH RATE CURVES	5-1 5-3
5.2	LIQUID OXYGEN TANK	

## TABLE OF CONTENTS, Contd

<u>Section</u>		<u>Page</u>
5.2.1	LO <sub>2</sub> Tank Safe-Life Analysis	5-3
5.2.2	LO <sub>2</sub> Tank Proof Factor and Apparent Factors of Safety	5-10
5.2.3	LO <sub>2</sub> Tank Weight Sensitivity to Flaw Growth Scatter Factor Perturbations	5-13
5.2.4	LO <sub>2</sub> Tank Safe-Life Sensitivity to Factor of Safety and Flaw Growth Scatter Factor	5-13
5.3	LIQUID HYDROGEN TANK	5-16
5.3.1	LH <sub>2</sub> Tank Safe-Life Analysis	5-16
5.3.2	LH <sub>2</sub> Tank Proof Factor and Apparent Factors of Safety	5-21
5.3.3	LH <sub>2</sub> Tank Weight Sensitivity to Flaw Growth Scatter Factor Perturbations	5-23
5.3.4	LH <sub>2</sub> Tank Safe-Life Sensitivity to Factor of Safety and Flaw Growth Scatter Factor	5-24
5.4	AFT ORBITER SUPPORT FRAME	5-26
5.4.1	Aft Orbiter Support Frame Safe-Life Analysis	5-26
5.4.2	Aft Orbiter Support Frame Safe-Life Sensitivity to Factor of Safety	5-28
5.5	WING BOX	5-30
5.5.1	Wing Spar Caps Safe-Life Analysis	5-30
5.5.2	Wing Spar Caps Safe-Life Sensitivity to Factor of Safety and Flaw Growth Scatter Factor	5-39
5.6	THRUST STRUCTURE	5-39
5.6.1	Thrust Beam Cap Safe-Life Analysis	5-39
5.6.2	Thrust Beam Cap Safe-Life Sensitivity to Factor of Safety and Flaw Growth Scatter Factor	5-42
5.7	VERTICAL TAIL	5-43
5.7.1	Vertical Tail Safe-Life Analysis	5-43
5.7.2	Vertical Tail Safe-Life Sensitivity to Factor of Safety and Flaw Growth Scatter Factor	5-46
5.8	CREW MODULE	5-48
6	FAIL-SAFE ANALYSIS	6-1
6.1	LIQUID OXYGEN TANK	6-1
6.1.1	Fail-Safe Analysis — LO <sub>2</sub> Tank Skin Under Internal Pressure	6-1
6.1.2	Sensitivity of LO <sub>2</sub> Tank Fail-Safe Capability to Factor of Safety Perturbations	6-4
6.2	LIQUID HYDROGEN TANK	6-6

## TABLE OF CONTENTS, Contd

<u>Section</u>		<u>Page</u>
6.2.1	Fail-Safe Analysis — LH <sub>2</sub> Tank Skin Under Internal Pressure	6-6
6.2.2	Fail-Safe Analysis — LH <sub>2</sub> Tank Skin Under Longitudinal Loads	6-7
6.2.3	LH <sub>2</sub> Tank Under Internal Pressure — Factor of Safety Perturbations for Fail-Safe	6-7
6.2.4	LH <sub>2</sub> Tank Under Longitudinal Loads — Factor of Safety Perturbations for Fail-Safe	6-10
6.3	WING BOX	6-10
6.3.1	Wing Box Fail-Safe Analysis	6-10
6.3.2	Wing Box Factor of Safety Perturbations for Fail-Safe	6-18
6.4	THRUST STRUCTURE	6-19
6.4.1	Thrust Structure Fail-Safe Analysis	6-19
6.4.2	Thrust Structure Factor of Safety Perturbations for Fail-Safe	6-20
6.5	VERTICAL TAIL BOX	6-26
6.5.1	Vertical Tail Fail-Safe Analysis	6-26
6.5.2	Vertical Tail Factor of Safety Perturbations for Fail-Safe	6-26
7	RELIABILITY ANALYSIS	7-1
7.1	METHOD OF ANALYSIS	7-1
7.2	RELIABILITY ANALYSIS AND SENSITIVITY TO FACTORS OF SAFETY	7-5
7.2.1	Reliability Analysis of Wing Spar Caps	7-5
7.2.2	Reliability Analysis of Other B-9U Components	7-10
8	SYSTEM SAFETY ANALYSIS	8-1
8.1	RELIABILITY AND CREW SAFETY	8-1
8.2	SAFETY OF COMPONENTS	8-1
8.3	CREW SAFETY AND DESIGN CRITERIA	8-2
8.4	DESIGN FOR CREW SAFETY	8-4
8.5	CREW SAFETY AND WEIGHT	8-4
9	OPTIMUM FACTORS OF SAFETY IDENTIFICATION	9-1
9.1	METHOD OF FACTOR OF SAFETY SELECTION AND ASSOCIATED WEIGHT CHANGE	9-1
9.2	SAMPLE FACTOR OF SAFETY SELECTION AND WEIGHT CHANGE DETERMINATION	9-2

## TABLE OF CONTENTS, Contd

<u>Section</u>		<u>Page</u>
9.2.1	Establishment of Critical Types of Design Requirements	9-2
9.2.2	Selection of Critical Design Requirement Values and Philosophy	9-3
9.2.3	Determination of Factors of Safety Necessary to Fulfill Design Requirements	9-3
9.2.4	Component Factor of Safety Selection	9-5
9.2.5	Component Weight Change Determination	9-7
9.3	OPTIMUM FACTORS OF SAFETY FOR VARIOUS SETS OF DESIGN REQUIREMENTS	9-9
9.3.1	Baseline Design Requirements Analysis with Safe-Life Approach	9-10
9.3.2	Fail-Safe Design Requirements Analysis	9-10
9.3.3	Extended Service Life and Inspection Interval Analysis with Safe-Life Approach	9-13
9.3.4	Increased Safe-Life Scatter Factor Analysis with Safe-Life Approach	9-13
10	COSTS	10-1
10.1	APPROACH	10-1
10.1.1	Direct Costs	10-1
10.1.2	Cascaded Costs	10-2
10.1.3	Growth Costs	10-2
10.2	GROUND RULES AND ASSUMPTIONS OF ANALYSIS	10-5
10.3	RESULTS	10-6
11	CONCLUSIONS AND RECOMMENDATIONS	11-1
12	REFERENCES	12-1
Appendix		
I	EXPERIMENTAL TEST PROGRAM	I-1





## LIST OF FIGURES

<u>Figure</u>		<u>Page</u>
1-1	Load Probability Density Distribution	1-2
1-2	Strength Probability Distribution	1-3
1-3	Factor of Safety Concept	1-4
1-4	Proof Test Concept	1-8
2-1	Elements of Space Shuttle Operations	2-2
2-2	Booster Flight Profile	2-3
2-3	Ascent Trajectory Parameters	2-4
2-4	Booster Entry Trajectory Key Events	2-5
2-5	B-9U Booster Vehicle Configuration	2-7
2-6	B-9U Booster Three View	2-7
2-7	B-9U Booster Inboard Profile	2-8
2-8	B-9U Booster Body Structure	2-11
2-9	B-9U Liquid Oxygen Tank	2-12
2-10	B-9U Liquid Hydrogen Tank	2-12
2-11	B-9U Intertank Section	2-13
2-12	B-9U Thrust Structure	2-14
2-13	B-9U Wing General Arrangement	2-16
2-14	B-9U Nacelle Location, Retracted and Deployed Positions	2-17
2-15	B-9U Vertical Tail Structure	2-18
2-16	B-9U Crew Module	2-19
2-17	B-9U Booster Peak Limit Load Intensities	2-31
2-18	LH <sub>2</sub> Tank Gage Pressures vs Tank Station	2-33
2-19	LO <sub>2</sub> Tank Gage Pressures vs Tank Station	2-33
2-20	Wing Loads (Limit)	2-34
2-21	Canard Loads (Limit)	2-35
2-22	Vertical Tail Loads (Limit)	2-35
2-23	Body Design Temperatures	2-36
2-24	Aerodynamic Surfaces Temperature and Materials Distribution	2-36
2-25	Acoustics on Launch Pad	2-37
2-26	Contours of Equal Overall Sound Pressure Levels, Wing	2-37
2-27	Contours of Equal Overall Sound Pressure Levels, Vertical Tail	2-38
2-28	B-9U Wing Load Spectra	2-40
2-29	B-9U Vertical Tail Load Spectra	2-41
2-30	B-9U Fuselage Station 2600 Load Spectra	2-42
2-31	B-9U Orbiter Forward Attachment Load Spectra	2-43
2-32	B-9U Orbiter Aft Attachment Load Spectra	2-44
2-33	Total Mean Booster Main Engine Thrust	2-45
2-34	Thrust Spectrum (One Flight)	2-45
2-35	Booster Main LH <sub>2</sub> Tank Pressure Schedule	2-46

# LIST OF FIGURES, Contd

<u>Figure</u>		<u>Page</u>
2-36	Booster Main LO <sub>2</sub> Tank Pressure Schedule	2-46
2-37	Crew Module Pressure Schedule	2-47
3-1	LO <sub>2</sub> Tank Plate-Stringer Sizing	3-5
3-2	Upper LO <sub>2</sub> Tank Dome Weight Sensitivity to Factor of Safety Perturbations	3-6
3-3	Lower LO <sub>2</sub> Tank Dome Weight Sensitivity to Factor of Safety Perturbations	3-6
3-4	LO <sub>2</sub> Tank Skin Weight Sensitivity to Factor of Safety Perturbations	3-7
3-5	LO <sub>2</sub> Tank Stringer Weight Sensitivity to Factor of Safety Perturbations	3-7
3-6	Liquid Oxygen Tank Weight Sensitivity to Factor of Safety Perturbations	3-7
3-7	LH <sub>2</sub> Tank Plate-Stringer Effective Thickness Versus Frame Spacing	3-9
3-8	Forward LH <sub>2</sub> Tank Dome Assembly Weight Sensitivity to Factor of Safety Perturbations	3-16
3-9	Aft LH <sub>2</sub> Tank Dome Assembly Weight Sensitivity to Factor of Safety Perturbations	3-16
3-10	LH <sub>2</sub> Tank Belt Frames and TPS Support Frames Weight Sensitivity to Factor of Safety Perturbations for Selected Load Conditions	3-17
3-11	LH <sub>2</sub> Tank Cylindrical Section Skin-Stringer Weight Sensitivity to Factor of Safety Perturbations for Selected Load Conditions	3-19
3-12	Liquid Hydrogen Tank Weight Sensitivity to Factor of Safety Perturbations for Selected Load Conditions	3-20
3-13	Liquid Hydrogen Tank Weight Sensitivity to Reduced FS <sub>u</sub> on Thrust and Drag Loads Only	3-21
3-14	Critical Applied Loads (Ultimate), Aft Orbiter Attachment Frame	3-22
3-15	Aft Orbiter Attachment Frame Element Identification	3-22
3-16	Aft Orbiter Support Frame Weight Sensitivity to Factor of Safety Perturbations for Critical Conditions	3-24
3-17	Thrust Structure Finite Element Model	3-26
3-18	Thrust Structure Model Elements	3-27
3-19	Thrust Structure Weight Sensitivity to Factor of Safety Perturbations for all Critical Conditions	3-34
3-20	Thrust Structure Weight Sensitivity to Perturbation of FS <sub>u</sub> for Thrust Loads Only	3-34

# LIST OF FIGURES, Contd

<u>Figure</u>		<u>Page</u>
3-21	B-9U Wing Structural Simulation Model	3-35
3-22	Wing Box Weight Sensitivity to Factor of Safety Perturbations for All Critical Conditions	3-40
3-23	Wing Box Weight Sensitivity to Factor of Safety Perturbations for Various Critical Load Conditions	3-40
3-24	Vertical Tail Configuration	3-41
3-25	Vertical Tail Box Weight Sensitivity to Factor of Safety Perturbations for All Critical Conditions	3-44
3-26	Vertical Tail Box Weight Sensitivity to Factor of Safety Perturbations for Various Critical Load Conditions	3-44
3-27	Crew Module Stress Intensity Factor Versus Crack Length for a Crack Initiating from a Frame Rivet	3-45
3-28	Crew Module Skin, Frames, and Bulkhead Sensitivity of Weight to Factor of Safety Perturbations for Maximum Operating Pressure	3-46
4-1	Estimated Fatigue Curves for 2219-T87 Aluminum Alloy at Room Temperature with $K_t=3.0$	4-1
4-2	Fatigue Curves for Annealed Ti-6Al-4V at Room Temperature with $K_t=3.0$	4-2
4-3	Fatigue Curves for Annealed Ti-6Al-4V at 650°F with $K_t=3.0$	4-2
4-4	Liquid Oxygen Tank Sensitivity of Fatigue Life to Factor of Safety Perturbations	4-5
4-5	Liquid Oxygen Tank Fatigue Life (for Crack Initiation) Versus Scatter Factor	4-5
4-6	Liquid Hydrogen Tank Sensitivity of Fatigue Life to Factor of Safety Perturbations	4-10
4-7	Liquid Hydrogen Tank Fatigue Life (for Crack Initiation) Versus Scatter Factor	4-10
4-8	Sta. 2666 Orbiter Support Frame Sensitivity of Fatigue Life to Factor of Safety Perturbations	4-11
4-9	Sta. 2666 Orbiter Support Frame Fatigue Life (for Crack Initiation) Versus Scatter Factor	4-11
4-10	Thrust Beam Cap Sensitivity of Fatigue Life to Factor of Safety Perturbations	4-14
4-11	Thrust Beam Cap Fatigue Life (for Crack Initiation) Versus Scatter Factor	4-15
4-12	Wing Spar Cap Sensitivity of Fatigue Life to Factor of Safety Perturbations	4-15
4-13	Wing Spar Cap Fatigue Life (for Crack Initiation) Versus Scatter Factor	4-17

# LIST OF FIGURES, Contd

<u>Figure</u>		<u>Page</u>
4-14	Vertical Stabilizer Sensitivity of Fatigue Life to Factor of Safety Perturbations	4-20
4-15	Vertical Stabilizer Fatigue Life (for Crack Initiation) Versus Scatter Factor	4-20
4-16	Crew Module Sensitivity of Fatigue Life to Factor of Safety Perturbations	4-21
4-17	Crew Module Fatigue Life (for Crack Initiation) Versus Scatter Factor	4-22
5-1	Cyclic Flaw Growth Rate for 2219-T87 Aluminum Alloy at Room Temperature	5-2
5-2	Sustained Flaw Growth Rate for 2219-T87 Aluminum Alloy at Room Temperature	5-2
5-3	Cyclic Flaw Growth Rate for 2219-T87 Aluminum Alloy at -320° F	5-2
5-4	Sustained Flaw Growth Rate for 2219-T87 Aluminum Alloy at -320° F	5-2
5-5	Cyclic Flaw Growth Rate for Ti-6Al-4V (ELI) Annealed Titanium Alloy at Room Temperature	5-3
5-6	Sustained Flaw Growth Rate for Ti-6Al-4V(ELI) Annealed Titanium Alloy at Room Temperature	5-3
5-7	Crack Growth in LO <sub>2</sub> Tank for Pressure Load Spectrum (Surface Flaw, $a/2c = 0.1$ )	5-8
5-8	Crack Growth in LO <sub>2</sub> Tank for Pressure Load Spectrum (Surface Flaw, $a/2c = 0.4$ and Equivalent Through Crack)	5-9
5-9	LO <sub>2</sub> Tank Stress Intensity Ratio Versus Flights to Failure	5-10
5-10	Upper LO <sub>2</sub> Tank Dome Assembly Weight Sensitivity to Flaw Growth Scatter Factor	5-14
5-11	Lower LO <sub>2</sub> Dome Assembly Weight Sensitivity to Flaw Growth Scatter Factor	5-14
5-12	LO <sub>2</sub> Tank Skin Weight Sensitivity to Flaw Growth Scatter Factor	5-14
5-13	LO <sub>2</sub> Tank Skin and Domes Weight Sensitivity to Flaw Growth Scatter Factor	5-14
5-14	LO <sub>2</sub> Tank Safe-Life Versus Factor of Safety	5-15
5-15	Liquid Oxygen Tank Safe-Life (Flaw Growth to Failure) Versus Scatter Factor	5-16
5-16	Crack Growth in LH <sub>2</sub> Tank for Pressure Load Spectrum (Surface Flaw, $a/2c = 0.1$ )	5-20
5-17	Crack Growth in LH <sub>2</sub> Tank for Pressure Load Spectrum (Surface Flaw, $a/2c = 0.4$ and Equivalent Through Crack)	5-20

# LIST OF FIGURES, Contd

<u>Figure</u>		<u>Page</u>
5-18	LH <sub>2</sub> Tank Stress Intensity Ratio Versus Flights to Failure	5-22
5-19	Upper and Lower LH <sub>2</sub> Tank Dome Assembly Weight Sensitivity to Flaw Growth Scatter Factor	5-25
5-20	LH <sub>2</sub> Tank Safe-Life Versus Factor of Safety	5-25
5-21	Liquid Hydrogen Tank Safe-Life (Flaw Growth to Failure) Versus Scatter Factor	5-26
5-22	Aft Orbiter Support Frame Critical Flaw Size Versus Applied Stress	5-29
5-23	Aft Orbiter Support Frame Safe-Life Versus Factor of Safety	5-29
5-24	Crack Growth in Titanium Wing Spar Caps	5-32
5-25	Stress Intensity Factor ( $\Delta K_I$ ) Multiple for a Crack Initiating at a Fastener Hole	5-36
5-26	Stress Level Versus Critical Flaw Size for the Titanium Wing Spar Caps	5-37
5-27	Allowable Maximum Operating Stress Level Versus the Number of Flights to Failure (Safe-Life) for the Titanium Wing Spar Caps	5-38
5-28	Wing Spar Caps Factor of Safety Versus Safe-Life	5-40
5-29	Wing Spar Caps Safe-Life (Flaw Growth to Failure) Versus Scatter Factor	5-41
5-30	Crack Growth in the Titanium Thrust Beam Caps (Flaw Configuration - Corner Crack)	5-42
5-31	Crack Growth in the Titanium Thrust Beam Caps (Flaw Configuration - Crack Emanating from a Hole)	5-43
5-32	Thrust Structure Ultimate Factor of Safety Versus Critical Flaw Size	5-44
5-33	Thrust Structure Factor of Safety Versus Safe-Life	5-44
5-34	Thrust Beam Caps Safe-Life (Flaw Growth to Failure) Versus Scatter Factor	5-45
5-35	Crack Growth in the Vertical Tail Skin	5-46
5-36	Vertical Tail Applied Stress Versus Critical Crack Length for a Thru-Crack	5-47
5-37	Vertical Tail Ultimate Factor of Safety Versus Safe-Life	5-47
5-38	Vertical Tail Safe-Life (Flaw Growth to Failure) Versus Scatter Factor	5-48
5-39	Crew Module Applied Stress for a Thru-Crack Versus Critical Crack Length	5-49
5-40	Crew Module Ultimate Factor of Safety Versus Flights to Tear and Arrest	5-50

# LIST OF FIGURES, Contd

<u>Figure</u>		<u>Page</u>
5-41	Crew Module Safe-Life (Flaw Growth to Failure) Versus Scatter Factor	5-50
6-1	LO <sub>2</sub> Tank Crack Arrest Effectiveness of Graphite/Epoxy Tear Straps	6-3
6-2	LO <sub>2</sub> Tank Crack Arrest Effectiveness of Graphite/Epoxy Tear Straps, 36-Inch Strap Spacing	6-5
6-3	Liquid Oxygen Tank Critical Initial Crack Length Versus Ultimate Factor of Safety	6-5
6-4	LH <sub>2</sub> Tank Crack Arrest Effectiveness of Graphite/Epoxy Tear Straps	6-7
6-5	LH <sub>2</sub> Tank Crack Arrestment by Integral Stringers for Longitudinal Loading	6-9
6-6	Liquid Hydrogen Tank Critical Initial Crack Length Versus Ultimate Factor of Safety for Internal Pressure	6-9
6-7	Liquid Hydrogen Tank Longitudinal Loading Crack Arrestment by Integral Stringers for Various Factors of Safety	6-11
6-8	Wing Box Weight Penalty for Fail-Safe Versus Ultimate Factor of Safety	6-20
6-9	Thrust Structure Sensitivity of Weight to Ultimate Factor of Safety for Fail-Safe	6-26
6-10	Vertical Tail Box Stress Intensity Factor Versus Crack Length	6-27
6-11	Vertical Tail Box Stress Intensity Factor Versus Crack Length for Various Ultimate Factors of Safety	6-28
7-1	Estimate of B-9U Wing Load Distribution	7-5
7-2	Percent of Room Temperature Tensile Strength and Coefficient of Variation of Strength Versus Temperature for Ti-6Al-4V Annealed	7-7
7-3	Percent of Room Temperature Tensile Strength and Coefficient of Variation of Strength Versus Temperature for René 41	7-7
7-4	Wing Yield Reliability Versus Factor of Safety at Room Temperature	7-8
7-5	Wing Ultimate Strength Reliability Versus Factor of Safety at Room Temperature	7-9
7-6	Wing Yield Reliability Versus Factor of Safety at 650° F	7-11
7-7	Wing Ultimate Strength Reliability Versus Factor of Safety at 650° F	7-12
7-8	Structural Reliability at Ultimate Strength for Several B-9U Components Versus Factor of Safety	7-13

## LIST OF FIGURES, Contd

<u>Figure</u>		<u>Page</u>
7-9	Structural Reliability at Yield Strength for Several B-9U Components Versus Factor of Safety	7-14
10-1	Theoretical First Unit Cost Estimating Relationship	10-3
10-2	Engineering Design and Development Cost Estimating Relationships	10-4

111

-

---

---



## LIST OF TABLES

<u>Table</u>	<u>Page</u>
1-1	Booster Entry Condition Load Parameters
1-2	Typical Factors of Safety for Aerospace Vehicle Primary Structures
2-1	B-9U Basic Data
2-2	Booster Materials
2-3	Weight Summary
2-4	B-9U Component Structural Weight Breakdown
2-5	Sequence Mass Properties Statement, B-9U Booster
2-6	Design Criteria
2-7	Service Life Factors
2-8	Safe-Life Design Environments
2-9	Summary of Booster Design Conditions and Loads
2-10	Summary of Design Conditions for Aerodynamic Surfaces
2-11	Booster/Orbiter Interconnection Loads
2-12	External Noise Levels on Booster Structure
3-1	LO <sub>2</sub> Tank Critical Ultimate ( $FS_u = 1.4$ ) Load Intensities
3-2	LH <sub>2</sub> Tank Critical Design Loads (Ultimate), $FS_u = 1.4$
3-3	LH <sub>2</sub> Tank Plate Stringer Sizing
3-4	Aft Orbiter Attachment Frame, Cap Axial Loads and Cross-Sectional Areas
3-5	Aft Orbiter Attachment Frame, Web Shear Flows and Thicknesses
3-6	Thrust Structure Ultimate Design Loads
3-7	Thrust Structure Model Element Loads, Areas, Thicknesses, Stresses, and Weights
3-8	Spar Cap Loads, B-9U Wing
3-9	Sizing Data — Spar No. 1 (WS 515), B-9U Wing
3-10	Sizing Data — Spar No. 2 (WS 633), B-9U Wing
3-11	Sizing Data — Spar No. 3 (WS 751), B-9U Wing
3-12	Sizing Data — Spar No. 4 (WS 941), B-9U Wing
3-13	Sizing Data — Spar No. 5 (WS 1042), B-9U Wing
4-1	LO <sub>2</sub> Tank Pressure Spectrum and Damage Analysis at Upper Dome Equator
4-2	LH <sub>2</sub> Tank Pressure Spectrum and Damage Analysis at Upper Dome Equator
4-3	Fuselage Damage Analysis — Station 2600 Bottom Centerline
4-4	Aft Orbiter Support Frame Load Spectrum and Damage Analysis
4-5	Thrust Beam Cap Fatigue Damage Analysis
4-6	B-9U Wing Spar Caps Fatigue Damage Analysis

# LIST OF TABLES, Contd

<u>Table</u>		<u>Page</u>
4-7	B-9U Vertical Tail Fatigue Damage Analysis	4-18
4-8	Crew Module Fatigue Damage Analysis	4-19
5-1	Aft Orbiter Support Frame Loading Spectrum	5-26
5-2	Wing Spar Cap Loading Spectrum	5-31
6-1	Wing Box Ultimate and Fail-Safe Internal Loads	6-12
6-2	Margins of Safety for Baseline Structure, and Area Increases for Fail-Safe Design, Wing Box	6-17 6-21
6-3	Thrust Structure Fail-Safe Analysis	6-21
7-1	Component Materials, Strength Values and Coefficients of Variation	7-15
9-1	Optimum Factor of Safety Identification, Baseline Design Requirements (Safe-Life Approach)	9-11
9-2	Optimum Factor of Safety Identification, Fail-Safe Design Requirements	9-12
9-3	Optimum Factor of Safety Identification, Extended Service Life and Inspection Interval Requirements (Safe-Life Approach)	9-15
9-4	Optimum Factor of Safety Identification, Increased Safe-Life Scatter Factor Requirement (Safe-Life Approach)	9-16 10-6
10-1	Delta Weights for Costing	10-6
10-2	Baseline B-9U Program — WBS Level 4 Summary Cost (\$ million)	10-7
10-3	Baseline B-9U Structural Group Cost Calculation (\$ million)	10-8
10-4	Baseline Design Requirements, Delta Costs	10-9
10-5	Fail-Safe Design Requirements, Delta Costs	10-9
10-6	Extended Service Life and Inspection Interval Design Requirements, Delta Costs	10-10 10-10
10-7	Increased Safe-Life Scatter Factor Requirements, Delta Costs	10-10
11-1	Summary of Analytical Results for Baseline B-9U Booster	11-2
11-2	Trade Study Weight and Cost Changes	11-3
11-3	Optimum Design Criteria (Fail-Safe Design Approach)	11-4

## LIST OF SYMBOLS AND ABBREVIATIONS

$a$	Surface flaw depth, through-crack half-length, radius of corner crack, length of flaw emanating from hole
$a_{cr}$	Critical value of $a$
$a_i$	Initial value of $a$
$a_o$	Initial through-crack half-length
$A$	Area
$A_{sk}$	Area of skin
$A_{str}$	Area of stringer
ABES	Air Breathing Engine System
ACPS	Attitude Control Propulsion System
A.L.	Axial Load
APU	Auxiliary Power Unit
AREF	Distance from hole for which GKT is equal to GMIN
B.L.	Boundary layer
$c$	Chord, surface flaw half length
$(2c)_{cr}$	Critical surface flaw length
$(2c)_i$	Initial surface flaw length
c.g.	Center of gravity
$C$	Stress intensity correction factor for stiffened sheet, stress intensity correction factor for bulge due to internal pressure
$C_D$	Drag coefficient
$C_f$	Shell instability coefficient = $6.25 \times 10^{-6}$
$C_L$	Lift coefficient
$C_{VL}$	Coefficient of variability of stress = $\frac{\ell}{L}$
$C_{VS}$	Coefficient of variability for strength = $\frac{s}{S}$
CS	Center Spar
$d$	Standard deviation of $D$ , frame depth
$d^2$	Variance of $D$

$\frac{da}{dn}$	Cyclic flaw growth rate
$\frac{da}{dt}$	Sustained flaw growth rate
D	Tank diameter, drag, random load variable with normal distribution = S - L
$\bar{D}$	Mean of D = S - L
e	Base of natural logarithms = 2.71828
E	Young's modulus
$E_c$	Young's modulus, compression
$E_f$	Young's modulus for tank stiffening frame
ECLSS	Environment Control Life Support System
ED&D	Engineering Design and Development
$f_c$	Compression stress
$f_s$	Shear stress
$f_{sp}$	Maximum shear stress
$f_t$	Tension stress
$f_{limit}$	Maximum operating stress
F	Allowable stress
$F_A$	A-value of material strength
$F_B$	B-value of material strength
$F_c$	Compression allowable stress
$F_s$	Shear allowable stress
$F_{su}$	Ultimate shear strength
$F_t$	Tension allowable stress
$F_{tu}$	Ultimate tensile strength
$F_{ty}$	Tensile yield strength
$F_{ult}$	Ultimate allowable stress
FS	Factor of safety, front spar
$FS_u$	Ultimate Factor of Safety
$FS_y$	Yield Factor of Safety

FTH	Flight Test Hardware
FTS	Flight Test Spares
g	Acceleration of gravity
GKT	Stress intensity corrections to account for stress concentration around a hole
GMAX	Maximum value of GKT (at periphery of hole)
GMIN	Minimum value GKT at some distance from hole
GN <sub>2</sub>	Gaseous Nitrogen
GO <sub>2</sub>	Gaseous Oxygen
GSE	Ground Service Equipment
GTH	Ground Test Hardware
h	altitude
I	Moment of inertia, product of interia
I <sub>f</sub>	Required moment of inertia of tank stiffeneing frame
IA&C/O	Installation, Assembly and Checkout
JP	Jet Propulsion
K	Stress intensity factor
K <sub>I</sub>	Stress intensity factor, opening mode
K <sub>C</sub>	Plane stress fracture toughness, critical stress intensity factor
K <sub>I<sub>C</sub></sub>	Plane strain fracture toughness
K <sub>I<sub>i</sub></sub>	Initial value of stress intensity factor
K <sub>t</sub>	Stress concentration factor
K <sub>TH</sub>	Threshold value of stress intensity factor
ℓ	Standard deviation of L
ℓ <sup>2</sup>	Variance of L
L	Load variable with normal distribution, frame spacing, lift, length
$\bar{L}$	Mean load
L'	Effective column length
LH <sub>2</sub>	Liquid Hydrogen
LO <sub>2</sub>	Liquid Oxygen
LN <sub>2</sub>	Liquid Nitrogen

M	Mach number, bending moment
$M_k$	Deep flaw correction factor
M.S.	Margin of safety, mid-spar
n	Applied number of fatigue cycles, test sample size, load factor
$n_e$	Number of exceedences
N	Fatigue cycles to failure
$N_x$	Axial load intensity
$N_y$	Circumferential load intensity
NDE	Nondestructive evaluation
NDI	Nondestructive inspection
p	Pressure
P	Force, pressure
$P_{ult}$	Ultimate member load for baseline $FS_u$
$P'_{ult}$	Ultimate member load for non-baseline $FS_u$
$P ( )$	Probability of ( )
q	Shear load intensity, dynamic pressure
r	Crew module radius of circular section
R	Tank radius, reliability
RS	Rear Spar
R.T.	Room Temperature
s	Standard deviation of S
$s^2$	Variance of S
S	Strength variable with normal distribution, fatigue stress for failure
$S_a$	Amplitude of fatigue stress for failure
$S_m$	Mean fatigue stress for failure
$\bar{S}$	Mean strength
SE&I	System Engineering and Integration
S.F.	Scatter factor
S.L.	Sea Level
SS	Span Station

t	Wing thickness, material thickness, time
$t_s$	Skin thickness
$\bar{t}$	Equivalent skin thickness
T	Thrust, temperature, torque
TAC	Test article conversion
TFU	Theoretical First Unit
TPS	Thermal Protection System
V	Velocity, shear
w	Material weight density
W	Weight, tear strap or crack stopper spacing
$W_B$	B-9U booster weight at liftoff
$W_0$	B-9U booster weight at separation
WBS	Work Breakdown Structure
WS	Wing station
WT	Weight
WTR	Western Test Range
$\bar{x}$	Mean material strength
z	Number of standard deviations = $\frac{\bar{D}}{d}$
$z_p$	Number of standard deviations corresponding to a given probability
$z_\gamma$	z-value for a given confidence level
Z	$\frac{D - \bar{D}}{d}$
$\alpha$	Proof factor, angle of attack
$\beta$	Angle of sideslip
$\Delta$	Increment or change
$\rho$	Radius of gyration, material weight density
$\sigma$	Stress, standard deviation
$\sigma_{alt}$	Alternating applied fatigue stress
$\sigma_c$	Critical hoop stress for onset of crack instability

$\sigma_{\text{limit}}$	Maximum operating stress.
$\sigma_{\text{mean}}$	Mean applied fatigue stress
$\sigma_y$	Tensile yield stress
$\sigma_{ys}$	Tensile yield stress
$\sigma_Y$	Tensile yield stress
$\sigma_{yB}$	Material yield strength in a 2:1 biaxial stress field



## SUMMARY

A study was made of the factors governing the structural design of the fully reusable Space Shuttle booster to establish a rational approach to select optimum structural factors of safety. The study included trade studies of structural factors of safety versus booster service life, weight, cost, and reliability. Similar trade studies can be made on other vehicles using the procedures developed.

The major structural components of a selected baseline booster were studied in depth, each being examined to determine the fatigue life, safe-life, and fail-safe capabilities of the baseline design. Each component was further examined to determine its reliability and safety requirements, and the change of structural weight with factors of safety. The apparent factors of safety resulting from fatigue, safe-life, proof test, and fail-safe requirements were identified. The feasibility of reduced factors of safety for design loads such as engine thrust, which are well defined, was examined.

It was found that:

- a. Fatigue is not a critical design criterion for the baseline B-9U due to its short design service life.
- b. All baseline B-9U components except the wing have safe-lives in excess of the 100 mission design life.
- c. The baseline propellant tanks are not fail-safe, and attempts to provide fracture arrest capability result in prohibitive weight increase. The baseline wing and thrust structure require beef-up to attain a fail-safe capability of 100% of limit load.
- d. All baseline components except the aft orbiter support frame have structural reliability well in excess of the required 0.9999 for ultimate strength and 0.999 for yield strength. The support frame, with a yield reliability of 0.998, just barely falls short of the requirement.
- e. Of the four design approaches for which factors of safety were studied, the only approach that produces a cost and weight decrease is the one for which fail-safe design is applied to components that lend themselves to this design philosophy and safe-life to the remaining components. This approach and its associated criteria are selected as the optimum design approach.
- f. For pressure-designed structure it was found that large apparent factors of safety resulted from proof test and fail-safe considerations for tension structure. Conversely, it was found that reduced factors of safety are feasible on highly redundant structural systems (i.e. thrust structure and wing) using a fail-safe design approach.

- g. Weight and cost decreases for the optimum approach are approximately 1%.
- h. The factor of safety selection procedure is found to be highly sensitive to fracture mechanics calculations.
- i. The data used in the study for fracture mechanics analysis was found to be highly conservative as a result of an experimental test program, which was conducted for two candidate materials. On the basis of the experimental data, the safe-lives of the components should be much larger than those calculated.

## SECTION 1

### INTRODUCTION

#### 1.1 DISCUSSION

Structural factors of safety for aerospace systems have traditionally been established on a deterministic basis, relying on experience and engineering judgment. Parameters considered in establishing factors of safety have included 1) confidence in determining critical loads, 2) mission, 3) design service life, 4) redundancy, 5) replacement/repair philosophy, 6) development status of the selected materials, 7) confidence in analysis methods, and 8) the scope of the structural development and qualification test program. Typical ultimate factors of safety of 1.5 for aircraft and 1.3 for unmanned space launch vehicles have provided generally satisfactory structures on past systems.

The Space Shuttle system represents a major advance in structural technology. It embodies the characteristics of aircraft, spacecraft, and launch vehicles and their associated severe environments and loads, long mission life, high reliability requirement, and considerations for low cost and weight. Conventional aircraft factors of safety could result in excessive structural weight, cost, reliability, and service life. Conversely, use of low launch vehicle factors of safety could result in an unreliable structure with inadequate service life. For the Space Shuttle it will become necessary to carefully select structural design criteria (i.e., factors of safety, service life factors, etc.) on a rational basis that account for the previously mentioned considerations, yet are optimum with respect to mission requirements, performance, service life, cost, reliability, and safety, and that will lead to the most effective Space Shuttle system.

New requirements (Reference 19) for "fracture control" to prevent catastrophic service failures of propellant tanks, crew cabins, and other primary structural components necessitate consideration of fracture mechanics analysis, fail-safe and safe-life design practices, and the additional factors of reduced design stresses and proof testing. Preliminary fracture control studies serve notice that large "apparent factors of safety" may result from this requirement.

#### 1.2 MAIN STRUCTURAL SAFETY VARIABLES

**1.2.1 DESIGN LOADS.** The Space Shuttle booster will experience a large number of applications of a wide variety of loads during its service life. Considering any one particular loading (e.g., loads arising from lateral gusts or winds during ascent, or loads arising from booster entry after staging) it is apparent that the vehicle is subjected to a large number of small-magnitude loads, a small number of high-magnitude loads, and, between, a decreasing number of loads of increasing magnitude.

Loads selected to design the structure are usually based upon a statistical treatment of the mission, aerodynamic, control, and aero-structural parameters that influence the load magnitude. These loads are then expressed deterministically for use in designing the structure. Table 1-1 presents examples of parameters that are examined and varied in selecting design loads for the Space Shuttle booster entry condition.

Table 1-1. Booster Entry Condition Load Parameters

Type of Parameter	Parameter	Effect when Varied
Mission	Staging velocity Staging altitude	Establishes boundary of a design entry corridor with variable velocities, accelerations, and transition altitudes
Aerodynamic	Life coefficient ( $C_L$ ) Drag coefficient ( $C_D$ )	
Control	Autopilot accuracy and redundancy Control system response	
Aero-Structural	Aeroelastic Stiffness Buffet response	Results in load redistribution or magnification

The usual procedure is to vary the parameters from the nominal values in a rational manner and produce a load probability density distribution, as illustrated in Figure 1-1. The design load is then selected as that load that has the probability density of approximately 1/1000 (i. e., one chance in 1000 of occurring). Expressed in statistical terms, the design load is the mean load plus three times the standard deviation ( $\bar{L} + 3\sigma$ ). This approach is "the use of probabilistic methods to arrive at deterministic loads."

Determining design loads on this basis was beyond the scope of the study. Loads from Phase B Space Shuttle and/or loads that resulted from References 22 through 26 will be used to provide design load information for this study.

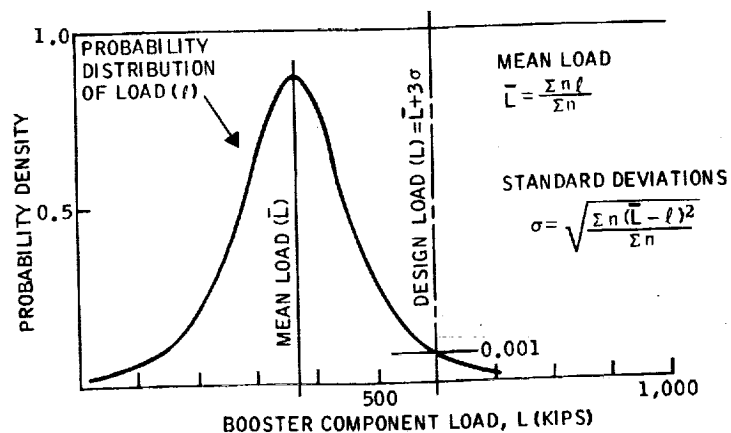


Figure 1-1. Load Probability Density Distribution

**1.2.2 STRUCTURAL STRENGTH.** An effort is made to restrict the variation of strength between apparently identical structures by controlling the manufacturing of the materials employed and the fabrication of the structure. Materials are controlled by adherence to strict limits in the chemical composition and in the manufacturing methods (heat treatment, rolling, etc.). For most metallic materials, this control alone minimizes variation among various samples of materials to the same specification. In certain cases, where it is less easy to control the manufacturing process (e.g., in casting) the results are more scattered. Inspection controls are superimposed on these controls. By visual examination, radiographic examination, and strength tests of specimens, it is possible to maintain a check on variations by rejecting batches that include bad samples.

The same general remarks apply to assembled structures. Strict control of dimensional tolerances and workshop practices (e.g., riveting, welding) is practiced. Visual inspection or, in certain cases, strength checks of sample pieces of construction minimize variation. However, in spite of this rigid control some variation in strength between apparently identical structures still results.

When plotted, these results appear as shown in Figure 1-2. As might be expected, the majority of specimens have strength values at or near the average, and the number of specimens having strength less or greater than average becomes less as the deviation from the average increases. Though the variation of the strength of the structure arises from a large number of individual causes, the resulting scatter generally produces a smooth curve. There are, however, two points to note. The ratio of the width of the diagram to the mean strength differs for different materials and forms of construction, corresponding to the degree of scatter. Materials or structures subject to wide scatter are represented by a broad curve shape. Second, in some cases, the diagram is not symmetrical about the vertical axis; for example, the inspection methods applied may prevent very low strengths from being included, but may accept very high strengths.

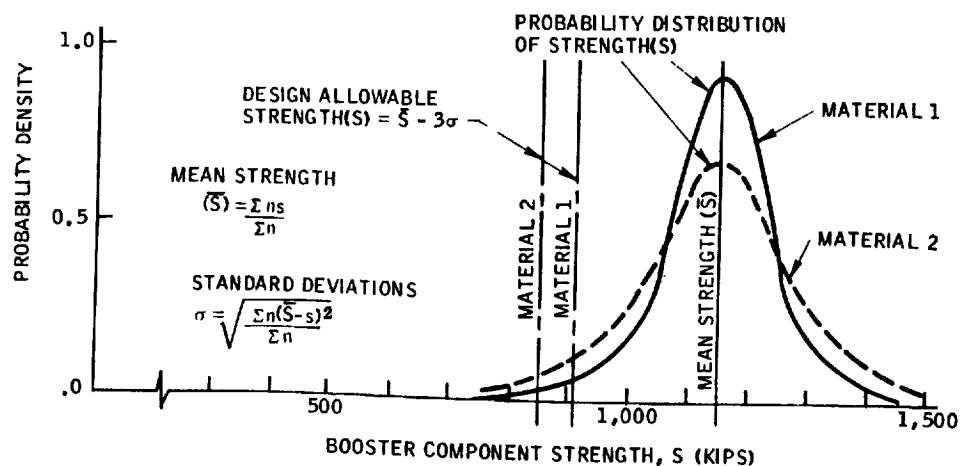


Figure 1-2. Strength Probability Distribution

Material design allowables are usually obtained by testing enough material to establish the minimum strength (i. e. , "A" basis) that has the probability density of approximately 1/1000 (i. e. , one coupon in 1000 has the chance of having this low strength). Tests of structural components to establish component design allowable strengths on this basis are usually not done because of the large costs required to fabricate and test a large number of complex test components. To gain confidence in the strength of structural components, additional factors, conservative analytical methods, and development tests should be considered.

Determining component and material design allowable strengths was beyond the scope of this study. Existing material and component strength data has been used to determine the variation of strength of the candidate Space Shuttle materials.

**1.2.3 FACTORS OF SAFETY AND RELIABILITY.** Most current aerospace vehicles use the factor of safety approach for structural component design. This factor is designed to account arbitrarily for the load and strength variability described in Sections 1.2.1 and 1.2.2, and to allow for unknowns in internal stress distribution and uncertainties in strength analysis methods.

The factor of safety concept is illustrated in Figure 1-3, where the probability density of load distribution of Figure 1-1 and the probability density of structural strength of Figure 1-2 are superimposed. It can be seen that there is a remote possibility that an applied load (greater than the design load) can exceed the strength of the structure (less than the design allowable strength) represented by the area where the probability load distribution curve and the probability strength distribution curve overlap. It can also be seen that the spacing between the design load and the design allowable strength is a measure of the factor of safety used. The area of overlap between the load and

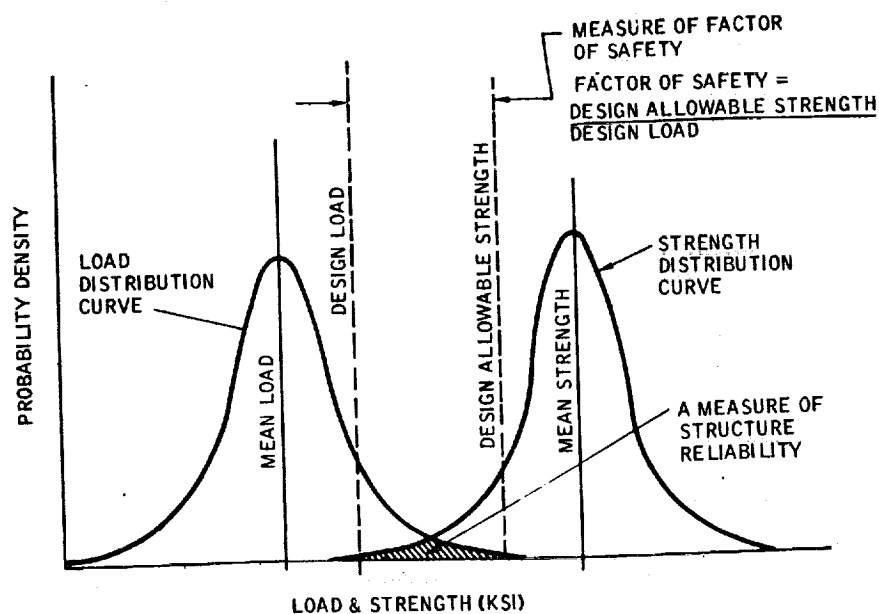


Figure 1-3. Factor of Safety Concept

strength curve is a measure of the probability of a structure's failing and can be related to structural reliability, as discussed in Section 7. It can be seen that the probability of structural failure can be reduced and the structural reliability increased with the use of larger factors of safety.

In practice, this factor is applied to the maximum anticipated loads or combinations of loads (defined as design limit loads) that the vehicle is expected to experience (Figure 1-1). The formal definition of limit load is "the maximum anticipated load, or combination of loads, that a structure may be expected to experience during the performance of missions." At limit load, the structure is required to have sufficient strength to withstand the limit loads with other accompanying environmental phenomena without excessive elastic or plastic deformation.

Ultimate load is the product of limit load and the ultimate factor of safety. At ultimate load, the structure is designed to withstand simultaneously the ultimate loads and other environmental phenomena without failure but with no limit on yielding or deformation. No factor of safety is applied to any environmental phenomena except loads.

An additional load is often defined and denoted as yield load. Yield load is defined as the product of limit load and the yield factor of safety. The rationale and usage of this factor and load condition are to provide a small margin of safety against excessive yielding and deformation at limit load conditions.

Burst and proof loads and factors of safety are specified for such pressure-carrying structures as pressure vessels and cabins. Burst or proof factors are applied to these tanks to provide extra engineering checks because of the high hoop stresses to which these structures are subjected. Of these, the burst pressure is the pressure that a test article must sustain at a singular loading without rupture. Burst tests are usually limited to one or two test specimens in the case of large tanks and a statistical sampling of production units in the case of smaller bottles.

Proof pressure is a pressure applied to each vessel in a production run as a test to demonstrate adequate workmanship, material quality, and service life. Requirements for proofing and the derivation of proof factors are discussed in detail in Section 5.

Different values of factors of safety are used for aerospace vehicles to reflect the designers' varying confidence in different structures, or increased conservatism when the vehicle is manned. In addition, different factors are used for flight or non-flight conditions. A typical set of these factors is presented in Table 1-2. Of interest is that factors in the major structure are divided into two categories pertaining to pressure-loaded and nonpressure-loaded structures.

The effects of temperature must be considered in the vehicle design. Heat sources are aerodynamic heating using critical trajectories, engine gas radiation, and internal heat and cold sources. The effect of these fluxes will be different on different sections

Table 1-2. Typical Factors of Safety for Aerospace Vehicle Primary Structures

Type of Vehicle	Type of Structure	Factor of Safety			
		Limit	Yield	Ultimate	Burst
Aircraft	General structure	1.0	1.0 to 1.2	1.5	—
	Pressure cabins	1.0	1.33	1.5	2.0
Unmanned Launch Vehicle	General structure critical for flight loads	1.0	1.1	1.25	
	General structure designed by nonflight loads and dangerous to ground personnel	1.0	1.1	1.5	
	Propellant tanks	1.0	1.1	1.25	1.25
Manned Launch Vehicle	General structure critical for flight loads	1.0	1.1	1.4	
	General structure designed by nonflight loads and dangerous to ground personnel	1.0	1.1	1.5	
	Propellant tanks	1.0	1.1	1.5	1.5

of the vehicle. Hence, it is necessary to generate time-temperature histories for all pertinent vehicle structures. These temperatures are used unfactored during analysis at both limit and ultimate conditions.

Main integral propellant tanks normally fall into the class of pressure-relieved structures, meaning that axial and bending loads on the tank walls are relieved by the tank internal pressure. In calculating design loads, this relief is used unfactored with factored airloads.

**1.2.4 BRITTLE FRACTURE.** Pressure vessels are stressed to very high levels and use welding to save weight or prevent leakage. Discontinuity stresses, structural defects, and initial flaws always exist and are difficult to control or predict because of variations and limitations of manufacturing and inspection processes. As a result, any poor workmanship or material can cause premature tank failure.

Other structural components also contain flaws, defects, or anomalies of varying shape, orientation, and criticality that are either inherent in the basic material or introduced during fabrication. Most cracks found in aerospace structures are initiated by tool marks, manufacturing defects, and the like. Under the combined driving forces of environment and service loading, these flaws may grow to catastrophic proportions,



resulting in serious reduction of service life or complete loss of the vehicle. Final fracture is often sudden, unexpected, and totally devoid of gross plastic deformation or yielding. It is important to note here that this "brittle like" behavior (crack instability) while perhaps most spectacular in so-called "high-strength" alloys, does occur to some degree in most aerospace structural materials.

Recent cases of catastrophic failure in primary structure have emphasized the need for a fresh look at the structural integrity process currently used to design and qualify structural systems. Perhaps the most obvious deviation that becomes apparent is the need to consider the existence of flaws in "new" structures and to account for their presence during the criteria development, design analysis, and test phases.

Fortunately, linear elastic fracture mechanics analysis and testing techniques have reached the state of development where they can be used with some level of confidence to assess the degree of flaw criticality, to predict the extent of subcritical growth before catastrophic fracture, and to determine the resultant failure modes.

Much of the basic ground work for the current application of linear fracture mechanics to "real" structures can be attributed to the investigators associated with the examination and solution of tankage and pressure vessel failures in recent years. Application to other structural components, on the other hand, while numerous, have been almost entirely motivated by independent requirements and desires within the particular air-frame company to ensure adequate fracture control.

Specific criteria, guidelines, and requirements to consider fracture mechanics in the design and procurement cycle for the Space Shuttle are presented in References 10, 19, and 26. The role of the fracture mechanics discipline in pressure vessel design and proof test qualification is rather straightforward (Reference 19); however, its impact upon weight and performance, and its relationships to factors of safety are more complex. For long-life pressure vessels that require large proof factors, lower design stresses, and higher weights than those required for the specified factors of safety may exist and result in large apparent factors of safety that should be considered when selecting and trading off structural design criteria.

The role of the discipline in designing and qualifying other nonpressure-carrying structural components is less obvious. The approach to be taken in this program is to assume initial flaws and to select design stress levels that do not allow the flaw to grow to critical size during the design life of the vehicle. Again, large apparent factors of safety may exist and are determined.

**1.2.5 PROOF FACTORS AND TEST METHODS.** An approach using the principles of fracture mechanics has been developed recently by Tiffany (References 14 and 19) and can be used as a design tool for safe-life design of pressure vessels. Tiffany's approach, sometimes called a fracture control program, consists of integrating residual crack strength analysis, flaw growth, and a structural proof test into a closed loop.

As a result of the proof test, the vessel is said to be "crack proof," and catastrophic failures are "eliminated" at the operating stress levels over the design service life. Some limitations exist in such a program, and improper use can cause the component to be scrapped.

The proof test consists of statically loading the structure to a level of stress greater than the maximum level expected in service. In addition, the test should be conducted at a temperature consistent with the lowest expected operating level. If completed successfully, this scheme provides assurance that all existing flaws or defects are less than the critical size required for fracture. With the aid of linear elastic fracture mechanics, this critical level includes all flaws of equal stress intensity and thus a wide variety of shapes.

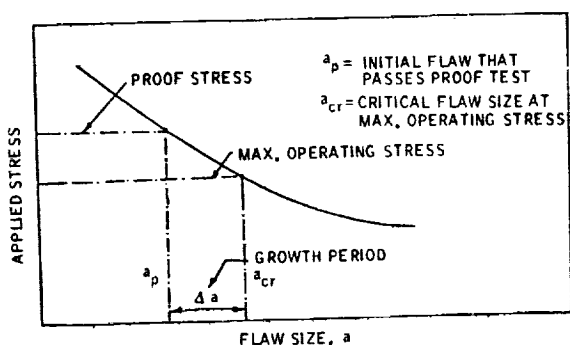


Figure 1-4. Proof Test Concept

The length of service life ensured by the proof test is the time required to grow the smaller "proof" stress flaw to the larger critical size associated with maximum service operating stress (Figure 1-4).

It is important to note that the length of service time achieved by proof testing is applicable only to those flaws, defects, and cracks present at the time of test.

No regard is given to flaws that may appear during service. Thus, the importance of separate fatigue test is fully realized since it is the only means available to detect design deficiencies that occur in service. Thus, for most applications, the single-cycle proof test concept cannot be extrapolated to cover the entire design or service lifetime of the aircraft.

Like components on individual vehicles may have different toughness values ( $K_{Ic}$ ). Thus, proof testing in production to equal values of stress will screen out smaller flaws in the less tough material. Life after proofing, however, is independent of  $K_{Ic}$  and dependent only on  $K_{Ii}/K_{Ic}$  (Figure 5-9). This is true so long as relatively short periods are considered and loading is fairly uniform. Catastrophic failure of each component will occur when the critical value of  $K$  is achieved; thus, for equal crack lengths the less tough component will fail first. It is not unreasonable to presume that in aerospace applications, unequal flaws, screened out in the proof test, will at some time during the service period be at the same length. This is due mainly to the wide variation in usage and environment. Thus, the tougher component can realistically be expected to achieve a longer life under these conditions.

The practical considerations of proof testing must be evaluated during the structural component design. Figure 2-19 shows the relationship of the proof test pressure envelope to the design and normal operating pressure envelopes for the B-9U Space Shuttle booster liquid oxygen tank. The cryogenic proof test with liquid nitrogen was

selected because it duplicated the tank operating temperature and provided a relatively safe proof test medium. It can be seen that the upper portion of the tank is overpressurized during the proof test and must be designed to account for this proof test limitation. For the design pressure, this overdesign for the proof test condition results in an apparent factor of safety larger than the ultimate factor of safety specified.

**1.2.6 SAFE-LIFE AND FAIL-SAFE DESIGN PHILOSOPHY.** All vehicles are designed for fatigue life in excess of the expected service life; however, the approach to providing residual strength or residual life in structures in the event of induced or inherent damage can be provided by designing for fail-safe or safe-life. For example, in commercial transport aircraft where safety is of utmost concern, fail-safe capability is provided to the greatest possible extent. For military aircraft where performance is of primary concern, fail-safe capability is not provided where it would cost weight to do so, reliance being placed on the fatigue analysis and tests to screen out potential structural damage, and safe-life analysis of assumed defects is used to establish safe inspection intervals. For single-mission launch vehicles and spacecraft, reliance is placed on safe-life analysis of assumed defects and proof tests of each article to provide safe-life in excess of the short service life.

Fail-safe design requires that the failure of any single structural component will not degrade the strength or stiffness of the remainder of the structure to the extent that the vehicle cannot complete the mission at a specified percentage of limit loads. Fail-safe design is normally achieved by providing structural redundancy and the means for arresting unstable crack growth. On the other hand, safe-life design requires sufficiently low design stresses that catastrophic failures of critical structural components will not occur during a specified service life due to initiation and growth of fatigue cracks, or due to the growth of flaws and defects that already exist in the structure. The safe-life of a structure is usually taken as an arbitrary multiple or increment of the specified service life depending on whether the concern is for the initiation of fatigue cracks or the growth of existing defects. For fatigue the arbitrary multiple is usually taken as four service lives, and for the growth of flaws or defects the increment is usually taken as the interval between major scheduled inspections.

Some confusion exists in Reference 26, the aerospace industry, and NASA regarding a precise definition of safe-life. Some engineers, particularly aircraft designers concerned with long life structures, define safe-life as the life of a component to the initiation of fatigue cracks. Other engineers, particularly those with fracture mechanics training, define safe-life as the component life for initial defects in the component to grow to critical size and failure. A third group, including the authors, feel that safe-life encompasses both of these failure modes. For purposes of this report and to be consistent with the definitions of Reference 26, two definitions are adopted: 1) fatigue life is the life of an unflawed structural component to the initiation of visible fatigue cracks, and 2) safe-life is the life for initial defects in a component to grow to a critical size for catastrophic failure.

### 1.3 OBJECTIVES OF STUDY

The present study was undertaken with the following objectives:

- a. To determine the required yield and ultimate factors of safety for selected Space Shuttle booster structural components.
- b. To determine the apparent factors of safety that exist due to other design considerations such as fatigue, safe-life, fail-safe, and proof testing.
- c. To determine the variation of component structural weight when the factors of safety are varied for all or only individual design conditions (i. e. , factor of safety varied on thrust loads but held at specified value for other design conditions).
- d. To provide the capability of making structural criteria trade studies in terms of performance, cost, service life, reliability, and crew safety.

### 1.4 STUDY APPROACH

The study approach consisted of selecting a baseline Space Shuttle booster vehicle, mission, preliminary criteria, and cost model, and performing theoretical and experimental studies using this vehicle and certain selected components as references to establish booster vehicle weight, cost, reliability, and safety sensitivities for variations in structural design criteria (i. e. , factors of safety, design life scatter factors, etc. ). Study results are then used to develop a procedure to identify the impact of design criteria changes (i. e. , factors of safety, design service life, life scatter factors, reliability factors, etc. ) on the total booster weight, performance, and cost. The procedures developed clearly show the relative criticality of the various design criteria on the selected baseline vehicle. Similar investigations and criteria trade studies can be performed on other Space Shuttle vehicles by following the procedures and examples presented.

Theoretical studies consisted of development of design loads, service load spectra, structural sizing, and performance of fatigue, safe-life, fail-safe, reliability, and cost analyses. Crew safety areas of risk were identified and evaluated qualitatively.

Preliminary investigations showed that safe-life and proof test requirements designed a large portion of the booster structure (i. e. , main propellant tanks and wing). Proof test factors (and hence the design) are based on analytical predictions of the rate of growth of crack-life flaws that exist or are assumed to exist in the structure. The analysis consists of calculating flaw growth under cyclic and sustained load conditions and assumed atmospheric environmental conditions. Conditions of alternate chilling, heating, drying, and exposure to a salt-laden sea-coast atmosphere could produce significantly higher crack growth rates that, in turn, would produce higher proof factors and structural weight, if accounted for.

Since these factors resulted in large apparent factors of safety and have a significant impact on the results of this study, a small experimental flaw growth test program was accomplished. Specific objectives of the experimental program were 1) to assess the effects of life cycle condition on crack growth rates, proof factors, factors of safety, and structural weight; and 2) to verify analytical predictions of flaw growth and proof factors.

The study did not include the orbiter because of lack of detail knowledge and data on the orbiter (i. e. , Convair Aerospace Phase B studies have been limited to the Space Shuttle booster) and the low funded effort. It is believed by the authors that the study results are generally applicable to the orbiter; however, caution should be exercised and orbiter studies accomplished before this conclusion can be fully satisfied.

The scope of the program also did not permit study of the entire booster structural system; however, the major structural components were studied. These included the crew cabin, main LO<sub>2</sub> and LH<sub>2</sub> propellant tanks, thrust structure, vertical tail box, aft orbiter support frame, and wing boxes, which represent approximately 45% of the booster primary structural weight, 25% of the booster dry weight, and 60% of the total booster structural system cost. Not included in the study were the thermal protection system, canards, intertank adapter, and other miscellaneous subcomponents.



## SECTION 2

### BASELINE BOOSTER DEFINITION

#### 2.1 BOOSTER MISSION

The Space Shuttle Program is designed to provide a space transportation system capable of placing and/or retrieving payloads in earth orbit. The specific mission considered in this study consists of launching an orbiter vehicle into a 100 n.mi. south polar orbit from WTR with a 40,000-pound payload. These objectives are achieved using a two-stage (booster and orbiter) vehicle capable of boost and earth entry with cruise-back to a designated landing site. This cycle is accomplished with reasonable acceleration levels and shirt-sleeve cabin environment. The significant elements of this mission are ground operations, mating of booster and orbiter, launch followed by staging of the two vehicles, with the booster returning to the launch area and the orbiter continuing on to its prescribed orbit. A complete mission cycle is shown in Figure 2-1.

A typical mission flight profile for the booster is shown in Figure 2-2.

**2.1.1 ASCENT.** The ascent phase is defined as beginning with engine ignition and ending with the initiation of separation. In the ignition/lift-off sequence, the thrust rises to 50 percent of full thrust and holds at that level until main-stage in all engines can be verified and holddown release is verified. Upon verification, the thrust is increased at a controlled rate to 100 percent. The vehicle lift-off occurs when the thrust-to-weight ratio (T/W) is greater than 1.

After the vehicle has cleared the service towers, the vehicle is oriented to the correct azimuth and pitch to provide the proper trajectory such that the vehicle assumes a wing-level, pilot-side-up attitude and correct azimuth. As propellant is depleted, along with increased thrust at altitude, the vehicle acceleration increases to 3 g. At this point, the main engines are throttled to maintain 3 g for crew comfort and vehicle design loads. Ascent phase is terminated by initiation of separation based on attainment of desired velocity or by indication of fuel depletion. Figure 2-3 gives a variety of ascent trajectory parameters.

**2.1.2 SEPARATION.** Near booster burnout, the booster engines are throttled to 50 percent thrust. When both sets of engines are at 50 percent thrust, the restraint mechanism between orbiter and booster is released, booster thrust decays to zero, and the orbiter rotates upwards and aft, relative to the booster, on separation system linkages until the orbiter is free and accelerating under its own thrust. The control of all sequencing functions necessary for separation and maintaining control of both orbiter and booster is accomplished by software in the main computer.

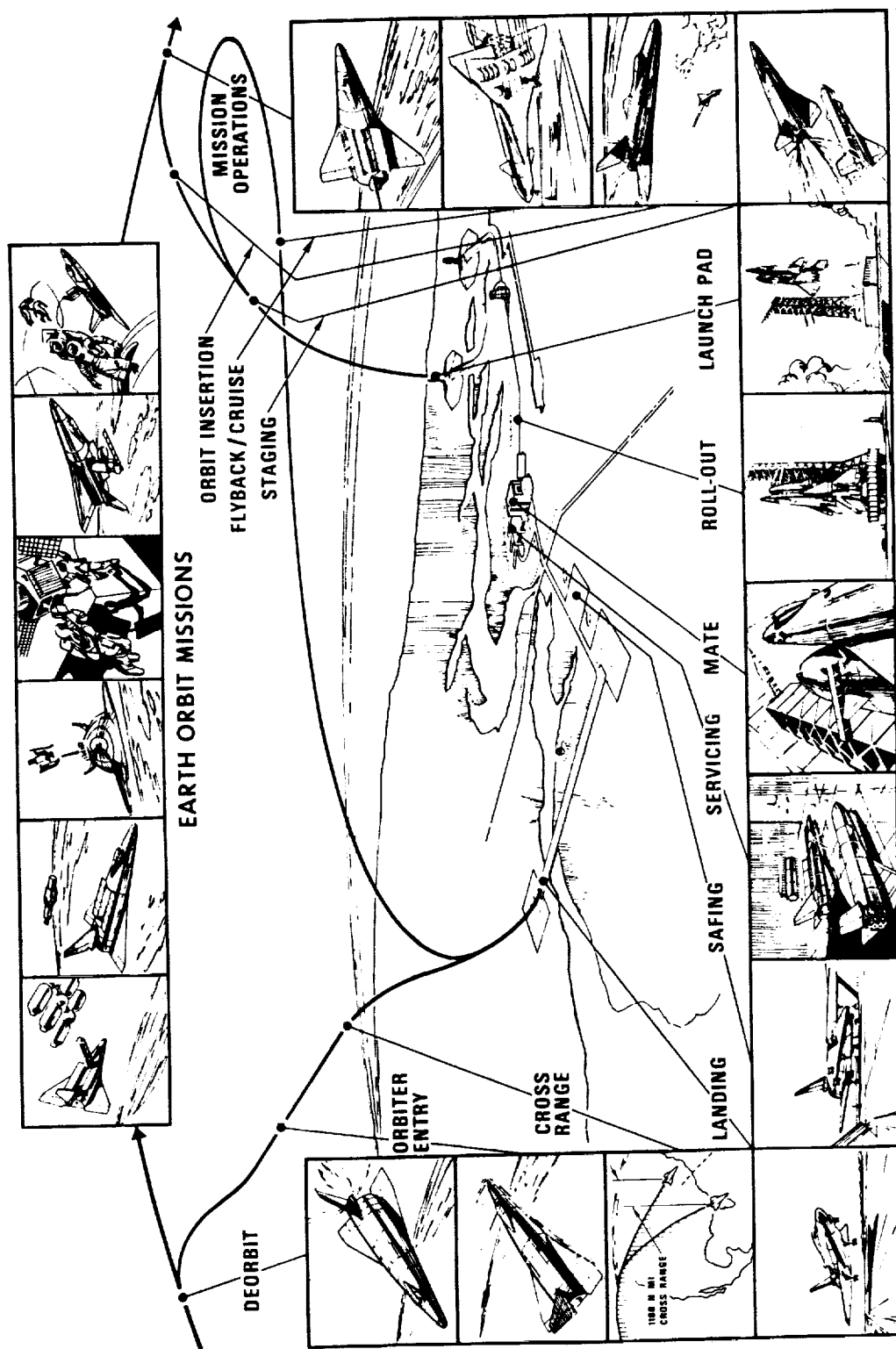


Figure 2-1. Elements of Space Shuttle Operations



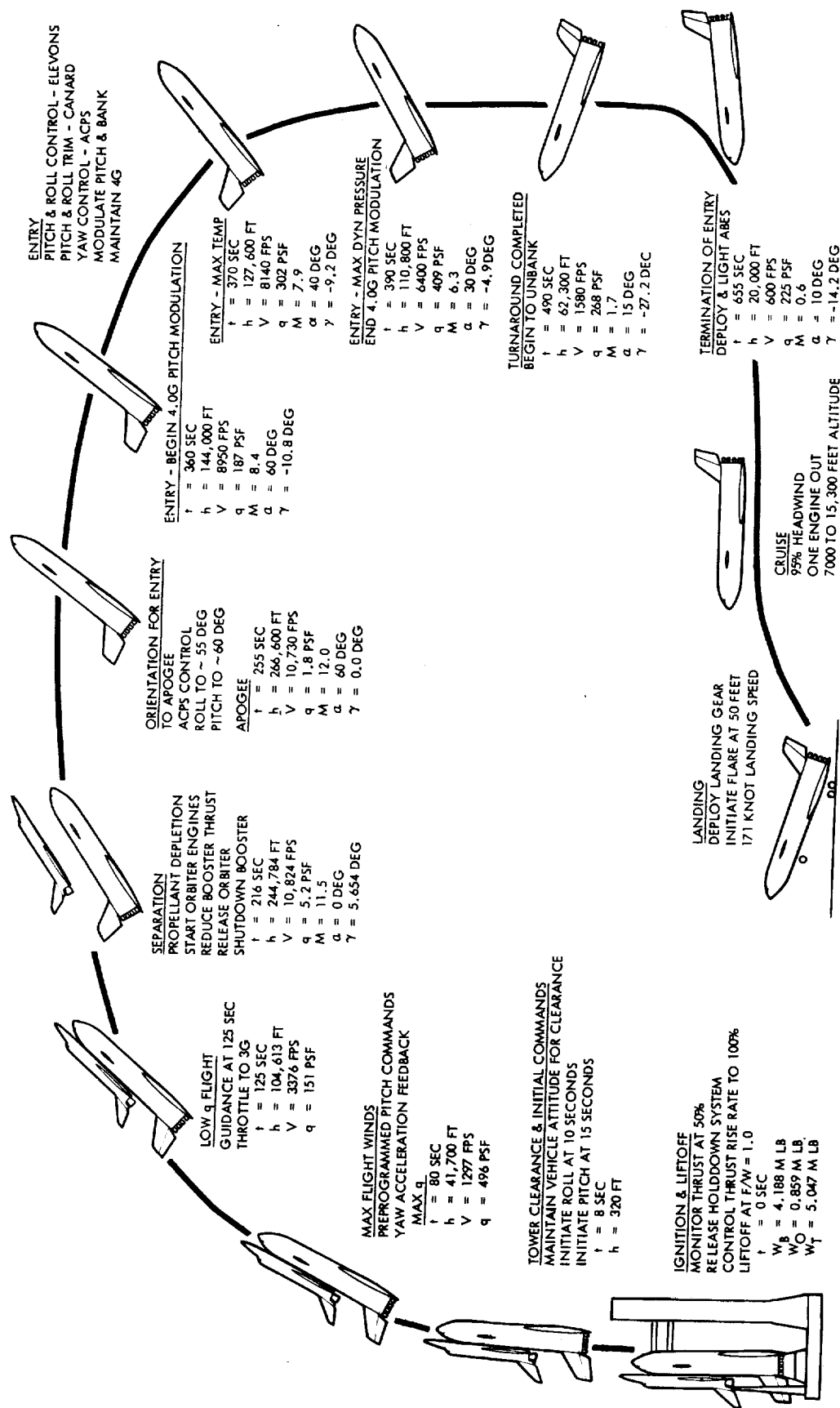


Figure 2-2. Booster Flight Profile

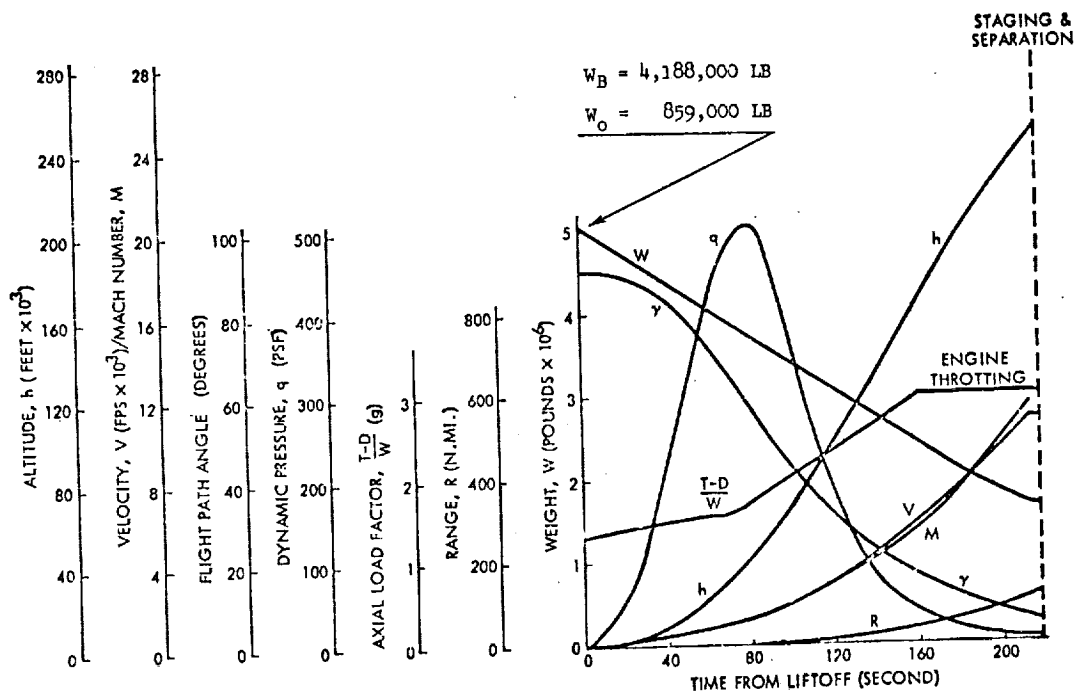


Figure 2-3. Ascent Trajectory Parameters

The staging conditions for the 100 n. mi. south polar circular orbit mission from WTR are:

Mission:	South Polar Launch
Altitude:	244,784 ft
Velocity:	10,824 fps
Gamma:	5.654 degrees
Heading Azimuth:	182.495 degrees

The booster weight decreases from 4,188,000 pounds at launch to about 808,000 pounds at separation. After separation the orbiter continues on its mission and the booster positions itself for entry, using ACPS engines.

**2.1.3 ENTRY.** The entry mode for the booster is a supersonic gradual transition. Highlights of the entry are shown in Figure 2-4. During the first 40 seconds after staging the booster pitches to 60 degrees angle of attack and banks to 48 degrees. That attitude is maintained until the resultant load factor reaches 4.0 g, occurring at Mach 8.4 and 144,000 feet altitude. Pitch modulation starts at this time to keep from exceeding 4.0 g. The lower stability limit constrains the angle of attack from going below 30 degrees during this maneuver. Upon reaching 30 degrees, the bank angle is raised to 75 degrees, which is held until the vehicle has completed its turn. A maximum  $q$  of 409 psf is reached at Mach 6.3 and 110,800 feet altitude. By Mach 3.25, the angle of attack has returned to 56 degrees. Beginning there, the angle of attack is constrained by the upper stability limit, reducing to 5 degrees at Mach = 1.1.

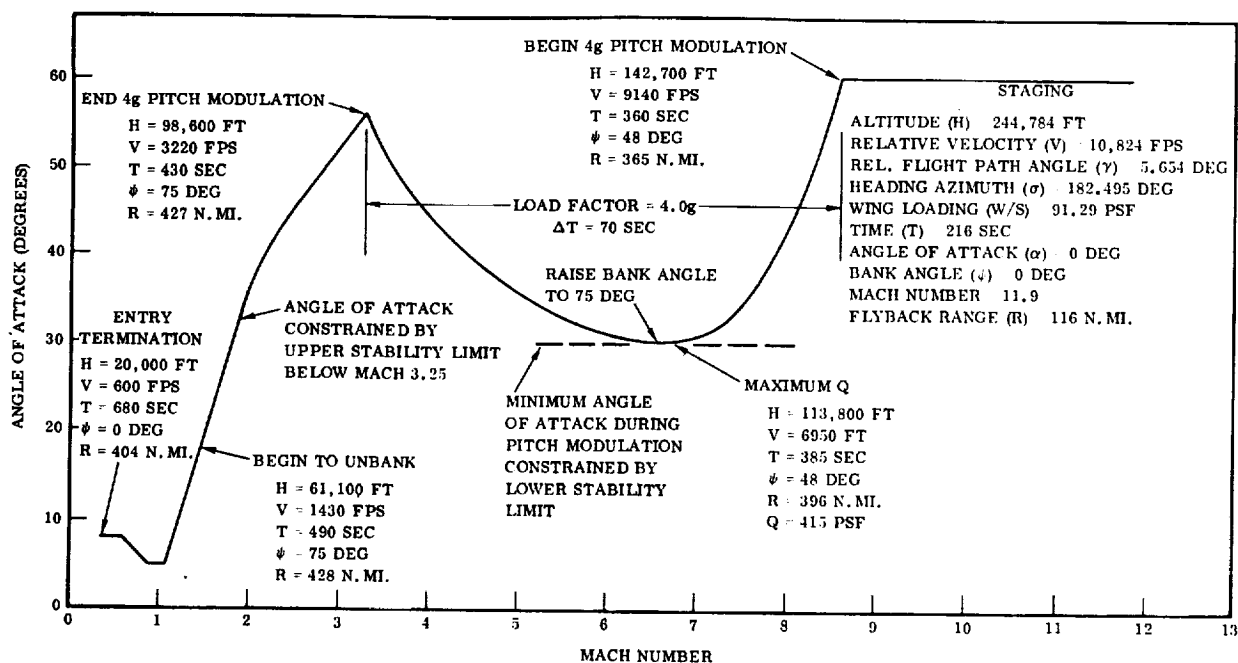


Figure 2-4. Booster Entry Trajectory Key Events

When the booster reaches 20,000 feet, the flyback range is 404 n. mi. At the completion of the entry phase the gross weight of the booster has decreased slightly to about 787,000 pounds.

**2.1.4 ABORT.** The space shuttle provides safe mission termination capability. This capability includes rapid crew and passenger egress prior to liftoff and intact abort after liftoff. Intact abort implies the capability of the booster and orbiter to separate and continue flight to a safe landing.

For flight test phases an ejection system is provided for the crew. The selected system was an open ejection seat using pressure and "g" suits.

The approach to abort in the operational program is intact abort. Prelaunch or pad abort is concerned with aborts during the 45-minute time period from when the crew and passengers enter the vehicle until liftoff. The failures in this time period that can be cause for abort can be classed as noncritical or critical. Noncritical failures are those failures in which there is no danger of vehicle or crew loss. The abort procedure would be vehicle shutdown and egress through the tower. Critical functional failures are those that present the danger of vehicle loss and personnel loss if they remain with the vehicle. The selected abort mode for critical pad failures is rapid egress using dedicated semi-free-fall elevators in the launch tower that would descend to a safe area below the tower.

Mated ascent refers to the time period from liftoff through staging. Noncritical failures are those that by definition allow continued safe mated flight to booster propellant

depletion. After separation the booster performs a conventional entry and flyback. Critical failures are those failures in which continued mated flight to booster propellant depletion is not possible and early separation is required. After separation, recovery procedures are initiated for both vehicles, providing the critical failure that caused the early separation does not prevent this.

The entry phase for the booster is that time period from stage separation through engine deployment and start. As with orbital entry vehicles, such as Apollo or Mercury, there is little that can be done in the way of abort procedures during this phase.

**2.1.5 ATMOSPHERIC FLIGHT.** At approximately 20,000 feet, the air-breathing engines are deployed and the return cruise is initiated.

The vehicle descends to approximately 13,000 feet and is flown at the altitude that is for best cruise specific range (maximum n. mi. per pound of fuel) for the required flyback range of 404 n. mi. Landing is based on a touchdown speed at the trimmed power-off  $C_L$  for an angle of attack of 14 degrees. The landing distance varies with the vehicle gross weight, but with a touchdown weight of 628,000 pounds, about 5625 feet are required for landing over a 50-foot obstacle. This distance is for a standard day condition at sea level using braking on a dry concrete runway.

**2.1.6 FERRY.** The basic design of B-9U is evolved from satisfying reference mission requirements; no design penalties are incorporated to accomplish ferry missions. The takeoff capability of the booster is critical to the ferry mission requirements. Cruise performance for the ferry mission consists of flying against a 50-knot headwind to the point of no return with all engines operating, and then cruising to the destination against the 50-knot wind with one engine inoperative. Cruise altitudes are selected that minimize total mission fuel requirements. Fuel reserves are included in the total mission fuel requirements.

## 2.2 BOOSTER STRUCTURAL CONFIGURATION

The space shuttle baseline configuration selected for this study consists of the GDC B-9U booster and the NR 161C orbiter, as reported in References 1 and 2. The B-9U booster is a low, delta wing vehicle with a single vertical tail and a small canard surface mounted forward above the body centerline. The body is basically a cylinder with fairings added to streamline the intersections with the aerodynamic surfaces. Figure 2-5 shows a general view of the booster, Figure 2-6 gives the three view, and the in-board profile is given in Figure 2-7.

The baseline booster configuration consists of cylindrical tanks to contain the launch propellants and to serve as the structural backbone. Surrounding the basic body structure is an outer heat shield assembly that provides the protective layer against

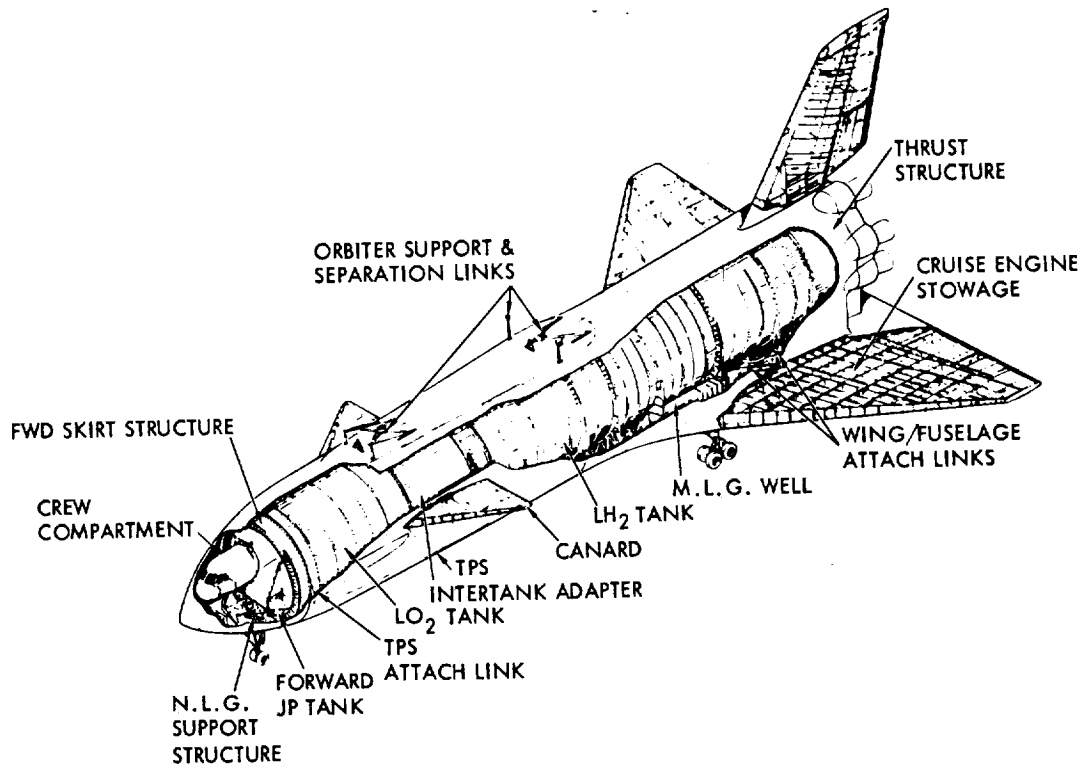


Figure 2-5. B-9U Booster Vehicle Configuration

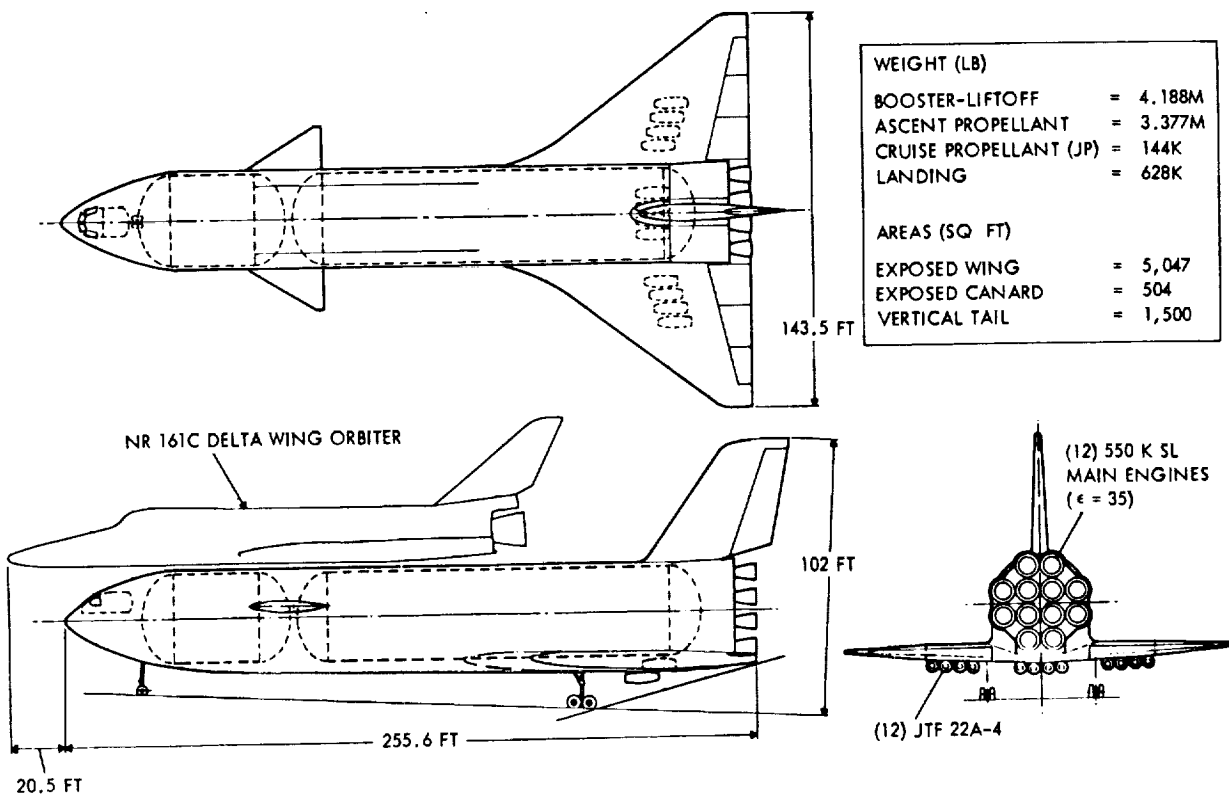
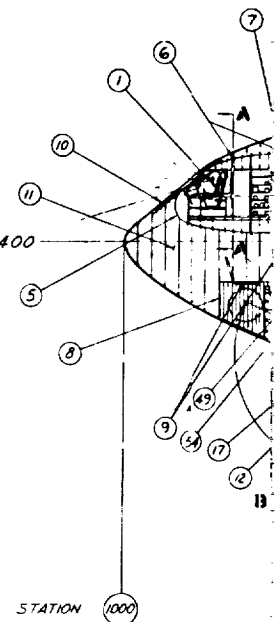
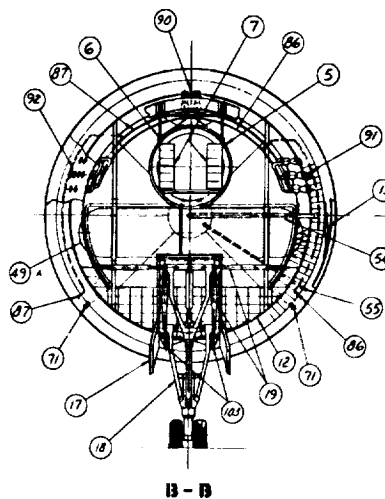
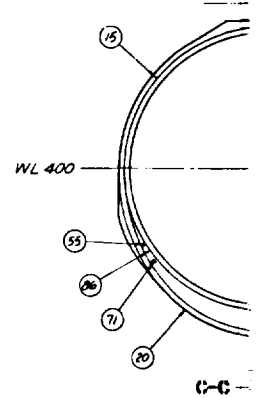
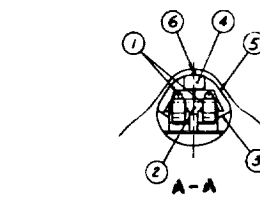


Figure 2-6. B-9U Booster Three View



## LEGEND

1. Pilot Seats
2. Instrument Panel
3. Consoles
4. Overhead Panel
5. Crew Module
6. Crew Module Support
7. Avionics Equipment Racks
8. Nose Gear Wheel Well
9. Crew Access Hatches
10. Retractable Heat Shield
11. Nose Structure
12. Nose Gear Support Bulkhead
13. TPS Support Lines
14. Main LO<sub>2</sub> Tank Structure
15. LO<sub>2</sub> Tank Frame
16. Orbiter Mechanism Support Bulkhead
17. Nose Landing Gear Doors
18. Nose Landing Gear Assembly
19. Nose Gear Support Structure
20. TPS Support Structure
21. Canard Structure Assembly
22. Canard Actuators
23. Forward Orbiter Attachment Mechanism
24. Orbiter Mechanism Attachment Fittings
25. Orbiter Mechanism Attachment Fitting
26. Orbiter Mechanism Support Bulkhead
27. Aft Orbiter Attachment Mechanism
28. Orbiter Mechanism Attachment Fittings
29. Orbiter Mechanism Attachment Fitting
30. Orbiter Mechanism Support Bulkhead
31. Orbiter Mechanism Support Bulkhead
32. Main Hydrogen Tank Structure
33. Main Landing Gear Support Bulkheads
34. Main Landing Gear Assembly
35. Main Landing Gear Doors
36. Landing Gear Drag Load Structural Link
37. Wing Drag Load Structural Link
38. Wing Body Vertical Attach Links
39. Wing Body Side Load Attach Link
40. Wing Structure Assembly
41. Vertical Tail Structure Assembly
42. Vertical Tail Attach Fittings
43. Thrust Structure Assembly
44. Base Heat Shield Assembly
45. Pad Hold-Down & Support Fittings
46. Main Rocket Engines
47. Air Breathing Engine Pods
48. Engine Deployment Power Hinge



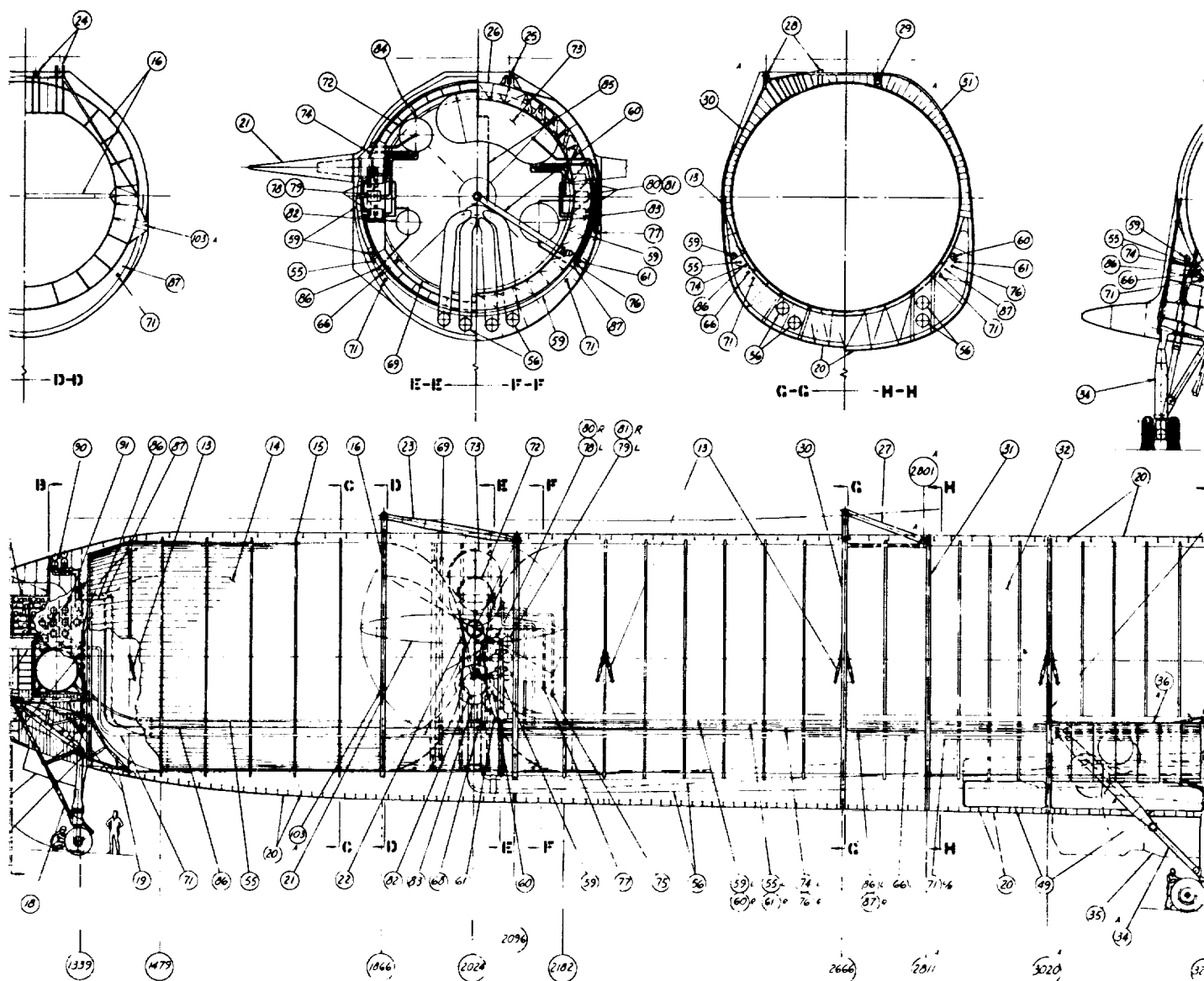
49. JP Fuel Tanks
50. JP Fuel Distribution System
51. JP Fuel Refuel Fitting (Level Attitude)
52. JP Fuel Vent Line to Wing Tip
53. JP Fuel Rise-Off Disconnect
54. Main LO<sub>2</sub> Tank Vent Line
55. LO<sub>2</sub> Tank Pressurization Line
56. Main LO<sub>2</sub> Feed Lines
57. Main LO<sub>2</sub> Distribution System
58. Main LO<sub>2</sub> Fill/Drain Line
59. Gas Exhaust Line
60. Main Hydrogen Tank Vent Line

61. Hydrog
62. Main L
63. Main L
64. Main L
65. Gas Ex
66. Purge
67. Aft Nit
68. Purge
69. Forward
70. Air Cy
71. Refrige
72. APS LC

Figure 2-7. B-9U Booster Inboard Profile







en Tank Pressurization Line  
 -H<sub>2</sub> Distribution System  
 -H<sub>2</sub> Fill/Drain Line  
 -H<sub>2</sub> Vent  
 -haust Vent  
 Nitrogen On-Pad Disconnect  
 rogen Purge Rings  
 Nitrogen To Hydrogen Tank  
 rd Nitrogen Purge Ring  
 cle Refrigeration System (2)  
 -eration Lines to Crew Module  
 O<sub>2</sub> Storage Supply

73. APS LH<sub>2</sub> Storage Supply  
 74. APS LO<sub>2</sub> Fill/Drain Line (On-Pad)  
 75. APS LO<sub>2</sub> Fill/Drain Fitting (Level Attitude)  
 76. APS LH<sub>2</sub> Fill/Drain Line (On-Pad)  
 77. APS LH<sub>2</sub> Fill/Drain Line (Level Attitude)  
 78. APS LO<sub>2</sub> Heat Exchanger (3)  
 79. APS LO<sub>2</sub> Turbopumps (3)  
 80. APS LH<sub>2</sub> Heat Exchanger (3)  
 81. APS LH<sub>2</sub> Turbopumps (3)  
 82. APS GO<sub>2</sub> Accumulator  
 83. APS GH<sub>2</sub> Accumulator  
 84. APS LO<sub>2</sub> Storage Tank Vent Line

85. APS LH<sub>2</sub> Storage Tank Vent  
 86. APS GO<sub>2</sub> Distribution Line  
 87. APS GH<sub>2</sub> Distribution Line  
 88. Auxiliary Power Unit (4)  
 89. APU Exhaust Lines  
 90. APS Thrusters - (4) Fwd. Pi  
 91. APS Thrusters - (8) LH Fwd  
 92. APS Thrusters - (8) RH Fwd  
 93. APS Thrusters - (5) LH Aft  
 94. APS Thrusters - (5) RH Aft  
 95. GHe Storage Supply  
 96. Helium Fill/Drain Disconnect







aerodynamic heating and an aerodynamic surface for the body. This aerodynamic surface varies from a round body section at the nose to a flat-bottomed section at the delta wing, which is attached to the underside of the body structure. The delta wing, with its elevons, canards, and the vertical tail, provides the aerodynamic surfaces required for stability and control for both supersonic and subsonic flight.

For the vertical launch, mated with the orbiter, the booster thrust is provided by 12 main propulsion engines, with a nominal thrust of 550,000 pounds per engine, that burn liquid hydrogen and oxygen and are arranged in the aft end of the vehicle.

Control of the vehicle during powered ascent is provided by gimbaling the main engines for thrust vector control and by using elevons for additional roll control. Subsonic cruise thrust for flyback after a space mission or for ferry flight is provided by 12 air-breathing engines mounted in nacelles. These engines are normally stowed within the wing and body structure envelope during the vertical flight and entry.

Attitude control outside the earth's atmosphere is provided by the attitude control propulsion system (ACPS) engines installed on the fuselage and wings. The ACPS engines use  $\text{LO}_2/\text{LH}_2$  propellants and provide 2100 pounds thrust each.

Landing is accomplished using a conventional tricycle landing gear, including two 4-wheel-bogie main landing gear assemblies and a dual-wheel steerable nose gear assembly.

The booster incorporates a mating and separation system on its top surface to support the orbiter during vertical flight and to perform the separation of the two vehicles. Basic data for the booster are given in Table 2-1.

Internally, the booster is arranged with the  $\text{LO}_2$  tank forward and the  $\text{LH}_2$  tank aft. The selection of cylindrical tanks with separate, state-of-the-art bulkheads, and of cylindrical intertank section and thrust barrel all combined into a primary load-carrying structure, was made to maintain simplicity of the design and manufacture, to increase confidence, and to reduce development risk. The breakdown of the booster body main load-carrying structure is shown in Figure 2-8.

The tanks have ellipsoidal bulkheads with radius-to-height ratios equal to  $\sqrt{2}$  to minimize hoop compression effects. The tanks are of aluminum alloy, with longitudinal integral T-stringers. They provide the primary load-carrying structure of the booster as well as functioning as pressure vessels. The tank diameters are 33 feet. All structural frames are external to the main tanks. The  $\text{LO}_2$  tank is 667 inches long and is shown in Figure 2-7 and Figure 2-9. The  $\text{LO}_2$  tank is not insulated.

Four main  $\text{LO}_2$  lines are routed through the lower body main structure/heat shield interspace, past the main landing gear and aft to the vehicle base.

Table 2-1. B-9U Basic Data

Item		Item	
Booster		Wing (Exposed)	
Launch weight, M lb	4.188	Area, ft <sup>2</sup>	5,047
Empty weight, M lb	0.627	Span (semi), in.	645
Cruise weight, M lb	0.787	Aspect ratio	2.289
Landing weight, M lb	0.639	MAC ( $\bar{c}$ ), in.	671.8
Orbiter weight, M lb	0.859	Wing station, in.	456
Landing c.g. station, in.	3,166	1/4 $\bar{c}$ , in.	167.9
Flyback range, n.mi.	404	1/4 $\bar{c}$ station, in.	3,563
Staging velocity (relative), fps	10,824	Load landing, lb/ft <sup>2</sup>	126.6
Staging altitude, ft	245,000	Max cruise, lb/ft <sup>2</sup>	155.9
Body		Location, c.g. to 1/4 $\bar{c}$ , in.	397
Planform area, ft <sup>2</sup>	8,728	Canard pivot to 1/4 $\bar{c}$ , in.	1,539
Volume, ft <sup>3</sup>	274,650	Wing 1/4 $\bar{c}$ to tail 1/4 $\bar{c}$ , in.	285
Tank diameters, in.	396	Thickness ratio t/c	0.101
Length, in.	3,067	Miscellaneous	
LH <sub>2</sub> tank volume, ft <sup>3</sup>	120,161	Canard area (exposed), ft <sup>2</sup>	504
LO <sub>2</sub> tank volume, ft <sup>3</sup>	40,901	Canard pivot to c.g., in.	1,142
Wing (Theoretical)		Canard span, in.	800.4
Area, ft <sup>2</sup>	8,451	Vertical tail area (exposed), ft <sup>2</sup>	1,500
Span, in.	1,722	Tail 1/4 $\bar{c}$ to c.g., in.	682
Aspect ratio	2.436	Tail span (exposed), in.	533.8
MAC ( $\bar{c}$ ), in.	860.6	Gear axis to c.g., in.	129.0
Wing station, in.	314.3		
1/4 $\bar{c}$ , in.	215.2		
1/4 $\bar{c}$ station, in.	3,421		

The LH<sub>2</sub> tank is similar in geometry to the LO<sub>2</sub> tank, except for the length of 1779 inches, and is shown in Figure 2-7 and Figure 2-10.

For the mixture ratio of 6:1, with added volume of 7.1 percent (for ullage, potential tanking at minimum specific impulse, and for internal insulation) a total LH<sub>2</sub> tank volume of 120,160 cubic feet results; for the LO<sub>2</sub> tank, which does not have any insulation, a factor of 4.5 percent is added to cover ullage and minimum specific impulse, for a tank volume of 40,900 cubic feet. The LH<sub>2</sub> tank construction is similar to the LO<sub>2</sub> tanks except that there are no anti-slosh baffles in the LH<sub>2</sub> tank because the low density fuel does not require them. Internal insulation is used to reduce thermal shock at tanking and to reduce heat leaks and cryopumping potentials associated with external insulation. The basic structural external frames are increased in section modulus at the aft attach points to the orbiter and in the main landing gear and wing box attach link pickup points.

The tanks are joined by a cylindrical intertank section that supports the canard pivot and the forward attach links to the orbiter. The intertank section is shown in Figure 2-11.

The intertank section is a conventional skin-stringer-frame assembly with built-up frames to support the orbiter attach links and the canard pivot points. The LO<sub>2</sub>

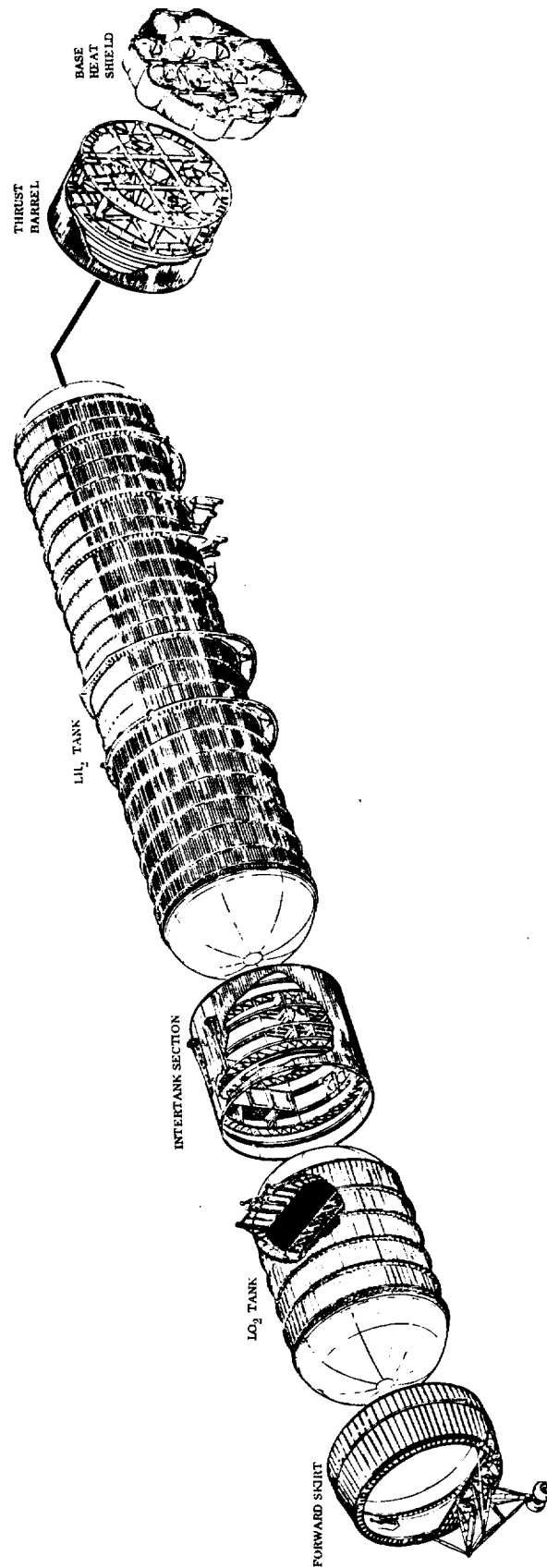


Figure 2-8. B-9U Booster Body Structure

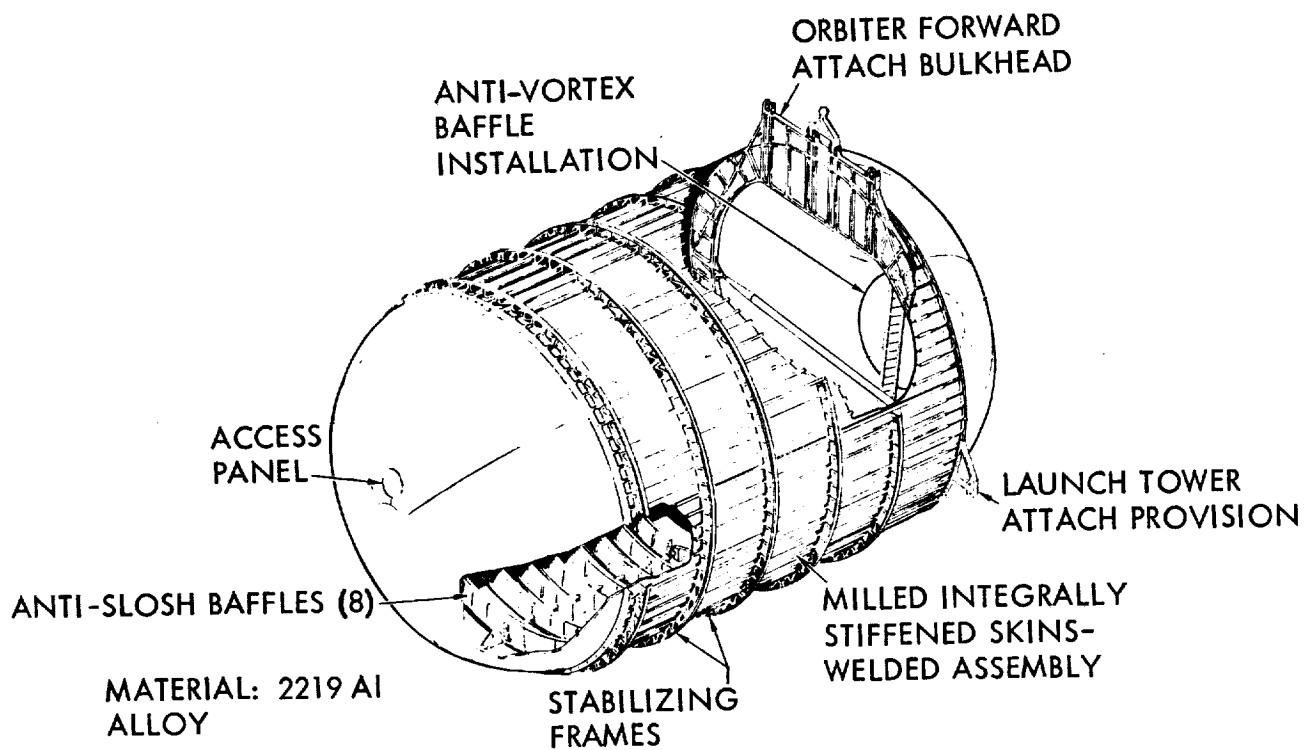


Figure 2-9. B-9U Liquid Oxygen Tank

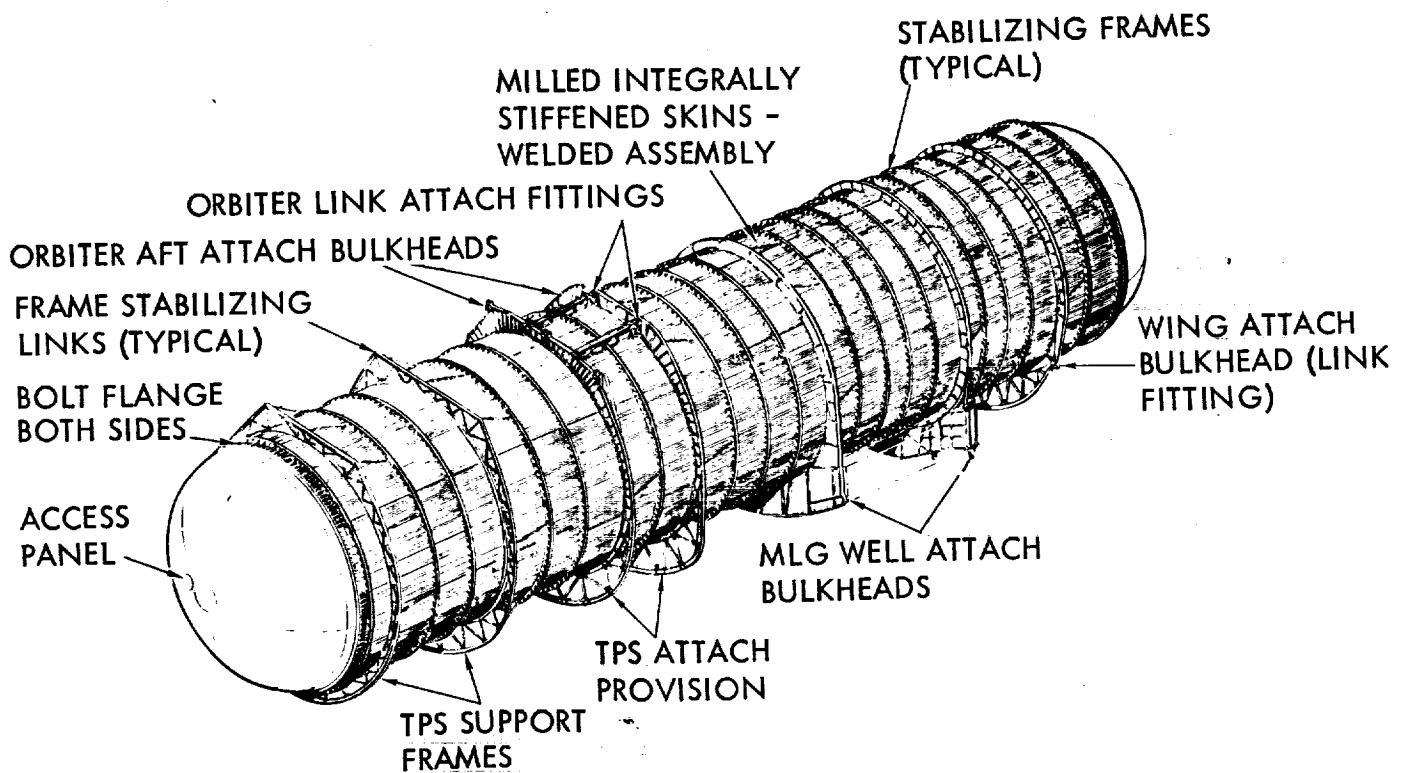


Figure 2-10. B-9U Liquid Hydrogen Tank



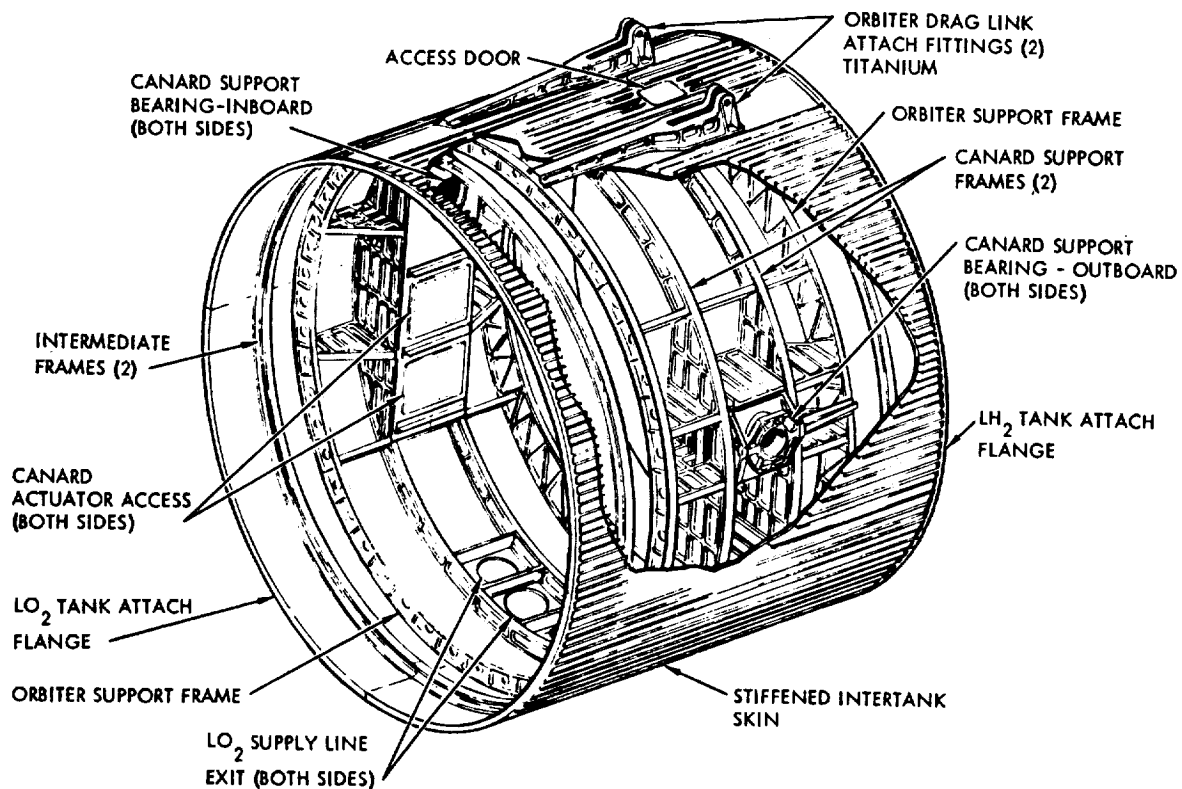


Figure 2-11. B-9U Intertank Section

lines run aft and occupy the lower intertank space. The canard pivot actuators are shown, four per side below the pivot point 50 inches above the body centerline. The intertank section contains the LH<sub>2</sub> and LO<sub>2</sub> tanks for the ACPS and auxiliary power unit (APU) supply. A single LH<sub>2</sub> tank for both systems is provided. The orbiter forward attach points are at the aft LO<sub>2</sub> dome/intertank joint and take the axial loads as well as pitch and side loads, while the aft attach points, which take pitch and sideloads only, are at Station 2666 in the LH<sub>2</sub> tank region (Section G-G of Figure 2-7.)

The top of the booster is flat in the stage interface region to fair out the attach frames of the booster and to accommodate the booster linkage after separation. The booster/orbiter separation system is a linkage type using booster thrust and orbiter inertia to produce positive separation. It is selected as the only system with the present configuration that will operate feasibly in the case of high dynamic pressure separation, as is required by abort criteria. The orbiter is arranged piggyback on the booster. This mating was initially done to allow rollout of the mated configuration to the launch pad on the booster main gear.

The aft end of the LH<sub>2</sub> tank picks up the cylindrical thrust skirt, which is also 33 feet in diameter and includes truss-type thrust beams that intersect to form the main engine thrust pad/gimbal support points. The thrust structure is a structurally connected titanium truss beam assembly with intersecting parallel vertical and horizontal beams, as shown in Figure 2-12. The beam intersections support the gimbal pad

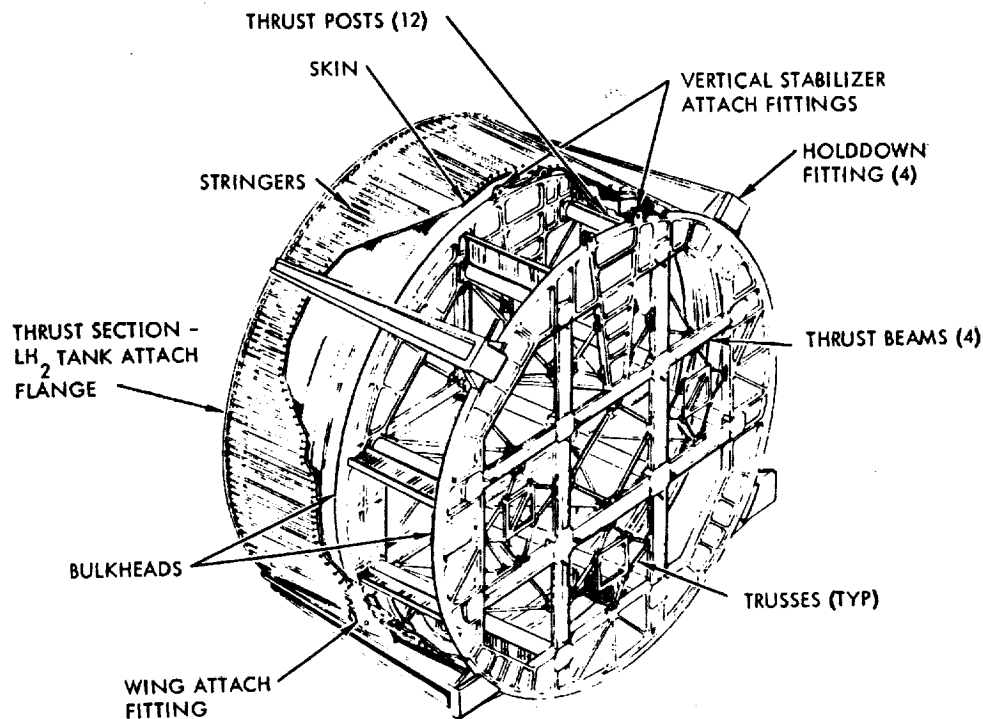


Figure 2-12. B-9U Thrust Structure

points. The beams are constrained by peripheral frames that transfer the loads into the cylindrical thrust skirt. The  $\text{LH}_2$  tank exits via a vortex baffle into a sump that branches into 12 fuel ducts to each engine. The engines have a fixed, low-pressure pump attached to the booster structure and a high-pressure pump on the engine. This arrangement allows the feed lines traversing the gimbal point to be of reduced diameter, eliminating the need for heavy pressure volume compensating ducts, and facilitating gimbaling to the required  $\pm 10$  degrees. The four  $\text{LO}_2$  lines branch at the aft end of the booster into three lines each to serve the 12 engines. The engine propellant inlets and thrust structure are arranged for acceptable clearance in the selected pattern. The  $\text{LO}_2$  lines are designed to have equal lengths from tank exit to pump inlet to minimize residuals. Each individual propellant feed line has a prevalue for a total of 12 for  $\text{LO}_2$  and 12 for  $\text{LH}_2$ .

The aft skirt that flares out for the rocket pump packages is an extension of the thermal protection system (TPS). The fairing is pocketed to accommodate the four support and hold-down longerons that transmit their axial load directly into the thrust barrel. The external skirt that protects the thrust structure and engine pump packages from thermal and aerodynamic loads is shaped to minimize booster base area as is seen in view M-M of Figure 2-7. The base heat shield consists of corrugated sheet with internal insulation. The heat shield is located in a plane through the nozzle throats of the main engines. Each engine has a spherical radius collar at the throat that wipes a matching hole in the heat shield to allow gimbal motion while maintaining a seal.

The base heat shield is penetrated by fill-and-drain lines and pressurization-and-purge lines. Electrical and other service disconnects are located as shown. The JP tank will be pressure fueled via a single point in the upper surface of the wing root.

The forward end of the LO<sub>2</sub> tank supports a tapered skirt that terminates in a bulkhead that supports the nose landing gear. The main landing gear is supported from trunnion points on external frames attached to the LH<sub>2</sub> tank. As shown in Figure 2-7, the main gear retracts forward into the wing root fillet region. The main gear bogies incorporate 60 x 20 inch 40 PR tires. The nose gear has dual 47 x 18 inch tires.

The outer heat shield provides an aerodynamic surface for the body which varies from a circular cross-section at the nose gear station to a gradually flattening lower surface transitioning into the wing fillet. The heat shield is primarily of shallow corrugated frame stiffened panels utilizing Rene '41 alloy principally, and titanium alloy in the regions of lower aerodynamic heating. The heat shield is supported via links from the primary structure to allow for expansion. The forebody ahead of Station 1479 is supported as an extension of the heat shield itself and moves with it, except for the nose gear that, as previously explained, is supported from an extension skirt on the primary load-carrying LO<sub>2</sub> tank. The body heat shield frames are on 20-inch centers below the body maximum breadth and on 40-inch centers above it.

The delta wing is mounted below the LH<sub>2</sub> tank. The wing carrythrough spars are tapered in the center section to allow the wing to overlap the tank in the side view and thus minimize base area. The wing attaches to the hydrogen tank frames and to the thrust structure via a series of links designed to take out relative expansion differentials between the wing and the body. See Figure 2-7. A low wing is selected principally to reduce the entry reradiation wing/body intersection temperature increase effects in a high wing arrangement. The low wing/fillet arrangement also provides main landing gear stowage space.

The wing is located aft for balance purposes. Because of the large weight of boost engines it is necessary to move the aerodynamic center aft to accommodate the aft cg in a balanced configuration. A low aspect ratio delta wing of 53-degree sweep is selected to provide minimum flyback system weight, within the constraints of satisfactory stability characteristics and landing speed. The delta wing also allows sufficient thickness to stow the flyback engines internally, which is particularly desirable since the shock impingement of lower surface nacelles creates excessively high temperatures. The high-sweep delta wing tends to minimize both heating and boost drag (also reduced with retracted flyback engines) and promises better transonic characteristics.

Figure 2-13 shows the general arrangement of the delta wing. The wing is spliced at span Station 507.5 to allow disassembly for shipping. Five ACPS engines are located next to the rear spar.

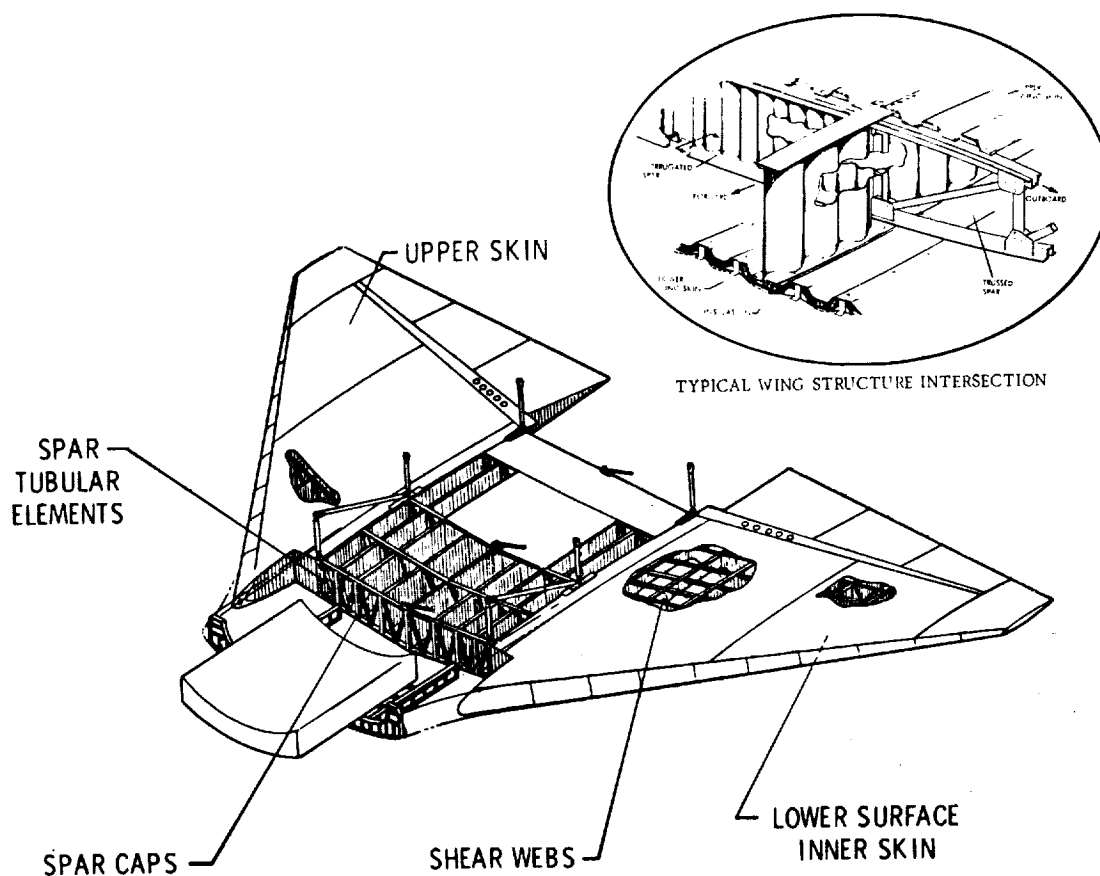


Figure 2-13. B-9U Wing General Arrangement

The delta wing has a theoretical area of 8451 square feet and an exposed area of 5047 square feet installed at +2-degree angle of incidence to the body centerline to facilitate cruise and to reduce landing angle within the constraints of the boost loads on the wing. The leading edge sweep is 53 degrees. The installation of the JTF22A-4 air-breathing engines in the wing requires a maximum thickness chord ratio of 10.3 percent at wing Station 507.5 just outboard of the outboard engine. Installation of these engines below the body in the center section requires a 7.1-percent theoretical root thickness at the vehicle centerline. The airfoils are NASA four digit series with modifications to the leading edge radii and with conical camber at the tips to improve L/D. The trailing edge of the wing is perpendicular to the body centerline with elevons segmented into three spanwise parts for varying degrees of control. The wing structure is primarily titanium alloy with two main structural boxes. The forward box accommodates the air-breathing engines. The lower surface of the wing is thermally protected by a system of dynaflex insulation with metallic radiation cover panels.

Flyback engines are selected from among off-the-shelf candidates. The JTF22A-4 is the lowest bypass ratio candidate and presents the smallest package for installation. This condition permits low wing thickness-to-chord ratio ( $t/c$ ) thus minimizing potential control problems during transonic passage at the end of entry. Overall system

weight differences between the JTF22A-4 and the F101 (higher bypass ratio engine) are small, the savings in fuel being offset by the increase in engine and installation weight and increased cruise drag effects. The air-breathing engines are installed in podded configurations, pivoted at the aft support point. Each engine assembly has its own deployment rotary actuators. Longitudinal doors in the lower surface open to allow deployment of the air-breathing engines to the subsonic cruise position. The engines rotate through 180 degrees to the locked-extended position. Upon engine deployment the engine bay doors close to present a clean surface for cruise and landing. See Figure 2-14.

The JP flyback fuel is currently stowed in a single tank on the booster centerline, near the center of gravity. While no fuel transfer is currently anticipated in the B-9U configuration for balance purposes, JP fuel presents an advantage in this respect for configurations having a closely coupled hypersonic/subsonic relationship requiring fuel transfer for cg control. The fuel is fed to the four engines under the body at Station 3560 and to the four engines in each wing.

The fully pivoting canard is selected as a trim and control device and as an adjunct to rotation for takeoff on ferry flights. The canard is located as far forward of the wing as feasible to increase control effectiveness. Use of the canard allows reduction in wing area and elevon size and permits the use of wing high-lift devices at landing and for cruise improvements in the typical high drag booster configuration. The canard

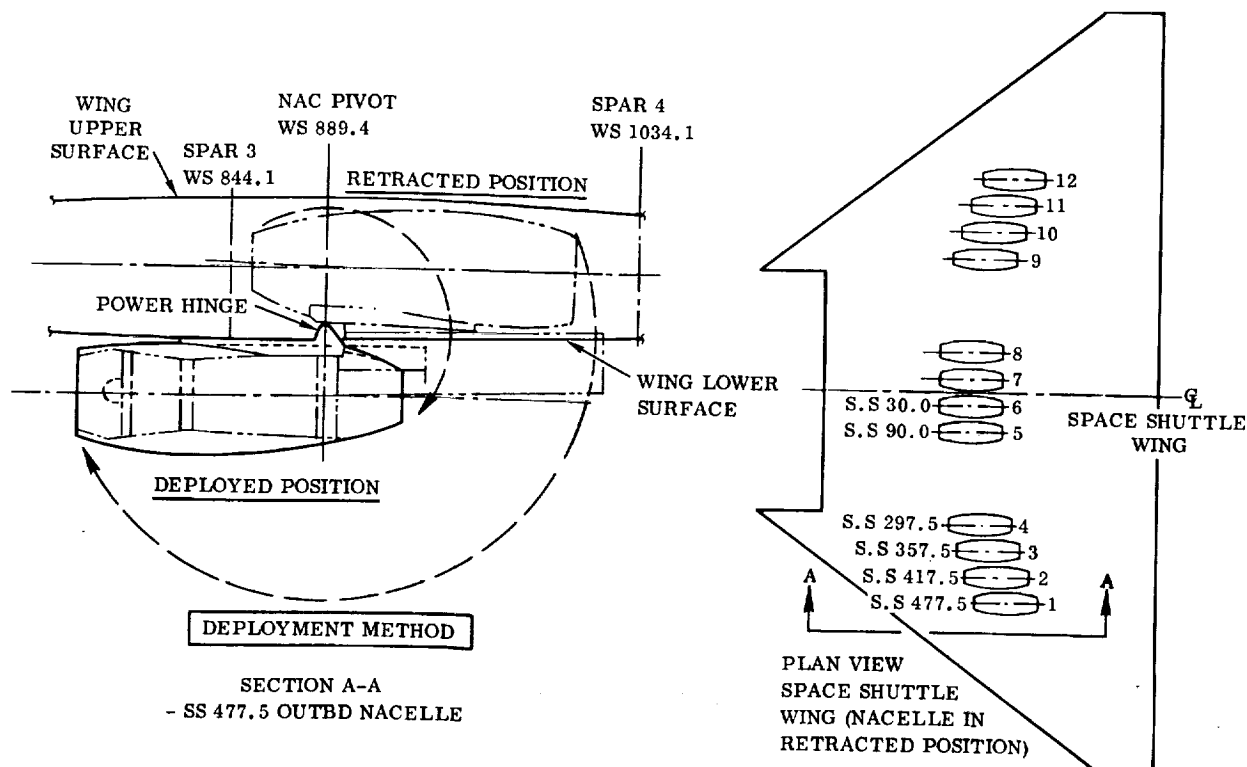


Figure 2-14. B-9U Nacelle Location, Retracted and Deployed Positions

provides a total exposed area of 540 square feet. The leading edge sweep is 60 degrees and the thickness is 14 percent. The entire surface is pivoted at 56 percent of the root chord and moves 65 degrees nose down to decouple the effect of the surface during hypersonic entry. The surface wipes a body fairing to maintain a seal at all points along the down travel. This seal is to minimize entry heating. Upward travel of the leading edge of the canard is 30 degrees.

The vertical tail is on the centerline of the body to minimize weight relative to tip fins that weigh more in themselves and impose an added weight to the outboard wing sections due to maximum boost  $\beta q$  loads and the attach complexity. Directional stability is maintained in the booster during reentry in the high-angle-of-attack mode by using the ACPS yaw engines. Even after the heat sink leading edge and the extra ACPS weights were incorporated, a centerline vertical still showed the least overall system weight. The general configuration of the vertical tail structure is shown in Figure 2-15.

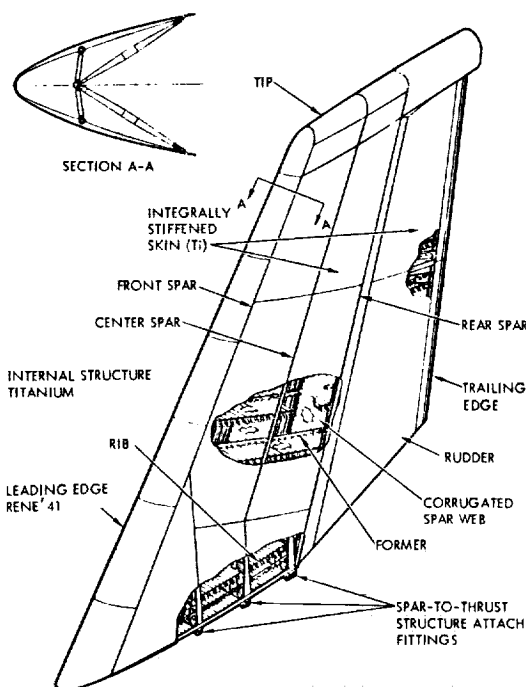


Figure 2-15. B-9U Vertical Tail Structure

The vertical stabilizer has an area of 1500 square feet with a leading edge sweep of 35 degrees to provide orbiter separation clearance consistent with weight and aerodynamic considerations. The tail thickness varies from 13 percent at the root to 11 percent at the tip. A 35-percent chord rudder is provided with  $\pm 25$  degrees of travel. The base of the rudder is cut off at 15 degrees to provide plume clearance for the upper rocket engines. Vent and exhaust lines are terminated at the fin tip trailing edge. The leading edge of the vertical tail has increased material thickness to act as a heat sink during the brief period of plume impingement during orbiter separation.

The crew module is conventionally located in the nose structure (see Figure 2-5). Swivel seats adjustable for the vertical flight, entry, and cruise flight are pro-

vided in conventional locations for captain and co-pilot. The crew module is pressurized for shirtsleeve environment. Heat shields are provided over the windshields, which are sized for adequate landing visibility at the maximum 15-degree touchdown angle. Access with the booster in the vertical position is via a door to the left of the pilot seat. Access with the booster in the horizontal position is via a door in the compartment floor reached through the nose-gear wheel well. Immediately behind the crew is space for an additional jump seat available for horizontal flight test or

checkout purposes. Aft of the crew compartment are the booster avionics systems installed in a controlled environment but separate from the crew compartment. Below the crew and avionics compartments is the nose-gear wheel well.

Figure 2-16 shows the general arrangement of the crew module. It is a semi-monocoque structure incorporating frames and longitudinal stringers. Where space between the module and the nose shell structure permits, structure is installed on the exterior side of the skin. There are four openings in the structure: the windshield, the aft compartment access hatch, and two hatches opposite the pilots' seats. The module consists of two compartments, the pilots' station and the electronics compartment. These compartments are separated by an internal bulkhead. The aft end of the module is closed by an ellipsoidal bulkhead. The electronics compartment is cylindrical in section while the crew compartment is faired to maintain as much curvature as is compatible with the hot nose structure contour and internal furnishing envelope.

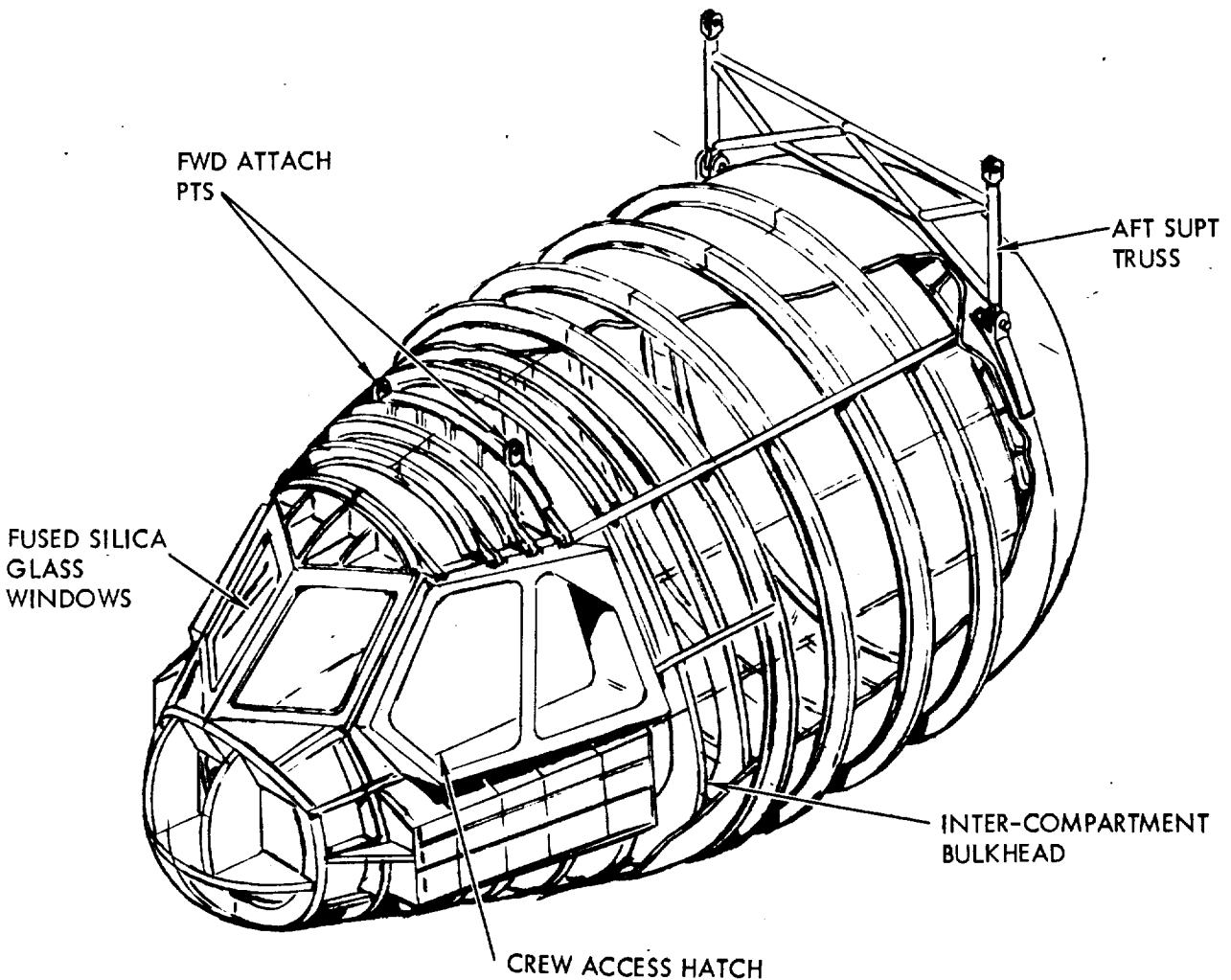


Figure 2-16. B-9U Crew Module

The crew module is supported by the nose structure at four points: at two points just aft of the crew compartment and at two points on the frame at the end of the electronics compartment. The gap between the nose structure and the crew compartment at the aft support is spanned by a pin-ended truss. This truss minimizes thermal loads on both the nose structure and the module structure as the outer shell expands.

The Environmental Control Life Support System (ECLSS) provides thermal and pressure control for equipment and personnel. The ECLSS also provides a shirt-sleeve environment for the crew and maintains atmospheric constituents within acceptable physiological limits. The following summarizes the operation of the ECLSS during various phases of the mission.

Prelaunch. During prelaunch operations, cooling is accomplished by supplying conditioned air from GSE to one of the air supply ducts through a rise-off disconnect. This air is then distributed to the flight deck and equipment bay. The airflow is exhausted through the outflow valves into the area between the liquid oxygen tank and the nose structure. This area is being purged with GN<sub>2</sub> and, therefore, the pressure in the crew module will be 15 psia which is higher than the purge area pressure which is in turn higher than the ambient pressure. At lift-off, blowers mounted in both the flight deck and equipment compartment are turned on and air is recirculated to provide continued cooling.

Boost. During boost, the cabin pressure regulator is closed and the module pressure decays because of leakage. Since it isn't possible to determine what the leakage rate will be, it is assumed for purposes of structural analysis that the internal cabin pressure remains at 15 psia throughout the mission. Cooling is maintained by recirculating air in the individual compartments which transfers personnel and equipment heat to structure and furnishings.

Reentry. Operation is continued as in the boost phase. The outflow valves remain closed and cabin pressure continues to decrease due to leakage. As decent continues, the outflow valve negative relief function prevents the module from becoming more than two to three inches of water negative with respect to ambient pressure. During this period, the thermal capacity of the system and the surrounding structure will limit temperature rise to an acceptable level. Because of the short time of closed-loop operation, the only life support needs are temperature and pressure control.

Flyback. After the cruise engines have been started, the air-cycle refrigeration system is used to provide cooling and cabin pressure control.

Post-Landing. Operation continues as during flyback until the cruise engines are shut down.



## 2.3 BOOSTER STRUCTURAL MATERIALS

Materials for the space shuttle booster structure fall into several categories: (1) aluminum alloys, (2) beryllium alloys, (3) titanium alloys, (4) nickel base alloys, (5) cobalt base alloys, (6) columbium alloys, and (7) composite materials. Primary candidate materials have been selected on existing properties data or data generated under space shuttle studies. To provide an efficient final design, the properties of some of these materials must be investigated to determine their allowable properties after exposure to the expected environments. Table 2-2 lists the primary structural materials for the B-9U major structural components selected for detailed study.

The wing box is primarily fabricated from titanium with a thermal limit of 800° F. Titanium was selected due to its high specific modulus and strength and low thermal stress index at 650° F. Titanium has well defined mechanical and physical properties and the fabrication, machining, and welding techniques are well known.

The basic structural concept of the wing is based on the use of a metallic standoff heat shield combined with insulation between the shield and the wing lower surface structure to provide thermal protection for the whole wing structure except for the hot leading edge. This allows efficient use of titanium for all of the primary and secondary structure above the TPS while the TPS shield itself can be made of HS188 and coated columbium. The Haynes 188 material is thermally limited to about 1900° F and the coated columbium to 2500° F. Both these materials were selected for their thermal strength properties.

The vertical stabilizer structural arrangement is a three-spar, multi-rib configuration with integrally stiffened skin/stringer panels. Spar and rib webs are of corrugated or trussed construction to allow for differential thermal expansion. The rudder is of similar construction. The entire structure is titanium except for the leading edge which is Inconel 718. The segment of leading edge that is subjected to the orbiter engine exhaust impingement is "heat sink" designed to withstand the increased temperature. Again titanium is selected due to its strength at temperatures that preclude aluminum, and its adaptability to a variety of proven fabrication techniques.

The crew module is constructed of 2219-T87 aluminum alloy except in those areas where the hot nose structure is in close proximity to the module structure. In these regions, such as the windshield frame and the pilots' hatches, the structure is fabricated from annealed 6Al-4V titanium alloy. With the exception of the glazed areas, the entire compartment is shrouded by a fibrous insulation blanket. The inner door windows are fabricated from heat tempered glass. The outer door windows are made from fused silica glass. The windshield is a laminated glass with an electrically conductive film for anti-icing. The floor and the bulkhead separating the electronics compartment from the crew station consist of aluminum alloy honeycomb panels backed up by a grid work of beams.

Table 2-2. Booster Materials

Booster Components	Sub-Components	Materials
Wing Box	Spar Caps	Annealed Titanium (6Al-4V)
	Spar Webs	Annealed Titanium (6Al-4V)
	Rib Caps	Annealed Titanium (6Al-4V)
	Rib Webs	Annealed Titanium (6Al-4V)
	Intercostals	Annealed Titanium (6Al-4V)
	Lower Surface Thermal Skins	Haynes HS-188/Coated Columbium
	Upper & Lower Structural Skins	Annealed Titanium
	Trusses	Annealed Titanium
	Fasteners	Conventional Except for Lower Thermal Skin
Vertical Tail Box	Spar Caps	Annealed Titanium (6Al-4V)
	Spar Webs	Annealed Titanium (6Al-4V)
	Ribs and Bulkhead Caps	Annealed Titanium (6Al-4V)
	Ribs and Bulkhead Webs	Annealed Titanium (6Al-4V)
	Integrally Stiffened Skins	Annealed Titanium (6Al-4V)
	Stiffeners	Annealed Titanium (6Al-4V)
	Fasteners	Conventional
LO <sub>2</sub> Tank	Integrally Stiffened Skins	Aluminum Alloy 2219-T87
	Frame Caps	Aluminum Alloy 2219-T87
	Frame Webs	Aluminum Alloy 2219-T87
	Bulkheads (Dome)	Aluminum Alloy 2219-T87
	Fasteners	Conventional
LH <sub>2</sub> Tank	Note LO <sub>2</sub> Tank	Same as LO <sub>2</sub> Tank Except for Polyphenylene Oxide Insulation
Orbiter Support Bulkhead	Beam Caps	Aluminum Alloy 2219-T87
	Beam Web	Aluminum Alloy 2219-T87
	Bulkhead Caps	Aluminum Alloy 2219-T87
	Bulkhead Webs	Aluminum Alloy 2219-T87
	Fasteners	Conventional
Thrust Structure	Skins	Annealed Titanium (6Al-4V)
	Thrust Beams	Annealed Titanium (6Al-4V)
	Thrust Posts	Annealed Titanium (6Al-4V)
	Bulkheads	Annealed Titanium (6Al-4V)
	Vertical Stabilizer Attach Fittings	Annealed Titanium (6Al-4V)
	Intermediate Frames	Annealed Titanium (6Al-4V)
	Attachment Flange	Annealed Titanium (6Al-4V)
	Fasteners	Conventional
	Base Heat Shield	René 41 & coated Columbium
Crew Module	Skin	Aluminum Alloy 2219-T87
	Frames	Aluminum Alloy 2219-T87
	Longerons	Aluminum Alloy 2219-T87
	Bulkheads	Aluminum Alloy 2219-T87
	Hatches	Annealed Titanium (6Al-4V)
	Windshield frame	Annealed Titanium (6Al-4V)

The main LO<sub>2</sub> and LH<sub>2</sub> fuel tanks are fabricated almost entirely of 2219 aluminum. Both 2219 and 2014 aluminum alloys were considered for the main tanks and other body structures. Both alloys possess excellent strength-toughness properties in the base metal at all temperatures down to -423° F, with the 2014 alloy being somewhat stronger than 2219. However, welded joints in the 2014 alloy exhibit a tendency towards brittle fracture and greater sensitivity to minor weld flaws at liquid oxygen to liquid hydrogen temperatures. The significantly greater resistance to stress corrosion possessed by the 2219 alloy has been thoroughly demonstrated, as has its superior weldability and weld repairability. The combination of better fracture toughness in welded joints at reduced temperatures and superior resistance to stress corrosion result in a significantly higher reliability for the 2219 alloy as compared to 2014.

Both 2219 and 2014 exhibit a decrease in strength properties as the plate thickness increases. Both the ultimate and the yield tensile strengths of 2014 decrease with increasing thickness at a greater rate than does the yield strength of 2219. Consequently, if the tank walls must be machined from 3 to 4 inch plate in order to accommodate integral stiffeners or weld lands, the strength advantage of 2014 is minimized.

Although 2014 shows an advantage in strength of the base metal, Convair Aerospace's choice of the 2219 aluminum alloy for the space shuttle propellant tankage is based upon its superior weldability, much better resistance to stress corrosion cracking, better overall toughness, and better reliability for the reusable manned space launch vehicle.

Table 2-3. B-9U Weight Summary

	Weight (lb)
Wing Group	59,063
Tail Group	17,908
Body	174,229
Induced environment, protection	86,024
Landing, recovery, dock	28,457
Propulsion-ascent	124,786
Propulsion-cruise	49,513
Propulsion-auxiliary	12,126
Prime power	1,930
Electrical	1,682
Hydraulics	2,201
Surface controls	9,620
Avionics	5,582
Environmental control	1,648
Personnel provisions	1,636
Contingency	50,705
Dry weight	627,110
Personnel	476
Residual fluids	11,503
Inert weight	639,089
Inflight losses	21,718
Propellant-ascent	3,382,307
Propellant-cruise	143,786
Propellant-ACS	1,500
Gross weight	4,188,400

## 2.4 BOOSTER WEIGHT SUMMARY

Table 2-3 is a summary weight statement for the B-9U booster in the launch condition. This launch condition is for the mission described in Section 2.1, and assumes that the orbiter launch weight will be about 859,000 pounds. In Table 2-3, weights are broken down to show individual major system weights. The weights were taken from Reference 6.

A more detailed breakdown of the weight of the major structural components chosen for study is given in Table 2-4.

Table 2-5 gives the booster mass properties sequence during the mission detailed in Section 2.1. Changes in weight, center of gravity, moment of inertia, and product of inertia are given.

Table 2-4. B-9U Component Structural Weight Breakdown

Description	Weight (lb)	Subtotal (lb)	Total (lb)
Wing Group		43,103	59,063
Box*			
Spar Caps, Upper	6,105.3		
Spar Caps, Lower	5,685.0		
Rib Caps, Upper	1,345.6		
Rib Caps, Lower	1,312.7		
Upper Cover	4,256.9		
Lower Cover	6,802.6		
Inner Spar Webs and Trusses	6,287.8		
Inner Ribs and Webs	7,248.4		
Miscellaneous	4,059.2		
Wing-Fuselage Attach Fittings and Links		1,056.8	
Leading Edge, Trailing Edge and Tips		3,825.7	
Secondary Structure		5,149.8	
Control Surfaces		5,926.9	
			17,908
Tail Group		4,629	
Canard		8,779	
Vertical Tail Box*			
Spar Caps	692.7		
Cover	4,168.0		
Spar Webs and Stiffeners	1,161.3		
Miscellaneous	705.0		
Vertical Tail Leading Edge, Trailing Edge and Tips		2,371	
Rudders		2,129	
			174,229
Body Group		67,645	
LH <sub>2</sub> Tank *			
Skin Panels	52,486		
Frames	2,966		
Forward Dome Assembly	2,483		
Aft Dome Assembly	2,468		
TPS Support Frames	1,201		
Orbiter Support Structure	5,754		
Miscellaneous	287		
LH <sub>2</sub> Tank Insulation		9,168	
LO <sub>2</sub> Tank*		15,127	
Skin Panels	7,090		
Frames	405		
Forward Dome Assembly	1,715		
Aft Dome Assembly	2,998		
Miscellaneous	2,919		
Forward Orbiter Support Structure		2,616	
Nose		9,598	
Forward Skirt Structure		3,652	
Intertank Structure		16,500	
Thrust Structure*		25,067	
Skin Panels	7,180		
Frames	1,721		
Thrust Beams	4,874		
Thrust Posts	1,134		
Ground Fittings	3,992		
Bulkheads	4,400		
Miscellaneous	1,766		
Crew Module		1,976.6	
Skin*	610		
Bulkhead and Frames*	271.6		
Longerons	36		
Doors	446		
Floor	194		
Windshield	145		
Miscellaneous	274		
Base Heat Shield		7,496	
Interstage Mechanism		4,603	
Main Landing Gear Provision		12,780	
			86,024
Thermal Protection System			

\* Component selected for study.

Table 2-5. Sequence Mass Properties Statement, B-9U Booster

Mission Event	Weight (lb)	Center of Gravity (inches)			Moment of Inertia (slug-ft <sup>2</sup> × 10 <sup>6</sup> )			Product of Inertia (slug-ft <sup>2</sup> × 10 <sup>6</sup> )		
		X	Y	Z	I <sub>x-x</sub>	I <sub>y-y</sub>	I <sub>z-z</sub>	I <sub>xy</sub>	I <sub>xz</sub>	I <sub>yz</sub>
Liftoff	4,188,400	2,163	0	392	13.160	549.200	549.300	0	-10.200	0
Prop to max q	-1,320,000									
Max q	2,868,400	2,389	0	388	12.370	404.700	404.800	0	- 8.490	0
Prop to 3-g	-1,320,000									
3-g	1,548,400	2,771	0	378	11.200	232.400	232.500	0	- 5.650	0
Prop to burnout	- 736,547									
Thrust decay prop	-3,340									
Burnout (entry)	808,513	3,167	0	333	8.782	102.000	102.700	0	- 1.380	0
Inflight losses	-18,332									
ACPS props	-3,450									
Start cruise	786,731	3,151	0	332	8.715	100.200	101.000	0	- 1.530	0
APU propellants	-4,218									
Flyback fuel (JP)	-143,786									
Landing (gear down)	638,727	3,166	0	353	8.386	99.710	100.400	0	- 2.000	0

## 2.5 DESIGN CRITERIA

The booster vehicle is designed to provide adequate structural strength for a safe-life of 100 missions, or for a ten year life, without the need for major repairs. This design is capable of withstanding the service life of flight and pressure loads combined with the thermal and acoustic environment. Booster structure is designed for minimum weight commensurate with overall costs and the vehicle is designed to minimize post-flight inspection requirements for rapid turnaround.

Structural components are designed to provide the yield and ultimate factors of safety and proof factors shown in Table 2-6. Service life factors (scatter factors) are given in Table 2-7, and safe-life design environments are presented in Table 2-8.

The LO<sub>2</sub> tank is designed to be proof-tested in segments because of weight savings, using a three-phase proof test. The entire LH<sub>2</sub> tank is designed to be pneumatically proof-tested at room temperature. The thermal protection system (TPS) structure is also designed for the load factors in Table 2-6, as applicable. In addition, an allowable creep strain of 0.2 percent per 10 hours exposure at maximum temperature will be used, and for corrugated panels in the transverse direction, 1.0 percent creep strain per 10 hours exposure at maximum temperature. A minimum clearance of 1.0 inch between the inner tank structure and the outer TPS structure will be maintained at limit load.

The booster is designed to withstand the repeated loads (fatigue) incurred in 400 flights without failure, including a scatter factor of four. Consideration will be given to the effects of acoustic fatigue loads. The booster will withstand the mission thermal environments with a minimum of post-flight inspection and subsequent structural refurbishment and/or replacement.

The primary structural components will be designed fail-safe insofar as practical, considering weight, cost, and manufacturing. When primary structure fail-safe design is not practical, a safe-life design concept will be applied. The primary structure includes the wing box, tanks, fin box, thrust structure, major bulkheads, intertank adapter, and similar major load-carrying structural components or elements such as spar caps and wing/body attach links.

Safe-life designs will be compatible with latest NDI (nondestructive inspection) techniques and limitations and residual strength and crack propagation analyses will be used to ensure that adequate safe-life has been provided. The booster is designed to provide a safe-life of 150 missions, including a scatter factor of 1.5.

Conventional strength, fail-safe, and fatigue analyses will be supplemented by fracture mechanics analysis to determine critical flaw sizes and residual life assuming pre-existing flaws.

Table 2-6. Design Criteria

Component	Yield	Ultimate	Proof	Applied On
Main Propellant Tanks	1.10	1.40	*	Maximum relief valve pressure only
	1.10	1.40	—	Loads (+ limit pressure)
	1.00	—	—	Proof pressures
Personnel Compartments	1.10	1.50	—	Loads (+ limit pressure)
	1.50	2.00	1.50	Maximum operating pressure only
Windows, Doors, Hatches	1.00	—	—	Proof pressure
Airframe Structure	—	3.00	2.00	Maximum operating pressure only
	1.10	1.40	—	Boost + entry loads
	1.10	1.50	—	Aircraft mode loads
Pressure Vessels	—	2.00	1.50	Maximum operating pressure
Pressurized Lines Fittings	—	2.50	1.50	Maximum operating pressure
All Components (Abort Conditions)	1.10	1.40	—	Abort loads (+ limit pressure)
All Components (Thermal Stresses)	1.00	1.00	—	Thermal forces (+ flight loads)
	1.00	1.25	—	Thermal forces (alone)
LO <sub>2</sub> Tank			1.23	Max. relief valve pressure
LH <sub>2</sub> Tank			1.13	Max. relief valve pressure

\* Based on fracture mechanics analysis  
Assumed service life = 100 missions

Table 2-7. Service Life Factors

Item	Factor	Applied On
Fatigue initiation	4.0	Design service life
Flaw growth to leak	1.5	Design service life
Flaw growth to failure	1.5	Design service life
Creep	4.0 and 2.0	Accumulated creep strain

Note: Design service life = 100 missions and 10 years of operation.

Table 2-8. Safe-Life Design Environments

Component	Design Environment
LO <sub>2</sub> Tank	LO <sub>2</sub> @ -320° F or GO <sub>2</sub> @ 70° F
LH <sub>2</sub> Tank	Air at 70° F
Intertank Adapter	Air at 70° F
TPS, Wing, Canard	
Empennage, Thrust Structure, and Orbiter Attachments	3-1/2% salt solution with alternate drying

## 2.6 DESIGN CONDITIONS

Booster design conditions were generated from ground handling procedures and from mission flight characteristics. The flight conditions investigated include: launch, ascent, entry, subsonic cruise, and horizontal takeoff and landing. Effects of Mach number, angle of attack, and control surface deflections on longitudinal and lateral directional characteristics were also included. The ground conditions investigated were taxi, towing, mating, and launch preparation and erection.

In most instances, the aerodynamic data was based on available experimental data adjusted for differences between tested and current configuration.

Table 2-9 summarizes limit flight loads and design load factors for a number of the critical mission conditions. Maximum loads on the body, wing, and canard occur during maximum  $g$  recovery (i. e. , entry), while maximum  $\beta q$  during ascent yields the greatest load on the vertical stabilizer. Critical design conditions and considerations for aerodynamic surfaces are summarized in Table 2-10.

Internal loads consisting of axial and shear loads and bending and torsion moments were determined at 48 stations along the body length for 25 load conditions. The conditions investigated are:

1. One-hour ground headwinds, fueled, unpressurized
2. One-hour ground tailwinds, fueled, unpressurized
3. One-hour ground sidewind, fueled, unpressurized
4. Liftoff + 1-hour ground headwinds
5. Liftoff + 1-hour ground tailwinds
6. Liftoff + 1-hour ground sidewinds
7. Maximum  $\alpha q$  headwinds
8. Maximum  $\alpha q$  tailwinds
9. Maximum  $\beta q$
10. Three-g maximum thrust
11. Booster burn-out
12. Maximum  $g$  entry
13. Subsonic gust
14. Two-point landing
15. Three-point landing



Table 2-9. Summary of Booster Design Conditions and Loads

Condition	Component (or Mass Item)	$n_x$	$n_y$	$n_z$	Limit Air Load (lb/panel)	Remarks
Two week standby		1.0				
One day hold		1.0				
One hour to launch		1.0				
Lift-off	(LO <sub>2</sub> mass)	1.31 ± 0.15				
	(LH <sub>2</sub> mass)	1.31 ± 0.25				
	(Orbiter & other)	1.31 ± 0.21				
Max. dynamic pressure						
Max $\alpha q$						
Headwind	Body	1.61	0	0.51	537,000	
	Wing	1.61	0	0.51	666,800	
	Canard	1.61	0	0.51	45,430	
Tailwind	Body	1.67	0	-0.19	-220,000	Provides, with booster burnout condition, critical loads for orbiter-booster attachment.
	Wing	1.67	0	-0.19	-98,600	
	Canard	1.67	0	-0.19	-45,360	
Max $\beta q$	Body	1.60	± 0.213	0.016	130,000	
	Wing	1.60	± 0.213	0.016	485,000	
	Canard	1.60	± 0.213	0.016	19,520	
	Vertical tail	1.60	± 0.213	0.016	±187,100	
Max. thrust	Body	3.3	0	0.242		Provides critical inertia loads for wing-to-body drag links, and together with max. $\alpha q$ condition, critical loads for orbiter-booster attachment.
	Wing	3.3	0	0.242		
	Canard	3.3	0	0.242		
Booster burnout	Body	3.3	0	0.343		
	Wing	3.3	0	0.343		
	Canard	3.3	0	0.343		
Max. g recovery	Body		0	4.0	1,507,000	
	Wing		0	4.0	808,600	
	Canard		0	4.0	0	
2.5g maneuver	Wing	0	0	2.5	617,600	
	Canard	0	0	2.5	71,370	
Rudder kick	Vertical tail				±204,000	
Subsonic gust	Body	0	0	2.1	488,000	
	Wing	0	0	2.1	591,500	
	Canard	0	0	2.1	-4,957	
	Vertical tail	0	0.5	1.0	±272,000	
Landing	Body	0	± 0.35	2.35	208,000	
	Wing	0	± 0.35	2.35	376,000	
	Canard	0	± 0.35	2.35	47,000	

16. Two-g taxi
17. One-day ground headwinds, fueled
18. One-day ground tailwinds, fueled
19. One-day ground sidewinds, fueled
20. Two-week ground headwinds, unfueled, unpressurized
21. Two-week ground tailwinds, unfueled, unpressurized
22. Two-week ground sidewinds, unfueled, unpressurized

Table 2-10. Summary of Design Conditions for Aerodynamic Surfaces

Structural Design Summary Chart		
Structural Component	Critical Condition	Design Considerations
<b>Wing:</b> Primary Sub-Structure Upper Skin Panels Lower Skin Panels TPS Heat Shield Elevon Sub-Structure Leading Edge	Max $\alpha q \sim$ Boost Liftoff Sound Pressure Max $g \sim$ Recovery Liftoff Sound Pressure Max $g \sim$ Recovery Max Heating $\sim$ Recovery	Wing Shear & Bending Sonic Fatigue Pressure & Temp Differential Sonic Fatigue Air Pressure Pressure & Temperature
<b>Wing/Body Attachment:</b> Fwd Vertical Attach Center Vertical Attach Aft Vertical Attach Drag Attach Fwd Side Load Attach Aft Side Load Attach Center Side Load Attach	Subsonic Gust $\sim$ Flyback Max $\alpha q \sim$ Boost Max $\alpha q \sim$ Boost Max Thrust $\sim$ Boost Max Thrust $\sim$ Boost Max Thrust $\sim$ Boost Taxi	Safe-Life Safe-Life Safe-Life Fail-Safe Fail-Safe Fail-Safe Fail-Safe
<b>Canard</b> Primary Substructure Torque Tube	Max $g \sim$ Recovery	Canard Structure & Torque Tube Shear, Bending, Torsion
<b>Vert. Tail</b> Primary Structure	Max $\beta q \sim$ Launch	Box Shear, Bending

23. 2.5 g positive maneuver

24. -1.0 g negative maneuver

25. Maximum operating pressure

An envelope of the resulting peak load intensities ( $N_x$ ) for the most critical conditions is shown in Figure 2-17, where  $N_x$  is the longitudinal axial load in the tank wall. The major loading conditions on the forward skirt are due to axial loads occurring during boost phase and shear loads during landing and taxiing conditions.

Proof pressures on the  $LO_2$  tank determine the skin gages of domes and the cylinder. Stiffening on the cylindrical body is required for flight and ground loads. The aft dome is grid-stiffened close to the equator because of compressive hoop loads occurring in the partially filled condition. External stiffening, consisting of tee stringers and trussed frames, was optimized for the low load intensities typical of the  $LO_2$  tank.

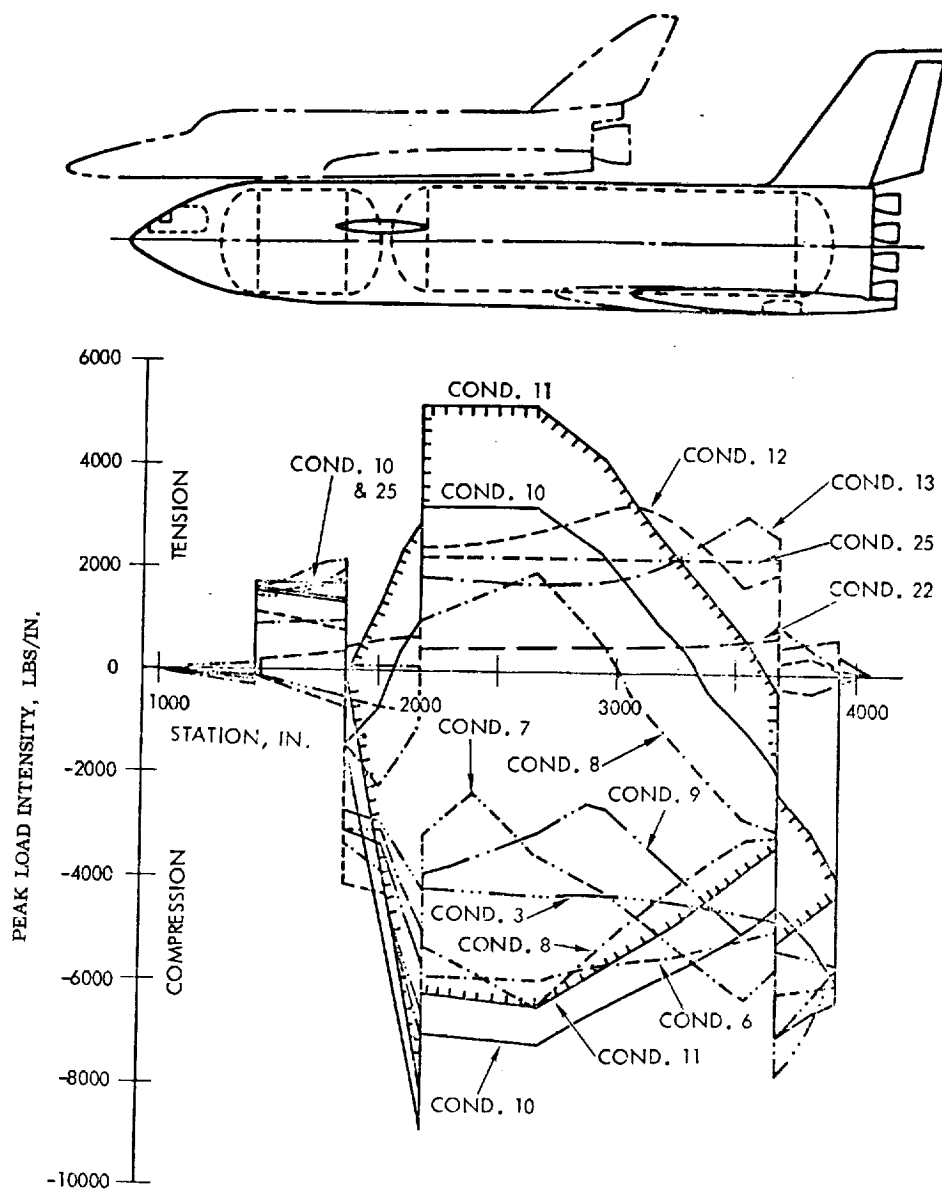


Figure 2-17. B-9U Booster Peak Limit Load Intensities

LH<sub>2</sub> tank skin gages of the domes and cylindrical section are determined by proof-test requirements at the forward end of the tank, and by ultimate shear and axial load plus pressure for flight conditions in the central and aft portions of the tank. Optimized tank stiffening in the form of tee stringers and external frames, critical for axial and bending loads occurring during ground winds and boost, is provided.

Critical design conditions for the intertank structure are derived from axial loads due to the LO<sub>2</sub> weight forward and the bending and axial load introduced at the forward attachment by the eccentric orbiter weight.

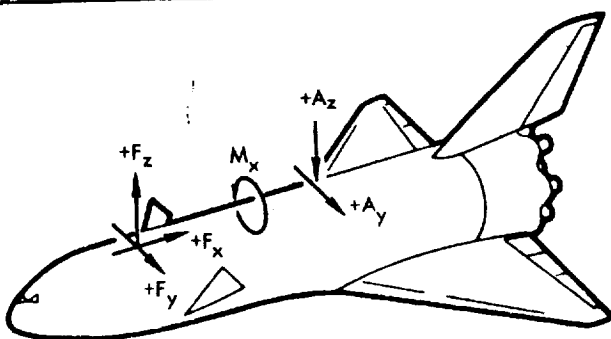
A total of 30 loading conditions on the thrust structure were investigated, including ground-wind, launch, and boost phase loads with and without engine-out conditions.

Ground-wind conditions are critical for hold-down fittings, back-up longerons, and adjacent skin on the skirt. Thrust beams, posts, frames, and skin away from hold-down longerons are critical for maximum  $\alpha q$  and 3g maximum thrust conditions with one engine out.

Table 2-11 summarizes the orbiter/booster interconnection loads, including loads for a number of critical conditions.

Net limit pressure (including dynamic head) versus tank station at various times during boost is shown in Figure 2-18 for the LH<sub>2</sub> tank. These pressures correspond to the upper bound of a 3 psi regulating band. Also shown is the pressure line for a pneumatic proof test, which requires a proof factor equal to 1.13 based on 150 missions.

Table 2-11. Booster/Orbiter Interconnection Loads



CONDITION	WIND	F <sub>x</sub> (KIPS)	F <sub>y</sub> (KIPS)	F <sub>z</sub> (KIPS)	A <sub>y</sub> (KIPS)	A <sub>z</sub> (KIPS)	M <sub>x</sub> (X 10 <sup>6</sup> IN-LB)
TWO-WEEK GROUND WINDS, UNFUELED, WITH TOWER SUPPORT	HEAD	268	0	56.9	0	-33.0	0
	TAIL	268	0	-119.0	0	149.0	0
	SIDE	268	±98.5	28.8	±30.2	34.9	±17.1
ONE-DAY GROUND WINDS, FUELED, WITH TOWER SUPPORT	HEAD	859	0	95.2	0	62.7	0
	TAIL	859	0	-0.1	0	161.0	0
	SIDE	859	±53.3	80.0	±16.3	99.5	±9.28
ONE-HOUR GROUND WINDS, FUELED, UNSUPPORTED	HEAD	859	0	89.5	0	76.5	0
	TAIL	859	0	30.0	0	138.0	0
	SIDE	859	±33.3	80.0	±10.2	99.5	±5.80
DYNAMIC LIFTOFF PLUS ONE-HOUR GROUND WINDS	HEAD	1296	0	119.0	0	134.0	0
	TAIL	1295	0	82.2	0	182.0	0
	SIDE	1296	±20.5	121.0	±2.92	150.0	±4.14
MAX $\alpha$ -q $\alpha$ -q = 2800 $\alpha$ -q = -2800	HEAD	1798	0	224.8	0	234.8	0
	TAIL	1804	0	83.0	0	950.3	0
	NO WIND	1808	0	137.4	0	625.6	0
MAX $\beta$ -q    ±2400	SIDE	1802	±81.2	128.8	±166.8	653.7	±72.3
3g MAX THRUST							
		2849	0	135.2	0	424.5	0
		2849	±55.4	179.3	±30.7	394.5	±7.6
BOOSTER BURNOUT							
		2841	0	62.9	0	459.0	0
		2841	±55.4	118.3	±30.7	428.0	±7.6

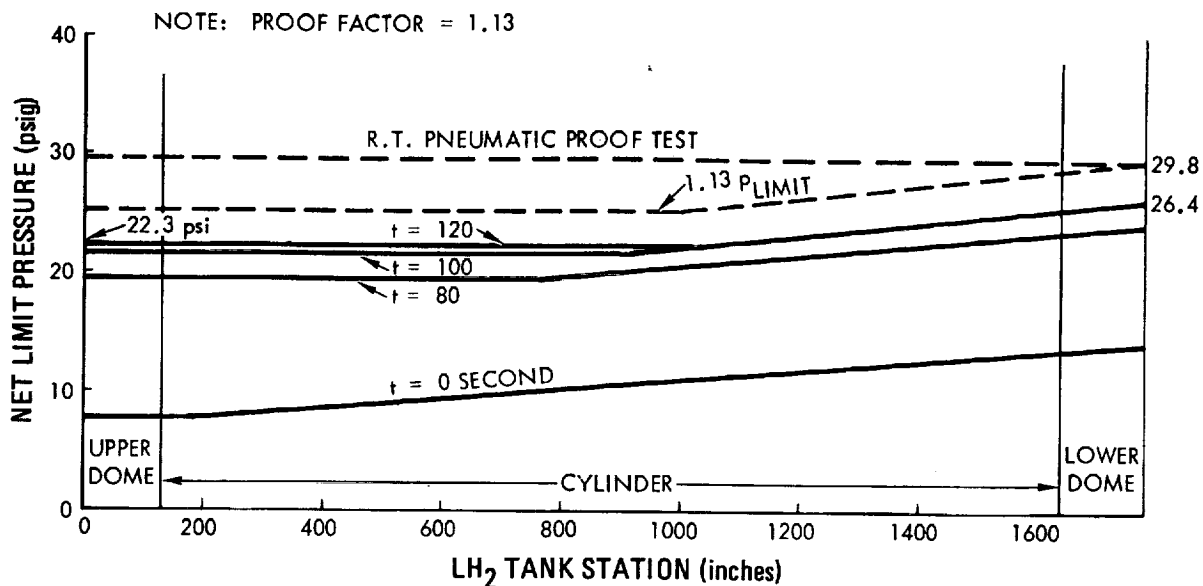


Figure 2-18. LH<sub>2</sub> Tank Net Pressures vs Tank Station

Net limit pressure for the LO<sub>2</sub> tank (including dynamic head) versus tank station at various times during boost is shown in Figure 2-19. These pressures pertain to the upper bound of the relief valve tolerance band. Also shown are the pressure lines for a three-phase proof test program using a 1g LN<sub>2</sub> head on a vertical tank position for the first two phases and a room-temperature pneumatic phase. A proof factor of 1.23 is required based on 150 missions.

The tank proof test factors of 1.13 and 1.23 are based on fracture mechanics analysis, assuming the given service life spectrum, material, and flaw growth characteristics.

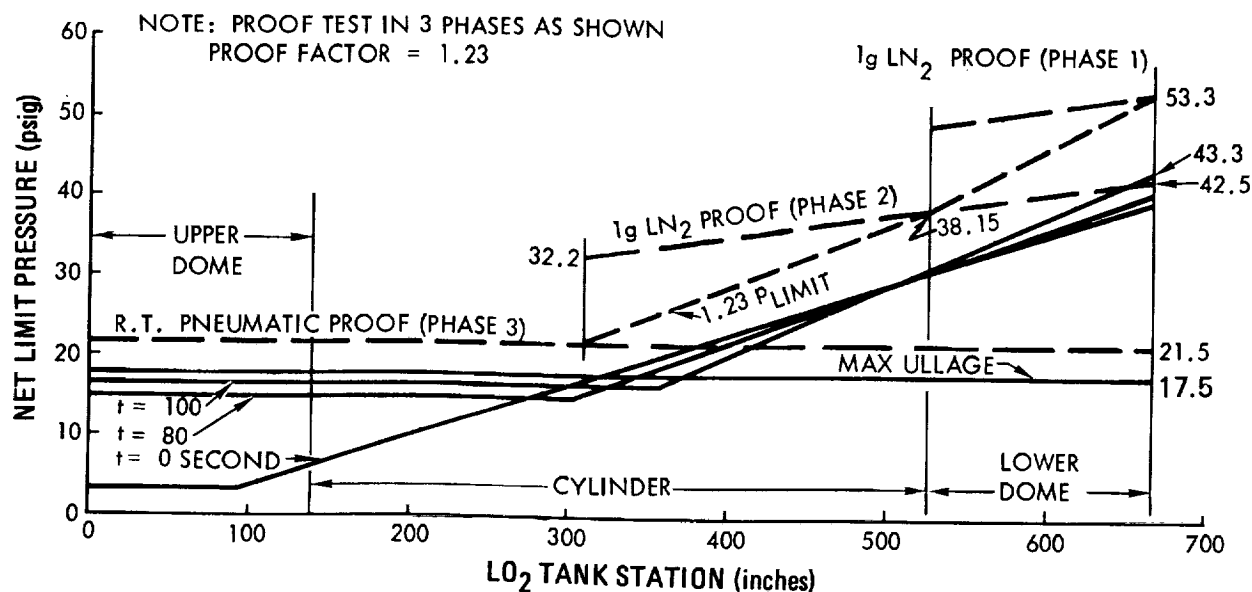


Figure 2-19. LO<sub>2</sub> Tank Net Pressures vs Tank Station

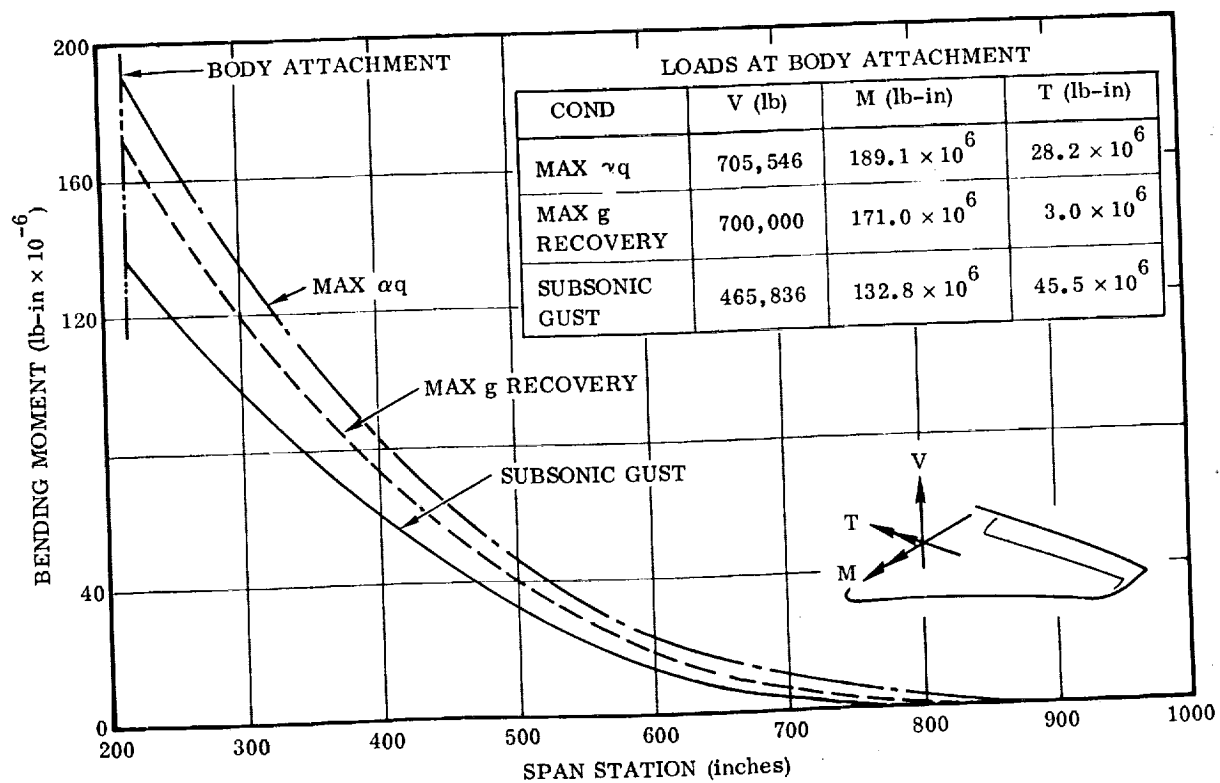
Critical design conditions for the body, wing, canard, and vertical tail structure are summarized in Table 2-7.

Figures 2-20, 2-21, and 2-22 present critical shear moment and torque values, together with bending moment curves, for the wing, canard, and vertical tail respectively.

The major critical thermal environment for the booster occurs during the entry portion of the mission. Local critical heating of the base heat shield and rudder occurs during ascent, and the top of the body and the vertical tail leading edge receive critical heating during orbiter separation.

Design temperatures used in sizing the booster outer thermal protection system structure are shown in Figures 2-23 and 2-24.

The acoustical environment to which the booster will be exposed during launch is shown in Figure 2-25, and summarized for all conditions in Table 2-12. For rocket noise at launch the exposure is general over the entire vehicle surface. For boundary layer shock wave interaction and for the air-breathing engine noise, the excitation is fairly localized. Figure 2-26 shows the wing acoustical environment for both booster noise at launch and air-breathing engine noise during cruise. The vertical tail acoustical inputs for launch are shown in Figure 2-27.



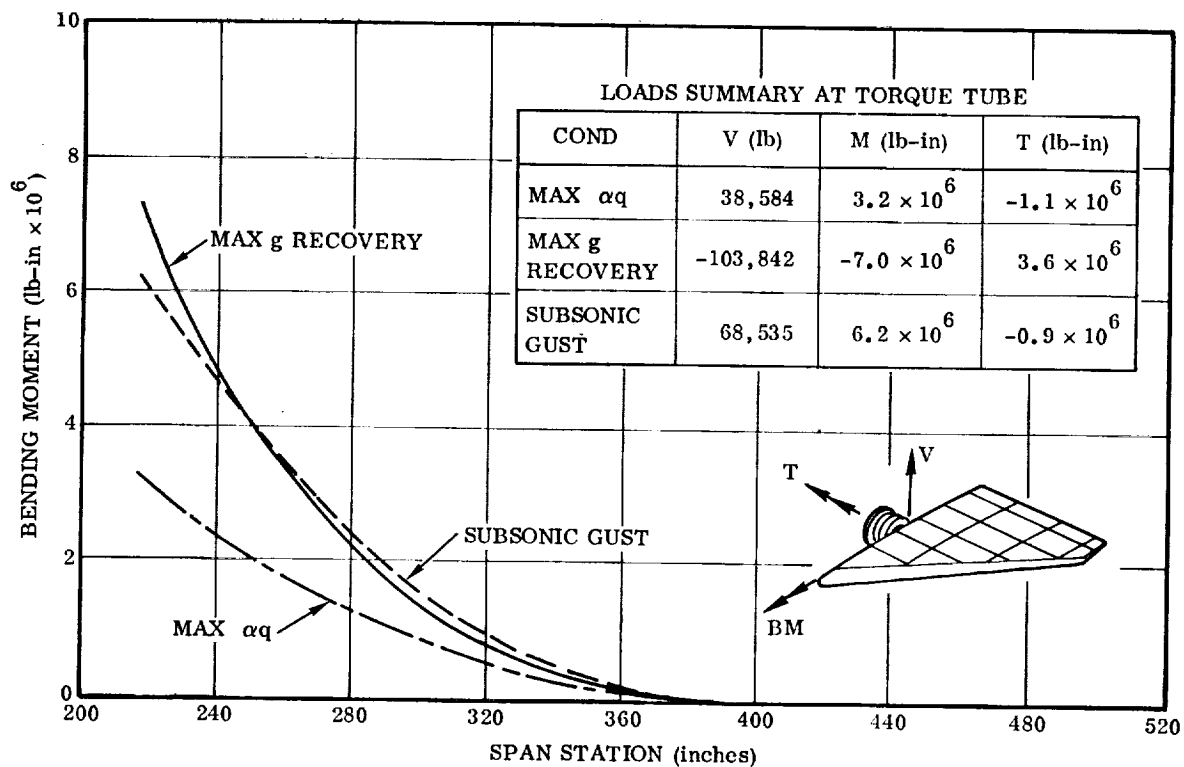


Figure 2-21. Canard Loads (Limit)

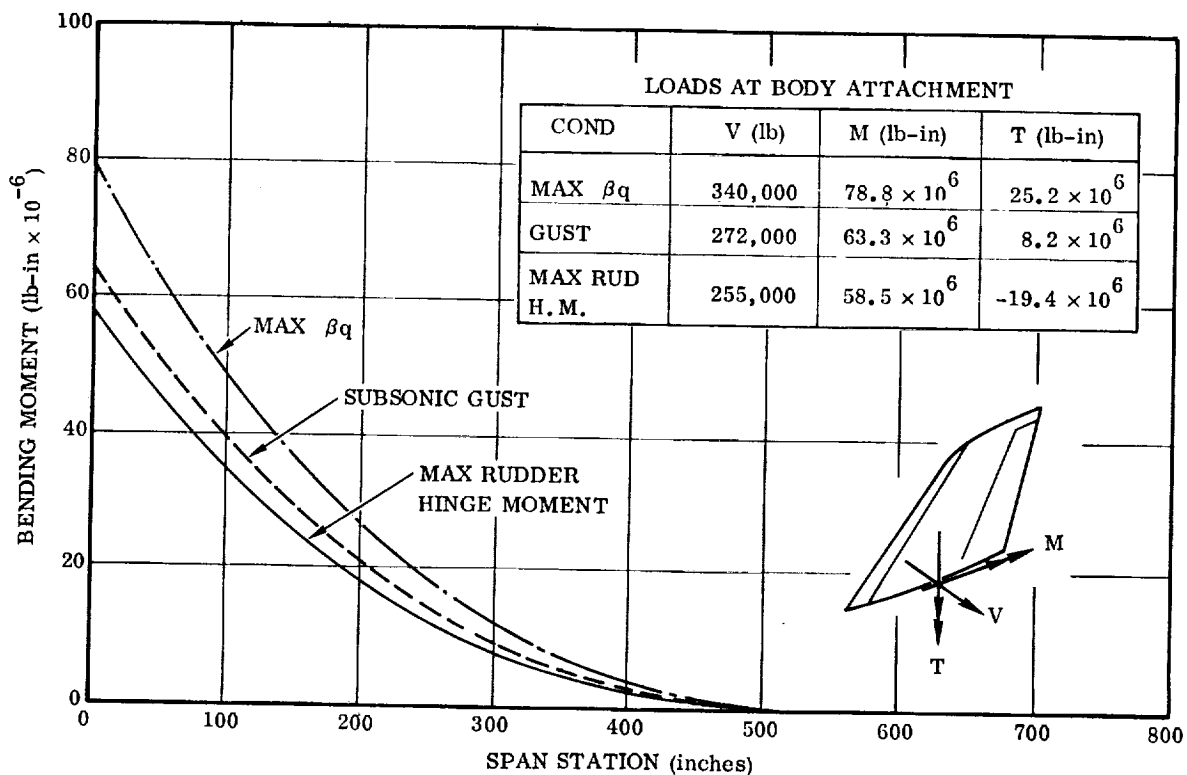


Figure 2-22. Vertical Tail Loads (Limit)

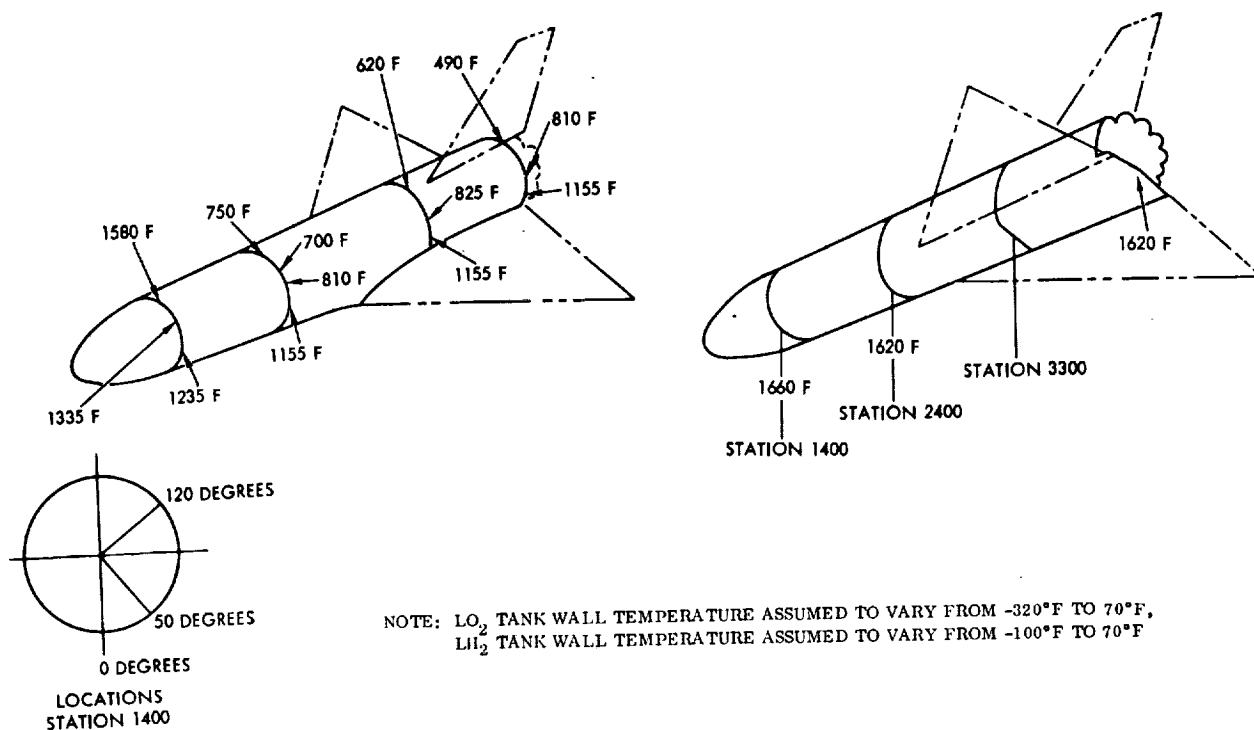


Figure 2-23. Body Design Temperatures

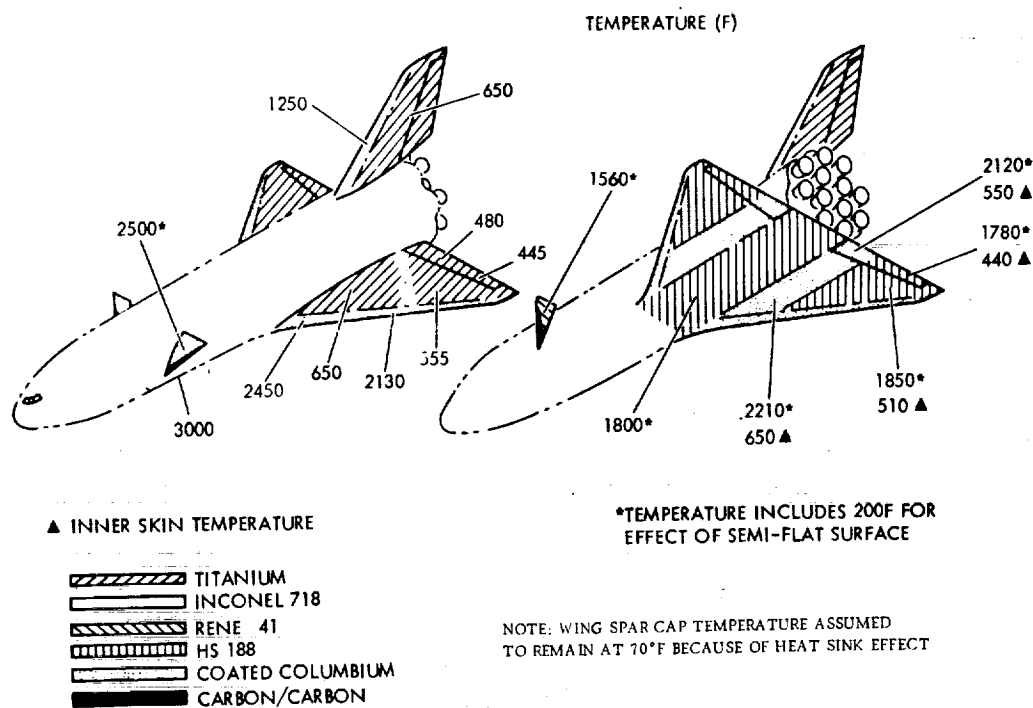


Figure 2-24. Aerodynamic Surfaces Temperature and Materials Distribution



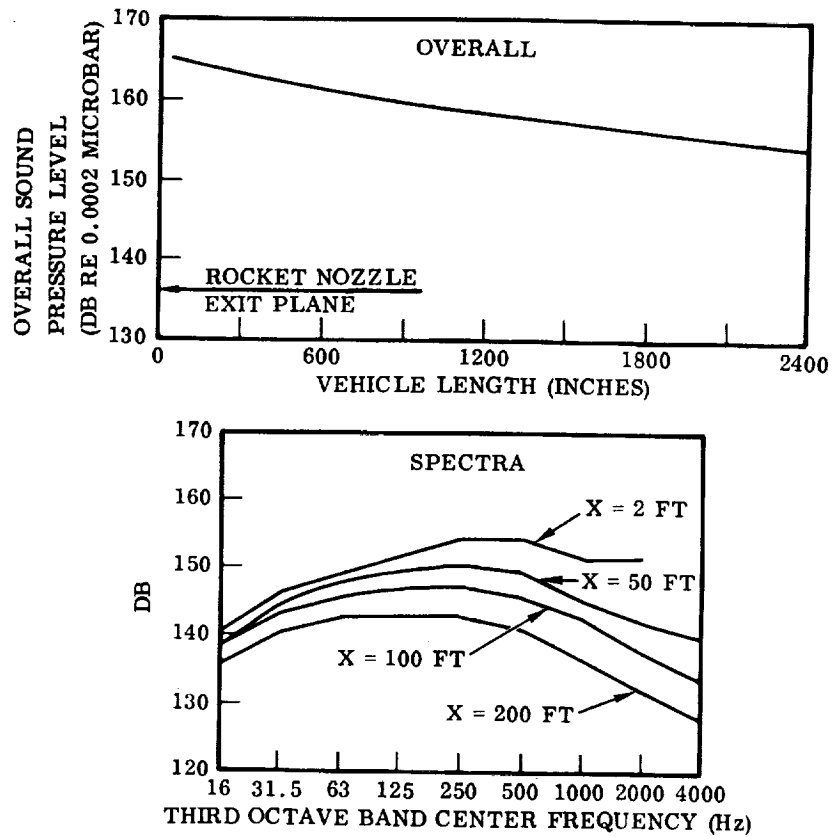


Figure 2-25. Acoustics on Launch Pad

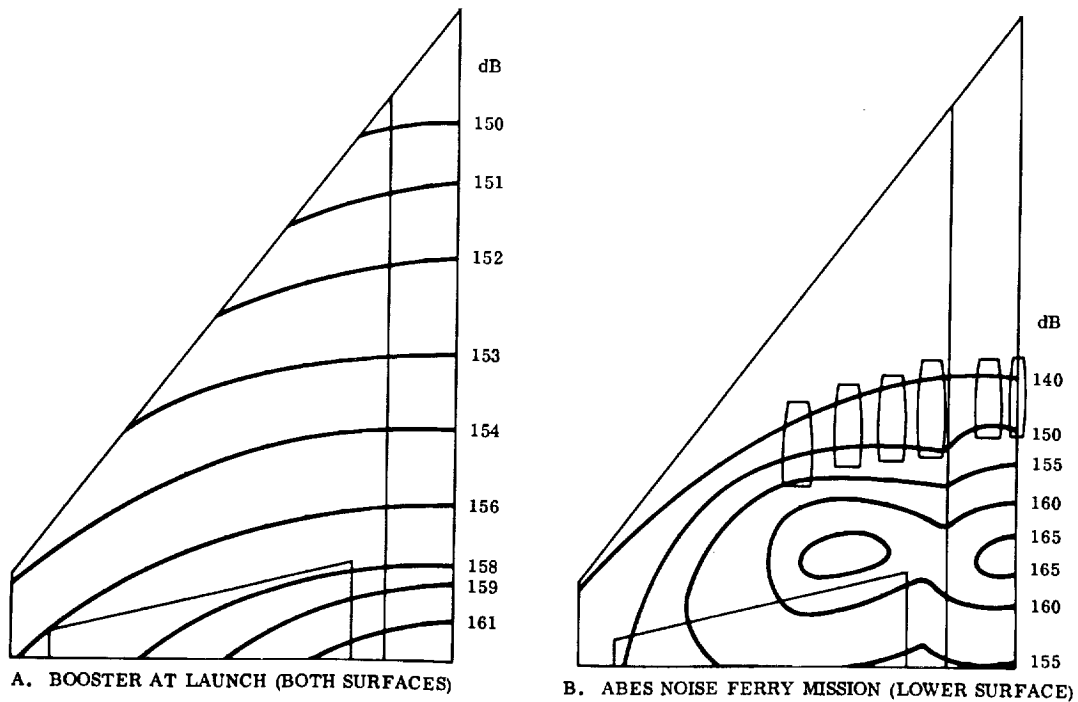


Figure 2-26. Contours of Equal Overall Sound Pressure Levels, Wing

Table 2-12. External Noise Levels on Booster Structure

Flight Condition	Noise Source	OASPL (db)(4)	Max. 1/3 OBSPL (db)(4)	Max. 1/3 OBSPL GMF(Hz) (4)	Incidence	Correlation Distance
Launch	Rockets	165(1) 154.5(2)	153 143	250 63-250	Random Random	Large Large
Ascent	Unperturbed boundary layer (B. L.)	149(2)	140	4000	Grazing	Small
	Shock - B. L. interaction	154.5(2)	146	10	Grazing	Small/medium
Reentry	Unperturbed B. L.	151(2)	141	4000	Grazing	Small
Cruise* (per engine)	ABES @ 10,000-ft alt. and 0.5 Mach	133(3)	123	560	Grazing/random	Small/medium
Ferry takeoff* (per engine)	ABES @ S. L. and zero air-speed	170(3)	160	1000	Grazing/random	Small/medium
<p>Notes: (1) 15 feet above rocket nozzle plane.            (2) Area of crew compartment.            (3) About 10 feet aft of engine exhaust nozzle and 5 feet off engine centerline.            (4) OASPL = overall sound pressure level            OBSPL = octave band sound pressure level            GMF = geometrical mean frequency</p> <p>*These levels are given per engine because they represent very near field data that are subject to wide variations for small changes in reference coordinates. The levels shown are for a plane through the apex of the jet exhaust core.</p>						

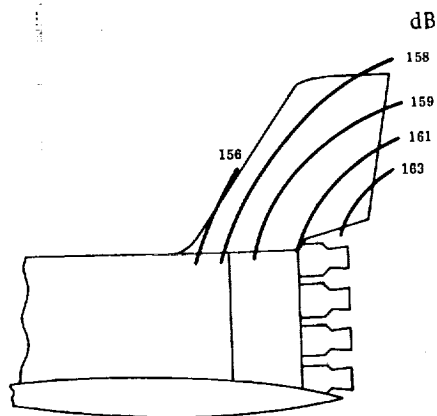


Figure 2-27. Contours of Equal Overall Sound Pressure Levels, Vertical Tail

## 2.7 SERVICE LOAD SPECTRA

This section presents the flight load and pressure load spectra expected during the 100-mission service life of the space shuttle booster. Load spectra for the components selected for detail study (i.e., tanks, wing, vertical tail, thrust structure, and orbiter support) are presented.

**2.7.1 WING LOAD SPECTRA.** Figure 2-28 presents the wing flight load spectra for a 100-mission vehicle life under ascent, entry, cruise/landing, and taxi conditions. The spectra are expressed in terms of number of exceedences versus alternating and mean bending moment, which are shown in percent of the critical value for the condition considered. These values are converted to number of cycles of mean and alternating stress, with the ascent condition represented by various segments of the total ascent flight to orbiter separation.

**2.7.2 VERTICAL TAIL LOAD SPECTRA.** The vertical tail flight load spectra are presented in Figure 2-29. As with the wing, the numbered lines represent various segments of the ascent flight.

**2.7.3 FUSELAGE LOAD SPECTRA.** The spectra of booster fuselage axial load intensity (i.e., net longitudinal load in the tank shell due to axial and bending loads, in lb/in.) are presented in Figure 2-30 for the top and bottom centerline locations at Fuselage Station 2600. Station 2600 is located at the aft orbiter-to-booster attachment and is the most highly loaded fuselage section. For the top centerline location, the design load intensity and cyclic load are compression. For the bottom centerline location, the design load intensity and cyclic loads are tension.

**2.7.4 ORBITER-TO-BOOSTER ATTACHMENT LOAD SPECTRA.** The forward orbiter-to-booster attachment flight load spectra are presented in Figure 2-31. Only vertical ( $F_z$ ) and lateral ( $F_y$ ) loads are shown, as the drag load (i.e.,  $F_x$ ) is taken through the aft attachment. The aft orbiter-to-booster attachment flight load spectra are given in Figure 2-32.

**2.7.5 THRUST LOAD SPECTRA.** Figure 2-33 is a plot of the total mean thrust versus time for the 12 booster main rocket engines. Superimposed on this is the transient thrust load spectrum presented in Figure 2-34.

**2.7.6 PROPELLANT TANK PRESSURE SPECTRA.** The main  $LH_2$  and  $LO_2$  propellant tank pressure schedules are presented in Figure 2-35 and 2-36, respectively. Nominal ullage and ullage plus fuel head pressure at the lower tank apex are shown. In addition, the maximum design pressure (i.e., maximum relief valve setting plus fuel head) assuming a pressure regulator malfunction is shown. For fatigue and flaw growth studies, it will be assumed that a pressure regulator malfunction occurs once every 20 flights.

**2.7.7 CREW MODULE PRESSURE SPECTRUM.** The pressure schedule for the crew module is presented in Figure 2-37. This curve is based on an absolute internal pressure of 15 psi at liftoff and no pressure leakage after the closing of the pressure regulator.

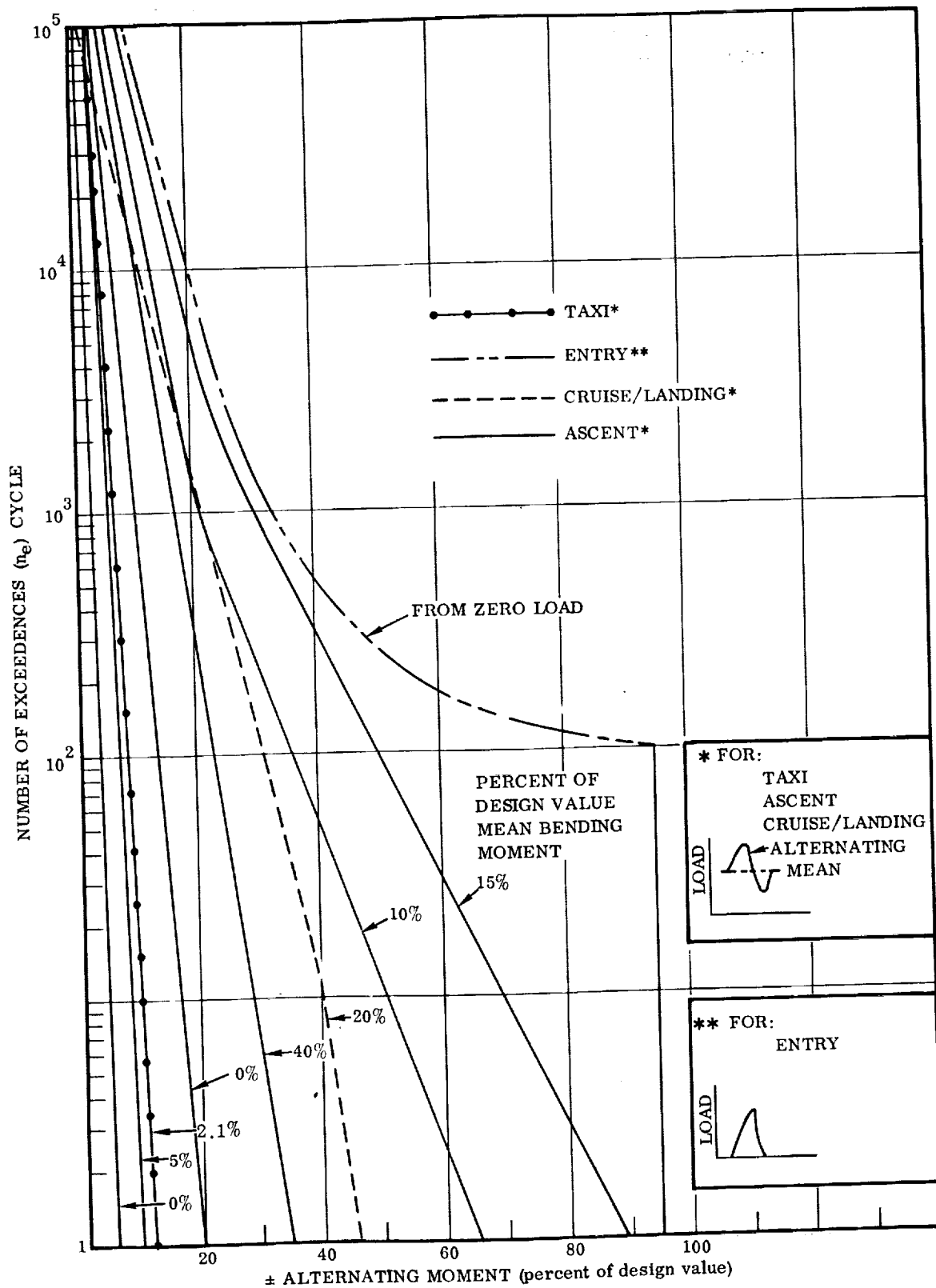


Figure 2-28. B-9U Wing Load Spectra

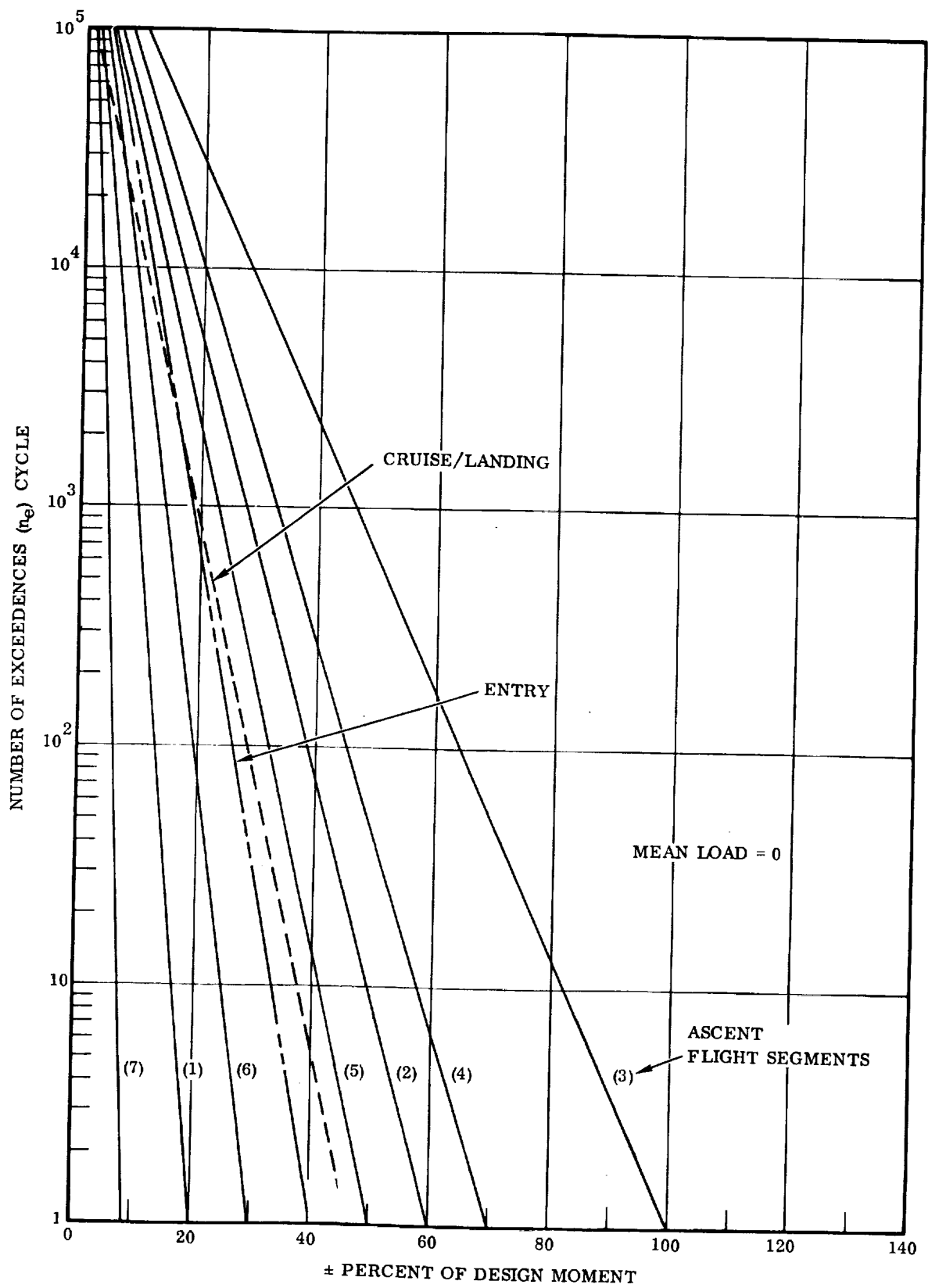


Figure 2-29. B-9U Vertical Tail Load Spectra

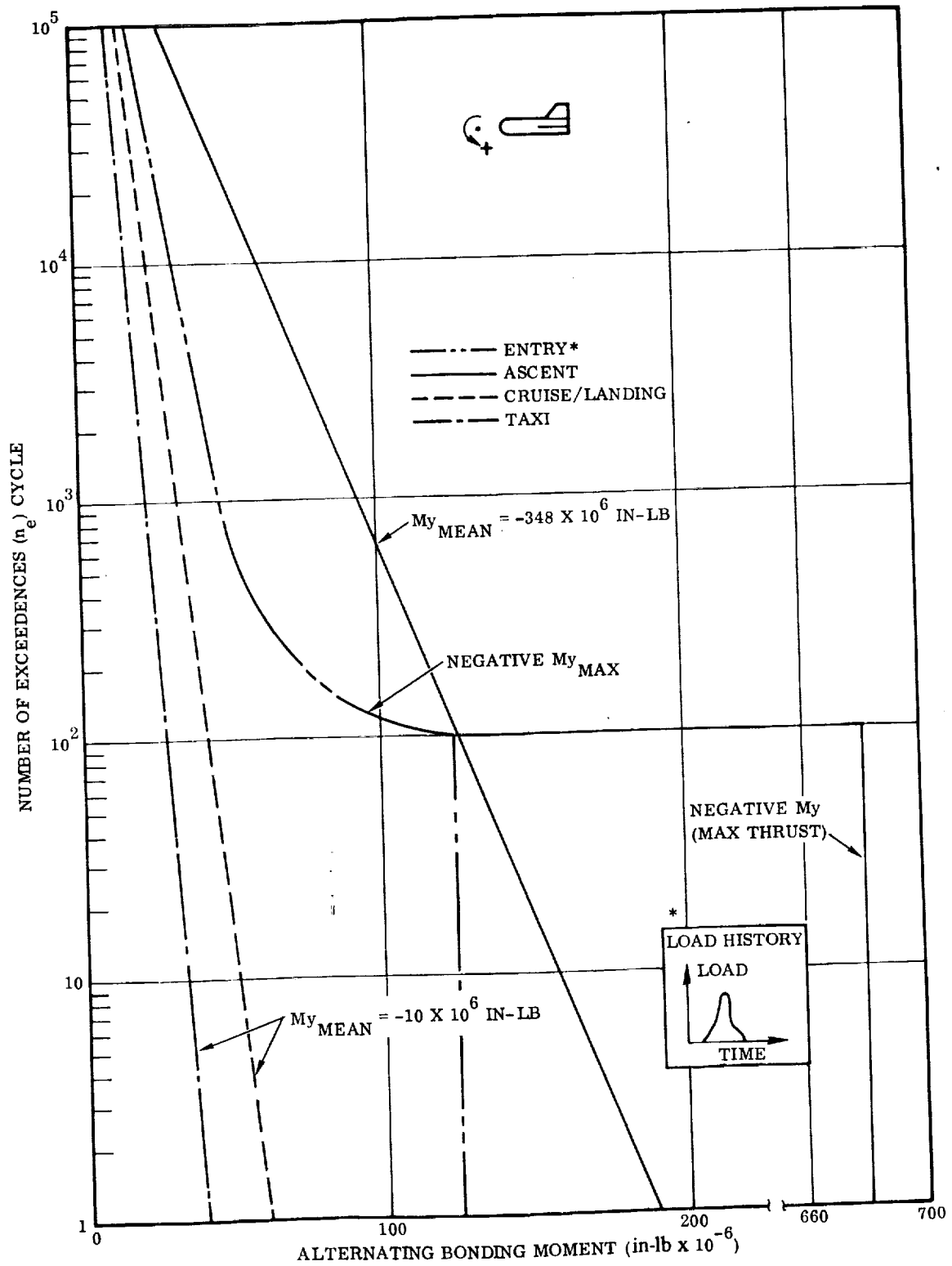


Figure 2-30. B-9U Fuselage Station 2600 Load Spectra

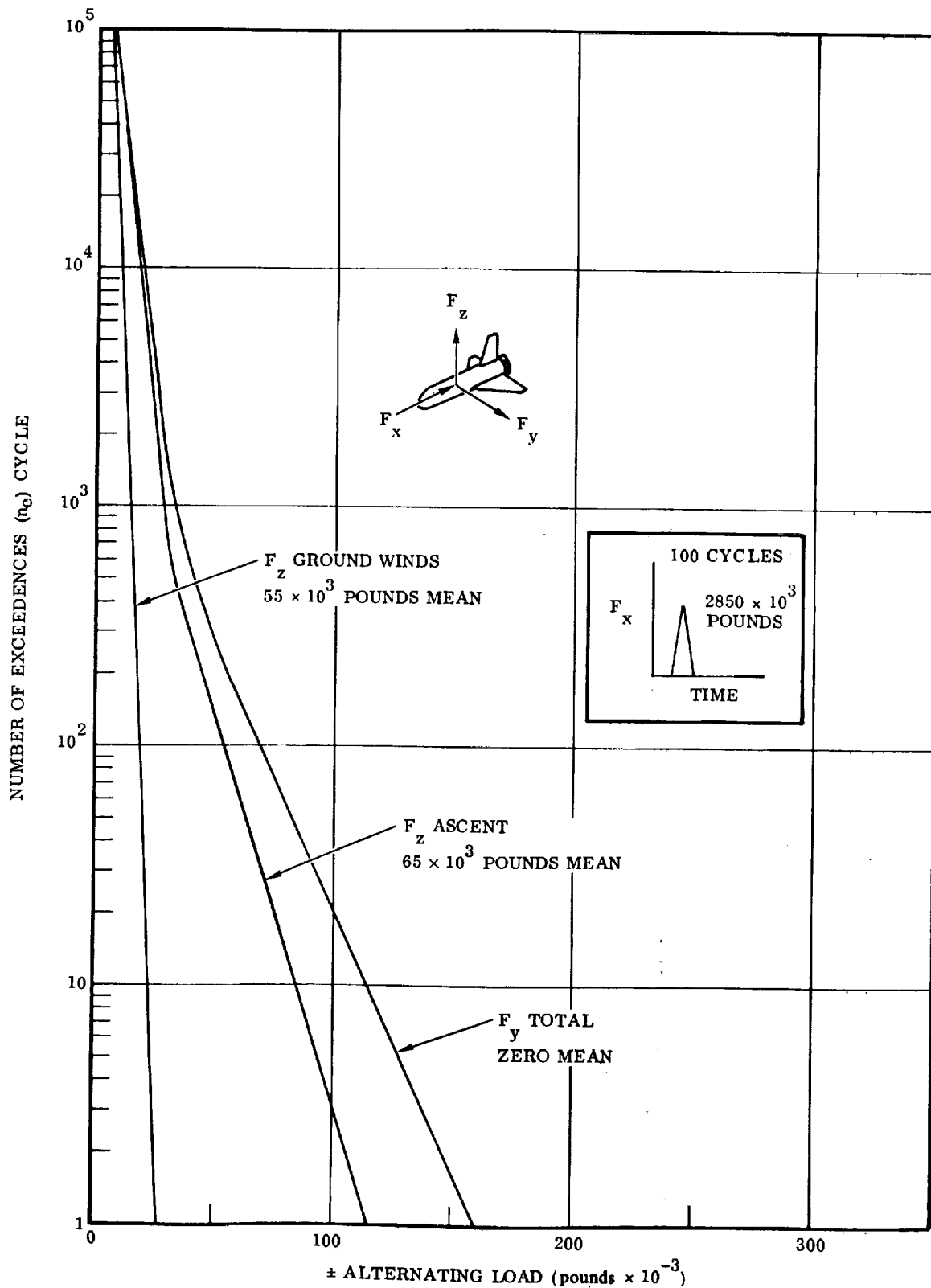


Figure 2-31. B-9U Orbiter Forward Attachment Load Spectra

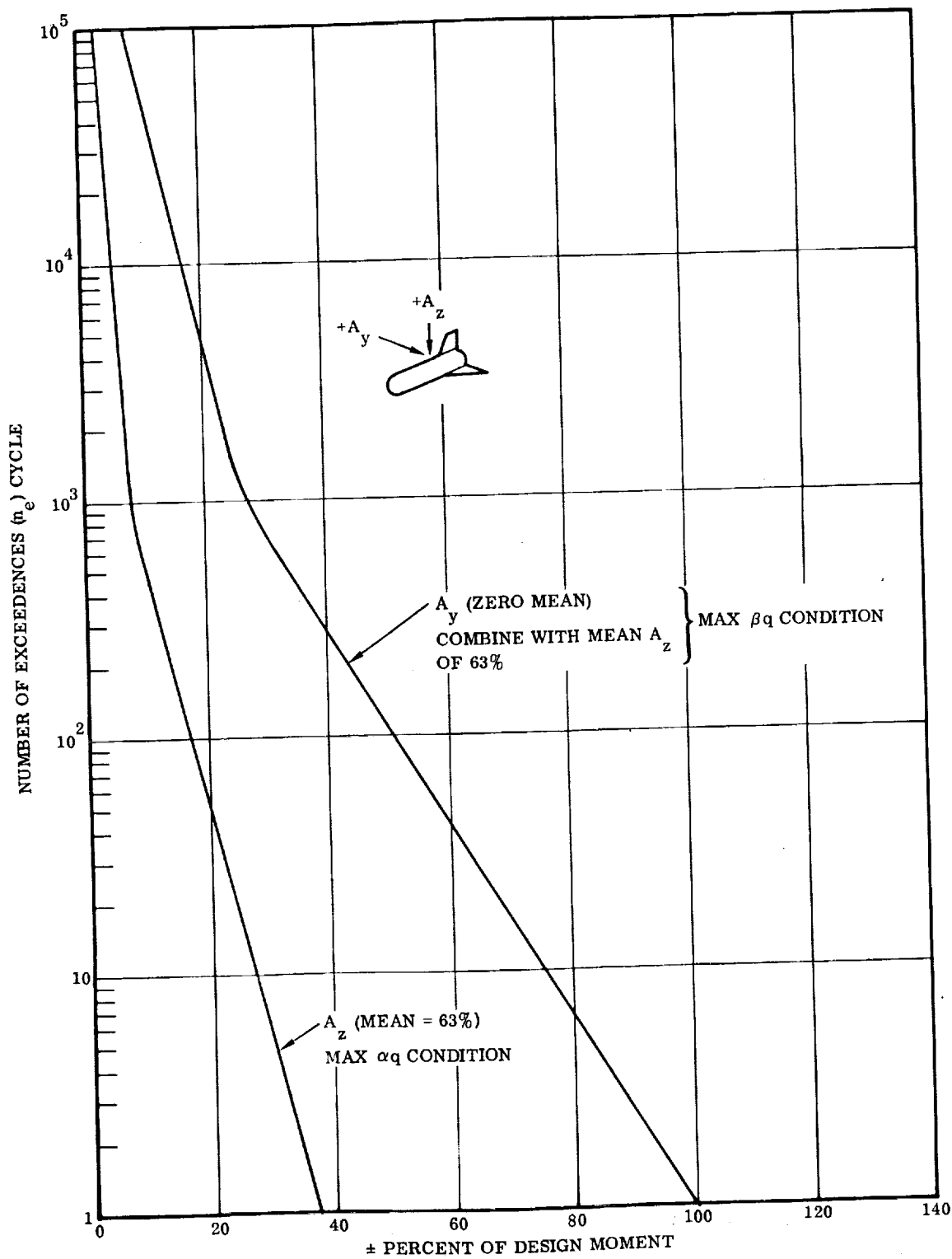


Figure 2-32. B-9U Orbiter Aft Attachment Load Spectra



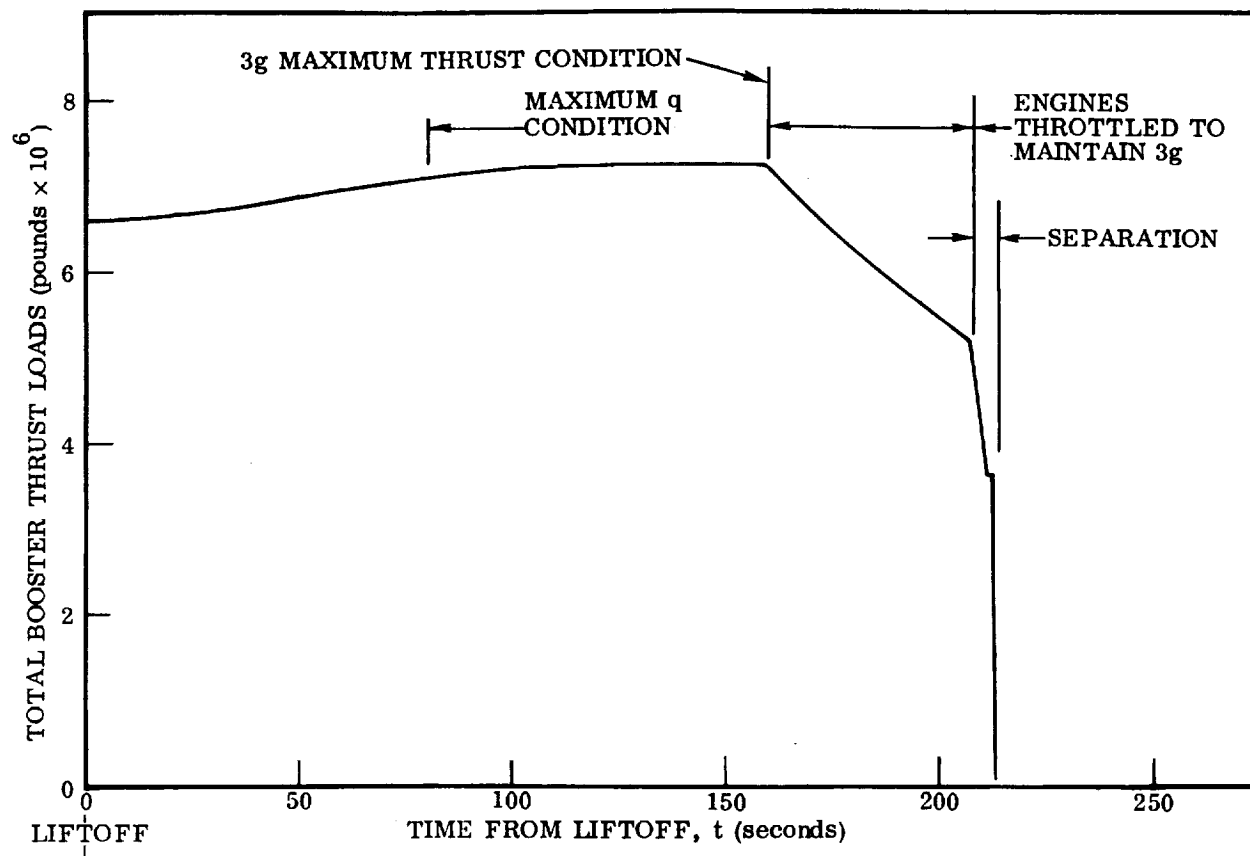


Figure 2-33. Total Mean Booster Main Engine Thrust

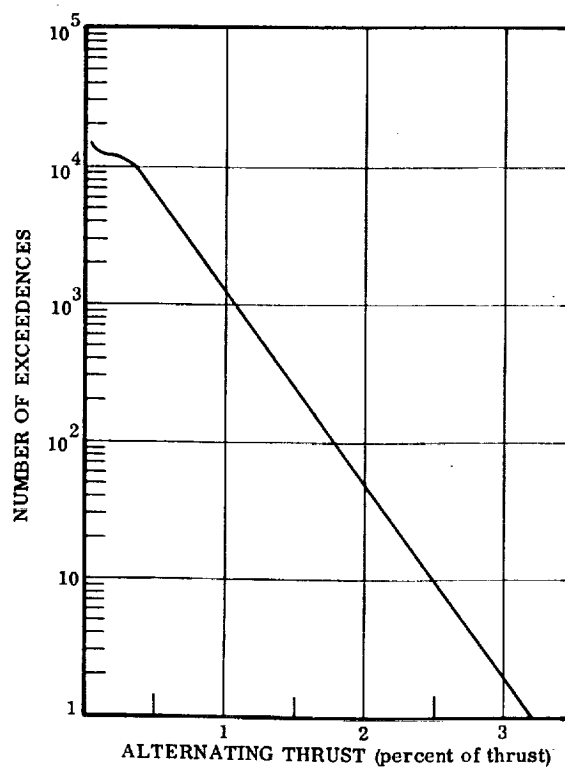


Figure 2-34. Thrust Spectrum (One Flight)

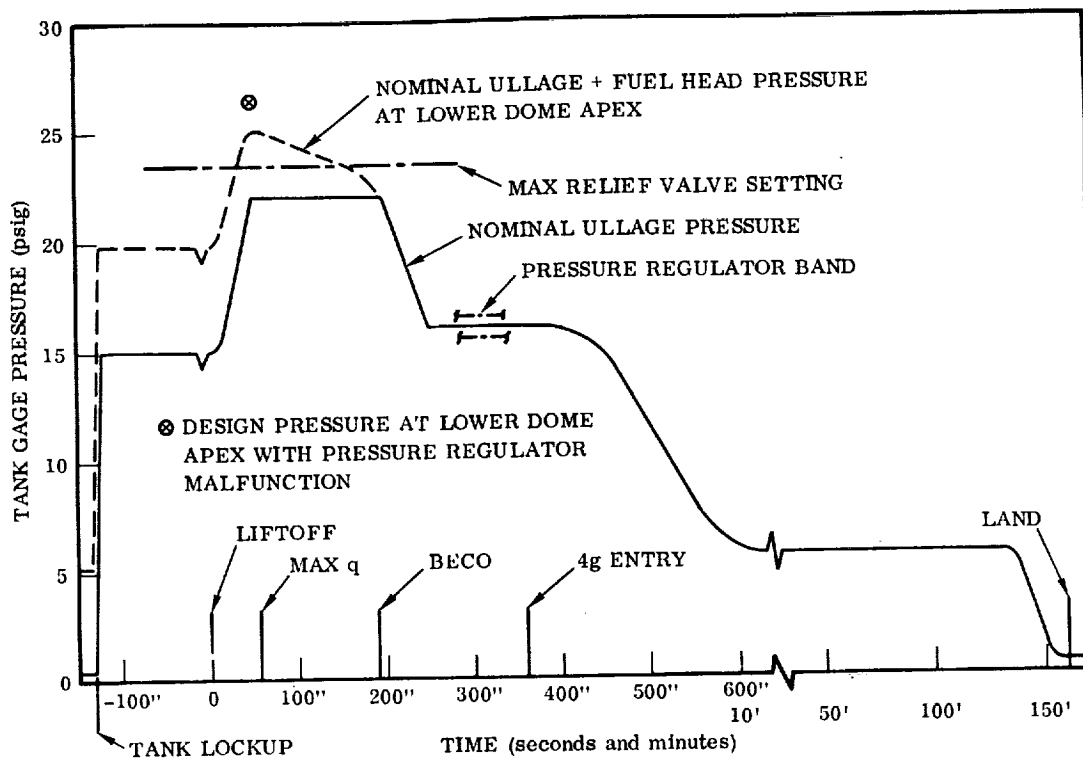


Figure 2-35. Booster Main LH<sub>2</sub> Tank Pressure Schedule

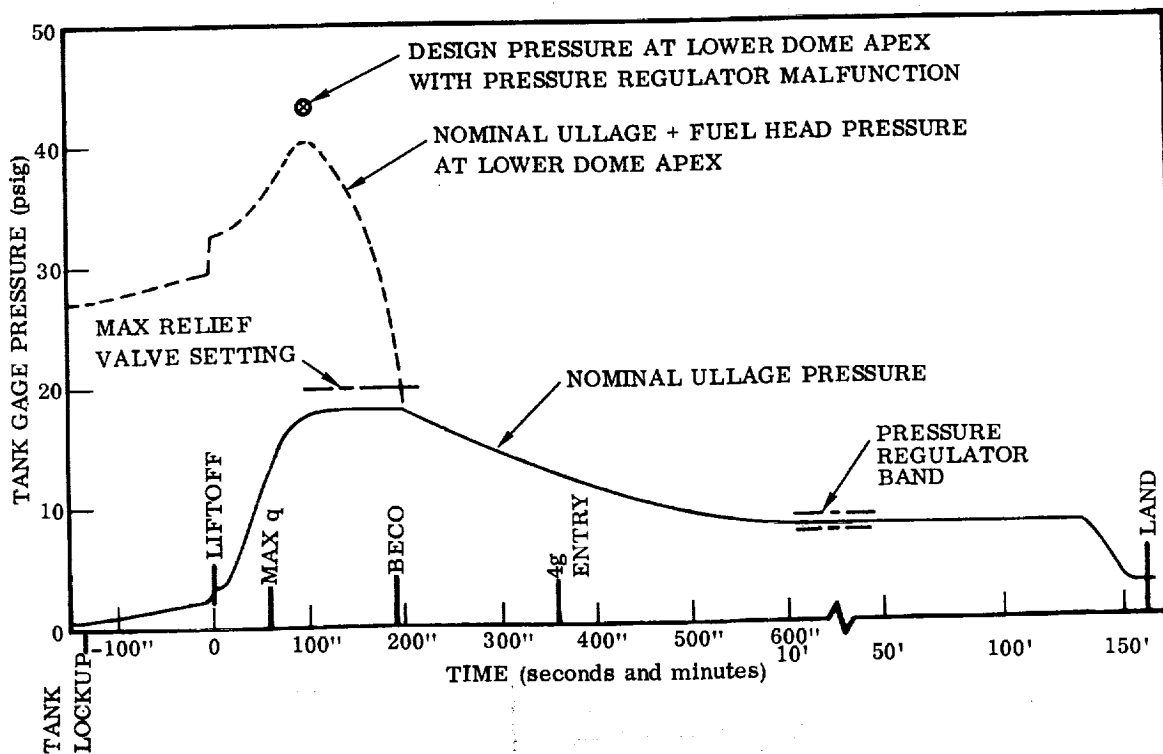


Figure 2-36. Booster Main LO<sub>2</sub> Tank Pressure Schedule

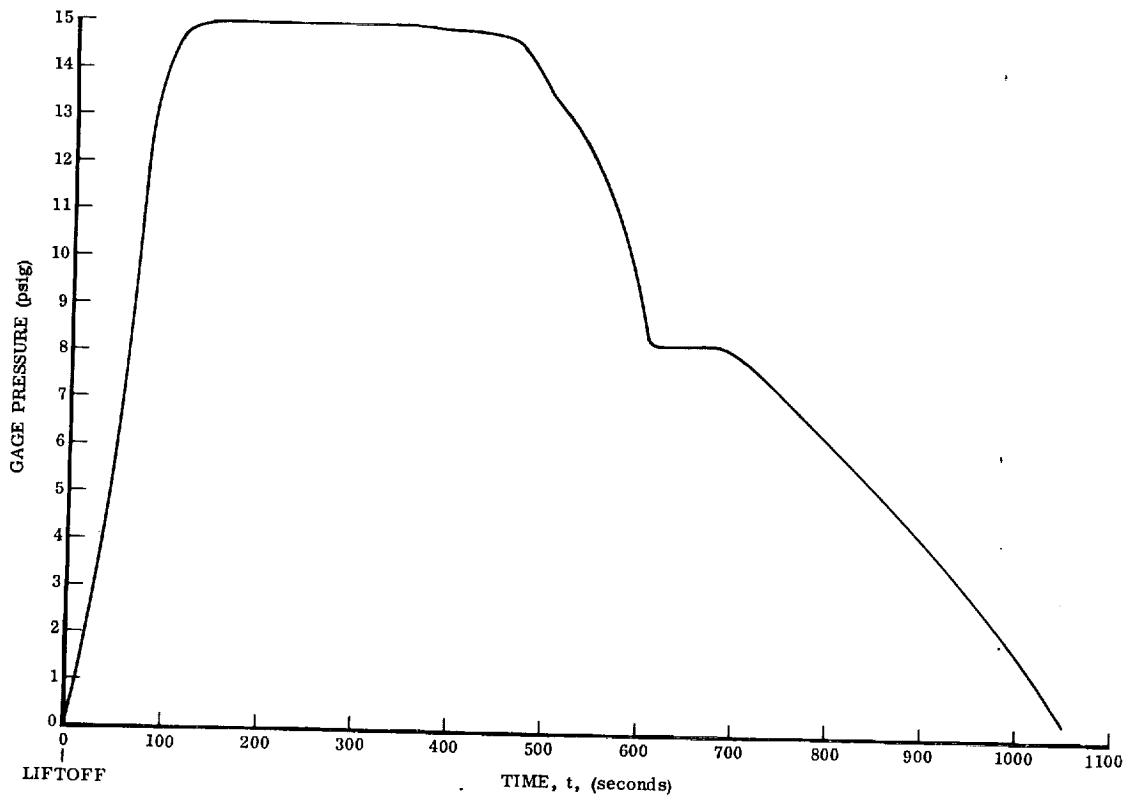


Figure 2-37. Crew Module Pressure Schedule

1

2

3

4

5

6

7

8

9

10

11

12

13

14

15

16

17

18

19

20

21

22

23

24

25

26

27

28

29

30

31

32

33

34

35

36

37

38

39

40

41

42

43

44

45

46

47

48

49

50

51

52

53

54

55

56

57

58

59

60

61

62

63

64

65

66

67

68

69

70

71

72

73

74

75

76

### SECTION 3

#### STRUCTURAL SIZING AND SENSITIVITY OF WEIGHT TO FACTOR OF SAFETY PERTURBATIONS FOR BASELINE BOOSTER

This section presents the sizing analysis of the booster structural components selected for study under this contract. The components studied are the liquid oxygen tank, liquid hydrogen tank, aft orbiter support frame, thrust structure, wing, vertical tail, and crew module. The sensitivity of the weights, determined through this sizing procedure, to factor of safety perturbations are then determined.

#### 3.1 LIQUID OXYGEN TANK

3.1.1 LO<sub>2</sub> TANK STRUCTURAL SIZING. The LO<sub>2</sub> tank is critical for the internal pressures and external loads presented in Section 2.6. Sizing of the various elements of the tank and the sensitivity of their weights to factor of safety perturbations are presented in the following paragraphs.

3.1.1.1 LO<sub>2</sub> Tank End Domes. Upper and lower LO<sub>2</sub> tank end domes have been sized for ultimate, yield, and proof test loads. Dome sizing and weight calculations were performed by means of a propellant tank dome synthesis computer program (Reference 12). This program determines the skin thickness requirements at four locations along a dome meridian and calculates dome weight assuming a stepped thickness change.

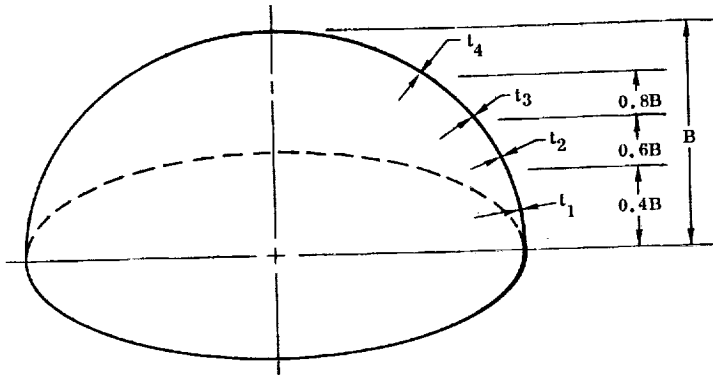
The upper dome is not in contact with liquid oxygen during critical design conditions; consequently, the structure will be near room temperature. Proof testing of the upper dome will be performed at room temperature.

The lower dome is in contact with liquid oxygen during critical design times and will be proof tested with liquid nitrogen.

Dome structural material is 2219-T87 aluminum alloy with the following properties:

	<u>Room Temperature</u>	<u>-297° F (liquid oxygen temperature)</u>	<u>-320° F (liquid nitrogen temperature)</u>
F <sub>tu</sub> (ksi)	63	75	78
F <sub>ty</sub> (ksi)	52	61	62
E <sub>c</sub> (psi)	10.8(10) <sup>6</sup>	10.8(10) <sup>6</sup>	10.8(10) <sup>6</sup>
w (lb/in <sup>3</sup> )	0.102	0.102	0.102

Design conditions are as follows:



Ultimate design,

Upper dome pressure = 17.5 psi

Lower dome pressure = 40.0 psi  
ullage

Ultimate factor = 1.4

Yield factor = 1.1

Proof pressure test design  
(proof factor,  $\alpha = 1.23$ )

Upper dome pressure = 17.5 (1.23)  
= 21.6 psi

Lower dome pressure = 40 (1.23)  
= 49.1 psi

LO <sub>2</sub> TANK END DOME SKIN THICKNESSES, IN.				
FORWARD DOME			AFT DOME	
	PROOF T: -320° F	ULTIMATE T RT	PROOF T: -320° F	ULTIMATE T: -297° F
t <sub>1</sub>	0.044	0.041	0.092	0.088
t <sub>2</sub>	0.048	0.045	0.099	0.095
t <sub>3</sub>	0.053	0.049	0.109	0.105
t <sub>4</sub>	0.058	0.054	0.120	0.115

Results of this analysis are shown in the accompanying sketch.

Both LO<sub>2</sub> tank domes are therefore designed by proof pressure for the baseline.

**3.1.1.2 LO<sub>2</sub> Tank Plate-Stringers.** Plate-stringers for the LO<sub>2</sub> tank have been sized to carry tank pressures and fuselage external loads. Plate-stringers were optimized by sizing the skin for pressure and then sizing longitudinal stiffeners (stringers) for axial loads. Skins are critical for proof pressure, as shown in this analysis, and stringers are sized for the maximum axial compression load.

Material: 2219-T87 plate, three inches thick

Properties at	Room Temperature	-320° F	-297° F
F <sub>tu</sub> (ksi)	63	63(1.24) = 78	63(1.19) = 75
F <sub>ty</sub> (ksi)	51	51(1.19) = 61	51(1.17) = 60
F <sub>su</sub> (ksi)	38		
E <sub>c</sub> (psi)	10.8(10) <sup>6</sup>		
w (lb/in <sup>3</sup> )	0.102		

Allowable working tension stress at limit pressure:

At room temperature,

$$\text{Ultimate design } \frac{63}{1.4} = 45.0 \text{ ksi (1.4 ultimate factor)}$$

$$\text{Yield design } \frac{51}{1.1} = 46.4 \text{ ksi (1.1 yield factor)}$$

$$\text{Proof design } \frac{51}{1.23} = 41.5 \text{ ksi (1.23 proof factor)}$$

At -297° F,

$$\text{Ultimate design } \frac{75}{1.4} = 53.6 \text{ ksi}$$

$$\text{Yield design } \frac{60}{1.1} = 54.5 \text{ ksi}$$

At -320° F,

$$\text{Proof design } \frac{61}{1.23} = 49.5 \text{ ksi}$$

For pressure design the skins are proof test critical.

Tank skins from the lower dome to LO<sub>2</sub> tank Station 310 will be tested with LN<sub>2</sub> at -320° F.

Proof pressure at lower dome equator:  $p = 38.8 \text{ psi}$

$$t_{\min} = \frac{pR}{F_{ty}} = \frac{38.8(198)}{61,000} = 0.126 \text{ in. (at lower dome equator)}$$

Proof pressure at LO<sub>2</sub> Station 310:  $p = 32.2 \text{ psi}$

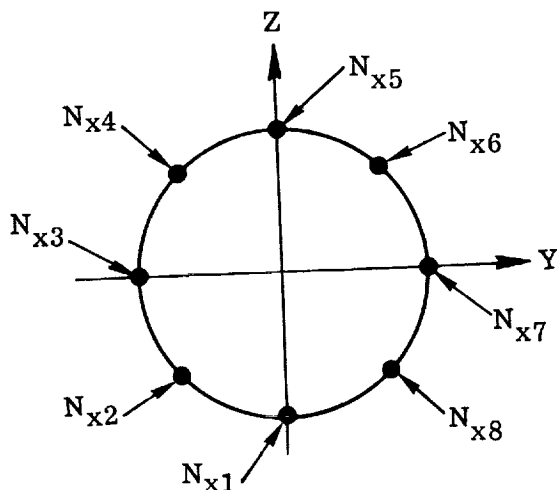
$$t_{\min} = \frac{pR}{F_{ty}} = \frac{32.2(198)}{61,000} = 0.105 \text{ in. (at Station 310)}$$

Tank skins from the upper dome to LO<sub>2</sub> tank Station 310 will be tested at room temperature.

Proof pressure:  $p = 21.5 \text{ psi}$

$$t_{\min} = \frac{pR}{F_{ty}} = \frac{21.5(198)}{51,000} = 0.084 \text{ in.}$$

The drawing skin thickness tolerance is  $\pm 0.015$  inch for nominal thicknesses less than 0.100 inch and  $\pm 0.010$  inch for 0.100 and over. A minimum thickness of 0.084 inch would require a callout of  $0.099 \pm 0.015$  because it is less than 0.100. A callout of  $0.100 \pm 0.010$  will be used, giving a minimum skin thickness of 0.090.



The critical ultimate load intensities in the liquid oxygen tank shell at eight points around the circumference of the tank, as shown in the accompanying sketch, are given in Table 3-1.

The baseline stringers have a tee cross-section and are integral with the 2219-T87 skin. Stringers are not critical for tension loading. The maximum longitudinal compression load in the LO<sub>2</sub> tank wall is  $N_x = -985$  lb/in ultimate, which is produced by the liftoff +1 hour ground headwinds condition.

Table 3-1. LO<sub>2</sub> Tank Critical Ultimate ( $FS_u = 1.4$ ) Load Intensities

	Station (in.)	$N_{x1}$ (lb/in)	$N_{x2}$ & $N_{x8}$ (lb/in)	$N_{x3}$ & $N_{x7}$ (lb/in)	$N_{x4}$ & $N_{x6}$ (lb/in)	$N_{x5}$ (lb/in)
Tension	1481	2654 (12)	2583 (12)	2425 (25)	2425 (25)	2425 (25)
	1600	2765 (12)	2658 (12)	2425 (25)	2425 (25)	2425 (25)
	1750	2943 (12)	2778 (12)	2425 (25)	2569 (8)	2887 (8)
	1864	3098 (12)	2883 (12)	2425 (25)	2674 (8)	3064 (8)
Compression	1481	—	—	—	—	—
	1600	-350 (6)	-233 (6)	—	—	—
	1750	-682 (4)	-480 (19)	—	—	—
	1864	-985 (4)	-702 (6)	-375 (22)	-214 (15)	-440 (15)

( ) Indicates condition number.

#### Section Data:

Stringer  $\Delta \bar{t} = 0.0246$  inch

$F_c = 8000$  psi

$L' = 70$  inches

$N_x = -997$  lb/in minimum allowable

The same stringer section is used for all of the tank. A plot of skin thickness,  $t_s$ , and equivalent plate stringer thickness,  $t$ , is presented in Figure 3-1.

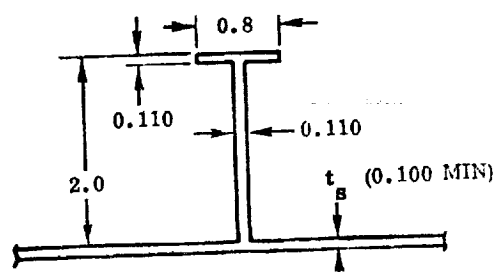


Plate-Stringer Section  
(Stringers are spaced at 12.0 inches on centers)



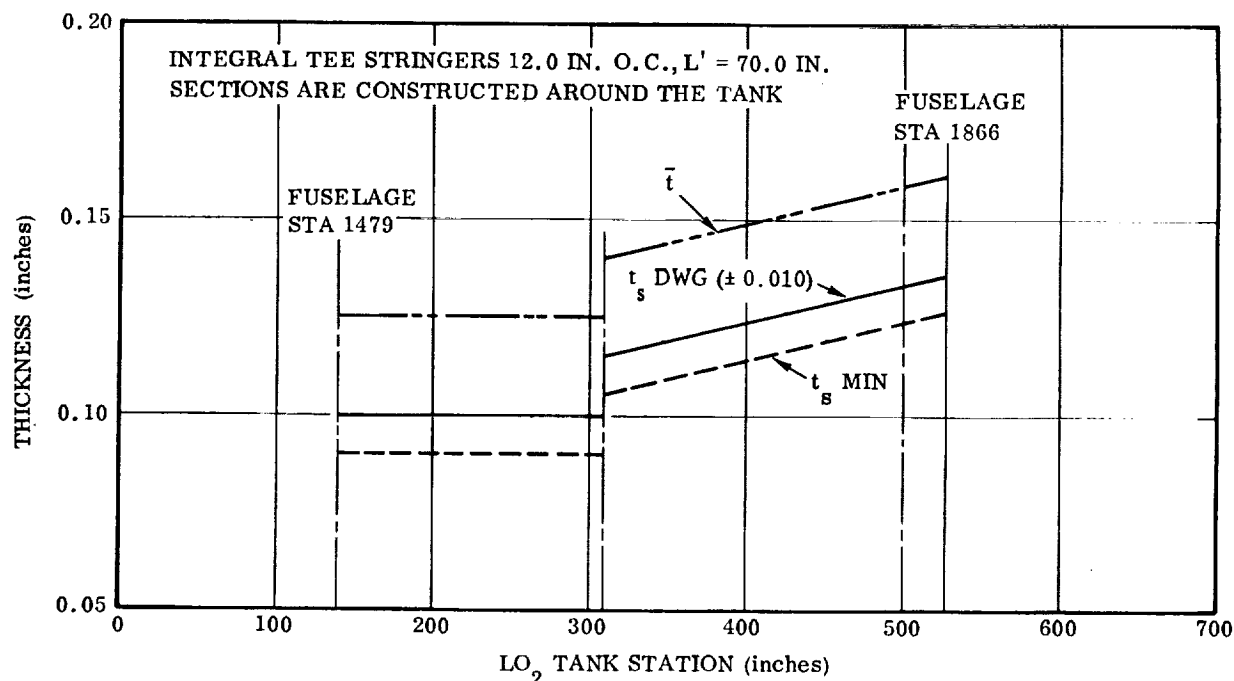


Figure 3-1.  $\text{LO}_2$  Plate-Stringer Sizing

### 3.1.2 $\text{LO}_2$ TANK WEIGHT SENSITIVITY TO FACTOR OF SAFETY PERTURBATIONS.

The results of weight sensitivity analyses for perturbations in ultimate and yield factors of safety are presented in this section for the liquid oxygen tank. All elements of the liquid oxygen tank except the orbiter support bulkhead at Station 1866 were included in the analysis. The curves presented, in general, show the variation of weight as a function of ultimate factor of safety ( $\text{FS}_u$ ) assuming ultimate design is critical. The figures also give cutoffs for certain yield factors of safety ( $\text{FS}_y$ ), assuming yield design is critical, and for proof design for a service life of 100 missions and a scatter factor of 1.5.

**3.1.2.1 Forward and Aft  $\text{LO}_2$  Tank Domes.** Figures 3-2 and 3-3 present the weight sensitivities of the  $\text{LO}_2$  tank forward (upper) and aft (lower) dome assemblies to factor of safety perturbations. The curves labeled ULTIMATE DESIGN are based on the assumption that the design of the domes is critical for the ultimate strength of the material when loaded by  $\text{FS}_u$  multiplied by the limit operating load. The two cutoffs for  $\text{FS}_y = 1.0$  and 1.1 are based on the assumption that the design of the domes is critical for the yield strength of the material when loaded by  $\text{FS}_y$  multiplied by the limit operating load. The cutoff for proof design establishes the baseline weights for the domes, and is shown in these figures for comparison purposes. The proof design cutoffs are determined by application of a proof factor to limit operating loads, and then designing the structure to withstand this load without yielding. The proof test at this load then guarantees a 100 mission safe-life for flaw growth at a scatter factor of 1.5. The proof factor,  $\alpha$ , is 1.23 for the liquid oxygen tank. The baseline weight for the forward dome is 1715 pounds, and for the aft dome it is 2998 pounds.

**3.1.2.2  $\text{LO}_2$  Tank Skins.** The weight sensitivity of the liquid oxygen tank skin to factor of safety perturbations is presented in Figure 3-4. Weights for the skin were determined

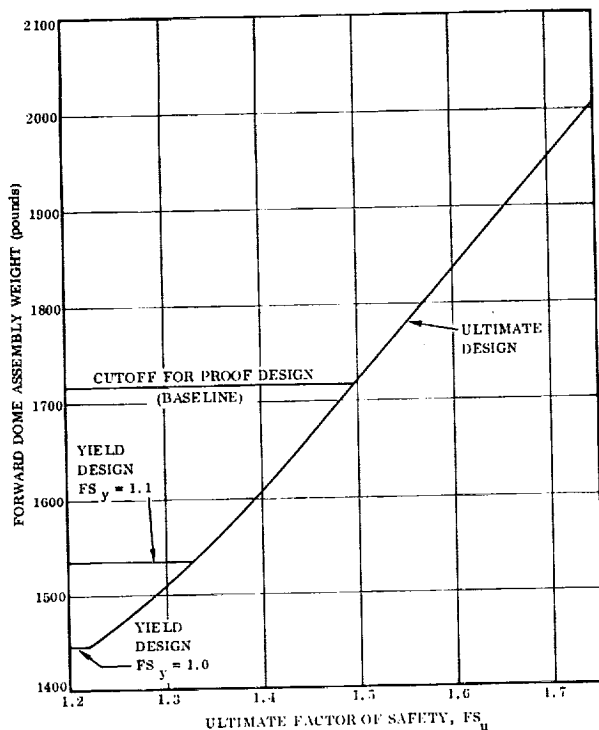


Figure 3-2. Forward LO<sub>2</sub> Tank Dome Assembly Weight Sensitivity to Factor of Safety Perturbations

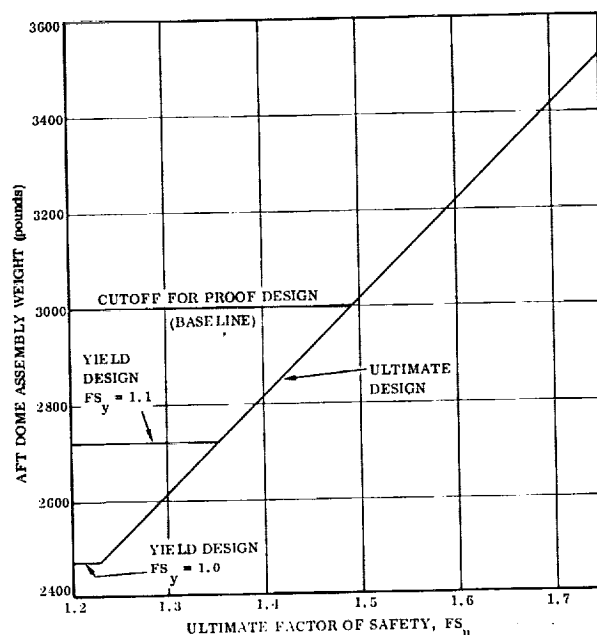


Figure 3-3. Aft LO<sub>2</sub> Tank Dome Assembly Weight Sensitivity to Factor of Safety Perturbations

in the same manner as for the domes (Section 3.1.2.1), except that for proof design, the proof pressure varies along the length of the tank due to the planned three-phase proof test. The baseline weight of the skin, as required for proof, is 5616 pounds.

**3.1.2.3 LO<sub>2</sub> Tank Stringers.** The weight sensitivity of the liquid oxygen tank stringers to factor of safety perturbations is presented in Figure 3-5. The upper curve in that figure is based on a skin designed by proof pressure for a safe-life of 100 missions and a scatter factor of 1.5, and constant section stringers designed for the maximum compression in the tank. The two lower curves give the stringer weight based on the design of the stringers for the actual maximum compression load at a given station. The upper curve of these two is based on the skin being designed for the same factor of safety as the stringers, whereas the lower curve uses a skin designed for proof pressure just as the curve for constant section stringers does. The baseline stringer weight is 1474 pounds.

**3.1.2.4 Liquid Oxygen Tank.** The weight sensitivity of the liquid oxygen tank to factor of safety perturbations is presented in Figure 3-6. The curve labeled **ULTIMATE DESIGN** is based on the design of all LO<sub>2</sub> tank elements for the ultimate strength of the material when loaded by  $FS_u$  multiplied by limit operating load. The two curves labeled **YIELD DESIGN** for  $FS_y = 1.0$  and  $1.1$  are based on the design of all LO<sub>2</sub> tank elements except the stringers for the yield strength of the material when loaded by  $FS_y$  multiplied by the limit operating load. The stringers are not critical for yield design, and therefore the weight of the stringers on the yield design curves increases with  $FS_u$ .

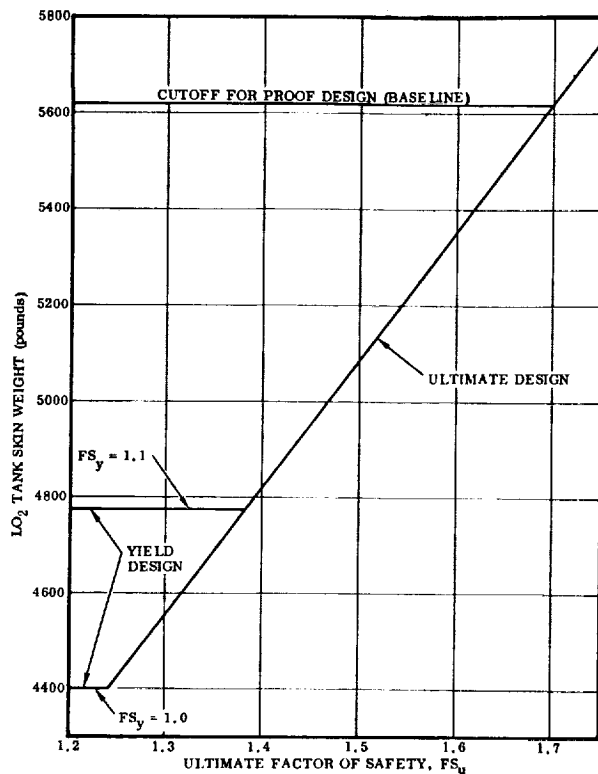


Figure 3-4. LO<sub>2</sub> Tank Skin Weight Sensitivity to Factor of Safety Perturbations

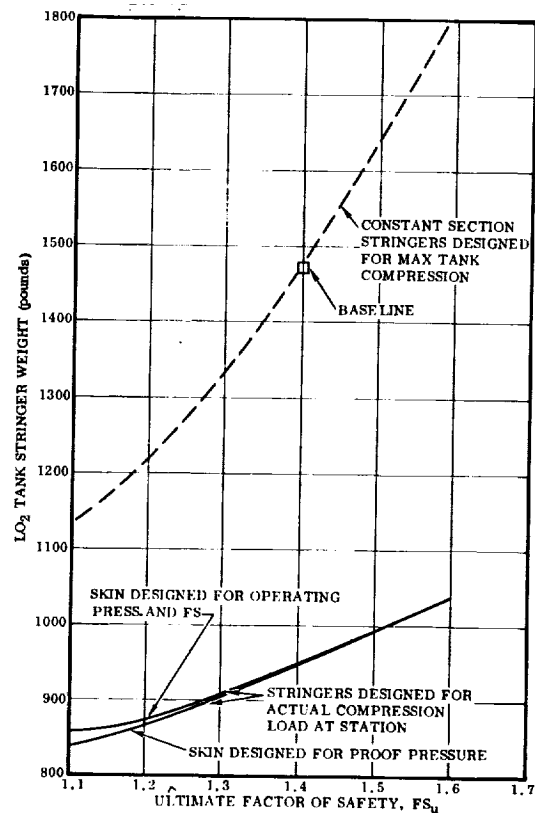


Figure 3-5. LO<sub>2</sub> Tank Stringer Weight Sensitivity to Factor of Safety Perturbations

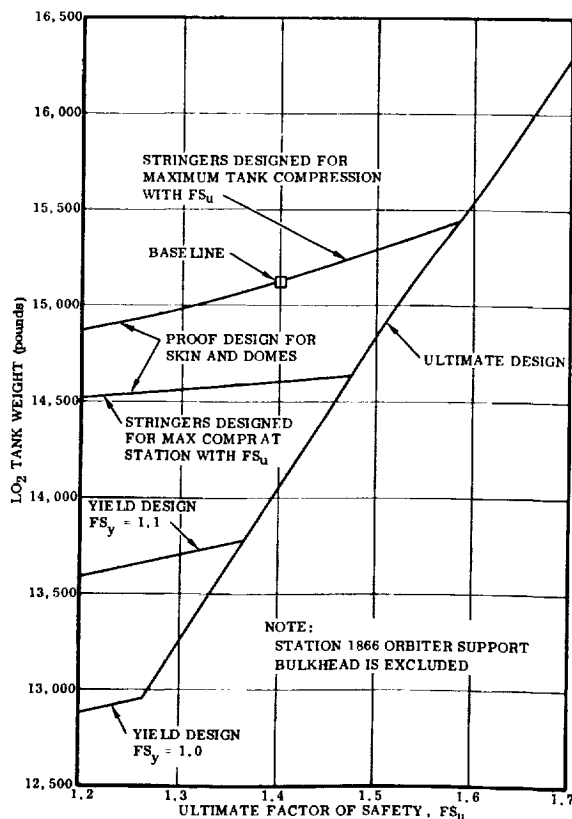


Figure 3-6. LO<sub>2</sub> Tank Weight Sensitivity to Factor of Safety Perturbations

as is indicated by the slope of the curves, which is in contrast to the horizontal cut-offs in Figures 3-2 through 3-4. The upper two curves in Figure 3-6, including the one which goes through the baseline weight point, are based on proof design for the end domes and skin. The curve through the baseline weight point, in addition, uses stringers designed for the maximum compression anywhere within the tank, whereas the lower of the two curves uses stringers designed for the maximum compression at a particular tank station. The baseline LO<sub>2</sub> tank weight is 15,127 pounds. This weight excludes the weight of the Station 1866 orbiter support bulkhead, which was not included in the study of the LO<sub>2</sub> tank.

## 3.2 LIQUID HYDROGEN TANK

**3.2.1 LH<sub>2</sub> TANK STRUCTURAL SIZING.** The LH<sub>2</sub> tank is critical for the pressure, axial, and shear loads presented in Section 2.6. Sizing of the various structural elements of the tank and the sensitivity of their weights to factor of safety perturbations are presented in the following paragraphs.

**3.2.1.1 LH<sub>2</sub> Tank End Domes.** Upper and lower LH<sub>2</sub> tank end domes have been sized for both ultimate design and proof test. Dome sizing and calculation of weights was performed by means of a propellant tank dome synthesis computer program (Reference 12). This program was also used to size LO<sub>2</sub> tank domes.

Dome structural material is 2219-T87 aluminum alloy with the following properties at room temperature:

$$F_{tu} = 63,000 \text{ psi}$$

$$F_{ty} = 52,000 \text{ psi}$$

Design conditions are:

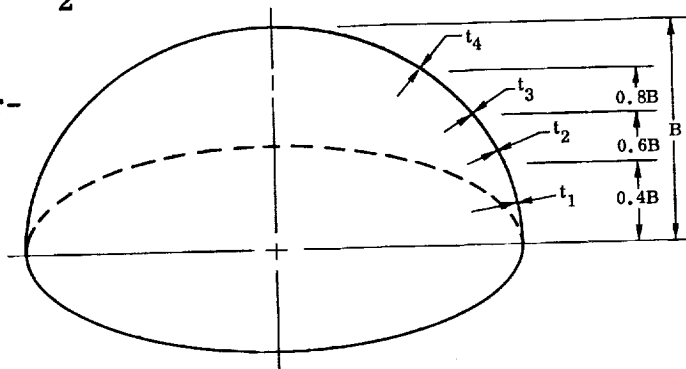
$$\text{Ultimate design, } FS_u = 1.4$$

$$\text{Upper dome pressure} = 22.3 \text{ psi}$$

$$\text{Lower dome pressure} = 26.4 \text{ psi}$$

Proof pressure test design  
(proof factor,  $\alpha = 1.13$ )

$$\text{Upper and lower dome pressure} = 26.4 (1.13) = 29.8 \text{ psi}$$



LH <sub>2</sub> TANK END DOME SKIN THICKNESSES, IN.				
	FORWARD DOME		AFT DOME	
	PROOF T=RT	ULTIMATE T=RT	PROOF T=RT	ULTIMATE T=RT
t <sub>1</sub>	0.061	0.053	0.061	0.063
t <sub>2</sub>	0.066	0.057	0.060	0.068
t <sub>3</sub>	0.073	0.063	0.073	0.074
t <sub>4</sub>	0.080	0.069	0.080	0.082

Results of this analysis are shown in the accompanying sketch.

The results indicate that the forward (upper) LH<sub>2</sub> tank dome is critical for proof pressure, while the aft (lower) dome is critical for ultimate pressure.

**3.2.1.2 LH<sub>2</sub> Tank Plate-Stringers and Belt Frames.** Plate-stringers for the LH<sub>2</sub> tank have been sized to carry tank pressures and fuselage external loads. The design criteria and loadings presented in Section 2 were followed in establishing factors of safety, minimum skin thickness for pressure design, and minimum thickness for stability design.

Plate-stringer and belt frame configurations were optimized for axial loads with the following constraints:

- Minimum skin required for pressure and/or shear.

- b. Minimum stringer spacing for machining.
- c. Maximum stringer height limited by available plate thickness.

Optimum frame spacing was determined for two basic integral stiffener configurations, tee and blade, by selecting average compressive load intensities and optimum stiffeners for various effective column lengths. Belt frame required moments of inertia were calculated by the Shanley criterion, which gives stiffening requirements for the prevention of shell general instability (Reference 13).

$$I_f = N_x \left( \frac{C_f \pi D^4}{4LE_f} \right)$$

Frame cross-sectional areas were calculated for 9.0-inch-deep frames with truss webs that would have the required moment of inertia. Effective thickness ( $\bar{t}$ ) was calculated for each configuration and plotted as shown in Figure 3-7. As a result of this study, integral stiffeners with an effective column length of 60 inches were selected for detailed sizing.

Various sizes of integral stiffener were analyzed to determine the effect of stringer spacing and height for several minimum skin thicknesses. As a result of this study, a stiffener spacing of 4.0 inches was selected for the LH<sub>2</sub> tank.

Detailed sizing of the plate-stringer includes the effects of internal pressure, axial load, and shear. Minimum skin thickness was determined for pressure design (ultimate,

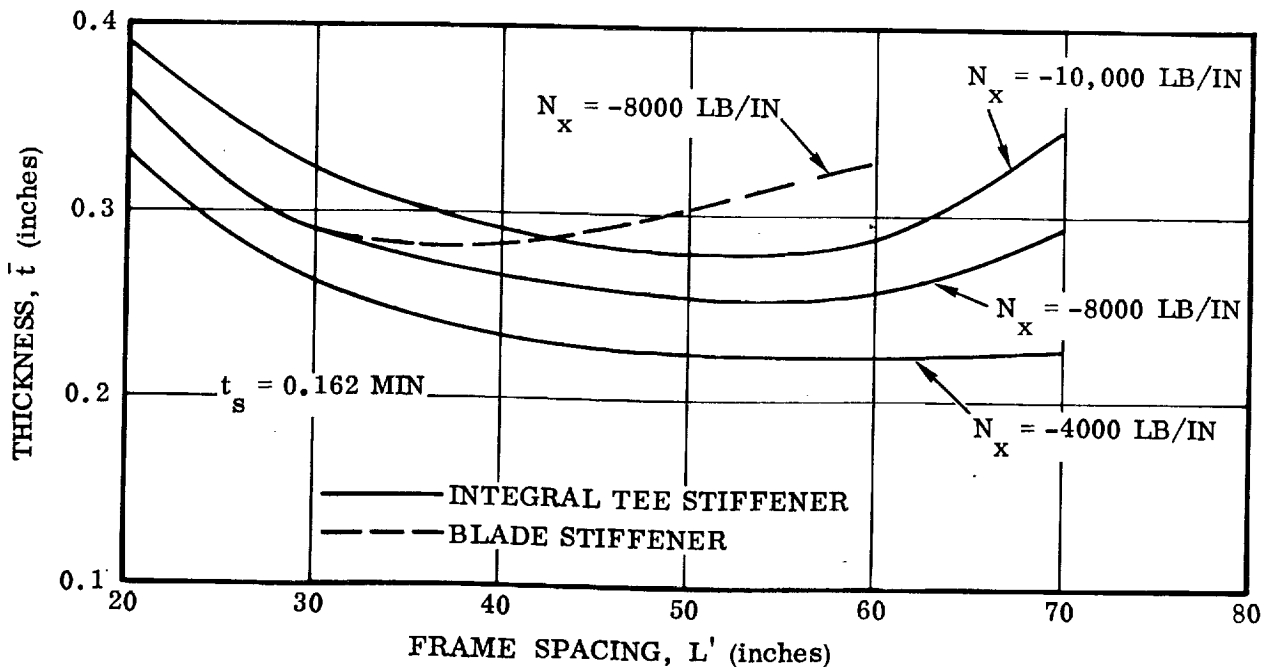


Figure 3-7. LH<sub>2</sub> Tank Plate-Stringer Effective Thickness Versus Frame Spacing

yield, and proof test), shear (principal stress), and axial load. Sizing of the skin is influenced by axial loads in determining optimum plate-stringer sizes for minimum weight to carry biaxial load and not exceed the allowable shear strength of the skin.

Four sections of the LH<sub>2</sub> tank were selected for detailed analysis of a clean structure. The effect of concentrated loads was calculated separately.

Loads for the selected stations are presented in Table 3-2. A typical analysis is presented and the final plate stringer sizes are in Table 3-3.

Material: 2219-T87 plate, 3 inches thick

Room temperature properties

$$F_{tu} = 63 \text{ ksi}$$

$$E_c = 10.8 (10)^6 \text{ psi}$$

$$F_{ty} = 51 \text{ ksi}$$

$$w = 0.102 \text{ lb/in}^3$$

$$F_{su} = 38 \text{ ksi}$$

Allowable working tension stress at limit pressure

$$\text{Ultimate design } \frac{63}{1.4} = 45.0 \text{ ksi (1.4 ultimate factor)}$$

$$\text{Yield design } \frac{51}{1.1} = 46.4 \text{ ksi (1.1 yield factor)}$$

$$\text{Proof design } \frac{51}{1.13} = 45.1 \text{ ksi (1.13 proof test factor)}$$

For pressure design the tank skins are ultimate critical. Minimum skin thickness for the tank will be determined by ultimate design pressure and proof pressure. The proof pressure is the maximum pressure in the tank multiplied by the proof test factor of 1.13.

Maximum tank pressure is at the lower dome apex (26.4 psi).

$$\text{Proof pressure} = 26.4 (1.13) = 29.83 \text{ psi}$$

Maximum tank pressure in constant section:  $p = 25.5 \text{ psi}$ .

The tank constant section is proof test critical

$$t_{\min} = \frac{pR}{F_{ty}} = \frac{29.83(198)}{51,000} = 0.116 \text{ inch}$$

$$\text{Drawing callout} = 0.126 \pm 0.010 \text{ inch}$$

$$\text{Stability design } t = 1.05 (0.116) = 0.122 \text{ inch}$$

Table 3-2. LH<sub>2</sub> Tank Critical Design Loads (Ultimate)

a. Ultimate Axial Load Intensities

Station	Bottom			Bottom Side			Side			Top Side			Top		
	N <sub>x</sub>	q	C*	N <sub>x</sub>	q	C	N <sub>x</sub>	q	C	N <sub>x</sub>	q	C	N <sub>x</sub>	q	C
2400	-4167	0	7	-4072	49	4	-6062	6	6	-8803	5	10	-10,923	0	10
2800	-6327	0	7	-5614	222	7	-6138	319	6	-8485	624	10	-10,412	0	10
3161	-7269	0	7	-6380	228	7	-6401	346	6	-7817	700	10	-9,206	0	10
3377	-8055	0	7	-7006	66	7	-6536	362	6	-7479	743	5	-8,349	0	10

b. Ultimate Hoop Load Intensities

Station	Condition 4		Condition 6		Condition 7		Condition 10	
	Press	N <sub>y</sub>	Press	N <sub>y</sub>	Press	N <sub>y</sub>	Press	N <sub>y</sub>
2400	11.9	2356	11.9	2356	27.3	5405	31.2	6178
2800	13.3	2633	13.3	2633	27.3	5405	31.2	6178
3161	15.4	3049	15.4	3049	28.7	5683	31.2	6178
3377	16.8	3326	16.8	3326	30.1	5960	32.2	6376

\* C = Condition number, see Section 2.6.

Table 3-3. LH<sub>2</sub> Tank Plate Stringer Sizing

Material: 2219-T87; Stringer Spacing: 4.0 inches on centers;  
Stringer Height: 3.0 inches

Sta 2182	2400	2800	3161	3377	3681	
	$t_s = 0.122$ $\bar{t} = 0.175$	$t_s = 0.140$ $\bar{t} = 0.200$	$t_s = 0.150$ $\bar{t} = 0.220$	$t_s = 0.150$ $\bar{t} = 0.236$		Bottom $\phi$
	$t_s = 0.122$ $\bar{t} = 0.174$	$t_s = 0.130$ $\bar{t} = 0.192$	$t_s = 0.140$ $\bar{t} = 0.206$	$t_s = 0.150$ $\bar{t} = 0.212$		Bottom Side
	$t_s = 0.140$ $\bar{t} = 0.190$	$t_s = 0.140$ $\bar{t} = 0.193$	$t_s = 0.140$ $\bar{t} = 0.207$	$t_s = 0.150$ $\bar{t} = 0.204$		Side
	$t_s = 0.160$ $\bar{t} = 0.242$	$t_s = 0.160$ $\bar{t} = 0.240$	$t_s = 0.150$ $\bar{t} = 0.236$	$t_s = 0.150$ $\bar{t} = 0.223$		Top Side
	$t_s = 0.170$ $\bar{t} = 0.292$	$t_s = 0.170$ $\bar{t} = 0.276$	$t_s = 0.160$ $\bar{t} = 0.252$	$t_s = 0.160$ $\bar{t} = 0.246$		Top $\phi$

- Note: 1.  $t_s$  is skin thickness for stability design.  
2.  $\bar{t}$  is the equivalent thickness of skin and stringers.  
3. Thickness shown does not include effects of local loads.

# Typical Plate Stringer Analysis — Section at Station 2800:

Tank Bottom Centerline:

Ultimate loads:  $N_x = -6327 \text{ lb/in}$ ;  $N_y = 5405 \text{ lb/in}$ ;  $q = 0$ .

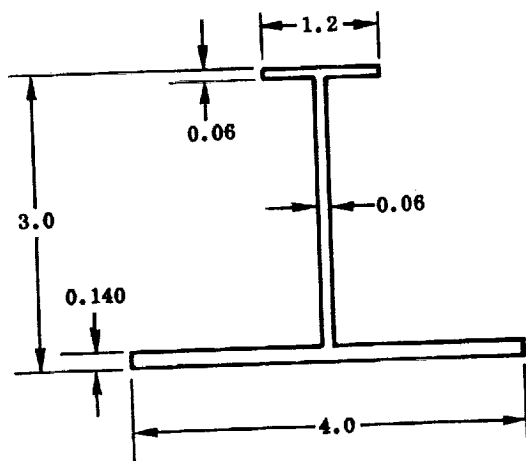


Plate-Stringer Section  
(Stringers are 4.0 inches on Centers)

Section Data:

$$t_s = 0.140 \text{ inch}$$

$$\bar{t} = 0.200 \text{ inch}$$

$$F_c = 33,500 \text{ psi } (L' = 60)$$

$$F_{su} = 38,000 \text{ psi}$$

Note: Thickness shown is for stability  
design:  $1.05 \times t_{\min}$

$$\text{for pressure } t_s = \frac{0.140}{1.05} = 0.133 \text{ inch}$$

$$\text{Compressive stress: } f_c = \frac{6327}{0.200} = 31,630 \text{ psi}$$

$$\text{Tensile stress normal to compressive: } f_t = \frac{5405}{0.133} = 40,700 \text{ psi}$$

Maximum shear stress:

$$f_{sp} = \left[ \left( \frac{f_t + f_c}{2} \right)^2 + f_s^2 \right]^{1/2}$$

$$f_{sp} = 37,000 \text{ psi}$$

$$\text{M. S.} = \frac{33,500}{31,630} - 1 = +0.05 \text{ (compression)}$$

$$\text{M. S.} = \frac{38,000}{37,000} - 1 = +0.02 \text{ (shear)}$$



Typical Plate-Stringer Analysis - Station 2800 - Upper Side

Maximum compressive condition: 3g maximum thrust

$$N_x = -8485 \text{ lb/in ultimate}$$

$$q = 621 \text{ lb/in ultimate}$$

Internal pressure maximum ultimate:  $p = 22.3 (1.4) = 30.7 \text{ psi}$

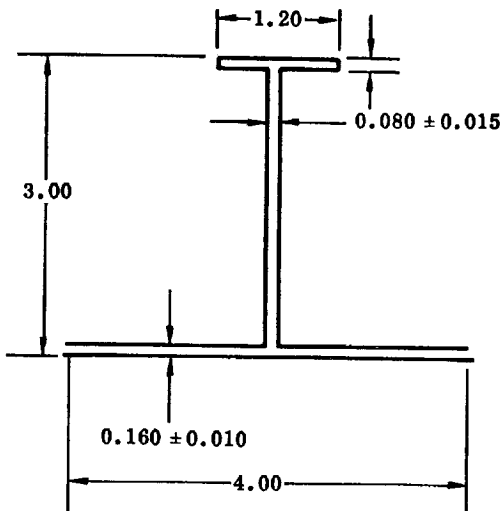
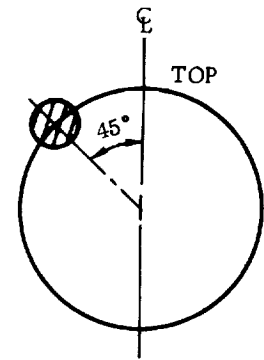


Plate Stringer Section

Nominal Section Properties

$$\bar{t} = 0.242 \text{ inch}$$

$$A = 0.9696 \text{ in}^2 / 4 \text{ inch width}$$

$$\rho = 1.099 \text{ inch}$$

Section for Stability Design

$$\text{Skin } t = 0.150 (1.05) = 0.157 \text{ inch}$$

$$\text{Stringer } t = 0.065 (1.05) = 0.068 \text{ inch}$$

$$A = 0.9029 \text{ in}^2$$

$$\bar{t} = 0.226 \text{ inch}$$

$$\rho = 1.014 \text{ inch}$$

Plate-stringer compression allowable:

Frame spacing is 66.7 inches

Column fixity is 1.5

$$L' = \frac{66.7}{\sqrt{1.5}} = 54.6$$

$$F_c = 37,600 \text{ psi}$$

$$f_c = \frac{8485}{0.226} = 37,500 \text{ psi}$$

$$\text{M.S.} = \frac{37,600}{37,500} - 1 = +0.0$$

Maximum skin shear: (nominal section)

$$f_t = \frac{pR}{t} = 38,000 \text{ psi}$$

$$f_c = \frac{N_x}{t} = 35,000 \text{ psi}$$

$$f_s = \frac{q}{t} = 3880 \text{ psi}$$

$$f_{s_{\max}} = \left[ \left( \frac{f_t + f_c}{2} \right)^2 + f_s^2 \right]^{1/2} = 36,500 \text{ psi}$$

$$\text{M. S.} = \frac{38,000}{36,500} - 1 = +0.04$$

LH<sub>2</sub> Tank Belt Frames:

Frames sized by Shanley criterion:

$$I_f = N_x \left( \frac{C_f \pi D^4}{4LE_f} \right)$$

Typical frame analysis:

Design load intensity:  $N_x = -8000 \text{ lb/in}$

Frame spacing:  $L = 60 \text{ inches}$

Tank diameter:  $D = 396 \text{ inches}$

Coefficient:  $C_f = 62.5 (10)^{-6}$

$$\text{Solution: } I_f = \frac{8000(62.5)(10)^{-6} \pi (396)^4}{4(60)(10.3)(10)^6}; \quad I_f = 15.63 \text{ in}^4$$

Frame section:

Frame depth:  $d = 9 \text{ inches}$

$$\text{Required cap area: } A = \frac{2I}{d_e^2}; \quad A = \frac{2(15.63)}{(8.75)^2} = 0.408 \text{ in}^2/\text{cap}$$

Effective depth:  $d_e = 8.75$

Equivalent web thickness of the truss:  $t_w = 0.06$

$$\text{Frame } \Delta \bar{t}: \Delta \bar{t} = \frac{[2(0.408) + 9(0.060)]}{60} = 0.023 \text{ inch}$$

### 3.2.2 LH<sub>2</sub> TANK WEIGHT SENSITIVITY TO FACTOR OF SAFETY PERTURBATIONS.

The results of weight sensitivity analyses for perturbations of ultimate and yield factors of safety are presented in this section for the liquid hydrogen tank. Analysis was performed for the forward and aft dome assemblies, the cylindrical section skin-stringer, the belt and TPS support frames, and the LH<sub>2</sub> tank as a whole. The curves presented, in general, show the variation of weight as a function of ultimate factor of safety ( $FS_u$ ) assuming ultimate design is critical. The figures also give cutoffs for certain yield factors of safety ( $FS_y$ ), and for proof design for a service life of 100 missions and a scatter factor of 1.5.

3.2.2.1 Forward and Aft LH<sub>2</sub> Tank Domes. Figures 3-8 and 3-9 present the weight sensitivities of the LH<sub>2</sub> tank forward (upper) and aft (lower) dome assemblies to factor of safety perturbations. The curves labeled ultimate design are based on the assumption that the design of the domes is critical for the ultimate strength of the material when loaded by  $FS_u$  multiplied by the limit operating load. Cutoffs for  $FS_y = 1.0, 1.1$ , and  $1.2$  are based on the assumption that the design of the domes is critical for the yield strength of the material when loaded by  $FS_y$  multiplied by the limit operating load. The cutoff for proof design establishes the baseline weight for the forward dome, and is shown in Figure 3-8 for comparison purposes.

The proof design cutoff is determined by application of a proof factor to limit operating loads, and then designing the structure to withstand this load without yielding. The proof test at this load then guarantees a 100 mission safe-life for flaw growth at a scatter factor of 1.5. The proof factor,  $\alpha$ , is 1.13 for the liquid hydrogen tank. The aft LH<sub>2</sub> tank dome is critical for ultimate operating pressure. Resizing of the end domes for perturbations of the factors of safety was accomplished by use of the computer program that was also used for the baseline sizing of the dome. The baseline weight for the forward LH<sub>2</sub> tank dome is 2483 pounds, and for the aft dome it is 2468 pounds.

3.2.2.2 Belt Frames and TPS Support Frames. The weight sensitivity of the LH<sub>2</sub> tank stabilizing belt frames and TPS support frames to factor of safety perturbations is given in Figure 3-10. Frame weight for the curves of Figure 3-10 was determined by means of a computer sizing program that uses the Shanley criterion (Section 3.2.1.2) and the maximum axial compression load at a station for a particular factor of safety. One point should be clearly understood when reading the curves of Figure 3-10. This point is that for these curves the factor of safety,  $FS_u$ , varies only for the load conditions for which the particular curve is so labeled. On that same curve the factor of safety,  $FS_u$ , for other load conditions is held constant at the baseline value. The curve with the highest slope, which is labeled ALL LAUNCH VEHICLE TYPE CONDITIONS (EXCLUDES CONDITIONS 13, 14, 15, 16, 23, 24) is actually the same as the curve that would have been produced had the factor of safety been varied for all 25 load conditions investigated. The reason is that the launch-vehicle-type conditions are so much more critical to the LH<sub>2</sub> tank structure than the aircraft-type load conditions

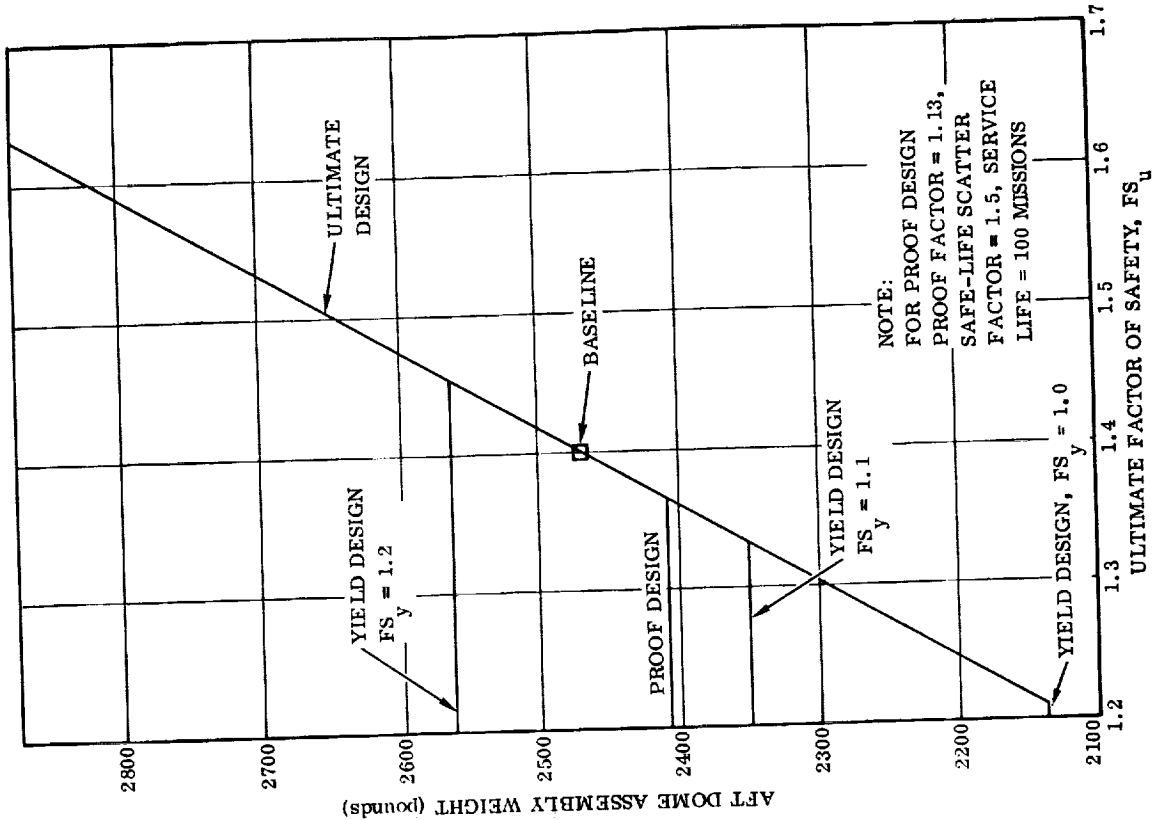


Figure 3-8. Forward LH<sub>2</sub> Tank Dome Assembly Weight Sensitivity to Factor of Safety Perturbations

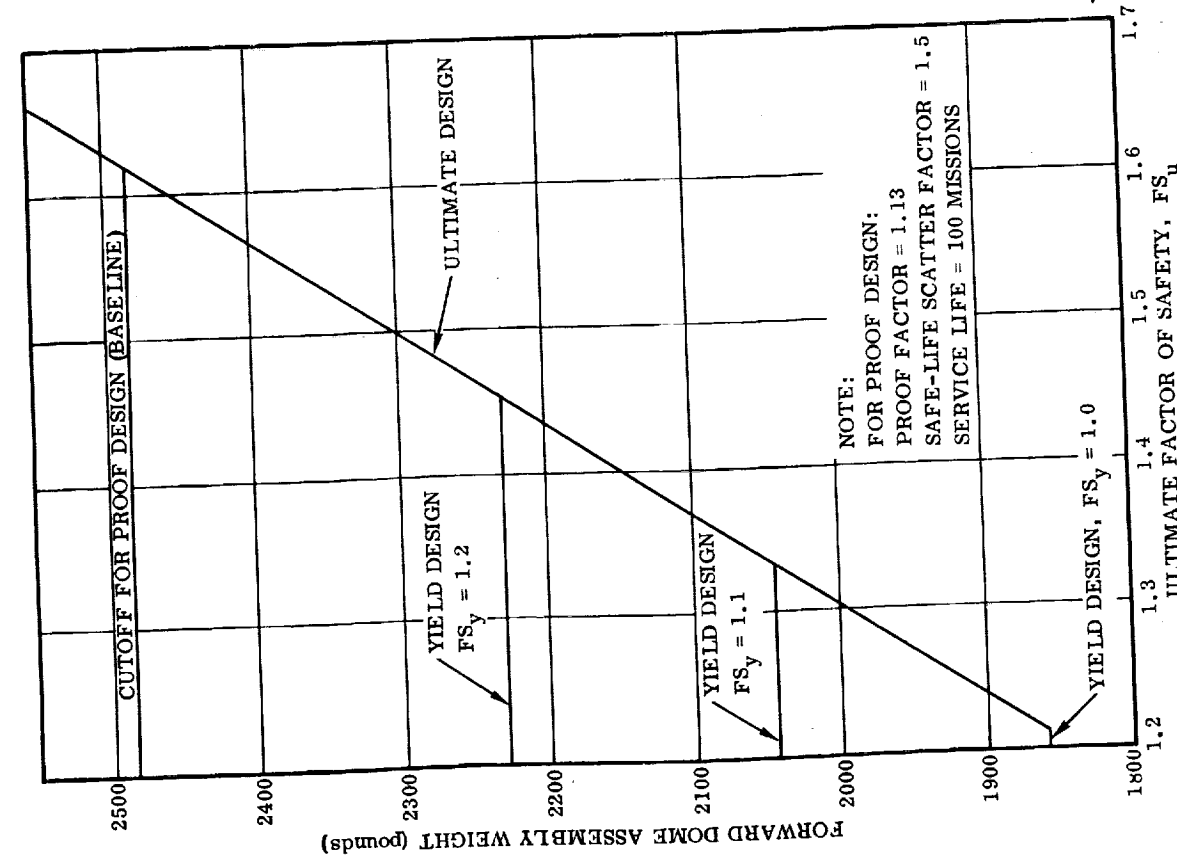


Figure 3-9. Aft LH<sub>2</sub> Tank Dome Assembly Weight Sensitivity to Factor of Safety Perturbations

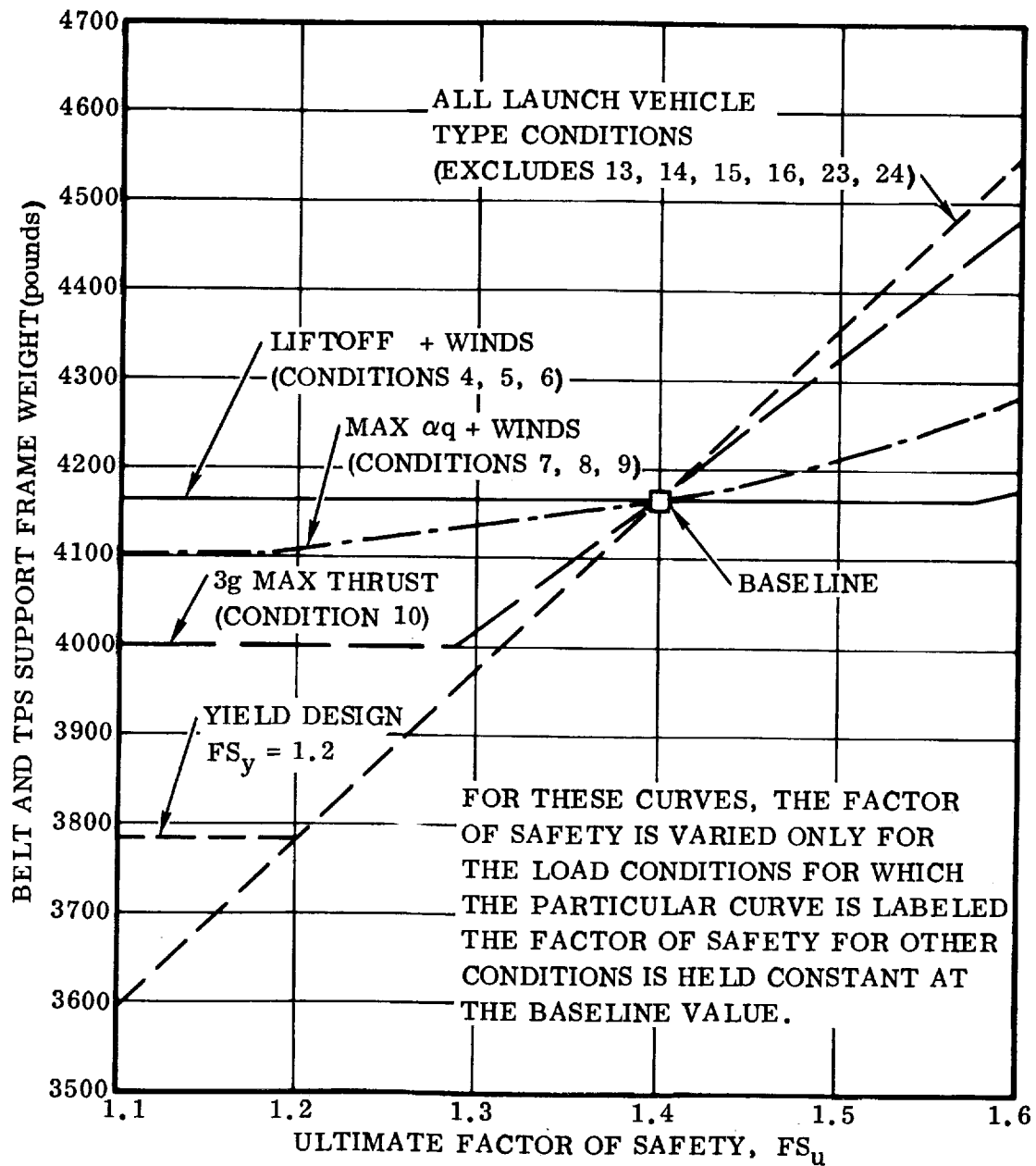


Figure 3-10. Belt Frames and TPS Support Frames Weight Sensitivity to Factor of Safety Perturbations for Selected Load Conditions

(13, 14, 15, 16, 23, 24) that even when the factor of safety on the launch-vehicle-type conditions was reduced to very low level, the aircraft-type load conditions were still not critical even with their high baseline factor of safety of 1.5. This curve therefore provides the overall weight sensitivity to factor of safety perturbations, and also provides a basis for comparison for the other curves presented in the figure.

Examination of Figure 3-10 reveals that that 3g maximum thrust condition (10) is the most critical condition for the stabilizing belt frames and TPS support frames and thus reduction of  $FS_u$  on this condition provides the greatest opportunity for weight savings, if it is not desired to alter  $FS_u$  on all conditions simultaneously as is illustrated by the curve labeled ALL LAUNCH VEHICLE TYPE CONDITIONS. On the other extreme, the figure shows that alteration of  $FS_u$  on the liftoff plus winds load conditions (4,5,6) produces no weight change for the frames except for large values of  $FS_u$ . It will be noted that the curves for maximum  $\alpha q$  plus winds (7,8,9) and 3g maximum thrust (10) remain constant for lower values of  $FS_u$ . This occurs because  $FS_u$  is being perturbed only for a load condition or group of load conditions at one time; thus, when the curve becomes constant below a certain  $FS_u$ , it means other conditions that still have  $FS_u$  at the baseline become critical. The baseline weight of the frames is 4167 pounds.

**3.2.2.3 LH<sub>2</sub> Tank Skin-Stringer.** The weight sensitivity of the liquid hydrogen tank skin-stringer to factor of safety perturbations is presented in Figure 3-11. Skin-stringer weights for the curves of Figure 3-11 were determined by means of the same computer sizing program used to size the baseline vehicle. In most areas the skin is designed by flight axial and shear loads. In locations where operating loads are low, however, the skin thickness is determined by proof pressure. In this case the proof pressure is determined by the requirement for a 100 mission service life with a scatter factor of 1.5.

Inspection of Figure 3-11 reveals that comments made in Section 3.2.2.2 for the belt and TPS support frames also apply to the skin-stringer structure, for the most part. However, the weight sensitivity of the skin-stringer is not as heavily influenced by individual conditions. Cutoffs are given where yield design is critical. For the range of safety factors investigated,  $FS_u = 1.1$  through 1.6 and  $FS_y = 1.0$  through 1.2, yield design is critical only for  $FS_y > FS_u$ . The cutoffs shown in the figure are for  $FS_y = 1.2$ . The baseline weight of the LH<sub>2</sub> skin-stringer is 52,486 pounds.

**3.2.2.4 Liquid Hydrogen Tank.** The weight sensitivity of the entire liquid hydrogen tank to factor of safety perturbations is presented in Figure 3-12. Curves are presented in Figure 3-12. Curves are presented in this figure for all of the critical design conditions and for  $FS_u = 1.1$  through 1.6 and  $FS_y = 1.0$  through 1.2. All LH<sub>2</sub> tank elements discussed in Sections 3.2.2.1 through 3.2.2.3 and presented in Figures 3-8 through 3-11 are included in Figure 3-12 with the addition of the orbiter support frames at Stations 2666 and 2866 and the associated tank beef-up required. For the curves of Figure 3-12, the forward tank dome assembly is designed by proof pressure for a 100 mission service life and a safe-life scatter factor 1.5; therefore, its weight does not

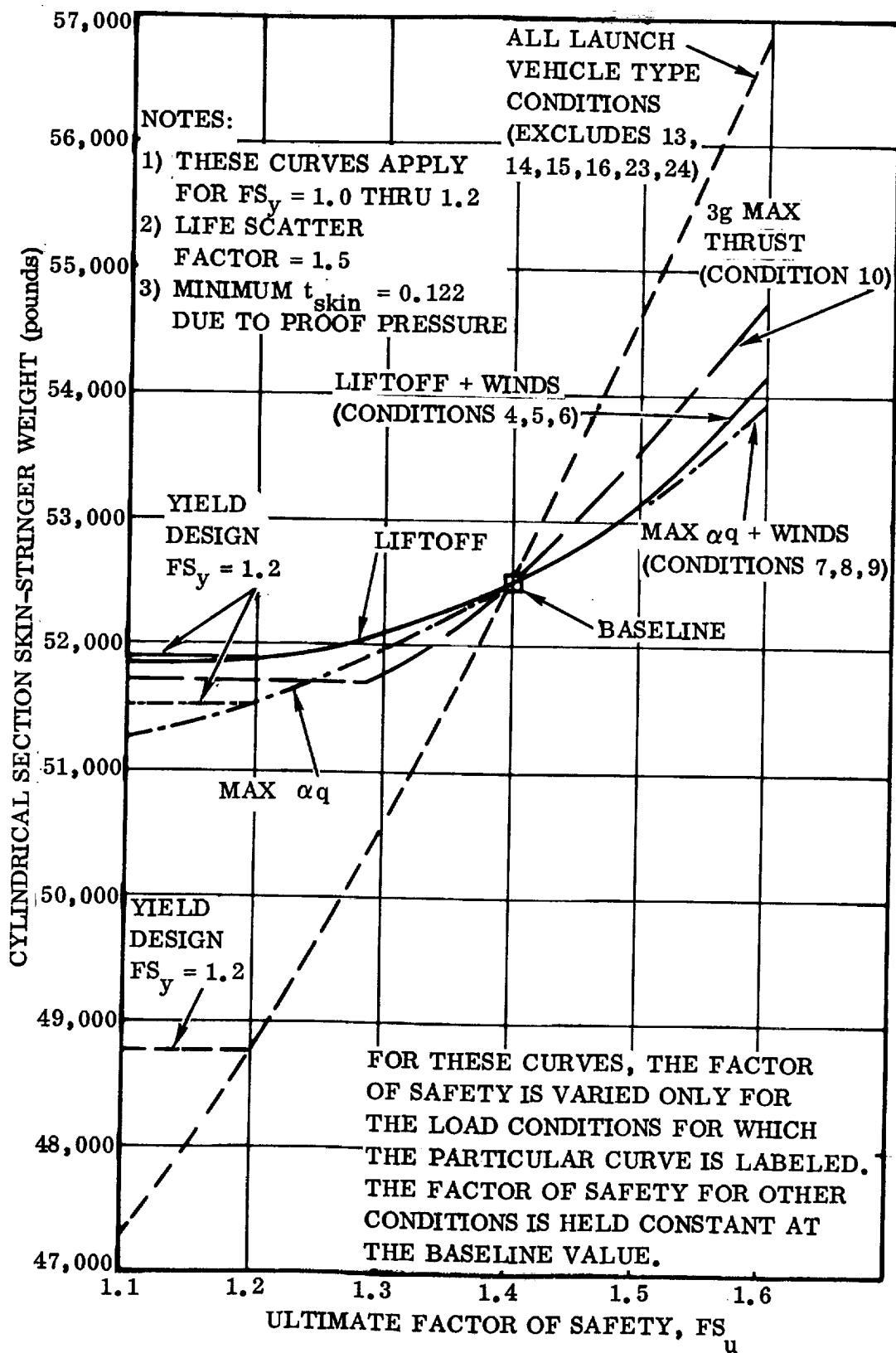


Figure 3-11. LH<sub>2</sub> Tank Cylindrical Section Skin-Stringer Weight Sensitivity to Factor of Safety Perturbations for Selected Load Conditions

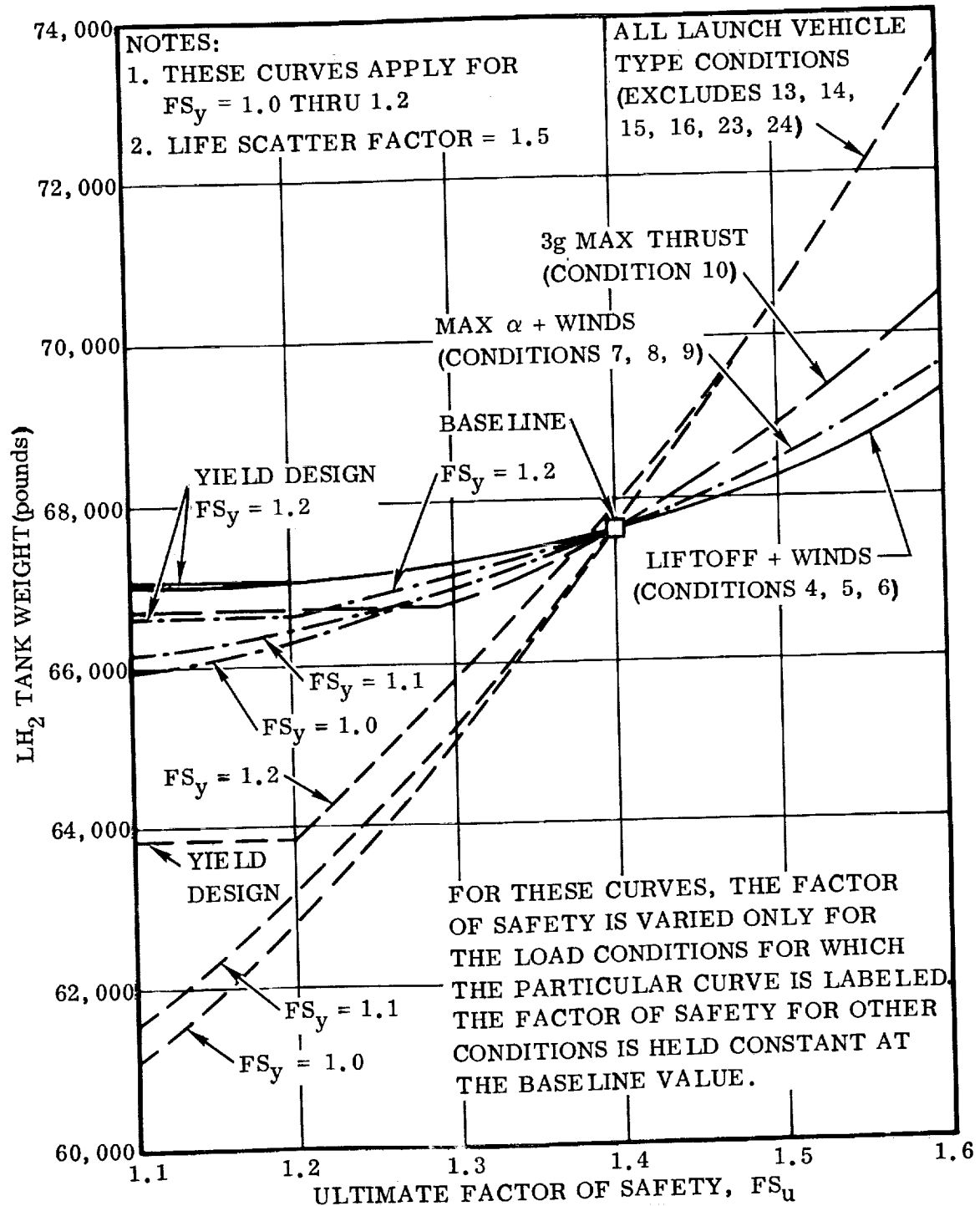


Figure 3-12.  $LH_2$  Tank Weight Sensitivity to Factor of Safety Perturbations for Selected Load Conditions



vary with factor of safety although the constant dome weight is included in the curves. For the liftoff plus winds curve (4,5,6) the weights of the lower dome and the aft orbiter support frames remain constant since they are not sensitive to factor of safety perturbations for this condition. For some of the load conditions of Figure 3-12, there are

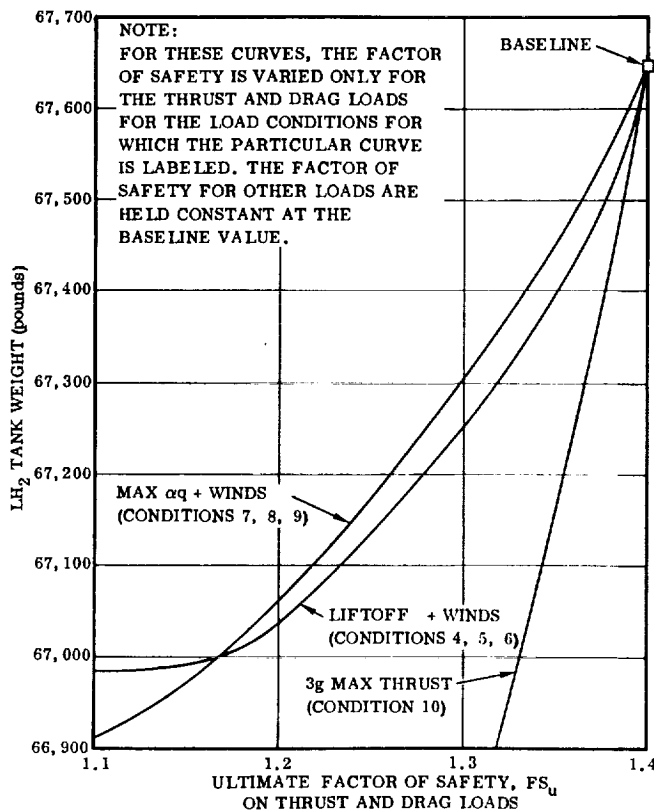


Figure 3-13. LH<sub>2</sub> Tank Weight Sensitivity to Reduced  $FS_u$  on Thrust and Drag Loads Only for Selected Load Conditions

separate curves for different values of  $FS_y$  for the lower values of  $FS_u$ . The presence of these differences is explained by the fact that various elements of the tank are critical for yield design when  $FS_u$  becomes low enough. The baseline weight of the LH<sub>2</sub> tank is 67,645 pounds.

Figure 3-13 presents the weight sensitivity to factor of safety perturbations on thrust and selected critical load conditions. The factor of safety is held constant at the baseline for all airload and tank pressure loads for these conditions. For these same curves other load conditions are used with their baseline factors of safety. The curves give the relative weight effectiveness of reducing the factor of safety on thrust loads. This type of information is desirable since thrust loads are more accurately predicted than, say, gust loads so that it is possible to use a reduced factor of safety. The service life was held constant at 100 missions and the safe-life scatter factor at 1.5 for the analysis and therefore the tank skin thickness did not drop below 0.122 inch.

### 3.3 AFT ORBITER SUPPORT FRAME

**3.3.1 AFT ORBITER SUPPORT FRAME STRUCTURAL SIZING.** The principal aft support point of the orbiter to the booster is located at Station 2666. A substantial body frame is provided at this station to distribute orbiter loads to the booster body shell. Figure 3-14 shows the critical applied loads (ultimate), and Figure 3-15 shows the element identification.

A finite element computer solution was used to size the frame, and the model, geometry, applied loads, section properties, and internal loads are shown on the following pages. The material of the frame is 2219-T87 aluminum alloy. The room temperature properties of this material are:

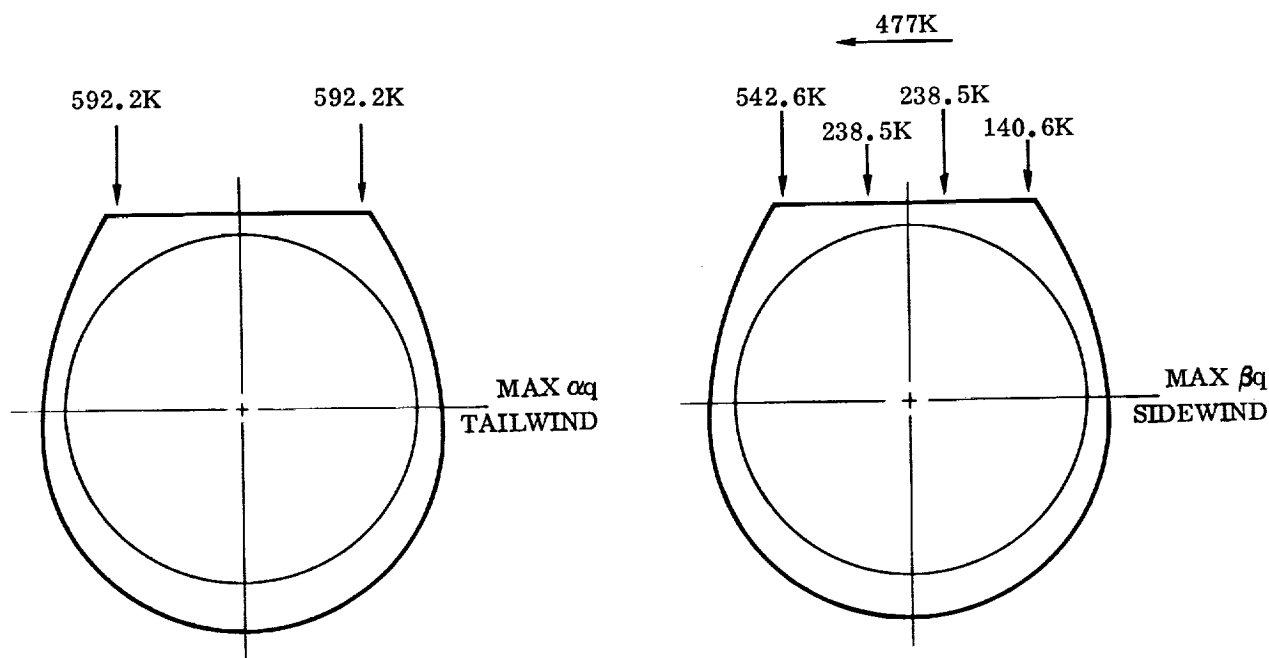


Figure 3-14. Critical Applied Loads (Ultimate),  
Aft Orbiter Attachment Frame

$$F_{tu} = 63 \text{ ksi}$$

$$F_t \text{ at limit load} = \frac{F_{tu}}{1.40} = \frac{63}{1.40} = 45 \text{ ksi}$$

$$F_{cy} = 51 \text{ ksi}$$

$$F_{su} = 37 \text{ ksi}$$

To allow for the effects of fastener holes, welds, and other strength reducers, these properties were reduced for member sizing to the following values for use with ultimate loads.

$$F_t = F_c = 50 \text{ ksi}$$

$$F_s = 20 \text{ ksi}$$

Table 3-4 lists cap axial loads and cross-sectional areas, and Table 3-5 lists the web shear flows and thicknesses.

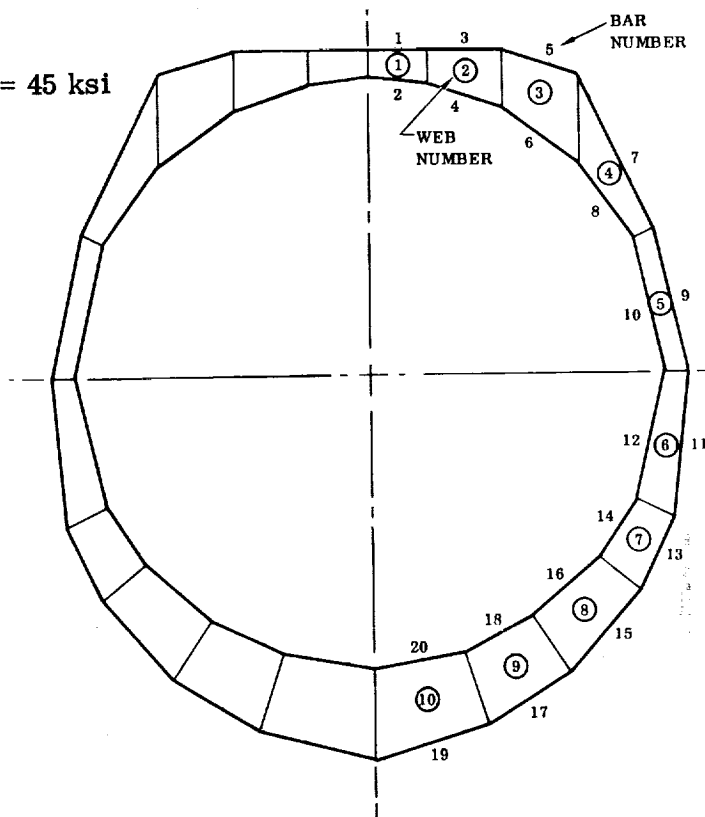


Figure 3-15. Aft Orbiter Attachment Frame  
Element Identification

Table 3-4. Aft Orbiter Attachment Frame, Cap Axial Loads and Cross-Sectional Areas

Bar	Length (inches)	Ultimate Axial Loads (kips)			Area* (in <sup>2</sup> )
		Max. $\alpha q$	Max. $\beta q$		
			Left	Right	
1	40	-56	302	-375	7.5
2	40	-227	-234	-11	4.6
3	50	-125	220	-376	7.5
4	53	-130	-180	87	3.6
5	52	-223	-1	-260	5.2
6	62	44	30	74	1.5
7	117	-424	-106	-373	8.5
8	64	63	87	-161	3.2
9	98	-110	-52	-62	2.2
10	91	-120	25	-185	3.7
11	102	19	-5	33	0.5
12	91	-82	-14	-87	1.7
13	55	1	1.7	0	0.5
14	47	3	-7.5	12	0.5
15	69	-5	0.6	-6.3	0.5
16	57	15	-0.5	22	0.5
17	67	-6	-0.9	-6.4	0.5
18	53	12	0.8	14.1	0.5
19	80	-6	-2.2	-4.2	0.5
20	62	6	1.1	5.6	0.5

\* Assume  $F_t = F_c = 50$  ksi ultimate

Table 3-5. Aft Orbiter Attachment Frame, Web Shear Flows and Thicknesses

Web	Area (in <sup>2</sup> )	Ultimate Shear Flow (kips/in)			t* (in.)
		Max. $\alpha q$	Max. $\beta q$		
			Left	Right	
1	722	1.1	4.3	5.7	0.29
2	1493	1.9	6.7	4.7	0.34
3	2441	1.8	2.1	0.11	0.11
4	2048	7.5	0.57	8.4	0.42
5	1471	3.5	1.00	2.9	0.50
6	2103	0.32	0.16	0.66	0.33
7	1631	0.21	0	0.26	0.13
8	2483	0.06	0	0.01	0.04
9	2854	0.01	0	0	0.04
10	3947	0	0	0.01	0.04

\* Assume  $F_s = 20$  ksi ultimate

**3.3.2 AFT ORBITER SUPPORT FRAME WEIGHT SENSITIVITY TO FACTOR OF SAFETY PERTURBATIONS.** The results of weight sensitivity analyses for perturbations of ultimate and yield factors of safety are presented in this section for the Station 2666 aft orbiter support bulkhead. The weight sensitivity curves are presented in Figure 3-16. The curve marked ULTIMATE DESIGN shows the weight variation of the frame for ultimate factors of safety ranging from 1.1 to 1.6 for the two critical design conditions, maximum  $\alpha q$  tailwinds and maximum  $\beta q$ . The cutoffs labeled YIELD DESIGN give the weights for  $FS_y = 1.0, 1.1,$  and  $1.2$ . The baseline weight of the frame is 2450 pounds.

The broken-line curve running between  $FS_u = 1.1$  and  $1.4$  shows the weight sensitivity of the frame to the reduction of  $FS_u$  on thrust loads only (and reacting drag and inertia loads) with  $FS_u$  and  $FS_y$  remaining at the baseline of  $1.4$  and  $1.1$  respectively on all airloads. The curve reveals that weight is a minimum for  $FS_u = 1.27$  on thrust and drag. The reason that the curve changes slope is that while the reduction of thrust  $FS_u$  relieves loading on the frame for maximum  $\alpha q$  plus tailwinds, the maximum  $\beta q$  condition becomes more critical for the frame as thrust  $FS_u$  is reduced. As a result the point at which optimum weight is reached is at  $FS_u = 1.27$ .

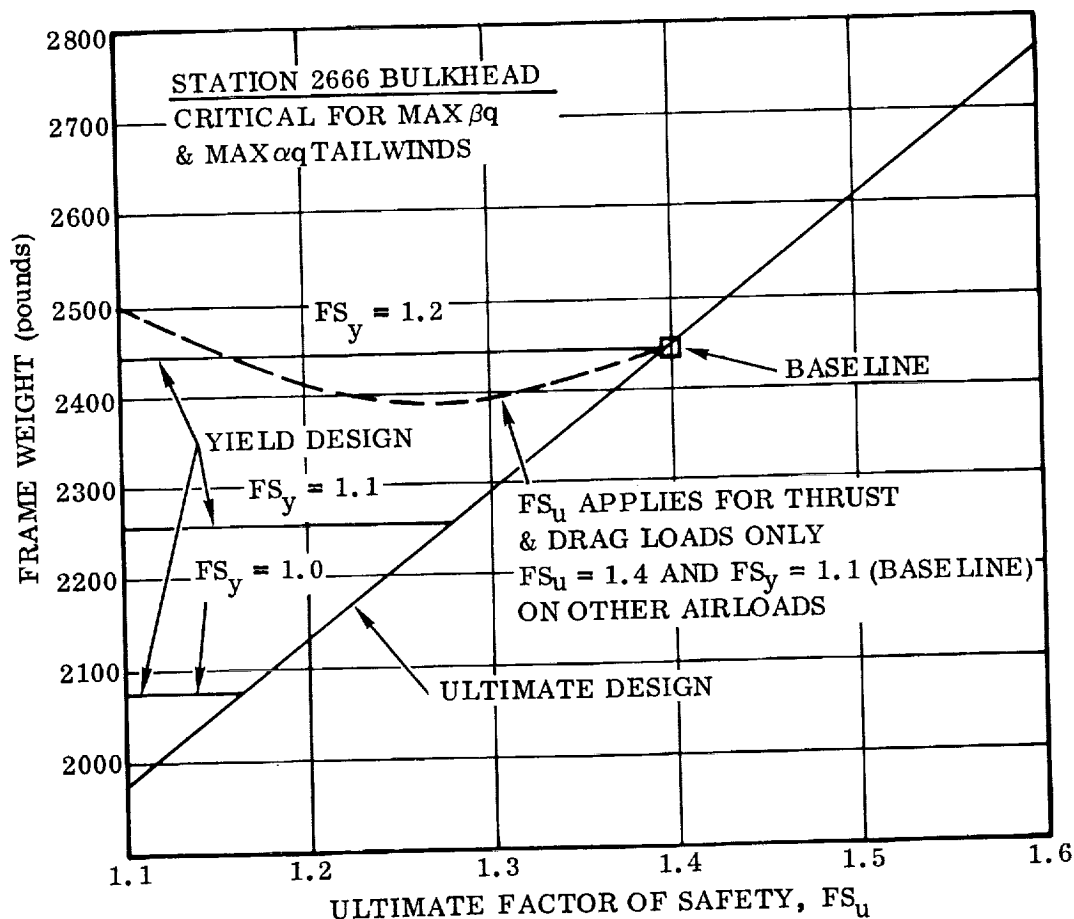


Figure 3-16. Aft Orbiter Support Frame Weight Sensitivity to Factor of Safety Perturbations for All Critical Conditions

### 3.4 THRUST STRUCTURE

**3.4.1 THRUST STRUCTURE STRUCTURAL SIZING.** A finite element model was utilized to determine the theoretical weight of the thrust structure. The idealized model and geometry is shown in Figures 3-17. Figure 3-18 shows thrust structure model elements.

A total of 14 basic loading conditions were initially investigated, plus one or two engine failures for the flight conditions. By assuming an identical structural configuration in each 45-degree segment of the thrust structure model, the number of possible loading combinations with engine failure was reduced. For one engine failed, one of the four inner engines or one of the eight outer engines was considered failed – reducing the number of combinations from 12 to 2. For two engines failed the number of combinations was reduced from 66 to 12. The thrust structure load conditions are:

- |   |                                      |
|---|--------------------------------------|
| 1. One hour ground headwinds              | 7. Maximum $\alpha q$ with headwinds |
| 2. One hour ground tailwinds              | 8. Maximum $\alpha q$ with tailwinds |
| 3. One hour ground sidewinds              | 9. Maximum $\beta q$                 |
| Conditions 4 through 11 were run with:    |                                      |
| a. No engines out.                        | 10. Three g maximum thrust           |
| b. With one engine out.                   | 11. Booster burnout                  |
| c. With two engines out.                  | 17. One day ground headwinds         |
| 4. Liftoff plus one hour ground headwinds | 18. One day ground tailwinds         |
| 5. Liftoff plus one hour ground tailwinds | 19. One day ground sidewinds         |
| 6. Liftoff plus one hour ground sidewinds |                                      |

A computerized analysis was made with these loading conditions. From the resulting internal loads it was determined that only seven loading conditions were critical for design. Conditions eliminated did not occur in the maximum/minimum search or were slightly critical in only a few areas; consequently, these conditions have a negligible effect on the overall results. The critical conditions are as follows:

- 7 Maximum  $\alpha q$  headwinds
- 7 IE Maximum  $\alpha q$  headwinds (inner engine failed)
- 7 OE Maximum  $\alpha q$  headwinds (outer engine failed)
- 10 Three g maximum thrust
- 10 IE Three g maximum thrust (inner engine failed)
- 10 OE Three g maximum thrust (outer engine failed)
- 19 One day ground sidewinds

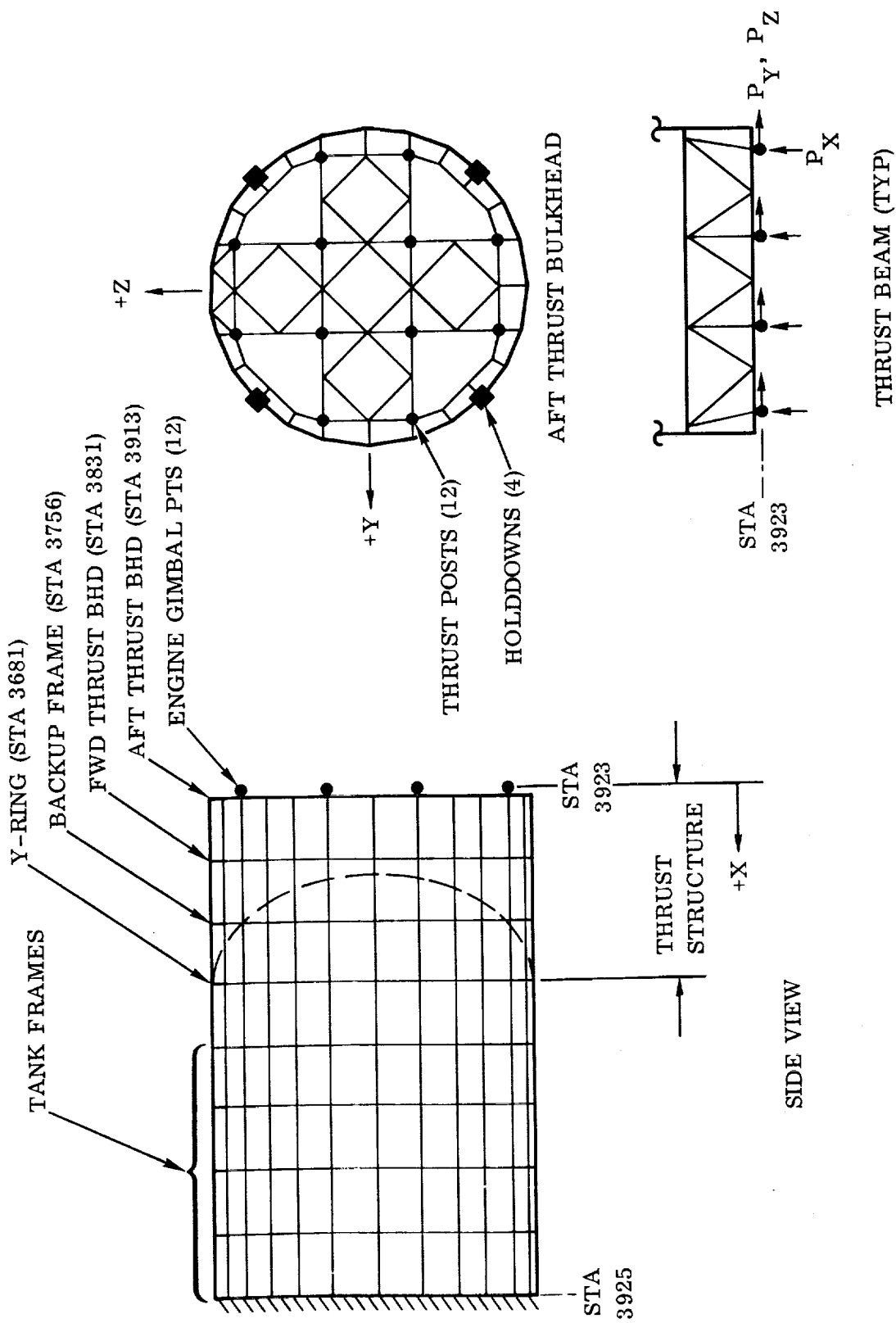


Figure 3-17. Thrust Structure Finite Element Model

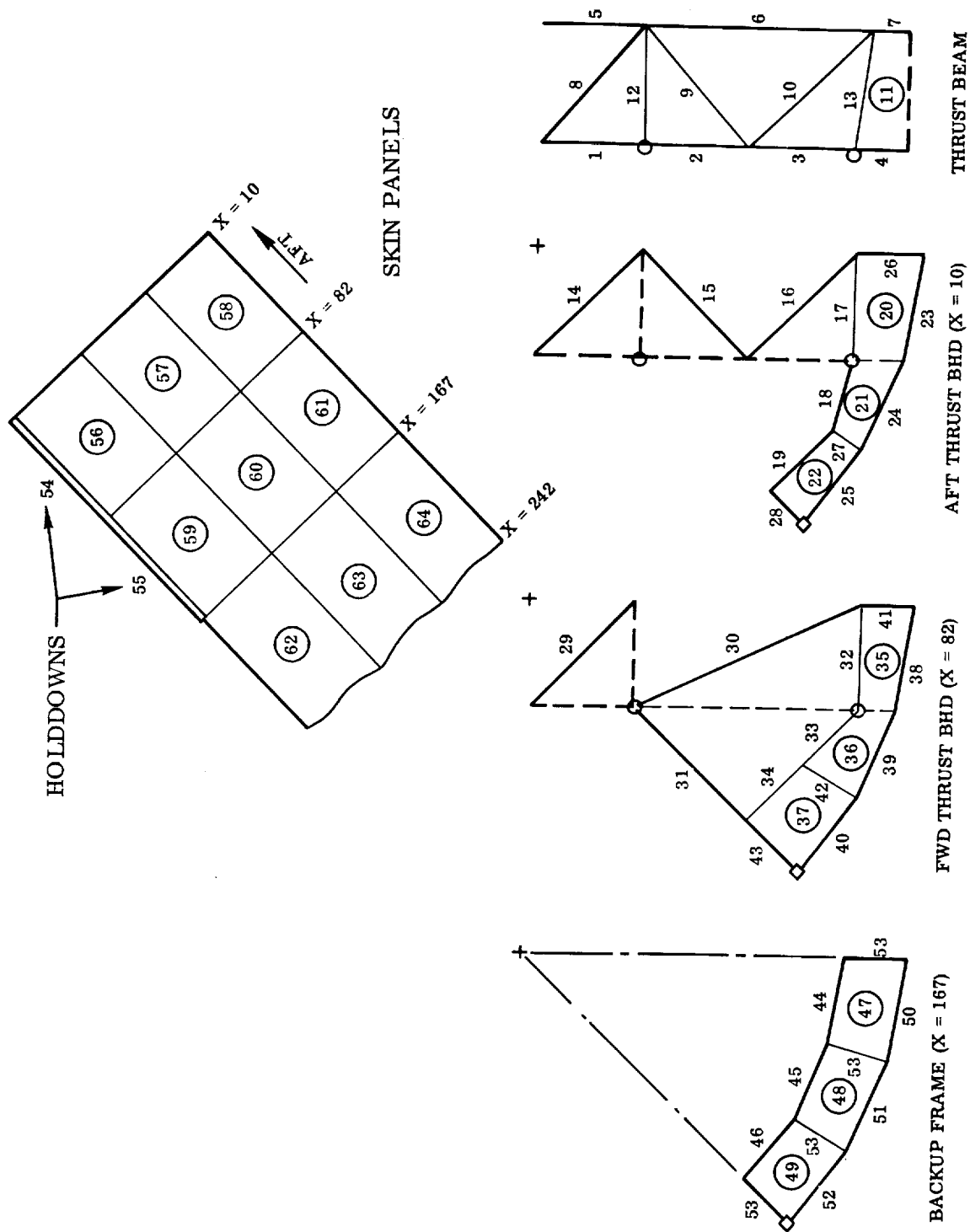


Figure 3-18. Thrust Structure Model Elements

Ultimate applied loads are shown in Table 3-6. Table 3-7 lists the element number, maximum load, cross-sectional area and thickness, applied and allowable stress, and element weight based on the material properties given below.

As noted in Section 2.3, the structural members of the thrust structure are of Ti-6Al-4V annealed titanium, having the following room temperature properties:

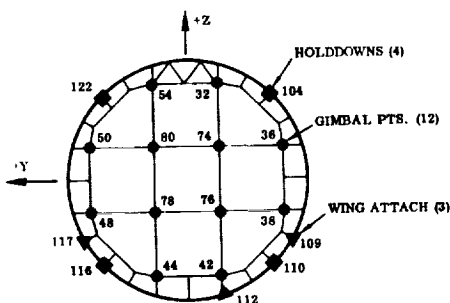
$$F_{tu} = 130 \text{ ksi (Reference 9)}$$

$$F_t \text{ at limit load} = \frac{F_{tu}}{1.40} = \frac{130}{1.40} = 92.86 \text{ ksi}$$

$$F_{cy} = 126 \text{ ksi}$$

$$F_{su} = 76 \text{ ksi}$$

Table 3-6. Thrust Structure Ultimate Design Loads



Conditions		Ultimate Loads (pounds)			Locations
		P <sub>x</sub>	P <sub>y</sub>	P <sub>z</sub>	
19	1 Day Ground Sidewinds	1,065,367	-38,280	4,202	104
		1,065,537	-104,926	4,212	110
		2,467,059	-104,926	70,858	116
		2,466,889	-38,280	70,858	122
7	Maximum alpha-q Headwinds	809,000	-187,920	32,36,38,42,44,48,50,54,74,76,78,80	109
			185,610	508,470	112
			46,300		117
			-185,610	508,470	117
7 IE	Maximum alpha-q Headwinds (Inner Engine Out)	882,610	-205,000	32,36,38,42,44,48,50,54,74,76,78,80	109
			185,610	508,470	112
			46,300		117
			-185,610	508,470	117
7 OE	Maximum alpha-q Headwinds (Outer Engine Out)	882,610	-205,000	32,36,38,44,48,50,54,74,76,78,80	109
			185,610	508,470	112
			46,300		117
			-185,610	508,470	117
10	3g Maximum Thrust	920,990	-67,680	32,36,38,42,44,48,50,54,74,76,78,80	
10 IE	3g Maximum Thrust (Inner Engine Out)	1,004,700	-73,832	32,36,38,42,44,48,50,54,74,78,80	
10 OE	3g Maximum Thrust (Outer Engine Out)	1,004,700	-73,832	32,36,38,44,48,50,54,74,76,78,80	



Table 3-7. Thrust Structure Model Element Loads, Areas, Thicknesses, Stresses, and Weights

THRUST BEAMS									
Element	A. L. (lb) q (lb/in)	A (sq in) t (in.)	Comments	Stress (psi)		L (in.) A (sq in)	No. of Elements	Weight (lb)	
				Applied	Allowable				
1	-1,013,000	10.31	Cruciform 7 x 7 x 0.78	$f_c = 98,300$	99,000	54.50	8	719.2	
2	-998,400	10.19	Cruciform 7 x 7 x 0.77	$f_c = 97,800$	99,000	54.50	8	710.9	
3	-263,300	3.44	Cruciform 7 x 7 x 0.25	$f_c = 76,600$	79,000	54.50	8	240.0	
4	-205,800	2.34	Cruciform 5 x 5 x 0.24	$f_c = 87,800$	88,500	26.85	8	80.4	
5	776,000	6.10	Cruciform 7 x 7 x 0.45	$f_t = 127,200$	130,000	109.00	4	425.5	Aft Flange Weight = 1750
6	476,300	3.71	Cruciform 7 x 7 x 0.27	$f_t = 128,400$	130,000	125.50	8	596.0	
7	-123,000	3.71	Cruciform (same as Element 6)		130,000	10.35	8	49.2	
8	-392,000	4.48	Tube 7 O. D. x 0.21 wall	$f_c = 87,500$	89,500	98.46	8	564.6	Fwd Flange Weight = 1071
9	818,400	6.32	Tube 8 O. D. x 0.26 wall	$f_t = 129,500$	130,000	98.46	8	796.5	
10	-901,500	10.23	Tube 8 O. D. x 0.43 wall	$f_c = 88,100$	90,600	108.47	8	1420.3	
11	(17,160)	(0.300)	Web	$f_s = 57,200$	58,700	(1525)	8	585.6	
12	A. L. = -882,600 M = 2,050,000	14.14	Tube 9.5 O. D. x 0.50 wall	$f_c = 62,400$	119,000		4	742.1	Diagonal and Web Weight = 3367
13	A. L. = -882,600 M = 2,050,000	14.14	Tube 9.5 O. D. x 0.50 wall (aft end)	$f_b = 67,800$	159,000	82.00			
	A. L. = 695,000	5.47	Tube 8.9 O. D. x 0.20 wall (fwd end)	$f_c = 62,400$	119,000				
				$f_b = 67,800$	159,000	83.64	8	1050.3	
				$f_t = 127,100$	130,000				Thrust Post Weight = 1792
									Thrust Beam Total Weight = 7980

Table 3-7. Thrust Structure Model Element Loads, Areas, Thicknesses, Stresses, and Weights, Contd

AFT THRUST BULKHEAD

Element	A. L. (lb) q (lb/in)	A (sq in) t (in.)	Comments	Stress (psi)		L (in.) A (sq in)	No. of Elements	Weight (lb)
				Applied	Allowable			
14	-26,400	0.7014	Tube 3.5 O.D. x 0.065 wall	$f_c = 37,600$	40,000	77.07	4	34.6
15	-64,500	0.9567	Tube 4.75 O.D. x 0.065 wall	$f_c = 67,400$	73,500	77.07	8	94.4
16	-64,500	0.9567	Tube 4.75 O.D. x 0.065 wall	$f_c = 67,400$	73,500	77.07	8	94.4
Brace Weight = 223								
17	-320,000	2.54	Tee	$f_c = 126,000$	126,000	54.50	8	177.2
18	-356,000	2.83	Tee	$f_c = 126,000$	126,000	37.44	8	135.6
19	-256,900	2.04	Tee	$f_c = 125,900$	126,000	44.81	8	117.0
Inner Flange Weight = 430								
20	(4.466)	(0.077)	Web	$f_s = 58,000$	58,700	(1672)	8	164.8
21	(12.340)	(0.211)	Web	$f_s = 58,500$	58,700	(962)	8	259.8
22	(2.542)	(0.060)	Web (0.060 = assumed minimum t)	$f_s = 42,400$	58,700	(1032)	8	79.3
Web Weight = 504								
23	-330,100	2.62	Tee	$f_c = 126,000$	126,000	55.03	8	184.5
24	-413,500	3.28	Tee	$f_c = 126,000$	126,000	50.02	8	210.0
25	-150,400	2.62	Tee (same as Element 23)		126,000	50.01	8	167.7
Outer Flange Weight = 562								
26	38,900	0.50	Assumed minimum area			34.50	4	11.0
27	233,000	2.33		$f_c = 100,000$	100,000	19.16	8	57.1
28	30,000	0.50	Assumed minimum area			24.86	4	8.0
Stiffener Weight = 76								
Aft Thrust Bulkhead Total Weight = 1795								

Table 3-7. Thrust Structure Model Element Loads, Areas, Thicknesses, Stresses, and Weights, Contd

FORWARD THRUST BULKHEAD									
Element	A. L., (lb) q (lb/in)	A (sq in) t (in.)	Comments	Stress (psi)		L (in.) A (sq in)	No. of Elements	Weight (lb)	
29	69,300	0.534	Tube	$f_t = 129,800$	130,000	77.07	4	26.3	
30	69,500	0.535	Tube	$f_t = 129,900$	130,000	136.82	8	93.7	
31	-82,500	1.464	Tube 5.0 O.D. x 0.095 wall	$f_c = 56,400$	61,500	88.74	4	83.1	
32	246,500	1.90	Tee	$f_t = 129,700$	130,000	54.50	8	132.5	Brace Weight = 203
33	353,500	2.72	Tee	$f_t = 130,000$	130,000	45.82	8	159.5	
34	408,000	3.14	Tee	$f_t = 129,900$	130,000	42.92	8	172.5	
35	(3693)	(0.063)	Web	$f_s = 58,600$	58,700	(773)	8	62.3	Inner Flange Weight = 465
36	(3538)	(0.061)	Web	$f_s = 58,000$	58,700	(830)	8	64.8	
37	(711)	(0.060)	Web (0.060 = assumed minimum t)			(1354)	8	104.0	
38	352,500	2.72	Tee	$f_t = 129,600$	130,000	55.03	8	191.6	Web Weight = 231
39	343,100	2.64	Tee	$f_t = 130,000$	130,000	50.02	8	169.0	
40	129,700	2.00	Tee		130,000	50.01	8	128.0	
41	-9,500	0.50	Assumed Minimum Area						Outer Flange Weight = 489
42	13,500	0.50	Assumed Minimum Area			18.00	4	5.8	
43	-73,300	0.73		$f_c = 100,000$	100,000	26.72	8	17.1	
						32.19	4	15.0	Stiffener Weight = 38
Forward Thrust Bulkhead Total Weight = 1425									

Table 3-7. Thrust Structure Model Element Loads, Areas, Thicknesses, Stresses, and Weights, Contd

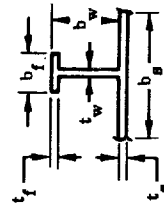
BACKUP FRAME									
Element	A. L. (lb) q (lb/in)	A (sq in) t (in.)	Comments	Stress (psi)		L (in.) A (sq in)	No. of Elements	Weight (lb)	
				Applied	Allowable				
44	-56,100	0.489	Tee 2 x 1 x 0.163	$f_c = 114,700$	115,000	48.09	8	30.1	
45	19,200	0.468	Tee 2 x 1 x 0.156		130,000	43.70	8	26.2	
46	58,400	0.450	Tee 2 x 1 x 0.150	$f_t = 129,800$	130,000	43.70	8	25.2	
						Inner Flange Weight = 81			
47	(594)	(0.040)	Web (0.040 = assumed minimum t)			(1277)	8	65.4	
48	(1302)	(0.040)	Web			(1162)	8	59.5	
49	(983)	(0.040)	Web			(1162)	8	59.5	
						Web Weight = 185			
50	-28,700	0.342	Tee 2 x 1 x 0.114	$f_c = 83,900$	84,500	55.03	8	24.1	
51	-20,900	0.316	Tee 2 x 1 x			50.02	8	20.2	
52	37,800	0.291	Tee 2 x 1 x 0.097	$f_t = 129,900$	130,000	50.01	8	18.6	
						Outer Flange Weight = 63			
53	6,300	0.500	Assumed minimum area			25.00	24	48.0	
						Stiffener Weight = 48.0			
						Backup Frame Total Weight = 377			

HOLDDOWN					
54	-1,916,300	15.21	H-section	$f_c = 126,000$	126,000
55	-1,113,100	8.84	H-section	$f_c = 125,900$	126,000
				Holddown Fittings Total Weight = 1223	

Table 3-7. Thrust Structure Model Element Loads, Areas, Thicknesses, Stresses, and Weights, Contd

SKIN PANELS

Element	Loads (lb/in)		$\bar{t}$ (in.)	Comments*	Stress (psi)				A (sq in)	No. of Elements	Weight (lb)
					Applied		Allowable				
	$N_x$	q			$f_c$	$f_s$	$F_c$	$F_s$			
56	20,334	7520	0.3021	$t_s^{**} = 0.160, t_w^{**} = t_f = 0.140$	67,309	47,000	108,870	80,000	4102	8	1586.2
57	4,752	6905	0.1821	$t_s = 0.120, t_w = t_f = 0.060$	26,100	57,540	63,270	80,000	4102	8	956.1
58	4,358	3167	0.1421	$t_s = 0.080, t_w = t_f = 0.060$	30,810	39,590	55,540	80,000	4512	8	820.7
Aft Bay Skin Panel Weight = 3363											
59	14,106	3910	0.2221	$t_s = 0.160, t_w = t_f = 0.060$	63,510	24,440	71,370	80,000	3751	8	1066.4
60	10,947	5372	0.2221	$t_s = 0.160, t_w = t_f = 0.060$	49,290	33,580	71,370	80,000	3752	8	1066.5
61	10,862	4033	0.2021	$t_s = 0.140, t_w = t_f = 0.060$	53,750	28,810	67,300	80,000	4127	8	1067.6
Center Bay Skin Panel Weight = 3201											
62	12,175	2719	0.2021	$t_s = 0.140, t_w = t_f = 0.060$	60,240	19,420	67,300	00,000	3751	8	970.4
63	11,567	3756	0.2021	$t_s = 0.140, t_w = t_f = 0.060$	57,230	26,830	67,300	80,000	3752	8	970.6
64	11,539	3675	0.2021	$t_s = 0.140, t_w = t_f = 0.060$	57,100	26,250	67,300	80,000	4127	8	1067.7
Forward Bay Skin Panel Weight = 3009											
										Skin Panels Total Weight = 9573	



$$b_s = 4, b_w = 3, b_f = 1.2$$

\*\*  $t_s$  and  $t_w$  were determined through the utilization of a plate-stringer optimization program.

**3.4.2 THRUST STRUCTURE WEIGHT SENSITIVITY TO FACTOR OF SAFETY PERTURBATIONS.** The weight sensitivity of the B-9U thrust structure to perturbations of factor of safety is presented in Figures 3-19 and 3-20. The curve labeled **ULTIMATE DESIGN** in Figure 3-19 gives the relationship of weight to  $FS_u$  for the assumption that structural members are designed for the ultimate allowable strength of the material when loaded by  $FS_u$  multiplied by limit operating load. The cutoffs labeled **YIELD DESIGN** are based on the assumption that members are critical for the yield allowable when loaded by  $FS_y$  multiplied by limit operating load. Weights for yield design are given for  $FS_y = 1.1$  and  $1.2$ . The baseline weight of the thrust structure is 25,067 pounds.

The weight sensitivity of the thrust structure to perturbations of  $FS_u$  on thrust loads only, while holding  $FS_u = 1.4$  and  $FS_y = 1.1$  (baseline) for other loads is shown in Figure 3-20. The broken-line curve in this figure is a duplicate of the curve for ultimate design in Figure 3-19, and is shown for comparison. This comparison shows that the thrust structure is highly sensitive to the thrust factor of safety, and that significant weight changes can be obtained by varying  $FS_u$  on thrust.

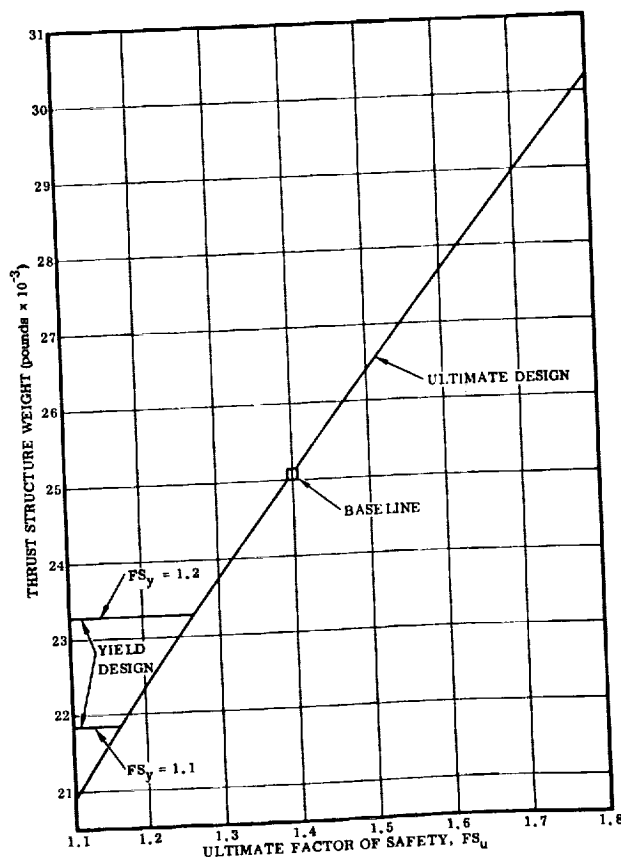


Figure 3-19. Thrust Structure Weight Sensitivity to Factor of Safety Perturbations for All Critical Conditions

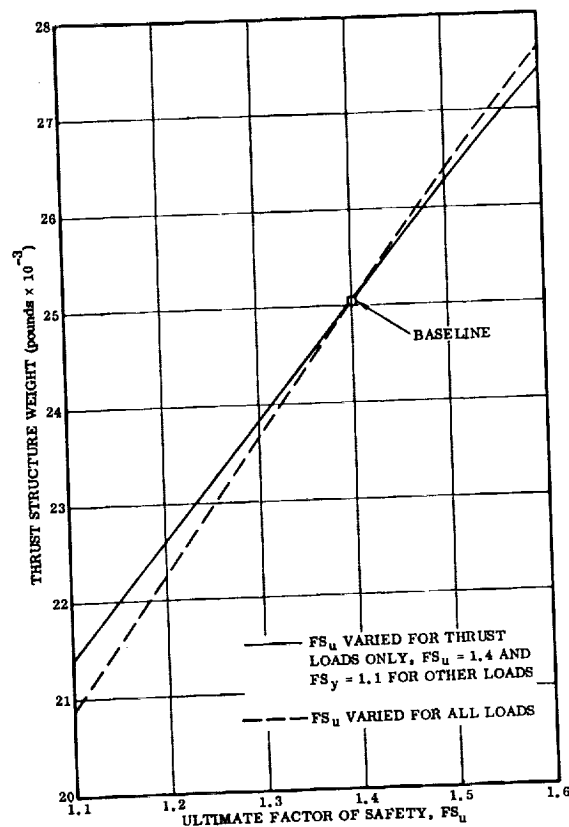
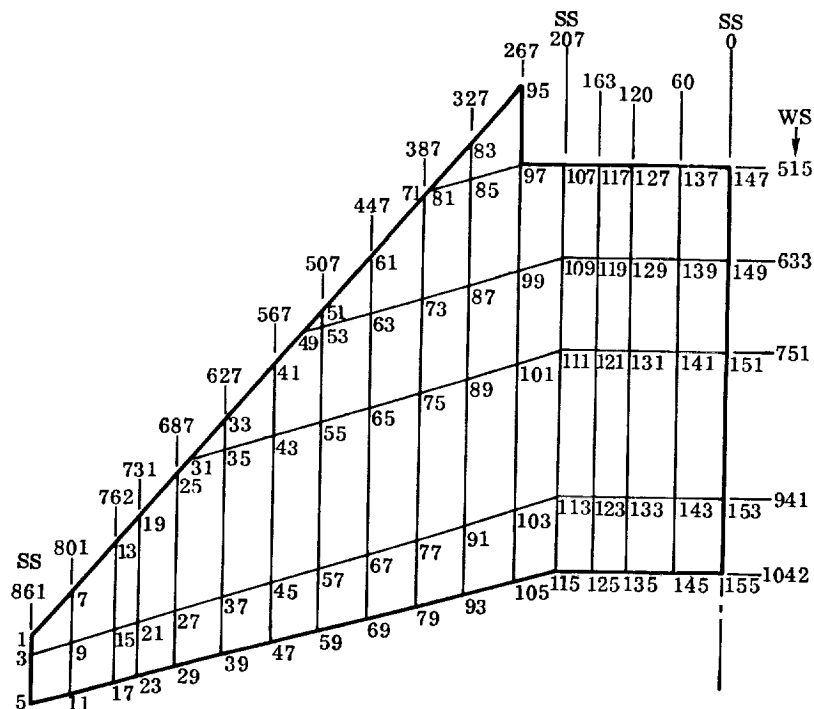


Figure 3-20. Thrust Structure Weight Sensitivity to Perturbation of  $FS_u$  for Thrust Loads Only

### 3.5 WING BOX

**3.5.1 WING BOX STRUCTURAL SIZING.** Primary structural components such as spars and ribs are sized by maximum  $\alpha q$  loads during boost (Condition W1). This condition is critical because it combines high air loads and low relieving inertia loads. A finite element solution was programmed using a structural simulation model consisting of 156 nodes and 1073 constant stress elements, as shown in Figure 3-21. Skin corrugations were simulated in shear with quadrilateral plate elements. Orthotropic triangles with negligible shear stiffness were superimposed to simulate the unidirectional extensional stiffness of the skins. Spar cap loads obtained from the computer solution are tabulated in Table 3-8 for Condition W1 and spar sizing data is presented in Tables 3-9 through 3-13.



B-9U space shuttle wing box simulation node points for upper surface. Add "1" to the upper surface nodes to obtain the node numbering for the lower surface.

Figure 3-21. B-9U Wing Structural Simulation Model

Table 3-8. Spar Cap Loads, B-9U Wing

S. STA.	P <sub>LE</sub>	P <sub>1</sub>	P <sub>2</sub>	P <sub>3</sub>	P <sub>4</sub>	P <sub>5</sub>		ΣP <sub>1</sub> -P <sub>5</sub>
	(KIPs)	(KIPs)	(KIPs)	(KIPs)	(KIPs)	(KIPs)		(KIPs)
861						-		
						-		
801	-3.2					-10.		-10
	+2.0				-	-		-
762	+1.0				-50	-25		-75
	-1.0				+20	+10		+30
731	+1.0				-105	-47		-152
	0.0				+50	+18		+68
637	-29.0			-75	-200	-85		-360
	+7.0			-	+100	+40		+140
627	-16.0			-235	-300	-120		-655
	+43.0			+110	+150	+80		+340
567	-51.0			-395	-360	-145		-900
	+33.0			+310	+170	+135		+615
507	-12.0		-145	-525	-430	-175		-1275
	+37.0		+90	+500	+240	+180		+1010
447	-15.0		-280	-650	-520	-240		-1690
	+33.0		+245	+415	+625	+220		+1505
337	-12.0		-425	-825	-650	-330		-2230
	+30.0		+385	+700	+660	+245		+1990
327	-4.0	-100	-480	-1000	-810	-410		-2800
	+8.0	+110	+440	+795	+935	+275		+2555
267	-2.0	-220	-595	-1250	-1035	-505		-3605
	+2.0	+255	+530	+880	+945	+320		+2930
207		-295	-730	-1385	-1180	-460		-4050
		+375	+670	+1020	+1245	+445		+3755
163		-315	-735	-1375	-1190	-465		-4080
		+415	+715	+1105	+1265	+500		+4000
120		-335	-755	-1400	-1215	-482		-4187
		+420	+540	+1150	+1290	+480		+3880
60		-365	-790	-1465	-1240	-480		-4340
		+440	+760	+1225	+1330	+515		+4270
0		-400	-830	-1555	-1360	-495		-4640
		+460	+765	+1305	+1360	+510		+4420



Table 3-9. Sizing Data — Spar No. 1 (WS 515), B-9U Wing

SS	$A_c$	$W_c$	$t_c$	$W_u$	$t_u$	$W_d$	$t_d$
327	3.56	4.08	0.218	2.09	0.074	4.14	0.036
267	5.19	4.54	0.285	2.64	0.099	4.39	0.055
207	6.56	4.86	0.338	3.88	0.18	4.62	0.075
163	6.84	3.90	0.44	3.25	0.107	3.77	0.034
120	7.06	3.93	0.45	3.50	0.11	3.68	0.023
60	7.30	4.81	0.38	2.96	0.081	4.23	0.016
0	7.50	4.84	0.387	2.48	0.060	4.14	0.016

$A_c$  = Spar cap area (in<sup>2</sup>)

$t_d$  = Spar diagonal gage (in.)

$W_c$  = Spar cap width (in.)

$t_w$  = Spar shear web gage

$t_c$  = Spar cap gage

$R$  = Spar shear web corrugation radius (in.)

$W_u$  = Spar upright width (in.)

$t_f$  = Spar shear web support cap gage (in.)

$t_u$  = Spar upright gage (in.)

SS = Spanwise station

$W_d$  = Spar diagonal width (in.)

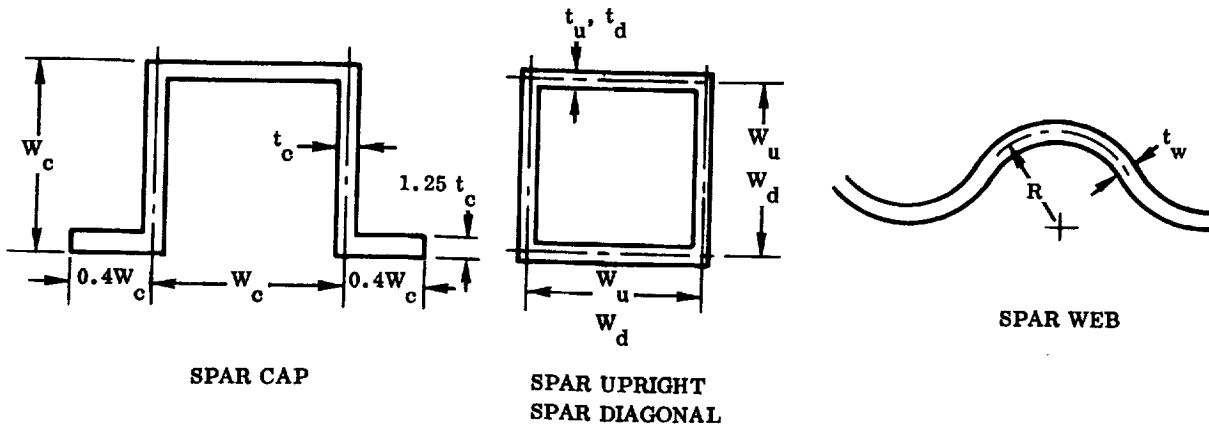


Table 3-10. Sizing Data — Spar No. 2 (WS 633), B-9U Wing

SS	A <sub>c</sub>	W <sub>c</sub>	t <sub>c</sub>	W <sub>u</sub>	t <sub>u</sub>	W <sub>d</sub>	t <sub>d</sub>
507	2.35	3.80	0.153	2.50	0.093	4.04	0.041
447	4.05	4.37	0.232	2.61	0.103	4.29	0.067
387	5.92	4.82	0.307	3.15	0.129	4.54	0.095
327	7.45	5.10	0.365	3.5	0.144	4.73	0.109
267	8.78	5.32	0.411	3.81	0.158	4.90	0.122
207	9.44	5.42	0.437	5.05	0.210	5.03	0.129
163	9.62	4.32	0.555	4.13	0.147	4.20	0.056
120	9.75	4.33	0.562	4.40	0.145	4.07	0.038
60	9.86	5.26	0.467	3.64	0.107	4.52	0.019
0	9.87	5.26	0.467	3.00	0.075	4.37	0.016

Table 3-11. Sizing Data — Spar No. 3 (WS 751), B-9U Wing

SS	A <sub>c</sub>	W <sub>c</sub>	t <sub>c</sub>	W <sub>u</sub>	t <sub>u</sub>	W <sub>d</sub>	t <sub>d</sub>	t <sub>w</sub>	R	t <sub>f</sub>
627	2.54	3.92	0.162	1.98	0.085	4.07	0.124			
567	3.64	4.42	0.206	2.82	0.125	4.24	0.118			
507	5.09	4.80	0.264	4.27	0.187	4.42	0.101	0.095	3.18	0.238
447	6.83							0.106	3.50	0.25
387	8.48							0.115	3.76	0.25
327	9.92							0.12	3.98	0.25
267	11.02	5.69	0.485	4.46	0.194	5.19	0.172	0.124	4.16	0.25
207	11.68	5.78	0.505	5.85	0.254	5.33	0.177			
163	11.80	4.59	0.643	4.77	0.177	4.51	0.077			
120	12.07	4.61	0.654	5.1	0.177	4.38	0.052	0.040	2.78	0.10
60	12.17							0.032	2.45	0.08
0	12.22							0.020	2.00	0.05

Table 3-12. Sizing Data - Spar No. 4 (WS 941), B-9U Wing

SS	A <sub>c</sub>	W <sub>c</sub>	t <sub>c</sub>	W <sub>u</sub>	t <sub>u</sub>	W <sub>d</sub>	t <sub>d</sub>	t <sub>w</sub>	R	t <sub>f</sub>
861	0.12	1.05	0.029	1	0.025	1	0.025			
801	0.22	1.61	0.034	1.5	0.062	3.01	0.029			
762	1.41	3.01	0.117	1.9	0.049	3.12	0.064			
731	1.82	2.42	0.188	2.08	0.096	2.17	0.085			
687	2.30	3.54	0.163	2.21	0.113	3.32	0.133			
627	3.50	4.36	0.200	2.53	0.117	4.07	0.124			
567	3.66	4.41	0.205	2.81	0.124	4.24	0.116			
507	4.26	4.55	0.234	2.43	0.090	4.42	0.101	0.080	2.82	0.199
447	5.17							0.080	2.90	0.200
387	6.02							0.081	3.00	0.203
327	6.79							0.082	3.09	0.205
267	7.49	5.07	0.37	3.41	0.137	4.72	0.096	0.084	3.21	0.211
207	7.86	5.13	0.383	4.40	0.176	4.81	0.098			
163	8.27	4.13	0.50	3.72	0.127	4.0	0.045			
120	8.89	4.21	0.52	4.12	0.133	3.95	0.033	0.032	2.31	0.080
60	9.86							0.025	2.12	0.062
0	10.96							0.020	1.95	0.050

Table 3-13. Sizing Data - Spar No. 5 (WS 1042), B-9U Wing

SS	A <sub>c</sub>	W <sub>c</sub>	t <sub>c</sub>	W <sub>u</sub>	t <sub>u</sub>	W <sub>d</sub>	t <sub>d</sub>
861	0.16	1.14	0.034	1	0.025	1	0.025
801	0.16	1.42	0.029	1	0.050	2.96	0.016
762	0.82	2.51	0.082	1.25	0.050	3.01	0.026
731	1.00	2.00	0.125	1.36	0.056	1.96	0.035
687	1.30	2.93	0.110	1.42	0.061	3.11	0.051
627	1.90	3.57	0.134	1.59	0.064	3.81	0.046
567	2.04	3.63	0.139	1.78	0.069	3.91	0.044
507	2.07	3.77	0.15	2.42	0.090	4.02	0.039
447	2.87	3.95	0.181	2.50	0.095	4.08	0.040
387	3.50	4.11	0.21	2.50	0.10	4.15	0.043
327	4.13	4.27	0.24	2.50	0.10	4.23	0.045
267	4.65	4.39	0.265	2.50	0.10	4.30	0.047
207	4.72	4.40	0.268	3.09	0.11	4.34	0.045
163	4.99	3.55	0.35	2.60	0.081	3.45	0.021
120	5.29	3.60	0.37	2.87	0.084	3.45	0.020
60	5.72	4.47	0.319	2.50	0.066	4.05	0.020
0	6.20	4.58	0.338	2.16	0.051	4.01	0.020

### 3.5.2 WING BOX WEIGHT SENSITIVITY TO FACTOR OF SAFETY PERTURBATIONS.

The weight sensitivity of the B-9U wing box to perturbations of factor of safety is presented in Figures 3-22 and 3-23 for all of the critical wing loading conditions. The critical wing loading conditions are shown in Figure 2-20. The curve of Figure 3-22 labeled ULTIMATE DESIGN is based on a structure critical for ultimate design loads at the plotted  $FS_u$ , whereas the cutoffs for yield design are based on a structure critical for yield loads at the indicated  $FS_y$ . Weights were determined by use of the same computer program used for the baseline analysis. The baseline weight of the wing box is 43,104 pounds.

In Figure 3-23 the weight sensitivity of the wing box to factor of safety perturbations for the launch vehicle type conditions, maximum  $\alpha q$  (W1) and maximum  $g$  recovery (W2), while holding the aircraft condition, subsonic gust (W3), at the baseline  $FS_u = 1.5$  is plotted along with the sensitivity to perturbations for the aircraft condition only while holding the launch vehicle conditions at the baseline of  $FS_u = 1.4$ . The curve for perturbations for all load conditions simultaneously is shown for comparison purposes. Inspection of the curves reveals that the aircraft loading condition has little effect on the wing box weight. The figure shows that the wing box weight is highly sensitive to the  $FS_u$  on launch vehicle type loading conditions, and that the weight can be significantly changed by varying  $FS_u$  for these conditions.

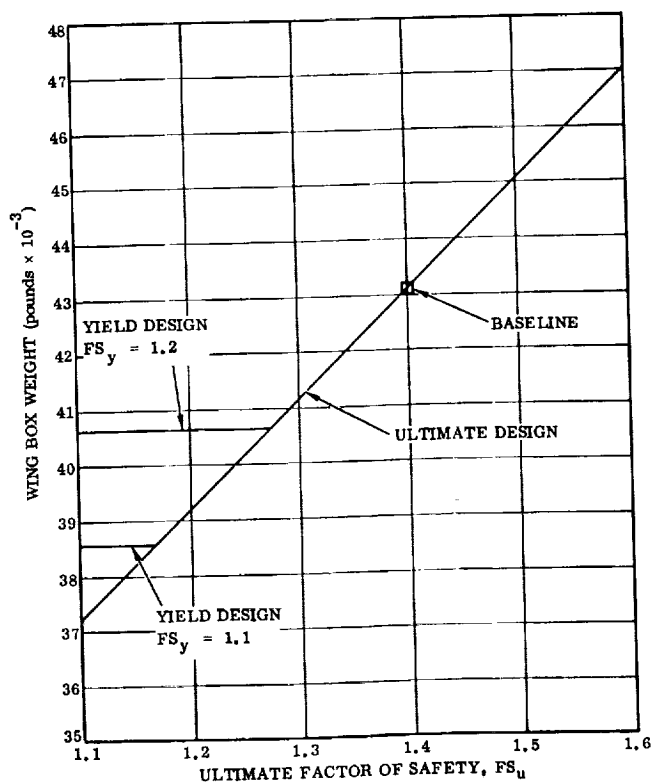


Figure 3-22. Wing Box Weight Sensitivity to Factor of Safety Perturbations for All Critical Conditions

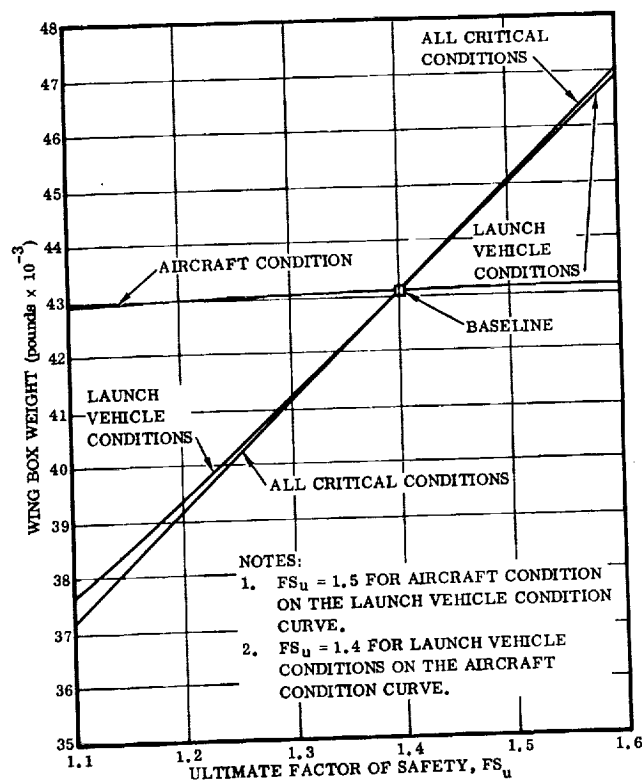


Figure 3-23. Wing Box Weight Sensitivity to Factor of Safety Perturbations for Various Critical Load Conditions

### 3.6 VERTICAL TAIL BOX

**3.6.1 VERTICAL TAIL BOX STRUCTURAL SIZING.** The vertical tail structural box is constructed of 6Al-4V titanium alloy and has a three-spar arrangement with the front spar on the 10% chord line, the rear spar on the 60% chord line, and the mid spar on the 37% chord line as shown in Figure 3-24. Spars and ribs are of corrugated construction. Welding is used to attach spar and rib caps to the corrugated webs. Surface coverings are of integrally stiffened extruded "planks," welded together. The rear spar and mid spar transfer the bending moments and shear into the body bulkheads through fittings.

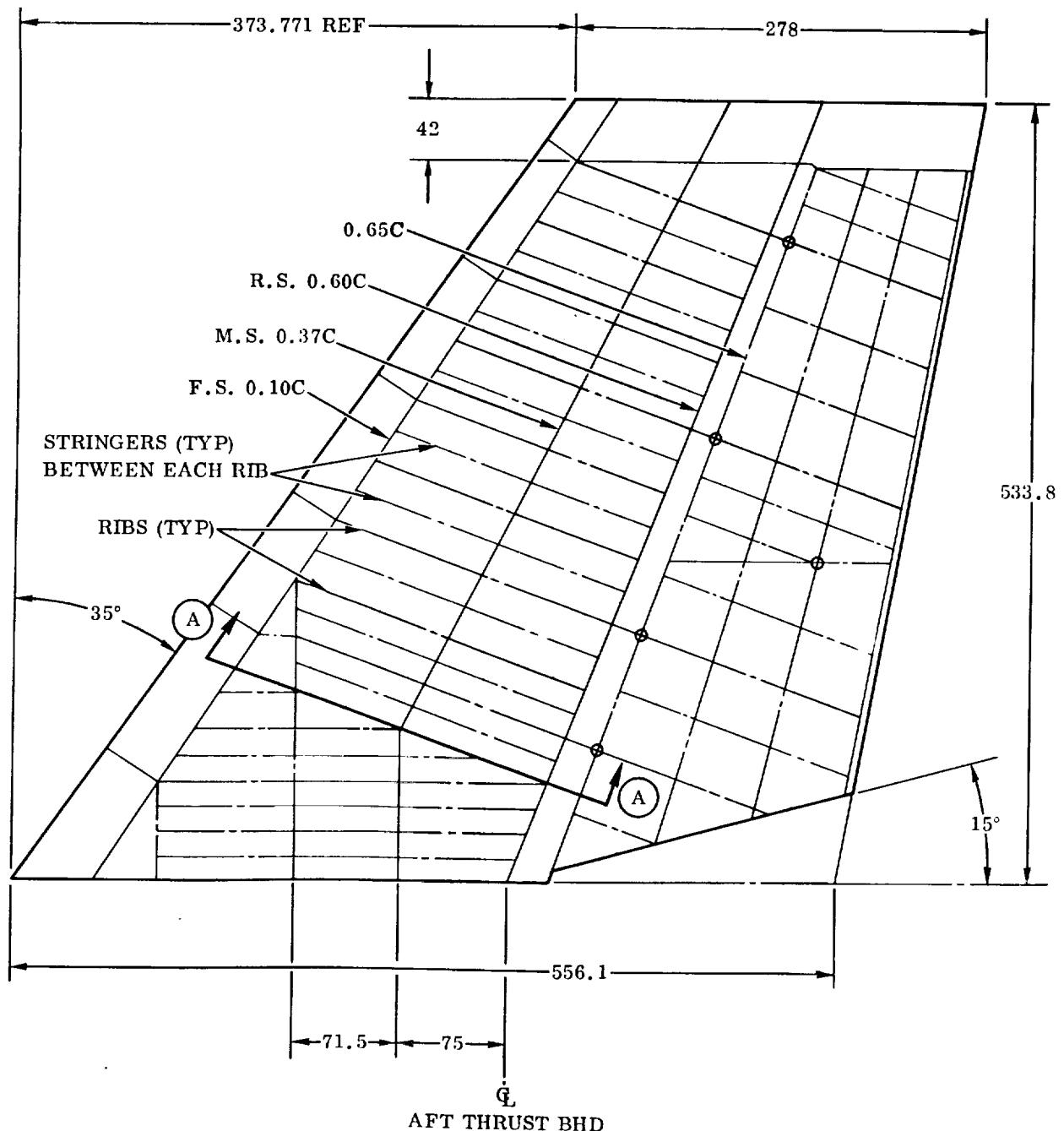
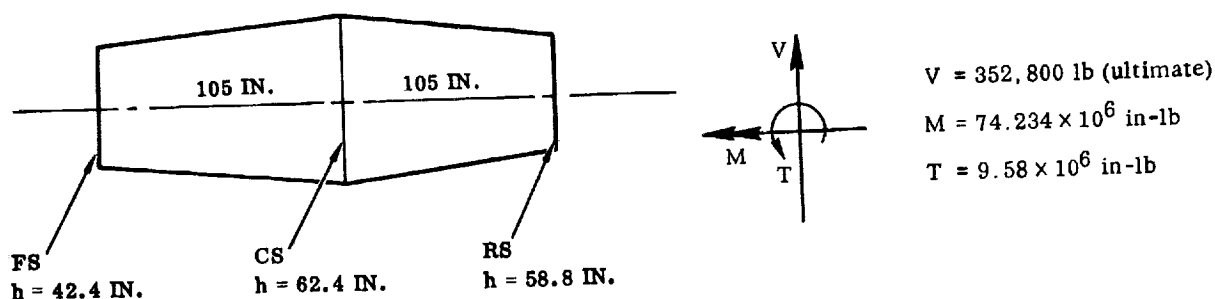


Figure 3-24. Vertical Tail Configuration

The vertical tail was simulated and analyzed by means of a Convair computer procedure that used the stiffness approach to obtain an internal load distribution. The spanwise bending moment distribution used for member sizing is shown in Figure 2-22. Another computer program was used to optimize the skin-stiffener configuration. The skins of the fin box are fully effective from the tip to the canted rib.

The section chosen for the fatigue calculations of the present study is at the canted rib, Section (A) - (A) of Figure 3-24. The spar cap sizing calculations for this section are shown below. The load distribution coefficients used were determined by computer.

Section A - A of Figure 3-24



$$q_{FS} = \frac{0.0176(352,800)}{42.4} = \frac{6209}{42.4} = 146 \text{ lb/in}$$

$$q_{CS} = \frac{0.123(352,800)}{62.4} = \frac{43,394}{62.4} = 695 \text{ lb/in}$$

$$q_{RS} = \frac{0.442(352,800)}{58.8} = \frac{155,938}{58.8} = 2652 \text{ lb/in}$$

Remainder of shear is carried in covers and caps, which are tapered.

#### Spar Cap Loads

$$\text{Forward } P_{cap} = \frac{0.013(74.234)10^6}{42.4} = 22,760$$

$$\text{Center } P_{cap} = \frac{0.032(74.234)(10^6)}{62.4} = 38,069$$

$$\text{Aft } P_{cap} = \frac{0.068(74.234)10^6}{58.8} = 85,849$$

Cap Areas, choosing  $f = 34 \text{ ksi}$

$$\text{Forward } A = \frac{22,760}{34,000} = 0.670 \text{ in}^2$$

$$\text{Center } A = \frac{38,069}{34,000} = 1.12 \text{ in}^2$$

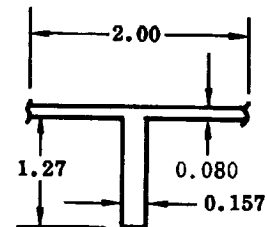
$$\text{Rear } A = \frac{85,849}{34,000} = 2.52 \text{ in}^2$$

Covers

$$0.89 (74,234,000) = 66,068,260 \text{ in-lb}$$

$$P_x = \frac{66,068,260}{55 \text{ in.}} = 1,201,240 \text{ lb}$$

$$N_x = \frac{1,201,241}{210 \text{ in.}} = 5725 \text{ lb/in}$$



For the configuration with  $t = 0.180$  we have  $\sigma_{cr} = 32,450 \text{ psi}$ .

This compares with  $\sigma_{eff} = \frac{5725 \text{ lb/in}}{0.180 \text{ in.}} = 31,805 \text{ psi}$

**3.6.2 VERTICAL TAIL BOX WEIGHT SENSITIVITY TO FACTOR OF SAFETY PERTURBATIONS.** The weight sensitivity of the B-9U vertical stabilizer box to  $FS_u$  perturbations is presented in Figures 3-25 and 3-26 for all of the critical vertical tail loading conditions. The curve of Figure 3-25 labeled ULTIMATE DESIGN is based on a structure critical for ultimate design loads at the plotted  $FS_u$ . Due to the low design ultimate stresses that remain within the elastic range of the material, yield design is not a consideration.  $FS_u$  was perturbed concurrently for all critical conditions. The critical loading conditions for the vertical tail box are maximum  $\beta_q$  (T1), subsonic gust (T2), and maximum rudder hinge moment (T3).

In Figure 3-26  $FS_u$  was perturbed for the launch vehicle condition only (condition T1) while holding the aircraft conditions (conditions T2 and T3) at the baseline  $FS_u = 1.5$ .  $FS_u$  was also perturbed for the aircraft conditions only while holding the launch vehicle condition at the baseline  $FS_u = 1.4$ . This was done to determine the relative sensitivity of the vertical tail box weight to the two types of conditions. The results are shown in Figure 3-25 with the curve for all conditions for comparison.

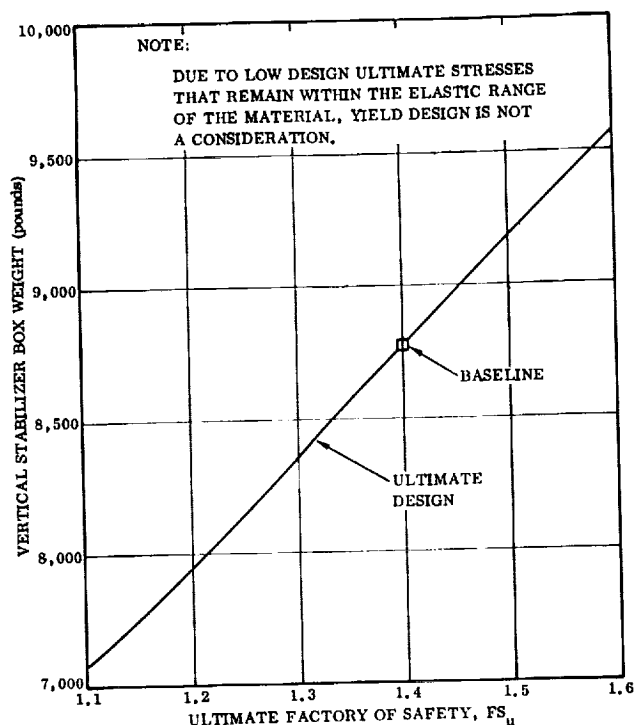


Figure 3-25. Vertical Stabilizer Box Weight Sensitivity to Factor of Safety Perturbations for All Critical Load Conditions

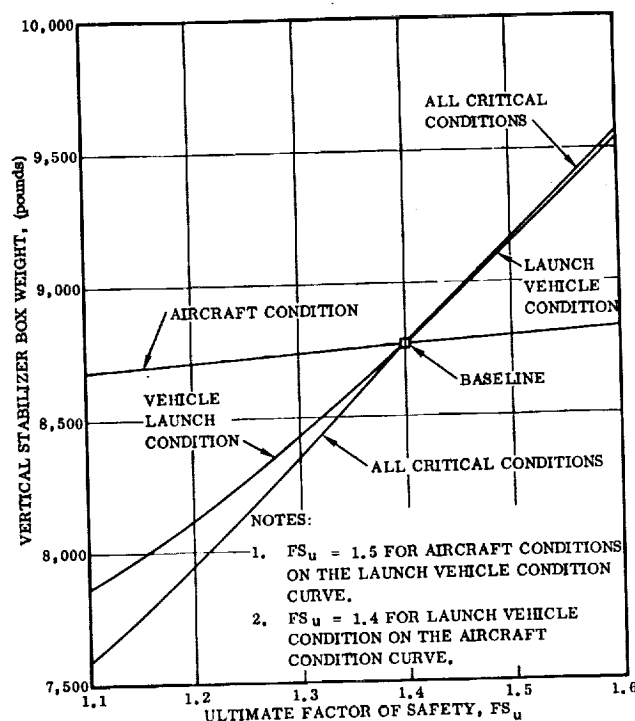


Figure 3-26. Vertical Stabilizer Box Weight Sensitivity to Factor of Safety Perturbations for Various Critical Load Conditions

Inspection of the curve reveals that the aircraft loading conditions T2 and T3 have little effect on the vertical tail box weight. The figure shows that the vertical tail box weight is highly sensitive to the  $FS_u$  on the launch vehicle type loading condition, maximum  $\beta q$  (T1), and that weight can be significantly changed by varying  $FS_u$  for this condition.

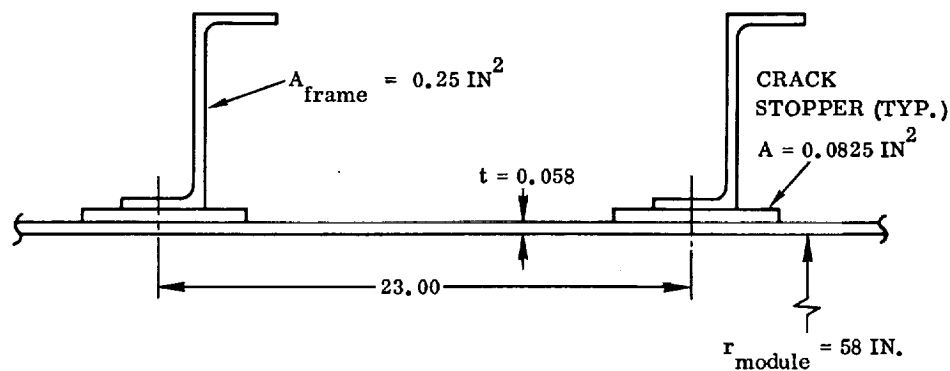
### 3.7 CREW MODULE

**3.7.1 CREW MODULE STRUCTURAL SIZING.** The crew module main structural shell is designed to be fail-safe through the use of crack-stoppers and beefed-up skins and frames. The aft ellipsoidal bulkhead of the crew module is one structural element on which it is difficult to employ ordinary fail-safe design techniques such as crack-stoppers. Therefore the same apparent factor of safety is used for the bulkhead as for the cylindrical section skin, and it is stiffened with a rectangular waffle pattern to provide crack arresting ability in both the circumferential and meridional directions.

The most critical loads applied to the crew module shell are those arising as a result of internal pressurization. The  $\Delta p$  across the shell is presented in Figure 2-37 as a function of time,  $t$ , from liftoff. For the  $\Delta p$  curve, an internal cabin pressure of 15 psia was used, and it was assumed that no leakage occurred.



An iterative analysis procedure shows that the longitudinal section through the skin wall in the cylindrical section of the module shown in the sketch will provide fail-safe capability for a longitudinal through-crack initiating from a frame rivet.



Using the method of Reference 11:

Percent stiffening = 20%

The stress intensity factor is

$$K = C \sigma \sqrt{\pi a}$$

Values of C were obtained from Figure 9 of Reference 11 for a crack initiating at a frame rivet. The largest value of S/p (frame spacing to rivet pitch ratio) was used due to the large frame spacing. The gross stress level,  $\sigma$ , is

$$\sigma = \frac{pr}{t} = \frac{(15 \text{ psi})(58 \text{ in.})}{0.058} = 15.0 \text{ ksi} = f_{\text{limit}}$$

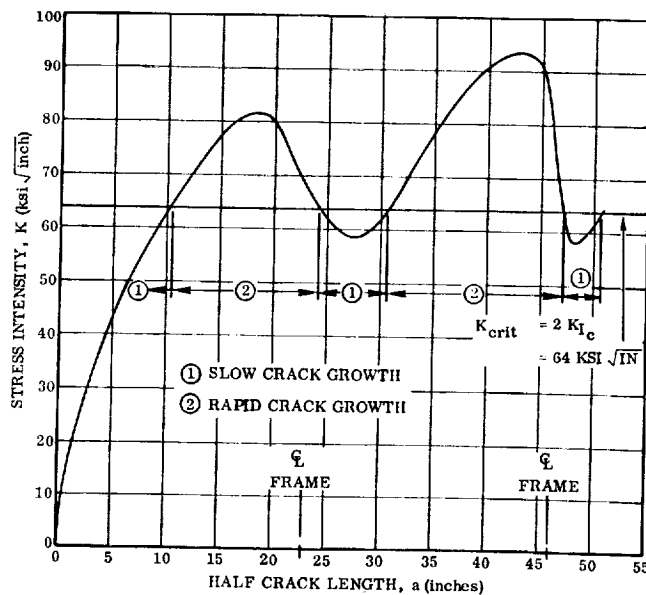


Figure 3-27. Crew Module Stress Intensity Factor Versus Crack Length for Crack Initiating from Frame Rivet

Figure 3-27 presents the stress intensity factor versus crack length for a longitudinal crack emanating from a frame rivet hole. The figure shows that fracture arrest is provided by both the first and the second frames. The main structural shell is therefore fail-safe for internal pressure loads. Fail-safe capability for the glazed areas is provided by use of double windows in the doors, and laminated glass in the windshield. The crew module is fail-safe for longitudinal loads by reason of the use of multiple stringers.

**3.7.2 APPARENT FACTORS OF SAFETY.** When reduced limit design stresses are required to meet yield, safe-life, or fail-safe criteria, the apparent factor of safety is given by the expression:

$$FS \text{ (apparent)} = \frac{F}{f_{\text{limit}}}$$

The skin of the crew module is designed by the fail-safe requirements. Therefore the skin has an apparent factor of safety greater than the baseline. For 2219-T87 aluminum at room temperature:

$$F_{tu} = 63,000 \text{ psi}, F_{ty} = 51,000 \text{ psi}$$

$$FS_u \text{ (apparent)} = \frac{63,000}{15,000} = 4.20, \quad FS_y \text{ (apparent)} = \frac{51,000}{15,000} = 3.40$$

Comparison of the actual and apparent ultimate safety factors, 2.0 and 4.2 respectively, reveals that the fail-safe requirement imposes a significant weight penalty on the skin over the weight required by static strength for which ultimate design is critical.

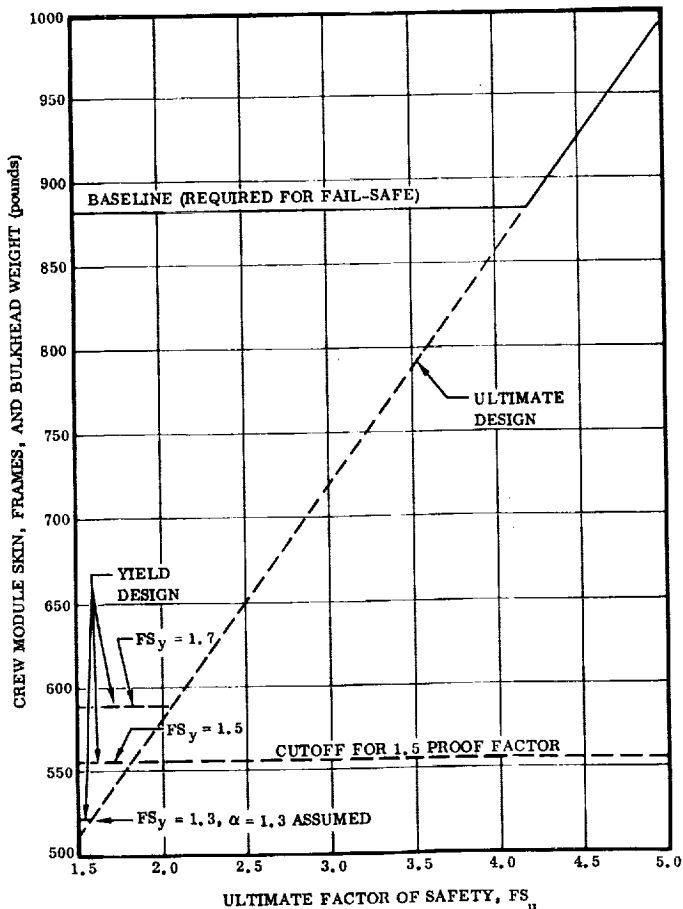


**Figure 3-28.** Crew-Module Skin Frames, and Bulkhead Sensitivity of Weight to Factor of Safety Perturbations for Maximum Operating Pressure

The bulkhead employs the same apparent safety factor for fail-safe purposes as the skin, and is therefore also subject to a large penalty over the weight required for static strength.

**3.7.3 CREW MODULE WEIGHT SENSITIVITY TO FACTOR OF SAFETY PERTURBATIONS.** The weight sensitivity of the crew module skin, frames, and bulkhead for perturbations of ultimate and yield factors of safety on the maximum operating pressure is presented in Figure 3-28. The ultimate factor of safety was perturbed over the range of 1.3 to 1.7. Inspection of Figure 3-28 reveals that the weight is determined by the fail-safe requirement for ultimate factors of safety of less than 4.2. The baseline weight of the skin, frames, and aft bulkhead is 882 pounds. The weight can go lower only if the fail-safe requirement is relaxed. Weight reductions to be obtained by relaxation of fail-safe and factor of safety criteria are further limited by the 1.5 proof factor requirement, which requires a weight of 555 pounds.

## SECTION 4

### FATIGUE ANALYSIS

On the following pages, a cumulative fatigue damage analysis is made for each of the baseline components to determine the safe-life number of missions to initiation of fatigue cracks, assuming initially flawless material. The service load spectra shown in Figure 2-28 through 2-37 are used.

Material information used in classical fatigue analysis is usually in the form of S-N curves, constant life diagrams, or some such presentation of stress versus cycles-to-failure of test specimens. Although this information is in terms of complete failure rather than fatigue crack initiation, S-N curves are being used as indicating crack initiation for purposes of this study. This interpretation is justified by the fact that the standard test specimen configuration used to generate S-N data has a small cross-section compared to space shuttle booster structural members. The specimen is therefore more sensitive to a given amount of fatigue damage, and progression of fatigue damage to complete failure is rapid. The fatigue curves of Figures 4-1, 4-2, and 4-3 provide S-N data for 2219-T87 aluminum alloy at room temperature, and Ti6Al-4V annealed titanium alloy at room temperature and 650°F, respectively. The sensitivity of fatigue life to factor of safety perturbations (i.e., stress level changes) and to fatigue crack initiation scatter factor perturbations is also presented for each of the baseline components.

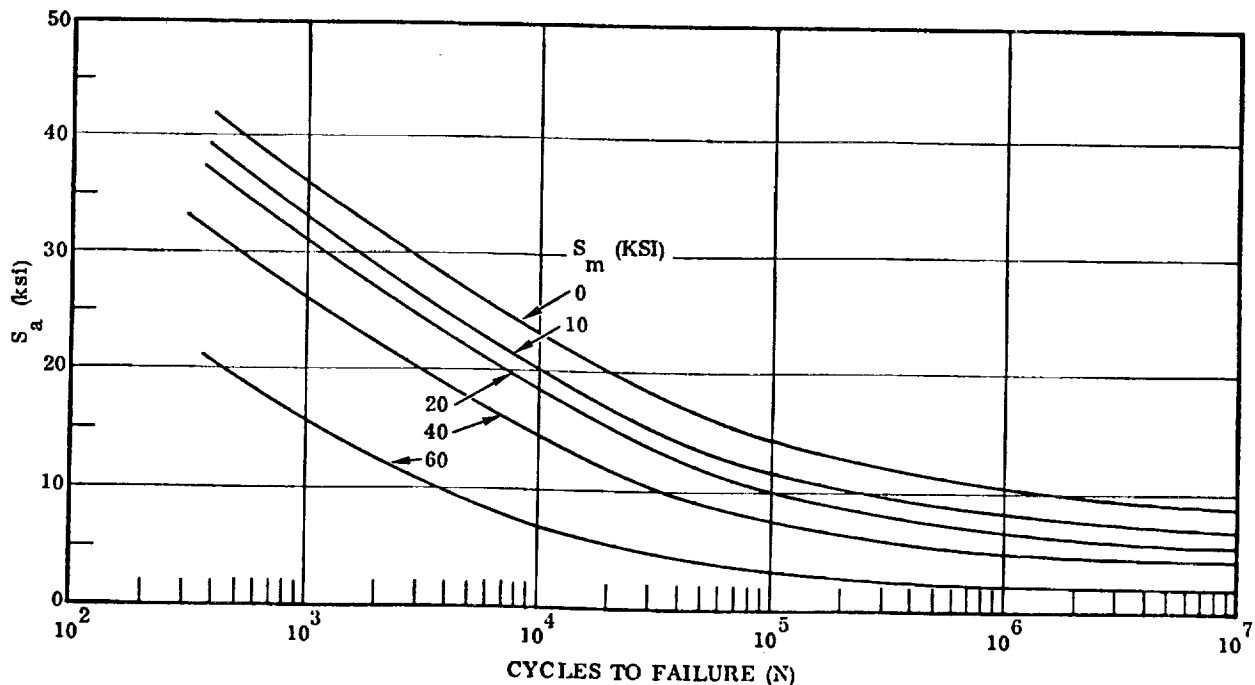


Figure 4-1. Estimated Fatigue Curves for 2219-T87 Aluminum Alloy at Room Temperature with  $K_t = 3.0$

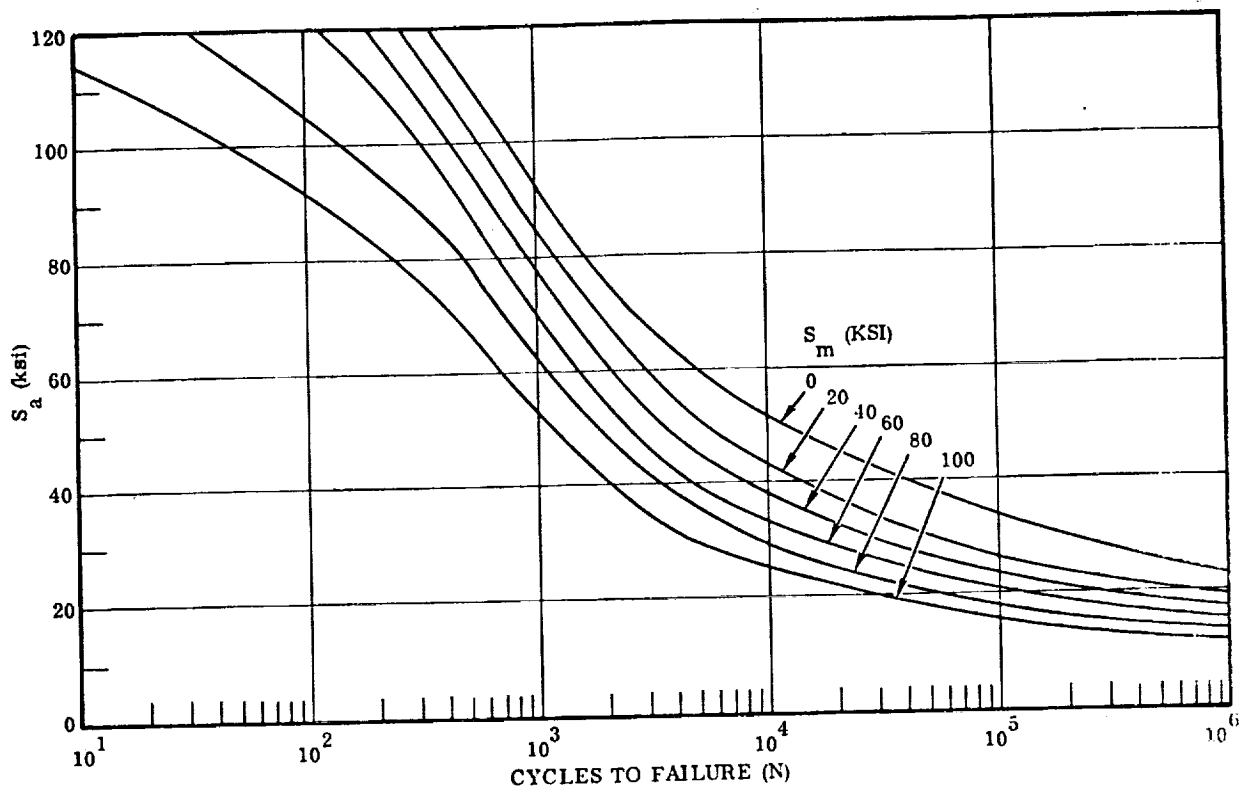


Figure 4-2. Fatigue Curves for Annealed Ti-6Al-4V  
at Room Temperature with  $K_t = 3.0$

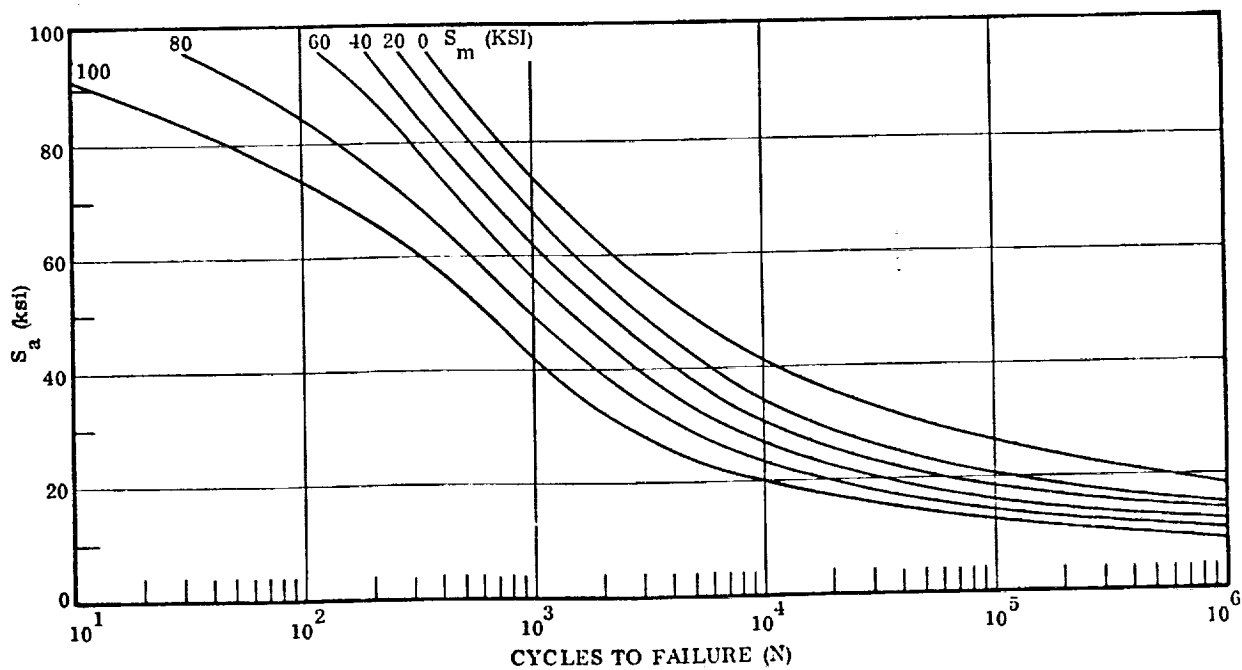


Figure 4-3. Fatigue Curves for Annealed Ti-6Al-4V  
at 650°F with  $K_t = 3.0$

#### 4.1 LIQUID OXYGEN TANK

This section presents the fatigue damage analysis for the baseline liquid oxygen tank and the sensitivity of its fatigue life to perturbations of factors of safety and fatigue crack initiation scatter factor. Table 4-1 gives the fatigue damage analysis for internal pressure for the most critical area of the LO<sub>2</sub> tank, which is the skin at the forward end of the tank cylindrical section. The calculated fatigue life for the LO<sub>2</sub> tank is 2049 missions based on a scatter factor of 4. Figure 4-4 presents the sensitivity of the LO<sub>2</sub> tank fatigue life to factor of safety perturbations. The fatigue life of the baseline tank is controlled by the proof design of the tank. Figure 4-5 presents the sensitivity of the LO<sub>2</sub> tank fatigue life to fatigue crack initiation scatter factor perturbations.

#### 4.2 LIQUID HYDROGEN TANK

This section presents the fatigue damage analysis for the baseline liquid hydrogen tank and the sensitivity of its fatigue life to perturbations of factor of safety and fatigue crack initiation scatter factor. Table 4-2 gives the fatigue damage analysis for internal pressure for the most critical area of the LH<sub>2</sub> tank, which is the skin at the forward end of the tank cylindrical section. The calculated fatigue life from this table is 2314 missions based on a scatter factor of 4. Table 4-3 presents the fatigue damage analysis at the fuselage Station 2600 bottom centerline for longitudinal loading due to flight and internal pressure. This table indicates a fatigue life of 6410 missions based on a scatter factor of 4. Therefore, the fatigue life of the LH<sub>2</sub> tank is critical for fatigue due circumferential loading from internal pressure as indicated by the 2314 mission fatigue life calculated in Table 4-2. Figure 4-6 presents the sensitivity of the LH<sub>2</sub> tank fatigue life to factor of safety perturbations. The fatigue life of the baseline tank is controlled by the proof design of the tank. Figure 4-7 presents the sensitivity of the LH<sub>2</sub> tank fatigue life, as calculated in Table 4-2, to fatigue crack initiation factor perturbations.

#### 4.3 AFT ORBITER SUPPORT FRAME

This section presents the fatigue damage analysis for the baseline aft orbiter support frame at Station 2666, and the sensitivity of its fatigue life to perturbations of factor of safety and fatigue crack initiation scatter factor. Table 4-4 presents the fatigue damage analysis for the frame. The critical member of the frame is Bar 6 of Figure 3-15 and Table 3-3. The calculated fatigue life from this analysis 4630 missions based on a scatter factor of 4. Figure 4-8 presents the sensitivity of the Station 2666 orbiter support frame fatigue life to perturbations of the factor of safety. The reduced fatigue life at low safety factors is due to the resulting higher limit operating stresses. The curve shows that even for a low ultimate factor of safety, the fatigue life of the bulkhead well exceeds the required 100 missions design life. Figure 4-9 presents the sensitivity of the orbiter support frame fatigue life to perturbations of the fatigue crack initiation scatter factor.

Table 4-1. LO<sub>2</sub> Tank Pressure Spectrum and Damage Analysis at Upper Dome Equator

Phase	Condition	P <sub>max</sub> (psig)	P <sub>min</sub> (psig)	σ <sub>max</sub> (1) (ksi)	σ <sub>min</sub> (1) (ksi)	n (2) (cycles)	σ <sub>mean</sub> (ksi)	σ <sub>alt</sub> (ksi)	K <sub>t</sub>	N (cycles)	n/N
Manufacture Preflight Flight	Proof Test	21.5	0	47.3	0	1	23.6	23.6	3.0	3 × 10 <sup>3</sup>	0.0003
	Fueling	5.0	0	11.0	0	100	5.5	5.5		∞	0
	Nominal Ullage Pressure	17.5 (3)	0	38.8	0	95	19.5	19.5		8.5 × 10 <sup>3</sup>	0.0112
Flight	Max. Relief Valve Pressure	19.5 (3)	0	42.8	0	5	21.4	21.4		5 × 10 <sup>3</sup>	0.0010
Post-Flight	GN <sub>2</sub> Purge	2.0	0	4.4	0	100	2.2	2.2		∞	0
	Solar Heating	4.0	0	8.8	0	3700	4.4	4.4	3.0	∞	0

$$\Sigma\left(\frac{n}{N}\right) = 0.0125 \text{ for one design lifetime of 100 missions}$$

$$\text{Fatigue life} = \frac{100}{4} \left( 1 + \frac{1 - 0.0125}{0.0125 - 0.0003} \right) = 2049 \text{ missions, based on a scatter factor of 4.}$$

NOTES:

- (1)  $\sigma = \frac{Pr}{t} = \frac{P(198)}{0.090}$
- (2) n is cycles for one design lifetime of 100 missions.
- (3) Proof test pressure from Figure 2-19; flight pressures from Figure 2-36. A pressure regulator malfunction is assumed to occur in 5% of the flights.
- (4) Material: 2219-T87 aluminum alloy

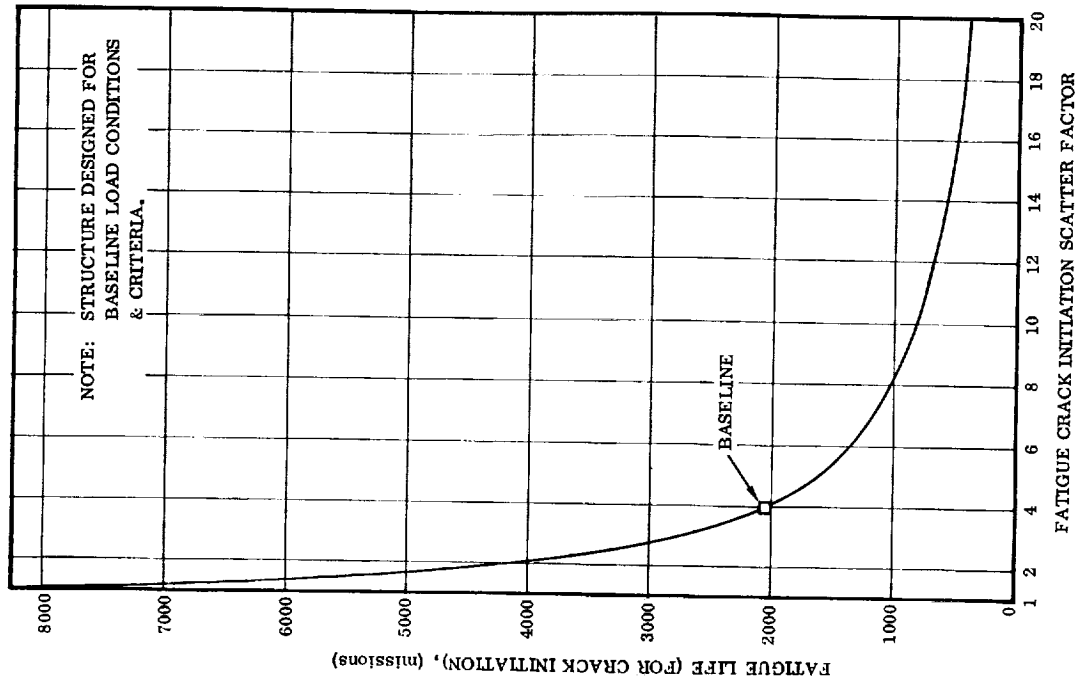


Figure 4-5. LO<sub>2</sub> Tank Fatigue Life (for Crack Initiation) Versus Scatter Factor

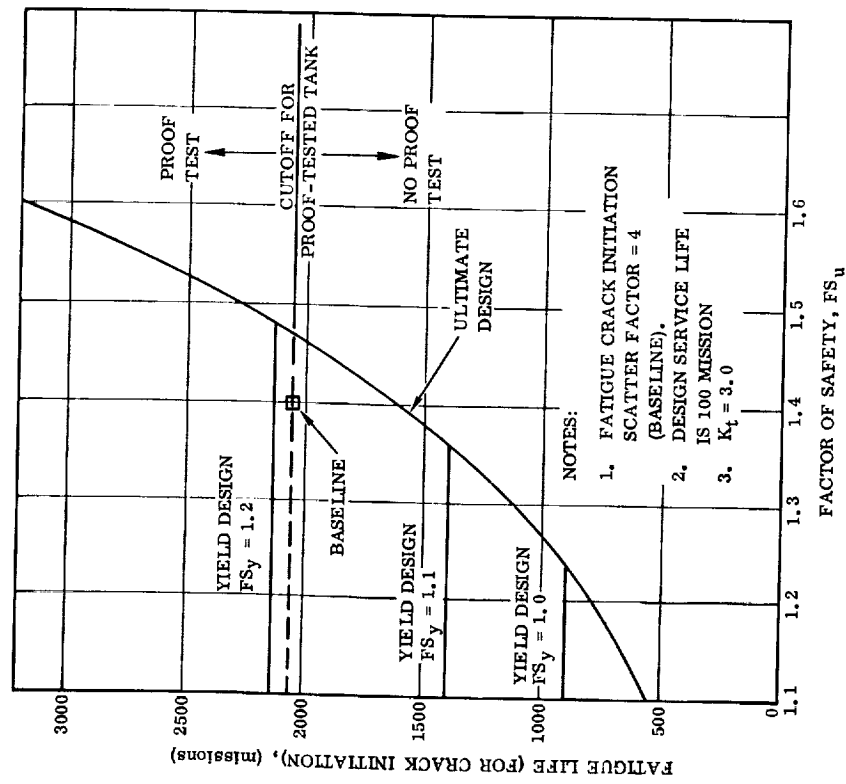


Figure 4-4. LO<sub>2</sub> Tank Sensitivity of Fatigue Life to Factor of Safety Perturbations

Table 4-2. LH<sub>2</sub> Tank Pressure Spectrum and Damage Analysis at Upper Dome Equator

Phase	Condition	P <sub>max</sub> (psig)	P <sub>min</sub> (1) (psig)	σ <sub>max</sub> (1) (ksi)	σ <sub>min</sub> (1) (ksi)	n (2) (cycles)	σ <sub>mean</sub> (ksi)	σ <sub>alt</sub> (ksi)	K <sub>t</sub>	N (cycles)	n/N
Manufacture Preflight Flight	Proof Test	29.8	0	50.9	0	1	25.4	25.4	3.0	2 × 10 <sup>3</sup>	0.0005
	Fueling	5.0	0	8.5	0	100	4.2	4.2	↔	∞	0
	Nominal Ullage Pressure	22.3 (3)	0 (3)	38.1	0	95	19.0	19.0		9.3 × 10 <sup>3</sup>	0.0100
Flight	Max. Relief Valve Pressure	23.8 (3)	0 (3)	40.6	0	5	20.3	20.3		6.6 × 10 <sup>3</sup>	0.0008
Post-Flight	GN <sub>2</sub> Purge	2.0	0	3.4	0	100	1.7	1.7		∞	0
	Solar Heating	4.0	0	6.8	0	3700	3.4	3.4	3.0	∞	0

$$\Sigma\left(\frac{n}{N}\right) = 0.0113 \text{ for one design lifetime of 100 missions.}$$

$$\text{Fatigue life} = \frac{100}{4} \left( 1 + \frac{1 - 0.0113}{0.0113 - 0.0005} \right) = 2314 \text{ missions, based on a scatter factor of 4.}$$

NOTES:

- (1)  $\sigma = \frac{Pr}{t} = \frac{P(198)}{0.116}$
- (2) n is cycles for one design lifetime of 100 missions.
- (3) Proof test pressure from Figure 2-18; flight pressures from Figure 2-35.
- (4) Material: 2219-T87 aluminum alloy.



Table 4-3. Fuselage Damage Analysis - Station 2600 Bottom Centerline

Mission Phase	T (°F)	$\bar{N}_{x \text{ mean}}$ (lb/in)	$\bar{N}_{x \text{ alt}}$ (lb/in)	$\bar{t}$ (inch)	$\sigma_{\text{mean}}$ (ksi)	$\sigma_{\text{alt}}$ (ksi)	$K_t$	n (cycles)	N (cycles)	n/N
Maximum Thrust	RT	4971	2761	0.188	26.4	14.7	3.0	100	$2.6 \times 10^4$	0.0038
Ascent		5036	361		26.8	1.9		90,000	$\infty$	0
			625			3.3		9,000	$\infty$	0
			885			4.7		900	$\infty$	0
Ascent		5036	1149		26.8	6.1		90	$7 \times 10^5$	0.0001
Entry			1413			7.5		9	$2.5 \times 10^5$	0
		1955	104		10.4	0.5		90,000	$\infty$	0
		2011	160		10.7	0.9		9,000		0
Entry		2198	347		11.7	1.8		900		0
		2354	503		12.5	2.7		99		0
Cruise/Landing (1)		1091	158		5.8	0.8		180,000		0
			231			1.2		18,000		0
			304			1.6		1,800		0
Cruise/Landing (1)		1091	378		5.8	2.0		180		0
			451			2.4		18		0
Taxi (1)		477	118		2.5	0.6		180,000		0
			162			0.9		18,000		0
			207			1.1		1,800		0
Taxi (1)	RT	477	252		2.5	1.3		180		0
			300	0.188		1.6	3.0	18	$\infty$	0
GAG (1)	RT				4.1	4.1	3.0	200	$\infty$	0

Mission Phase	n/N
Maximum Thrust	0.0038
Ascent	0.0001
Entry	0
Cruise/Landing	0
Taxi	0
GAG	0
$\Sigma (n/N)$	0.0039

$$\text{Fatigue} = \frac{100}{\text{S.F.} (\Sigma n/N)} = \frac{100}{4 (0.0039)} = 6410 \text{ missions, based on a scatter factor of 4}$$

NOTES:

- (1) To provide for one ferry flight per mission, the number of cycles for cruise/landing and taxi phases has been increased by a factor of 2.0, and two GAG cycles per mission added, using a minimum stress from the taxi phase and a maximum stress from the cruise/landing phase.
- (2) Material: 2219-T87 plate.

Table 4-4. Aft Orbiter Support Frame Load Spectrum and Damage Analysis

$A_z$ mean % (2)	$A_z$ alt % (2)	$A_y$ mean % (2)	$A_y$ alt % (2)	$A_z$ mean (kips) (3)	$A_z$ alt (kips) (3)	$A_y$ mean (kips) (4)	$A_y$ alt (kips) (4)	$\sigma_z$ mean (ksi) (5)	$\sigma_z$ alt (ksi) (5)	$\sigma_y$ mean (ksi) (6)	$\sigma_y$ alt (ksi) (6)	Total mean (ksi)	Total alt (ksi)	$\sigma_{alt}$ (ksi)	$n_e$ (Cycles)	$n$ (Cycles)	N (Cycles) (7)	n/N
Max. $\alpha$ -q Condition																		
63	2.8	0	0	488	22	0	0	12	1	0	0	12	1	1	100,000	90,000	1	0
63	5.1	0	0	488	40	0	0	12	1	0	0	12	1	2	10,000	9,000	1	0
63	7.9	0	0	488	61	0	0	12	2	0	0	12	2	2	1,000	900	1	0
63	17	0	0	488	132	0	0	12	3	0	0	12	3	4	100	90	1	0
63	27	0	0	488	209	0	0	12	5	0	0	12	5	6	10	9	1	0
63	37	0	0	488	287	0	0	12	7	0	0	12	7	1	1	1	1	0
Max. $\beta$ -q Condition																		
63	0	0	7.5	488	0	0	26	12	0	0	2	12	2	3	100,000	90,000	1	0
63	0	0	17	488	0	0	58	12	0	0	4	12	4	5	10,000	9,000	1	0
63	0	0	27	488	0	0	92	12	0	0	6	12	6	9	1,000	900	1	.0022
63	0	0	51	488	0	0	174	12	0	0	12	12	12	14	100	90	1	.0022
63	0	0	75	488	0	0	256	12	0	0	17	12	17	20	10	9	1	.0010
63	0	0	100	488	0	0	341	12	0	0	23	12	23	1	1	1	1	

Table 4-4. Aft Orbiter Support Frame Load Spectrum and Damage Analysis, Contd

NOTES:

1. Critical member judged to be Bar 6 (see Figure 3-15 and Table 3-3).
2. Percent of design values, from spectrum curves, Figure 2-32.
3. Design value of  $A_z = 775$  kips.  $A_z = \frac{\% A_z}{100} (775)$
4. Design value of  $A_y = 341$  kips.  $A_y = \frac{\% A_y}{100} (341)$
5. For a unit  $A_z$  of 1000 kips,  $\sigma_z$  in Bar 6 = 24.7 ksi
6. For a unit  $A_y$  of 1000 kips,  $\sigma_y$  in Bar 6 = 68.0 ksi
7. Cycles to failure (crack initiation) from Figure 4-1.
8. Material is 2219-T87 aluminum alloy.
9. Operating temperature for above conditions assumed to be RT.

Fatigue Life Computation:

$$\Sigma \frac{n}{N} = 0.0054 \text{ for 100 missions}$$

Fatigue Life

$$= \frac{100}{\text{S.F.} \times \Sigma (n/N)} = \frac{100}{4(0.0054)} = 4630 \text{ missions}$$

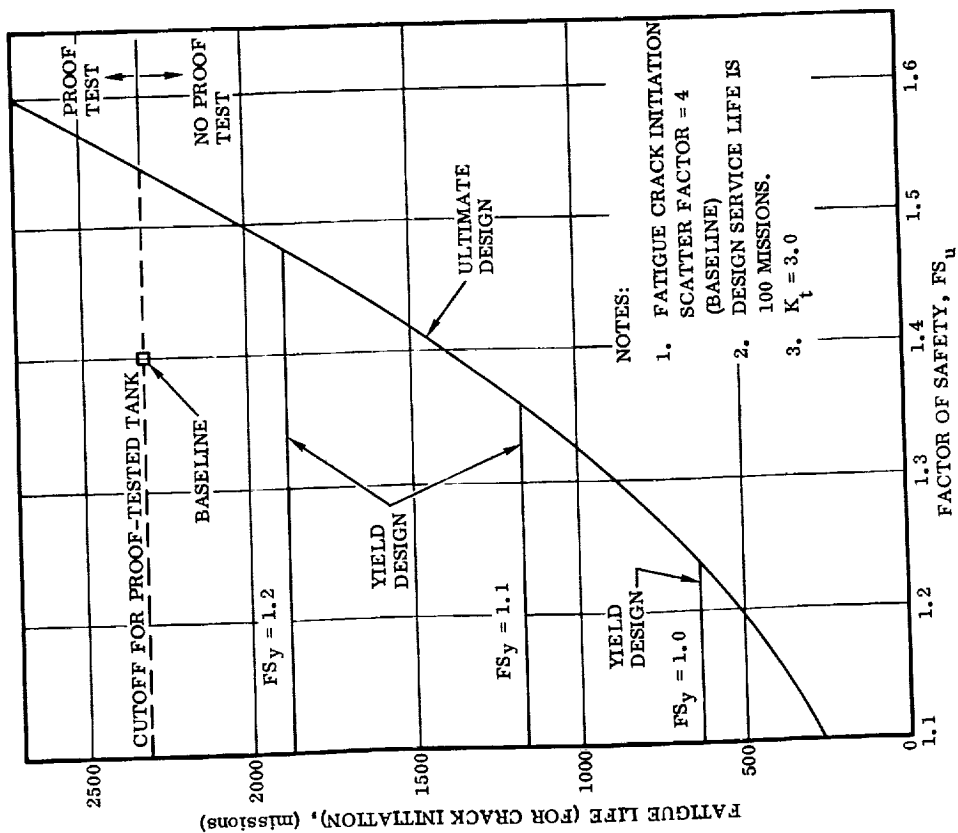


Figure 4-6. LH<sub>2</sub> Tank Sensitivity of Fatigue Life to Factor of Safety Perturbations

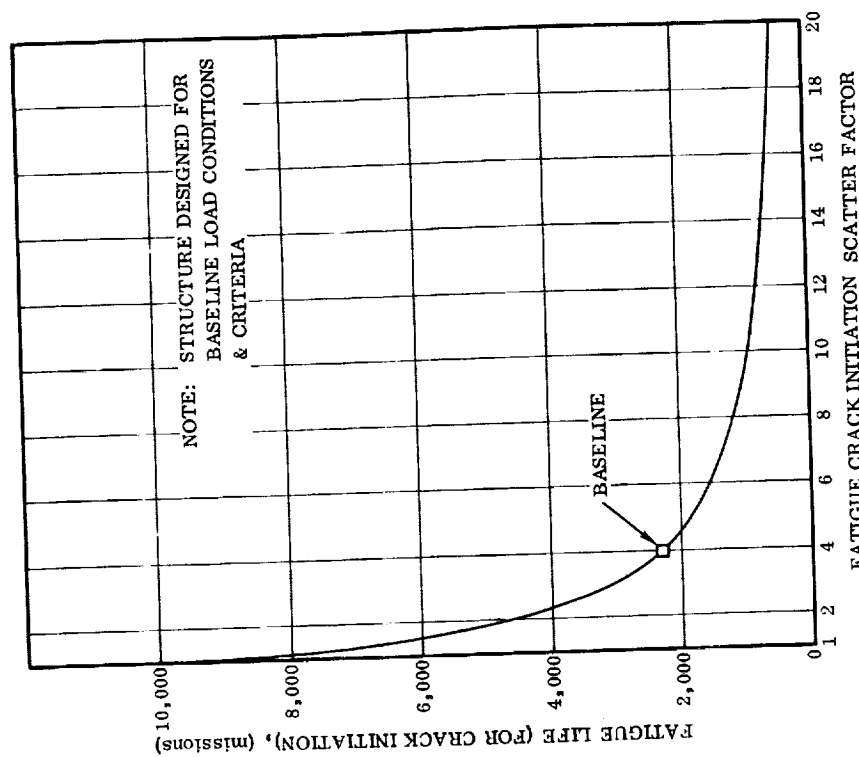


Figure 4-7. LH<sub>2</sub> Tank Fatigue Life (for Crack Initiation) Versus Scatter Factor

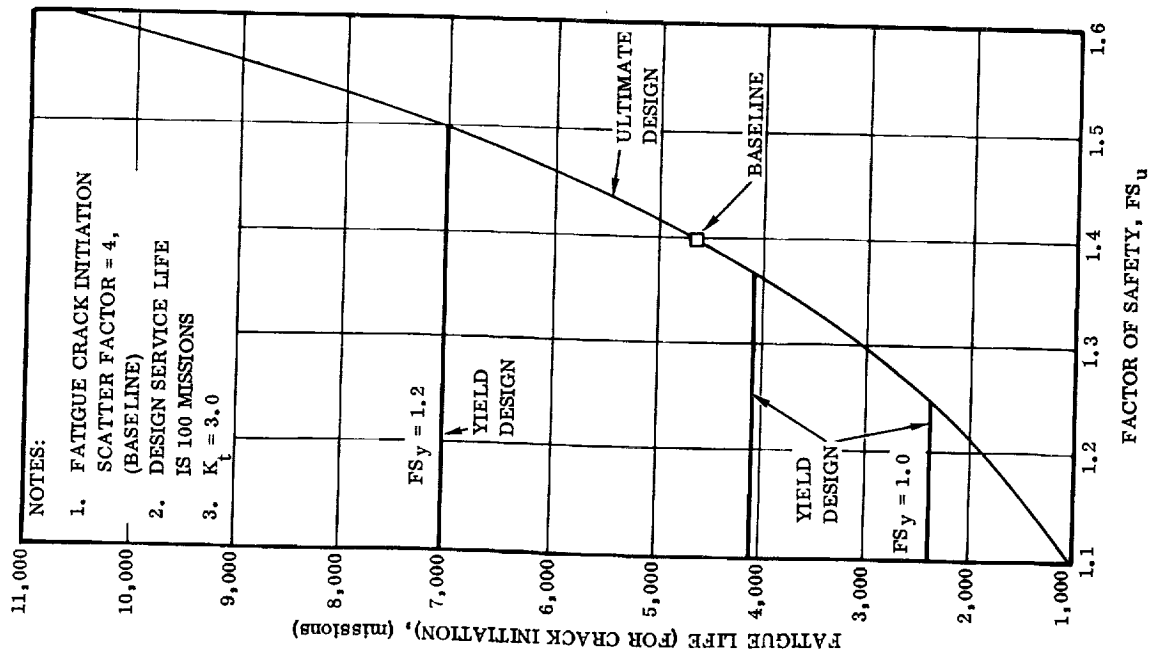


Figure 4-8. Station 2666 Orbiter Support Frame  
Sensitivity of Fatigue Life to Factor  
of Safety Perturbations

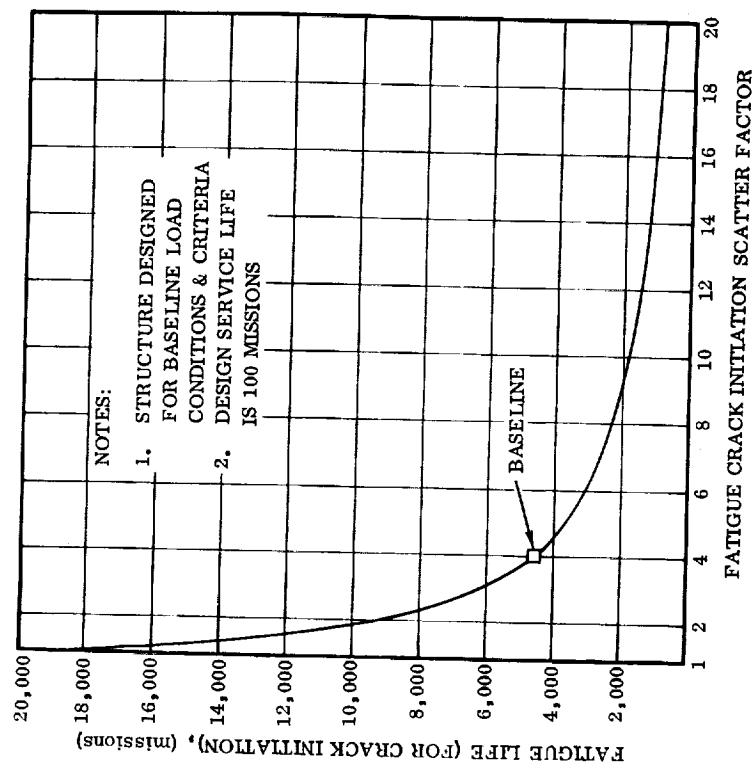


Figure 4-9. Station 2666 Orbiter Support Frame  
Fatigue Life (for Crack Initiation)  
Versus Scatter Factor

#### 4.4 THRUST STRUCTURE

This section presents the fatigue damage analysis for the baseline thrust structure and the sensitivity of its fatigue life to perturbations of factor safety and fatigue crack initiation scatter factor. Table 4-5 presents the fatigue damage analysis of the critical tension element of the thrust structure, which is the thrust beam cap. The analysis was made using the load spectrum of Figure 2-34, and based on a scatter factor of 4, gives a fatigue life of 877 missions, which is well in excess of the 100 mission baseline life requirement. Figure 4-10 gives the sensitivity of the thrust beam cap fatigue life to perturbations of the factor of safety. The reduced fatigue life at low safety factors is due the higher limit operating stresses resulting from these lower safety factors. The curve shows that for all safety factors investigated, the thrust structure has a fatigue life well in excess of the 100 mission requirement. Figure 4-11 presents the variation of the fatigue life as a function of the fatigue crack initiation scatter factor.

#### 4.5 WING BOX

This section presents the fatigue damage analysis for the baseline wing box and the sensitivity of its fatigue life to perturbations of factor of safety and fatigue crack initiation scatter factor. Table 4-6 presents the fatigue damage analysis for the wing spar caps, which are the most critical elements of the wing box. The analysis gives a baseline fatigue life of 182 missions whereas the design service life is 100 missions. This is the lowest fatigue life of any major structural assembly investigated and indicates the load spectrum for the wing to be severe. Figure 4-12 presents the sensitivity of the wing spar caps fatigue life to perturbation of the ultimate factor of safety. The reduced fatigue life at low safety factors is due to the resulting higher limit operating stresses. The curve shows that for the baseline fatigue crack initiation scatter factor of 4, a  $FS_u$  of 1.26 is needed to meet the requirement for a design service life of 100 missions. The curve also shows a fatigue life of only 65 missions for tension structure designed by the yield factor of safety,  $FS_y = 1.1$ . Although this is less than the design service life requirement of 100 missions, it is not critical unless  $FS_u$  is reduced to the point where yield design becomes critical. This cannot happen, however, because  $FS_u$  cannot be reduced below 1.26 without violating the 100 mission requirement.

Figure 4-13 presents the sensitivity of the wing box spar caps fatigue life to perturbations of the fatigue crack initiation scatter factor.

#### 4.6 VERTICAL TAIL BOX

This section presents the fatigue damage analysis for the baseline vertical tail box and the sensitivity of its fatigue life to perturbations of factor of safety and fatigue crack initiation scatter factor. Table 4-7 presents the fatigue damage analysis and gives the very large fatigue life of 125,000 missions based on a scatter factor of 4. Fatigue therefore is not critical for the vertical tail box. Figure 4-14 presents the sensitivity

Table 4-5. Thrust Beam Cap Fatigue Damage Analysis

Design $\sigma$ limit (ksi)	T (°F)	$K_t$	$T_m$ (%)	$T_a$ (%) (1)	$\sigma_m$ (ksi)	$\sigma_a$ (ksi)	$n_e$ (cycles) (2)	$n$ (cycles) (2)	$\bar{\sigma}_a$ (ksi)	N (cycles)	n/N
92.9	RT	3.0	96.8	0.05	89.9	0.05	15,000				
92.9	RT	3.0	96.8	0.37	89.9	0.34	10,000	5,000	0.195		0
92.9	RT	3.0	96.8	1.08	89.9	1.00	1,000	9,000	0.67		0
92.9	RT	3.0	96.8	1.79	89.9	1.66	100	900	1.33		0
92.9	RT	3.0	96.8	2.50	89.9	2.32	10	90	1.99		0
92.9	RT	3.0	96.8	3.20	89.9	2.97	1	9	2.64		0
92.9	RT	3.0	50	50	46.4	46.4	1	1	47.4	$3.5 \times 10^3$	0.000285

$$\sum \left( \frac{n}{N} \right)_{\text{thrust beam cap}} = 0.000285 \text{ for one flight}$$

$$\text{Fatigue life} = \frac{1}{4(0.000285)} = 877 \text{ missions}$$

NOTES:

- (1) Alternating thrust in percent of design thrust from Figure 2-34.
- (2) Cycles for one flight.
- (3) Material: Ti-6Al-4V annealed.

of the vertical tail box fatigue life to perturbation of the ultimate factor of safety. The reduced fatigue life at low safety factors is due to the resulting higher limit operating stresses. The curve shows that even for a low ultimate factor of safety, the fatigue life of the box far exceeds the required 100 mission design life. Figure 4-15 presents the variation of the vertical tail box fatigue life as a function of the fatigue initiation scatter factor.

#### 4.7 CREW MODULE

This section presents the fatigue damage analysis for the crew module and the sensitivity of its fatigue life to perturbations of factor of safety and fatigue crack initiation scatter factor. Table 4-8 presents the fatigue damage analysis for the baseline fail-safe crew module. The analysis indicates a fatigue life of 2,500,000 missions, which is very high and indicates that fatigue is not critical for the module. Figure 4-16 presents the sensitivity of the crew module fatigue life to factor of safety perturbations. The reduced fatigue life at lower safety factors is due to the resulting higher limit operating stresses. The ultimate factor of safety was perturbed over the range of 1.5 to 5.0, while the yield factor of safety was perturbed over the range of 1.3 to 1.7. The safe fatigue life is determined by the fail-safe requirement for ultimate factors of safety of less than 4.2. Lower fatigue lives result only if the fail-safe requirement is relaxed. Fatigue lives that result for lower safety factors, when fail-safe isn't required, are

shown in the inset of Figure 4-16. If fail-safe is not required and safety factors are reduced far enough, the reduction in fatigue life is limited by the 1.5 proof factor requirement. The figure shows that the crew module has far more than the required 100 missions service life for all factors of safety investigated. Figure 4-17 shows the variation of fatigue life as a function of the fatigue crack initiation scatter factor.

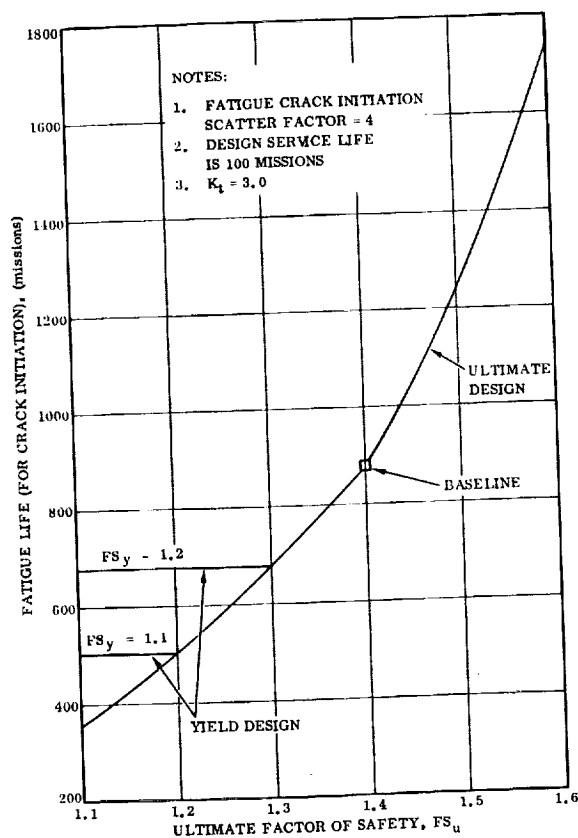


Figure 4-10. Thrust Beam Cap Sensitivity of Fatigue Life to Factor of Safety Perturbations



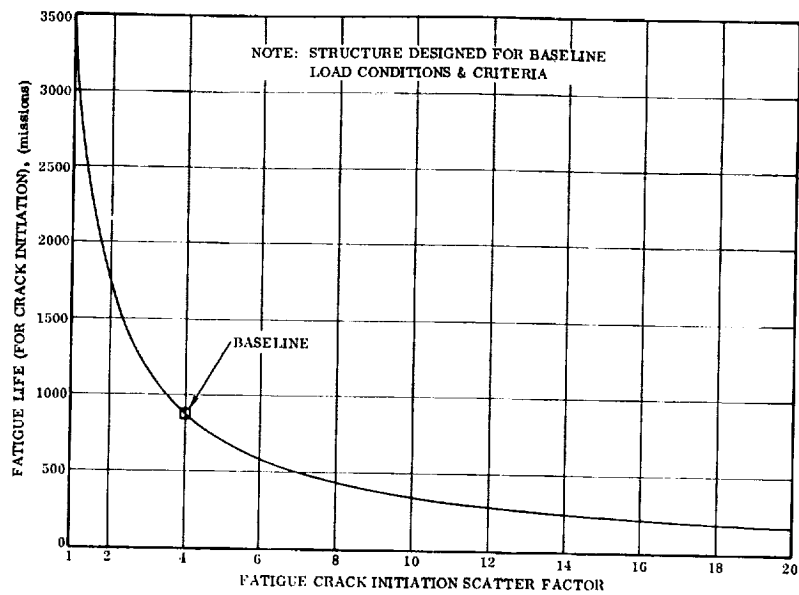


Figure 4-11. Thrust Beam Cap Fatigue Life (for Crack Initiation) Versus Scatter Factor

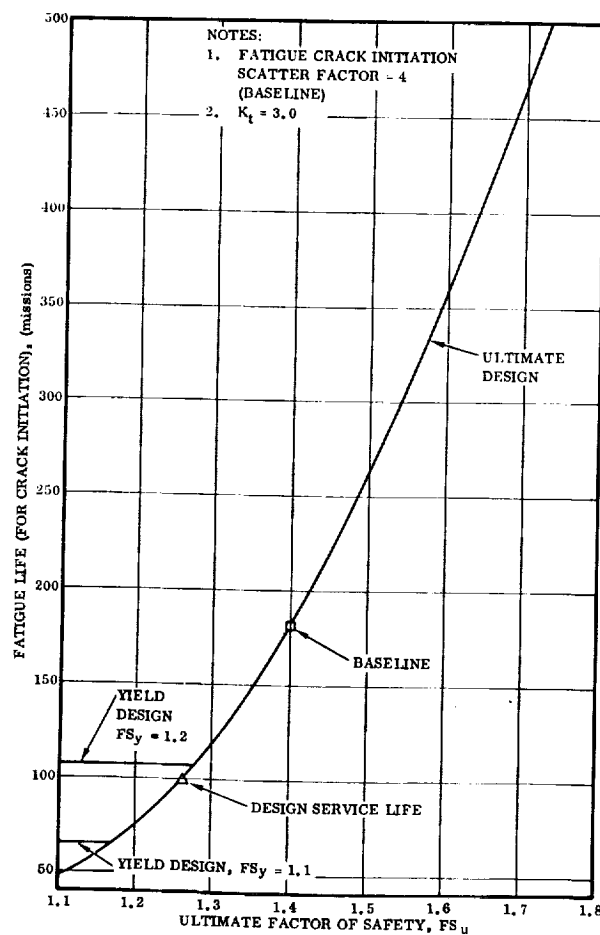


Figure 4-12. Wing Spar Cap Sensitivity of Fatigue Life to Factor of Safety Perturbations

Table 4-6. B-9U Wing Spar Caps Fatigue Damage Analysis

Mission Phase	T	$\sigma_{\text{limit}}$	$\sigma_{\text{mean}}$	$\sigma_{\text{alt}}$	$\sigma_{\text{mean}}$	$\sigma_{\text{alt}}$	$K_t$	N	n	$\frac{n}{N}$
	(°F)	(ksi)	$\sigma_{\text{limit}}$	$\sigma_{\text{alt}}$	(ksi)	(ksi)				
			(1)	(1)						
Ascent	RT	91.2	0	0.015	0	1.37	3.0	$\infty$	90,000	0
			0	0.025	0	2.28			9,000	0
			0	0.035	0	3.19			900	0
			0	0.045	0	4.10			90	0
			0	0.055	0	5.01			9	0
			0.15	0.035	13.7	3.2			90,000	0
			0.15	0.05	13.7	4.6			9,000	0
			0.15	0.065	13.7	5.9			900	0
			0.15	0.08	13.7	7.3			90	0
			0.15	0.09	13.7	8.2			9	0
			0	0.055	0	5.0			90,000	0
			0	0.09	0	8.2			9,000	0
			0	0.125	0	11.4			900	0
			0	0.155	0	14.1			90	0
			0	0.185	0	16.9			9	0
			0.40	0.08	36.5	7.3			90,000	0
			0.40	0.145	36.5	13.2			9,000	0
			0.40	0.21	36.5	19.2		500,000	900	0.0018
			0.40	0.27	36.5	24.6		90,000	90	0.0010
			0.40	0.33	36.5	30.1		30,000	9	0.0003
			0.10	0.105	9.1	9.6		$\infty$	90,000	0
			0.10	0.185	9.1	16.9		$\infty$	9,000	0
			0.10	0.30	9.1	27.4		170,000	900	0.0052
			0.10	0.45	9.1	41.0		20,000	90	0.0045
			0.10	0.605	9.1	55.1		5,500	9	0.0016
			0.15	0.135	13.7	12.3		$\infty$	90,000	0
			0.15	0.20	13.7	18.2		$4 \times 10^6$	9,000	0.0022
			0.15	0.37	13.7	33.7		50,000	900	0.0180
			0.15	0.61	13.7	55.6		5,000	90	0.0180
			0.15	0.80	13.7	72.9		1,900	9	0.0047
Ascent	RT	91.2	0.15	0.80	13.7	72.9				
Entry	650	91.2	0.075	0.075	6.8	6.8		$\infty$	90,000	0
			0.135	0.135	12.3	12.3		$\infty$	9,000	0
			0.185	0.185	16.9	16.9		$1 \times 10^6$	500	0.0005
			0.23	0.23	21.0	21.0		$8 \times 10^4$	250	0.0031
			0.37	0.37	33.7	33.7		$8 \times 10^3$	150	0.0188
			0.47	0.47	42.9	42.9		$3 \times 10^3$	100	0.0333
			0.50	0.50	45.6	45.6		$2.5 \times 10^3$	1	0.0004
Entry	650	91.2	0.50	0.50	45.6	45.6				
Cruise/Landing (2)	RT	91.2	0.20	0.07	18.2	6.3		$\infty$	180,000	0
			0.17	0.17	15.3	15.3		$\infty$	18,000	0
			0.27	0.27	23.9	23.9		$2.2 \times 10^5$	1,800	0.0082
			0.36	0.36	32.8	32.8		$3.8 \times 10^4$	180	0.0047
			0.20	0.43	18.2	39.6		$1.6 \times 10^4$	18	0.00131
Cruise/Landing (2)	RT	91.2	0.20	0.43	18.2	39.6				
Taxi (2)	RT	91.2	-0.021	0.040	-1.9	3.6		$\infty$	180,000	0
			0.060	0.060	5.5	5.5		$\infty$	18,000	0
			0.080	0.080	7.3	7.3		$\infty$	1,800	0
			0.095	0.095	8.7	8.7		$\infty$	180	0
			-0.021	0.110	-1.9	10.0		$\infty$	18	0
Taxi (2)	RT	91.2	-0.021	0.110	-1.9	10.0				
GAG (2)	RT	91.2	0.255	0.385	23.2	35.1	3.0	$2 \times 10^4$	200	0.0100

Table 4-6. B-9U Wing Spar Caps Fatigue Damage Analysis, Contd

Mission Phase	$n/N$	Fatigue life = $\frac{100}{4(0.1374)} = 182$ missions, based on a scatter factor of 4.	
Ascent	0.0573	<b>NOTES:</b>  (1) To provide for one ferry flight per mission, the number of cycles for the cruise/landing and taxi phases has been increased by a factor of 2.0, and two GAG cycles per mission added, using a minimum stress from the taxi phase and a maximum stress from the cruise/landing phase.  (2) Material: Ti6Al-4V annealed.	
Entry	0.0561		
Cruise/Landing	0.0140		
Taxi	0		
GAG	0.0100		
$\Sigma (n/N)$	0.1374		

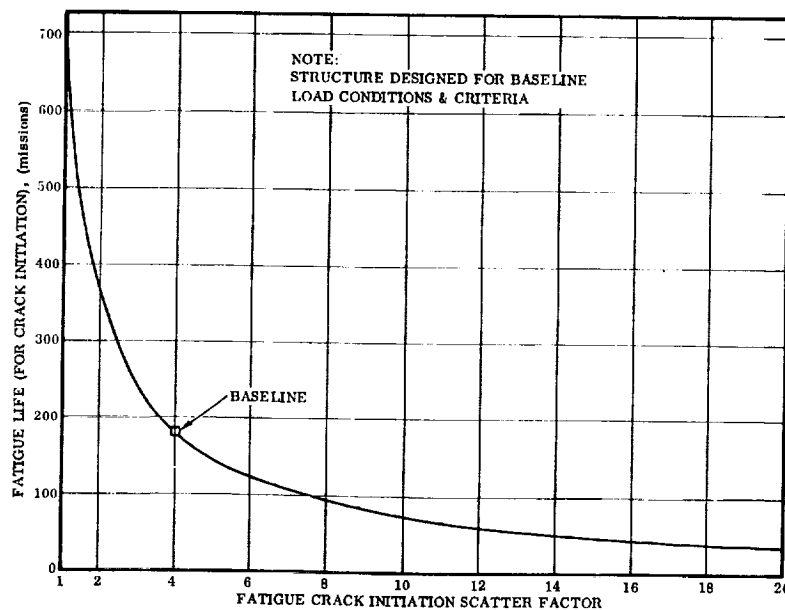


Figure 4-13. Wing Spar Caps Fatigue Life (for Crack Initiation) Versus Scatter Factor

Table 4-7. B-9U Vertical Tail Fatigue Damage Analysis

Mission Phase	T (°F)	$\sigma_{limit}$ ksi	$\frac{\sigma_{mean}}{\sigma_{limit}}$	$\frac{\sigma_{alt}}{\sigma_{limit}}$	$\sigma_{mean}$ (ksi)	$\sigma_{alt}$ (ksi)	$K_t$	N	n	n/N
Ascent - Segment (1)	RT	34	0	0.041	0	1.4	3.0	$\infty$	90,000	0
		34	0	.076	0	2.6	3.0	$\infty$	9,000	0
		34	0	.110	0	3.7	3.0	$\infty$	900	0
		34	0	.145	0	4.9	3.0	$\infty$	90	0
		34	0	.180	0	6.1	3.0	$\infty$	9	0
Ascent - Segment (2)	RT	34	0	.113	0	3.8	3.0	$\infty$	90,000	0
		34	0	.220	0	7.5	3.0	$\infty$	9,000	0
		34	0	.326	0	11.1	3.0	$\infty$	900	0
		34	0	.435	0	14.8	3.0	$\infty$	90	0
		34	0	.545	0	18.5	3.0	$10^7$	9	0
Ascent - Segment (3)	RT	34	0	.190	0	6.5	3.0	$\infty$	90,000	0
		34	0	.371	0	12.6	3.0	$\infty$	9,000	0
		34	0	.550	0	18.7	3.0	$10^7$	900	0
		34	0	.730	0	24.8	3.0	$6 \times 10^5$	90	0
		34	0	.910	0	30.9	3.0	$1.8 \times 10^5$	9	0
Ascent - Segment (4)	RT	34	0	.138	0	4.7	3.0	$\infty$	90,000	0
		34	0	.262	0	8.9	3.0	$\infty$	9,000	0
		34	0	.388	0	13.2	3.0	$\infty$	900	0
		34	0	.511	0	17.4	3.0	$\infty$	90	0
		34	0	.639	0	21.7	3.0	$1.9 \times 10^6$	9	0
Ascent - Segment (5)	RT	34	0	.091	0	3.1	3.0	$\infty$	90,000	0
		34	0	.184	0	6.3	3.0	$\infty$	9,000	0
		34	0	.276	0	9.4	3.0	$\infty$	900	0
		34	0	.366	0	12.4	3.0	$\infty$	90	0
		34	0	.455	0	15.5	3.0	$\infty$	9	0
Ascent - Segment (6)	RT	34	0	.058	0	2.0	3.0	$\infty$	90,000	0
		34	0	.114	0	3.9	3.0	$\infty$	9,000	0
		34	0	.166	0	5.6	3.0	$\infty$	900	0
		34	0	.216	0	7.3	3.0	$\infty$	90	0
		34	0	.270	0	9.2	3.0	$\infty$	9	0
Ascent - Segment (7)	RT	34	0	.026	0	0.9	3.0	$\infty$	90,000	0
		34	0	.036	0	1.2	3.0	$\infty$	9,000	0
		34	0	.050	0	1.7	3.0	$\infty$	900	0
		34	0	.065	0	2.2	3.0	$\infty$	90	0
		34	0	.079	0	2.7	3.0	$\infty$	9	0

Table 4-7. B-9U Vertical Tail Fatigue Damage Analysis, Contd

Mission Phase	T (°F)	$\sigma_{\text{limit}}$ (ksi)	$\frac{\sigma_{\text{mean}}}{\sigma_{\text{limit}}}$	$\frac{\sigma_{\text{alt}}}{\sigma_{\text{limit}}}$	$\sigma_{\text{mean}}$ (ksi)	$\sigma_{\text{alt}}$ (ksi)	$K_t$	N	n	n/N
Cruise/Landg	RT	34	0	.210	0	7.1	3.0	$\infty$	180,000	0
		34	0	.267	0	9.1	3.0		18,000	0
		34	0	.322	0	11.0	3.0		1,800	0
		34	0	.380	0	12.9	3.0		180	0
		34	0	.436	0	14.8	3.0		18	0

Summary

Mission Phase	n/N
Ascent	.0002
Cruise/Landg	0
$\Sigma(n/N)$	.0002

$$\text{Fatigue life} = \frac{100}{\text{S.F.} \times \Sigma(n/N)} = \frac{100}{4(.0002)} = 125,000 \text{ missions, based on a scatter factor of 4.}$$

NOTES:

- 1) To provide for one ferry flight per mission, the number of cycles for the cruise/landing phase has been increased to a factor of 2.
- 2) Material is Ti-6Al - 4V annealed.

Table 4-8. Crew Module Fatigue Damage Analysis

Phase	Design $\sigma_{\text{limit}}$ (ksi)	T Deg. F	$K_t$	$\Delta P_{\text{max}}$ (psi)	$\Delta P_{\text{min}}$ (psi)	$\sigma_{\text{max}}$ (ksi)	$\sigma_{\text{min}}$ (ksi)	$\sigma_{\text{mean}}$ (ksi)	$\sigma_{\text{alt}}$ (ksi)	n	N	$\frac{n}{N}$
Proof $\alpha = 1.5$	15.0	RT	3.0	22.5	0	22.5	0	11.25	11.25	1	$1.1 \times 10^5$	$8.9 \times 10^{-6}$
Flight	15.0	RT	3.0	15	0	15.0	0	7.5	7.5	100	$1.0 \times 10^7$	$10 \times 10^{-6}$
Ferry @ 20,000 ft.	15.0	RT	3.0	8.5	0	8.5	0	4.25	4.25	100	$\infty$	0

$$\Sigma \left( \frac{n}{N} \right) = 0.0000189 \text{ for 1 lifetime of 100 missions.}$$

$$0.0000100 = \text{damage due to flight for 100 missions.}$$

$$1 - 0.0000189 = 0.9999811 = \text{available damage after 1 lifetime.}$$

$$\text{Safe fatigue-life} = \frac{100}{4} \left( 1 + \frac{0.9999811}{0.0000100} \right) = 2.50 \times 10^6 \text{ missions.}$$

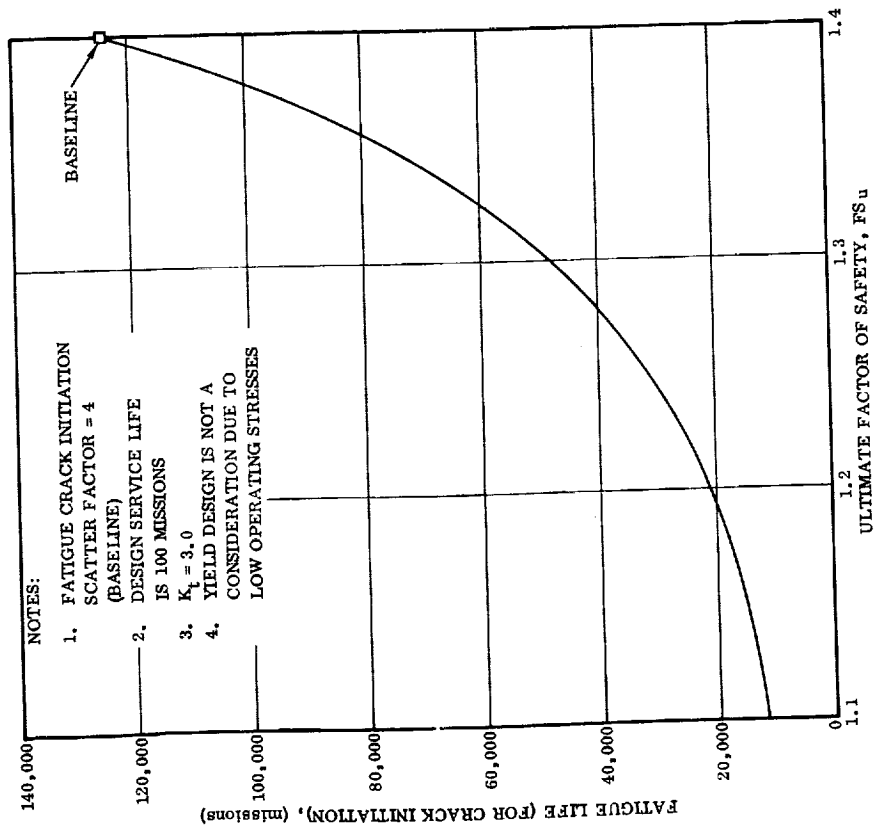


Figure 4-14. Vertical Stabilizer Sensitivity of Fatigue Life to Factor of Safety Perturbations

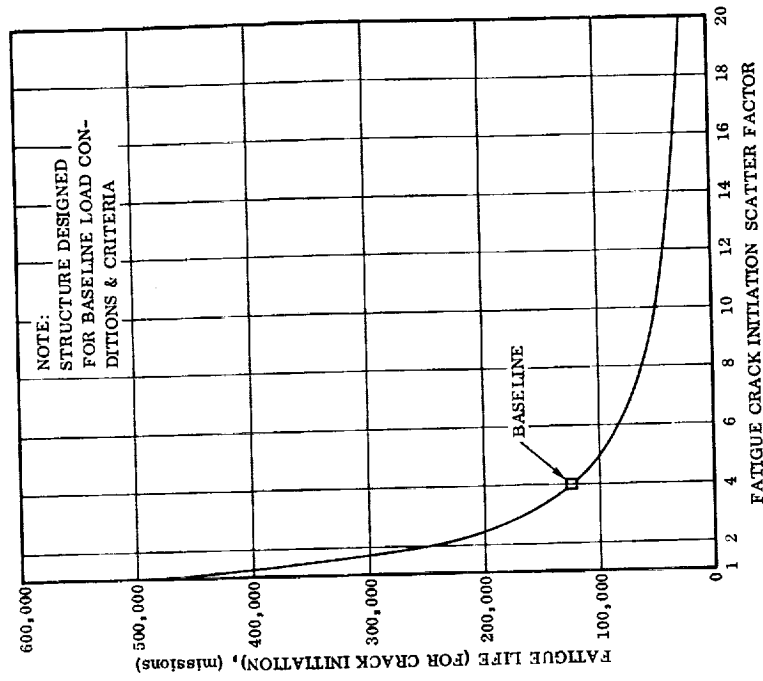


Figure 4-15. Vertical Stabilizer Fatigue Life (for Crack Initiation) Versus Scatter Factor

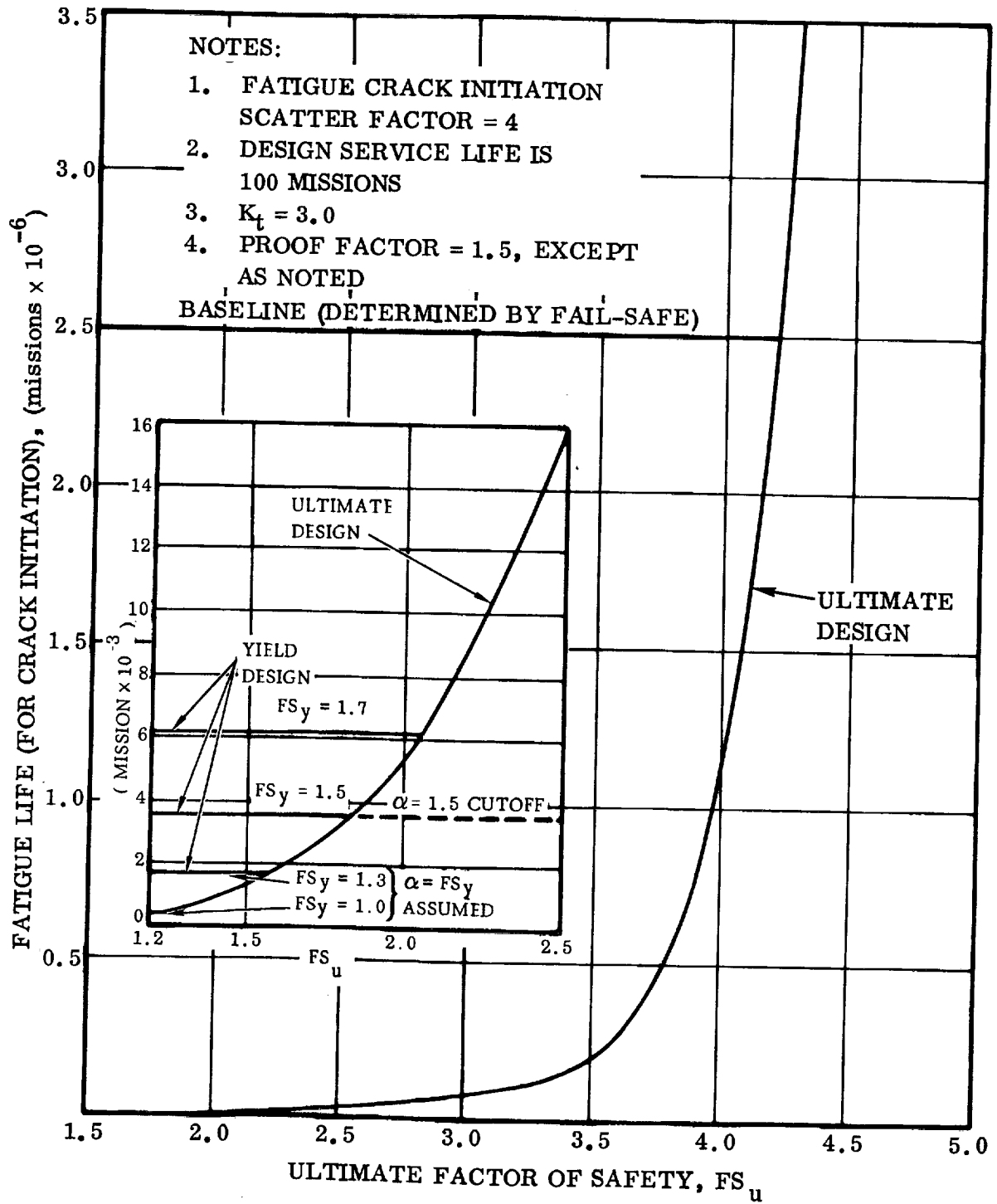


Figure 4-16. Sensitivity of Fatigue Life to  
Factor of Safety Perturbations

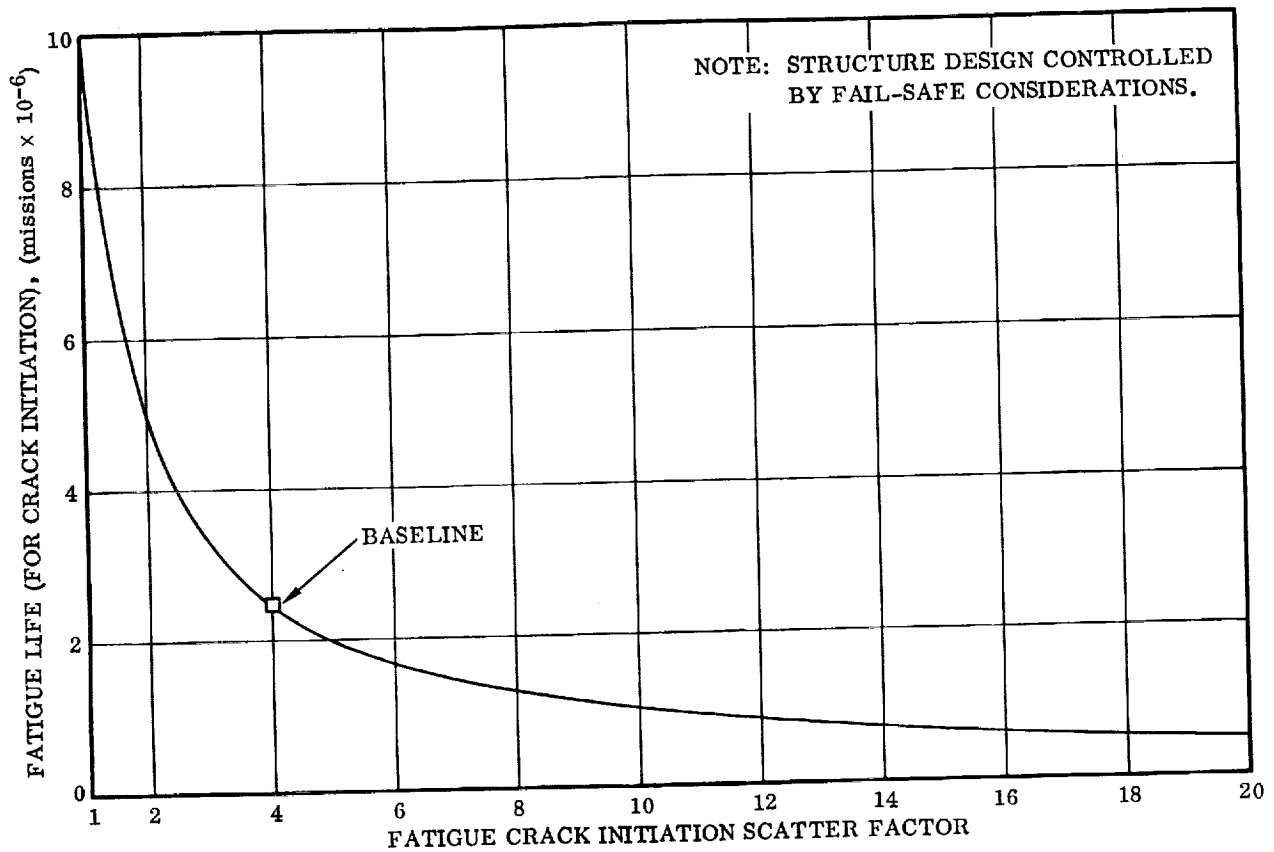


Figure 4-17. Crew Module Fatigue Life (for Crack Initiation) Versus Scatter Factor



## SECTION 5

### SAFE-LIFE ANALYSIS

This section presents the results of crack growth studies when the structural components are assumed to contain crack-like flaws. Flights to failure are calculated for all components.

The crack growth analyses are based on a Convair crack growth computer program called CRACKPROP, which calculates crack growth for both cyclic and sustained loads. Initial flaws are assumed to be elliptical surface flaws or through-cracks for the LO<sub>2</sub> and LH<sub>2</sub> propellant tank walls and the vertical stabilizer skin. Corner cracks emanating from flange edges are assumed for the thrust structure, orbiter support bulkhead, and wing spar caps. An analysis is also made assuming a crack initiating at a fastener hole in those components where mechanical fasteners may be used, i.e., the wing structure, thrust structure, and the orbiter aft support bulkhead.

For the LO<sub>2</sub> and LH<sub>2</sub> propellant tanks the initial flaw size is assumed to be that flaw screened by proof test using a plane strain fracture toughness ( $K_{Ic}$ ) value. When the calculated elliptical surface flaw screened by the proof test is greater than the tank wall thickness, an equivalent through-crack of an area equal to the area of a surface flaw on the verge of leakage is assumed.

Minimum fracture toughness values were used for all calculations of initial and critical flaw sizes. Because of this, the safe-lives calculated for the tanks should be treated with caution. However, where the initial flaw size was not dependent on material toughness the use of the minimum toughness in determining the critical flaw size does give the shortest life.

In addition to the basic safe-life analysis of the major structural components selected for study, this section also presents proof factor, apparent factors of safety, and weight sensitivity to flaw growth scatter factor for structure designed by proof pressure. In addition, the sensitivity of safe-life to factor of safety and flaw growth scatter factor is presented for all components.

#### 5.1 CYCLIC AND SUSTAINED FLAW GROWTH RATE CURVES

Figures 5-1 through 5-6 present crack growth rate curves of  $da/dn$  versus  $\Delta K_I$  and  $da/dt$  versus  $\Delta K_I$ , which are used in this section in the safe-life analysis of structural components containing flaws.

The cyclic growth rate curves ( $da/dn$  versus  $\Delta K_I$ ) for the 2219-T87 aluminum base metal at room temperature and at -320°F were derived from data found in Reference

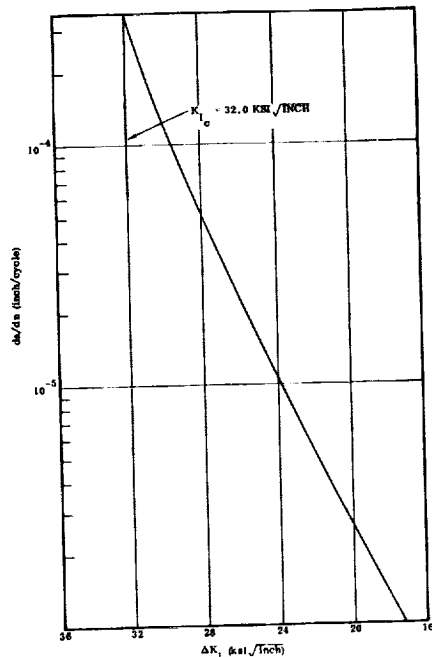


Figure 5-1. Cyclic Flaw Growth Rate for 2219-T87 Aluminum Alloy at Room Temperature

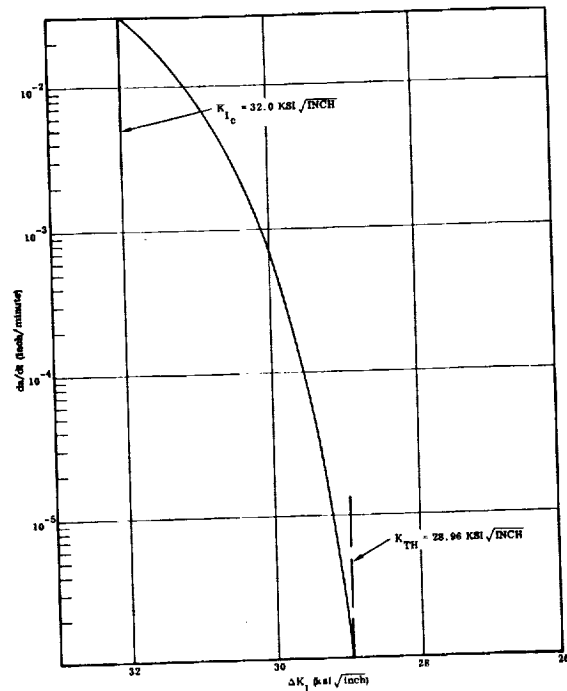


Figure 5-2. Sustained Flaw Growth Rate for 2219-T87 Aluminum Alloy at Room Temperature

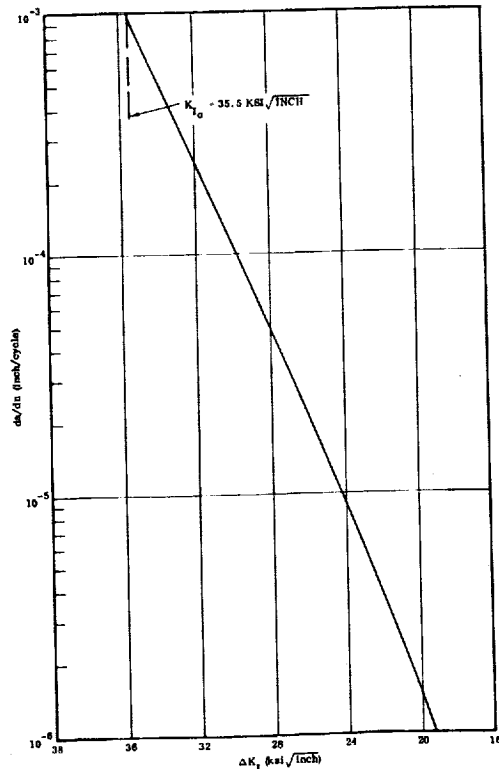


Figure 5-3. Cyclic Flaw Growth Rate for 2219-T87 Aluminum Alloy at -320°F

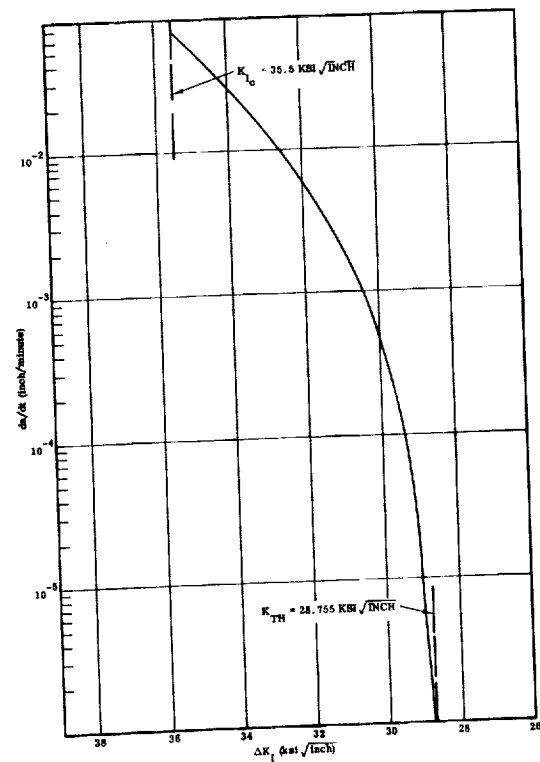


Figure 5-4. Sustained Flaw Growth Rate for 2219-T87 Aluminum Alloy at -320°F

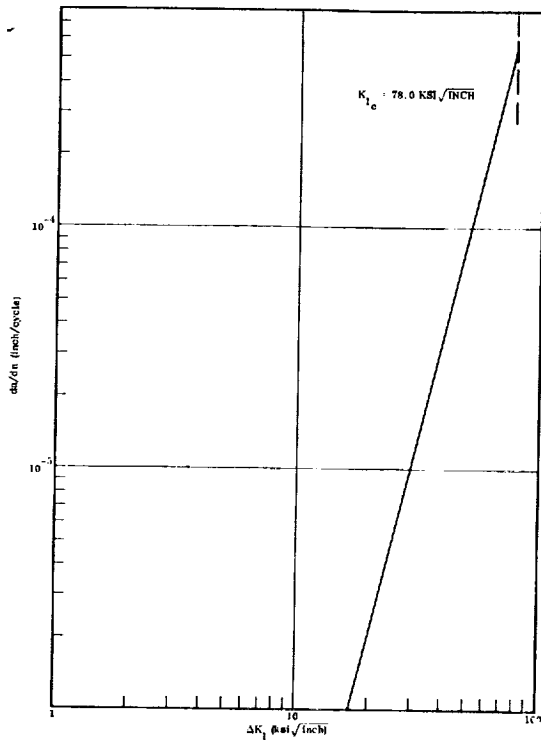


Figure 5-5. Cyclic Flaw Growth Rate for Ti-6Al-4V (ELI) Annealed Titanium Alloy at Room Temperature

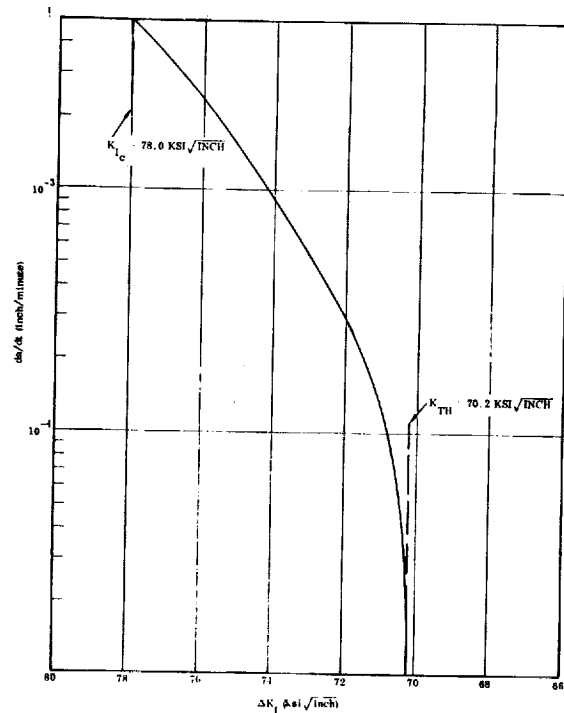


Figure 5-6. Sustained Flaw Growth Rate for Ti-6Al-4V (ELI) Annealed Titanium Alloy at Room Temperature

14. The sustained growth rate curves ( $da/dt$  versus  $\Delta K_I$ ) for the 2219-T87 aluminum base metal at room temperature and at  $-320^\circ\text{F}$  were derived from data found in Reference 15.

The cyclic growth rate curve ( $da/dn$  versus  $\Delta K_I$ ) for the Ti-6Al-4V annealed titanium base metal at room temperature was derived from data found in Reference 16. The sustained growth rate curve for the same material and temperature was derived from data found in References 16 and 17.

## 5.2 LIQUID OXYGEN TANK

5.2.1 LO<sub>2</sub> TANK SAFE-LIFE ANALYSIS. The LO<sub>2</sub> propellant tank is assumed to contain two distinct types of flaws. These are an elliptical surface flaw and a through crack, for which the initial size of each is developed in this section. These flaws are propagated to a specified failure criterion under the influence of the applied pressure spectrum loading. The critical crack lengths for both types of flaws are also developed here.

The applied pressure spectrum loading for the LO<sub>2</sub> tank was developed from the curve of Figure 2-36. Only those portions of the total loading spectrum that could contribute to the growth of the flaws were included in the spectrum for the tank. It should be noted here that it was necessary to take average pressures over a given time span to approximate the curve. The pressures used in developing the final spectrum are as follows:

#### LO<sub>2</sub> Tank Upper Dome Equator Pressures

Pressure (psi)	Time at Pressure (minutes)	Description
17.5	4.0	Nominal ullage pressure
12.0	6.0	Vent after staging pressure
19.5	4.0	Pressure regulator malfunction stress (assumed to occur once every 20 flights)

The tensile stresses in the LO<sub>2</sub> tank at the upper dome equator were developed from the pressures in the preceding list through the use of the following formula.

$$\sigma = \frac{pR}{t} = \frac{p(198)}{0.090}$$

p = internal pressure (psi)

R = 198 inches = tank radius

t = 0.090 inch = tank wall thickness at the upper dome equator

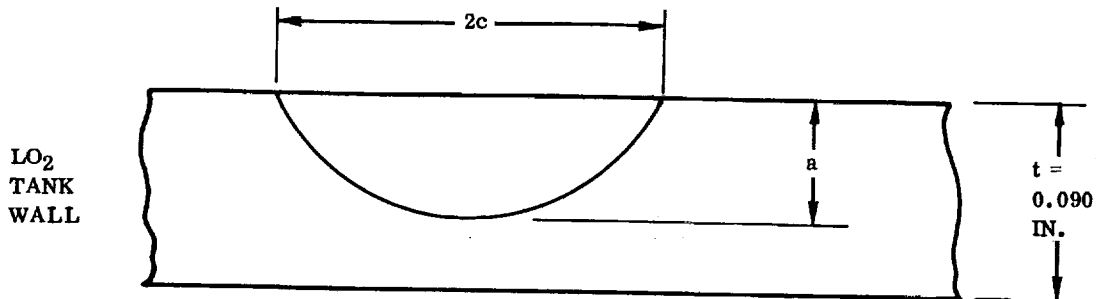
The results of this calculation and the final form of the pressure loading spectrum are as follows:

#### LO<sub>2</sub> Tank Pressure Loading Spectrum

Minimum Stress (ksi)	Maximum Stress (ksi)	Cycles per Flight	Time per Flight (minutes)
0.000	38.8*	1	4.0
0.000	38.8*		6.0
0.000	26.4		

\*Once every 20 flights, this nominal ullage pressure stress is replaced with the pressure regulator malfunction stress of 42.8 ksi.

The elliptical surface flaw is assumed to have two different initial aspect ratios,  $a/2c$  (see sketch below). These two aspect ratios are  $a/2c = 0.1$  and  $a/2c = 0.4$ .



The initial flaw size, which is calculated here for both the 0.1 and 0.4 aspect ratios, is the maximum flaw size that would be screened by a proof test of the tank, using a minimum value for the material toughness parameter,  $K_{Ic}$ , to be consistent with the value used in the crack growth analysis, and using the yield stress for the maximum stress developed in the tank wall during a proof test.

The equation for the maximum stress intensity factor for the elliptical surface flaw, which is used to calculate the maximum flaw size screened by a proof test, is as follows:

$$K_I = \frac{1.1 \sigma \sqrt{\pi} \sqrt{a} (M_K)}{\sqrt{\phi^2 - 0.212 (\sigma/\sigma_Y)^2}} \quad (\text{Reference 10, Equation IX-8})$$

where

$\sigma$  = applied stress (ksi)

$\sigma_Y$  = tensile yield stress (ksi)

$a$  = flaw size (inch)

$\phi^2$  = a function depending upon the value of  $a/2c$

for  $a/2c = 0.1$ ,  $\phi^2 = 1.10355$

for  $a/2c = 0.4$ ,  $\phi^2 = 2.01096$

$M_K$  = deep flaw correction factor, is a function of  $a/t$  and  $a/2c$ , from Reference 18, Page 135.

The LO<sub>2</sub> tank is proof tested at room temperature so that the value of  $K_{Ic}$  used in the following calculations will be the minimum value of  $K_{Ic}$  at room temperature. This value is  $K_{Ic} = 32.0 \text{ ksi } \sqrt{\text{inch}}$  (Reference 6, Figure 52, lower curve). Substituting this value of  $K_{Ic}$  into the equation for the stress intensity factor and using  $\sigma_Y = 51.0 \text{ ksi}$  (2219-T87 aluminum base metal at room temperature) as the proof test stress, we can arrive at a value of 'a' from the following equation:

$$32.0 = \frac{1.1 (51.0) \sqrt{\pi} \sqrt{a} (M_K)}{\sqrt{\phi^2 - 0.212 (51.0/51.0)^2}}$$

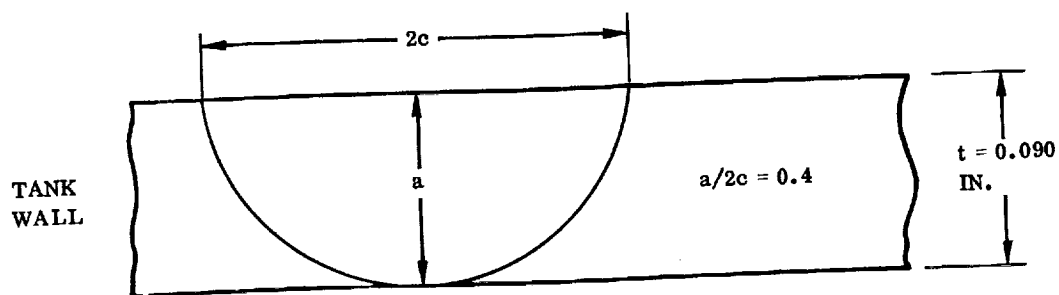
Note in the above equation that the variable  $M_K$  is a function of the flaw size, 'a', and that a trial and error solution is necessary to find the correct value of 'a'. The results of this solution for both aspect ratios of 0.1 and 0.4 are shown below.

For  $a/2c = 0.1$ , the maximum flaw size that would be screened by a proof test is:

$$a_i = 0.05464 \text{ inch}$$

For  $a/2c = 0.4$ , the maximum flaw size that would be screened by a proof test resulted in a flaw size, 'a', which was larger than the thickness of the tank wall,  $t = 0.090 \text{ inch}$ .

Since the 0.4 aspect ratio results in an initial flaw size greater than the thickness, an equivalent through crack, with an area equal to the area of a surface flaw of aspect ratio  $a/2c = 0.4$  on the verge of leakage, is calculated here.



Cross-sectional area of flaw =  $A_c$

$$A_c = \frac{\pi (a) (c)}{2} = 0.01590 \text{ in}^2$$

For a through crack, the area would be calculated by

$$A_c = (2c) \times t \text{ or } (2c) = \frac{A_c}{t}$$

Therefore the equivalent through crack would have a  $(2c)_i$  dimension of

$$(2c)_i = \frac{A_c}{t} = \frac{0.01590}{0.090} = 0.17671 \text{ inch}$$

The elliptical surface flaw of initial size  $a_i = 0.05464$  inch and the through crack of initial size  $(2c)_i = 0.17671$  inch are propagated to failure. The run to failure is made using material properties and growth rate curves for 2219-T87 aluminum base metal at  $-320^\circ\text{F}$ . The  $-320^\circ\text{F}$  temperature is used because growth rates at this temperature are more critical than those at room temperature, and the  $\text{LO}_2$  tank at the upper dome equator is assumed to be prechilled to  $-320^\circ\text{F}$ . The critical flaw sizes must therefore be calculated from the properties of the material at  $-320^\circ\text{F}$ .

The minimum value of  $K_{Ic}$  is used to calculate critical flaw sizes, and for the  $-320^\circ\text{F}$  temperature this value is  $35.5 \text{ ksi } \sqrt{\text{inch}}$  (Reference 6, Figure 52, lower curve at  $-320^\circ\text{F}$ ). The tensile yield at this temperature is taken to be  $\sigma_Y = 61.0 \text{ ksi}$ . The maximum stress in the spectrum, on which the critical flaw sizes must be based, is  $\sigma = 44.0 \text{ ksi}$ .

For the elliptical flaw of aspect ratio  $a/2c = 0.1$ , the critical flaw size,  $a_{cr}$ , is calculated from the equation

$$35.5 = \frac{1.1 (44.0) \sqrt{\pi} \sqrt{a_{cr}} (M_K)}{\sqrt{1.10355 - 0.212 (44.0/61.0)^2}}$$

which results in a value of  $a_{cr} = 0.07091$  inch.

For the through crack the equation for the stress intensity factor is

$$K_I = \frac{\sigma \sqrt{\pi} \sqrt{2c}}{\sqrt{2 - (\sigma/\sigma_Y)^2}} \quad (\text{Reference 18, Page 28})$$

Substituting the critical values into this equation results in

$$35.5 = \frac{44.0 \sqrt{\pi} \sqrt{(2c)_{cr}}}{\sqrt{2 - (44.0/61.0)^2}}$$

or  $(2c)_{cr} = 0.30660$  inch.

Results of flaw growth calculations:

Carrying out the analysis described above by use of a computer program, the following results were obtained.

Elliptical Surface Flaw,  $a/2c = 0.1$  (See Figure 5-7)

Starting with an initial flaw size of  $a_i = 0.05464$  inch, it took 294 flights for the flaw to grow to the critical size of  $a_{cr} = 0.07091$  inch (see sketch below). Note that a scatter factor of 1.5 was used on the number of flights to failure.

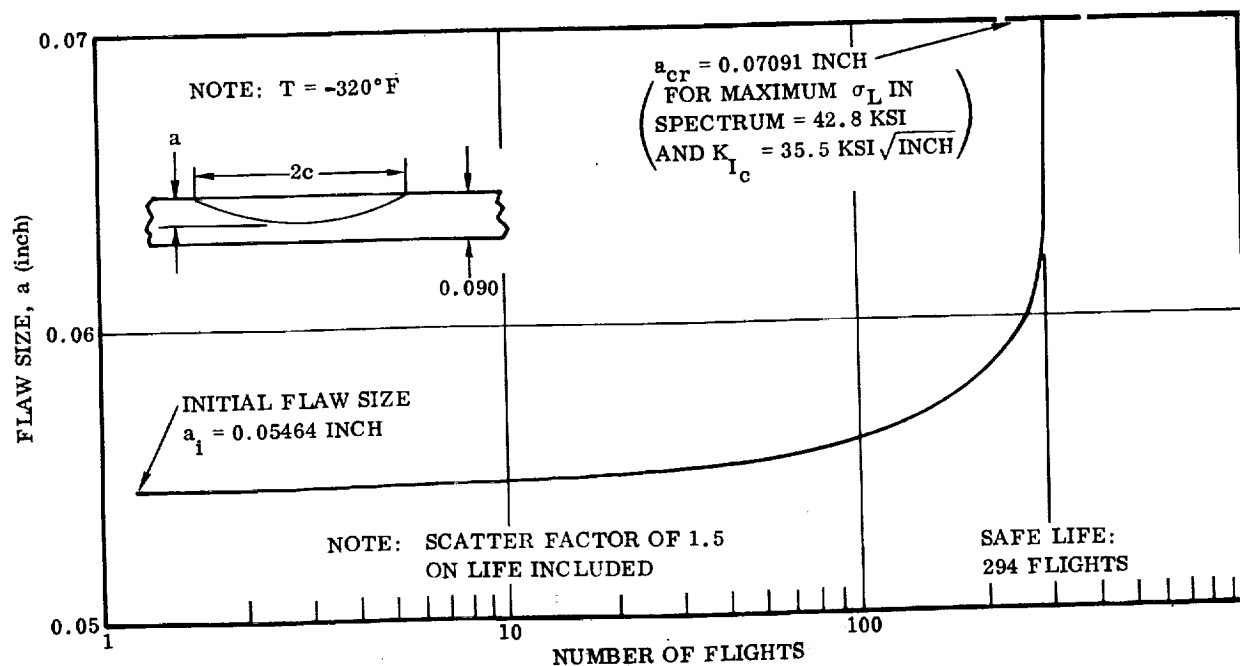
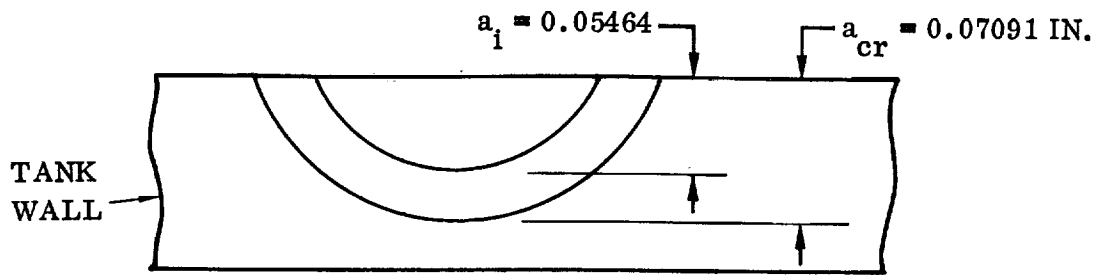


Figure 5-7. Crack Growth in  $\text{LO}_2$  Tank for Pressure Load Spectrum (Surface Flaw,  $a/2c = 0.1$ )





Through Crack (See Figure 5-8)

Starting with an initial flaw size of  $(2c)_i = 0.17671$  inch, it took 867 flights for the flaw to grow to the critical size of  $(2c)_{cr} = 0.30660$  inch. Again a scatter factor of 1.5 was used on the flights to failure.

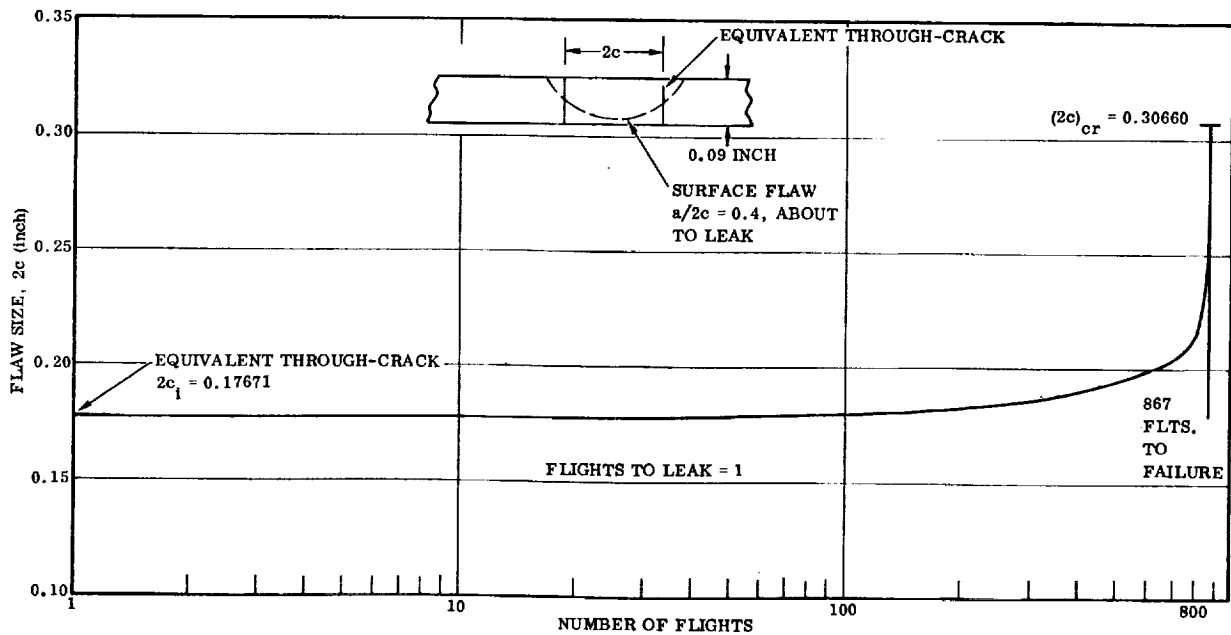


Figure 5-8. Crack Growth in  $\text{LO}_2$  Tank for Pressure Load Spectrum (Surface Flaw,  $a/2c = 0.4$  and Equivalent Through Crack)

5.2.2 LO<sub>2</sub> TANK PROOF FACTOR AND APPARENT FACTORS OF SAFETY. For final verification of the structural integrity of the main Space Shuttle booster LO<sub>2</sub> tank, primary reliance is placed in a pressure proof test prior to assembly into the booster vehicle.

The proof test logic is explained in detail in Reference 19, Fracture Control of Metallic Pressure Vessels, NASA SP8040. The proof test consists of loading the tanks to a stress level greater than the maximum stress level expected in service. In addition, the proof test should be conducted at a temperature consistent with the operating temperature. If the proof test is completed successfully, the proof test provides assurance that all existing flaws or defects are less than the critical size required for fracture at the proof stress level. In addition, the safe-life of the tank at the operating stress level can be determined by fracture mechanics analysis where the safe-life ensured by the proof test is the time required to grow the smaller "proof stress flaw" to the larger critical size associated with the maximum service operating stress. The task consists of developing a  $K_{Ii}/K_{Ic}$  versus number of flights curve by integrating the combined cyclic and sustained load flaw growth over arbitrarily selected flight increments using the flight pressure load spectrum and the flaw growth data. The final curve for the LO<sub>2</sub> is presented in Figure 5-9.

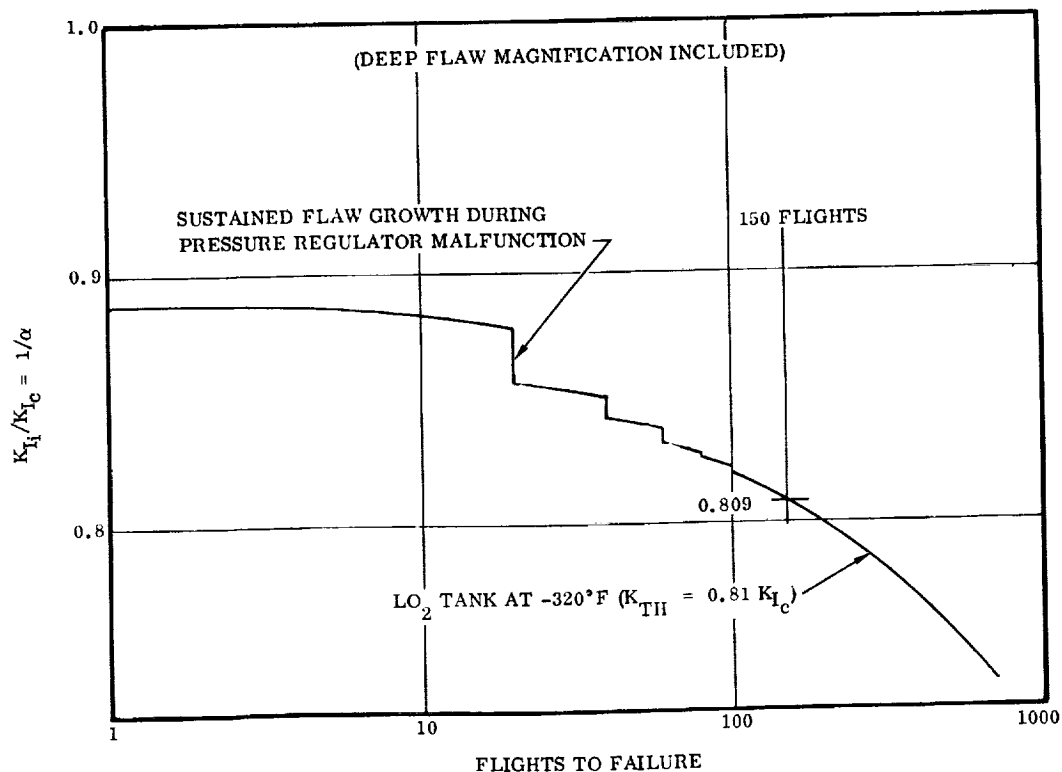


Figure 5-9. LO<sub>2</sub> Tank Stress Intensity Ratio Versus Flights to Failure

The method for obtaining the proof factor,  $\alpha$ , from this plot is to read  $K_{I_1}/K_{I_C}$  for the desired number of flights to failure. In this case, for the baseline, the flights to failure were 150; that is, the scatter factor of 1.5 multiplied by the design service life of 100 flights\*. Then,

$$\alpha = \frac{1}{K_{I_1}/K_{I_C}} = \frac{1}{0.809} = 1.23$$

The  $LO_2$  tank is proof tested as illustrated in Figure 2-19. For the  $LO_2$  tank, a three-stage proof test with  $LN_2$  and air as the proof test medium is selected to minimize the weight impact of the proof test. The proof test steps are:

- a. Assemble lower dome (segment 1) to a manufacturing bulkhead, erect and support vertically, and proof test with  $LN_2$  and 49 psi ullage.
- b. Assemble lower dome to lower  $LO_2$  tank barrel (i.e., segment 2), assemble lower dome and barrel assembly to a manufacturing bulkhead, erect and support vertically, and proof test with  $LN_2$  and 32.5 psi ullage.
- c. Assemble lower dome and barrel assembly (i.e., segments 1 and 2) to a upper dome and barrel assembly (i.e., segment 3), erect and support horizontally, fill tank with void reducing plastic balls, and proof test with room temperature dry air at 21 psi pressure.

Due to the reduced limit design stresses required by the proof test for the safe-life of the tank, there is an apparent ultimate factor of safety that results, and it is given by the expression;

$$FS_u(\text{apparent}) = \frac{F_{ult}}{f_{limit}}$$

---

\*Comparison of the number of flights to failure computed in Section 5.2.1 reveals a difference between the actual computed value of safe-life, 294 flights, and the number of flights to failure used to determine the proof factor above. The primary reasons for the difference in the lives calculated are the differences in assumptions and data used to generate the  $K_{I_1}/K_{I_C}$  versus flights to failure curve, Figure 5-9, and the  $LO_2$  tank safe-life analysis of Section 5.2.1. Although deep flaw magnification for both analyses was used, they assume different skin thicknesses and load spectra, and they also utilize different flaw growth data. Therefore, close consistency between the calculated safe-life and the 150 missions used to determine the proof factor should not be expected.

The apparent ultimate factors of safety for the various LO<sub>2</sub> tank elements are computed below.

Upper Dome. Since the upper dome is designed by proof pressure, the apparent ultimate factor of safety is calculated to compare to the nominal ultimate safety factor of 1.4.

$$F_{tu} = 63,000 \text{ psi (2219-T87 at RT)}$$

$$f \text{ (limit operating)} = \frac{F_{ty}}{\alpha} = \frac{52,000}{1.23} = 42,100 \text{ psi}$$

$$FS_u \text{ (apparent)} = \frac{63,000}{42,100} = 1.495$$

Lower Dome. The lower dome is also designed by proof pressures; the nominal ultimate safety factor is 1.4.

$$F_{tu} = 75,000 \text{ psi (2219-T87 at } -297^{\circ}\text{F)}$$

$$f \text{ (limit operating)} = \frac{F_{ty}}{\alpha} = \frac{62,000}{1.23} = 50,400 \text{ psi}$$

$$FS_u \text{ (apparent)} = \frac{75,000}{50,400} = 1.49$$

Skins. The nominal ultimate factor of safety for the skins is 1.4, and they are designed by proof pressure. See Section 3.1.1.2 for determination of the skin thickness.

#### Forward of Tank Station 310

$$F_{tu} = 63,000 \text{ psi (2219-T87 at RT)}$$

$$f \text{ (limit operating)} = \frac{pR}{t} = \frac{1.75}{0.09} \times \frac{198}{1.23} = 38,750 \text{ psi}$$

$$FS_u \text{ (apparent)} = \frac{63,000}{38,750} = 1.625$$

#### Aft of Tank Station 310

Just aft of Station 310:

$$F_{tu} = 75,000 \text{ psi (2219-T87 at } -297^{\circ}\text{F)}$$

$$f(\text{limit operating}) = \frac{pR}{t} = \frac{17.5(198)}{0.105} = 33,200 \text{ psi}$$

$$FS_u (\text{apparent}) = \frac{75,000}{33,200} = 2.26$$

Just forward of the intersection with the lower dome:

$$f(\text{limit operating}) = \frac{pR}{t} = \frac{31(198)}{0.126} = 48,750$$

$$FS_u (\text{apparent}) = \frac{75,000}{48,750} = 1.54$$

It will be noted that for all the cases checked, the apparent  $FS_u$  is greater than the nominal baseline  $FS_u$  of 1.4.

**5.2.3 LO<sub>2</sub> TANK WEIGHT SENSITIVITY TO FLAW GROWTH SCATTER FACTOR PERTURBATIONS.** Since the LO<sub>2</sub> tank end domes and skin are designed by proof pressure and the curve of  $K_{I_1}/K_{I_C}$  versus flights to failure is given in Figure 5-9, it is possible to determine the weight sensitivity of these items to perturbations of the flaw growth scatter factor. The procedure followed is:

- Enter Figure 5-9 for the scatter factor of interest multiplied by the service life, (e.g., 2.0 scatter factor  $\times$  100 mission life = 200 missions).
- Obtain the new  $1/\alpha$  from the curve of Figure 5-9, (e.g., for 200 missions,  $1/\alpha = 0.798$ ,  $\alpha = 1.255$ ).
- Calculate the new element weight for:

$$\text{Proof pressure} = \alpha \times \text{maximum operating pressure.}$$

The weight sensitivity of the upper dome, lower dome, skin, and combined skin and domes to flaw growth scatter factor perturbations, using this procedure, is presented Figure 5-10 through 5-13 respectively.

**5.2.4 LO<sub>2</sub> TANK SAFE-LIFE SENSITIVITY TO FACTOR OF SAFETY AND FLAW GROWTH SCATTER FACTOR.** Figure 5-14 presents the effects of ultimate and yield factor of safety on the propellant tank safe-life with a yield factor of safety during proof test maintained at a constant value of 1.0, (i.e.,  $FS_y = 1.0$  during proof test). These curves were developed from the stress intensity ratio versus number of flight curves (see Figure 5-9) for the LO<sub>2</sub> tank. These curves were generated assuming a semi-elliptical surface flaw in the tank walls and that the flaws propagated to failure

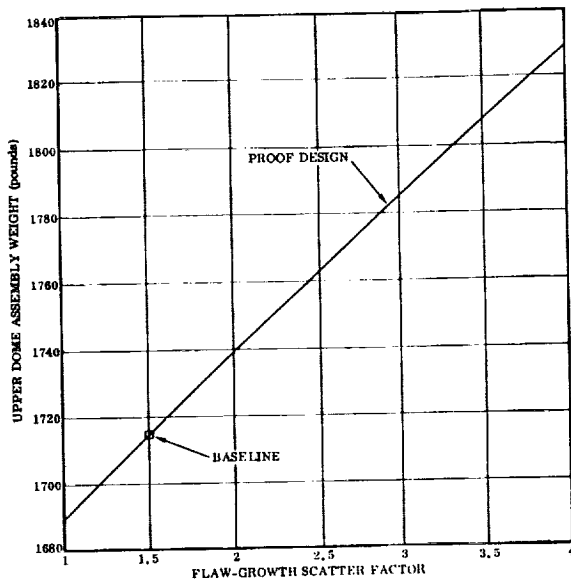


Figure 5-10. Upper LO<sub>2</sub> Tank Dome Assembly Weight Sensitivity to Flaw-Growth Scatter Factor

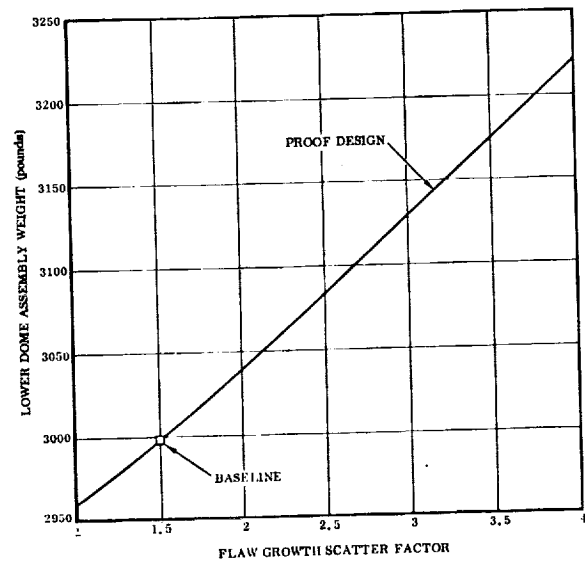


Figure 5-11. Lower LO<sub>2</sub> Dome Assembly Weight Sensitivity to Flaw-Growth Scatter Factor

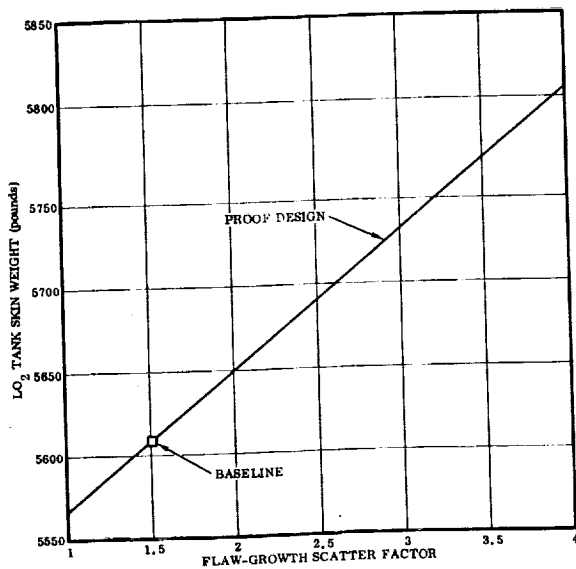


Figure 5-12. LO<sub>2</sub> Tank Skin Weight Sensitivity to Flaw-Growth Scatter Factor

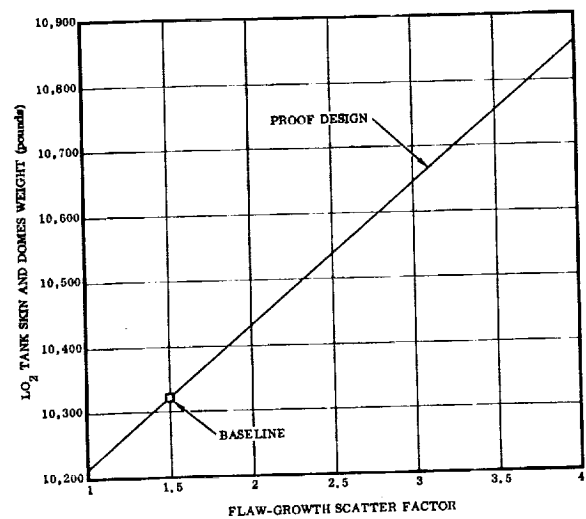


Figure 5-13. LO<sub>2</sub> Tank Skin and Domes Weight Sensitivity to Flaw-Growth Scatter Factor

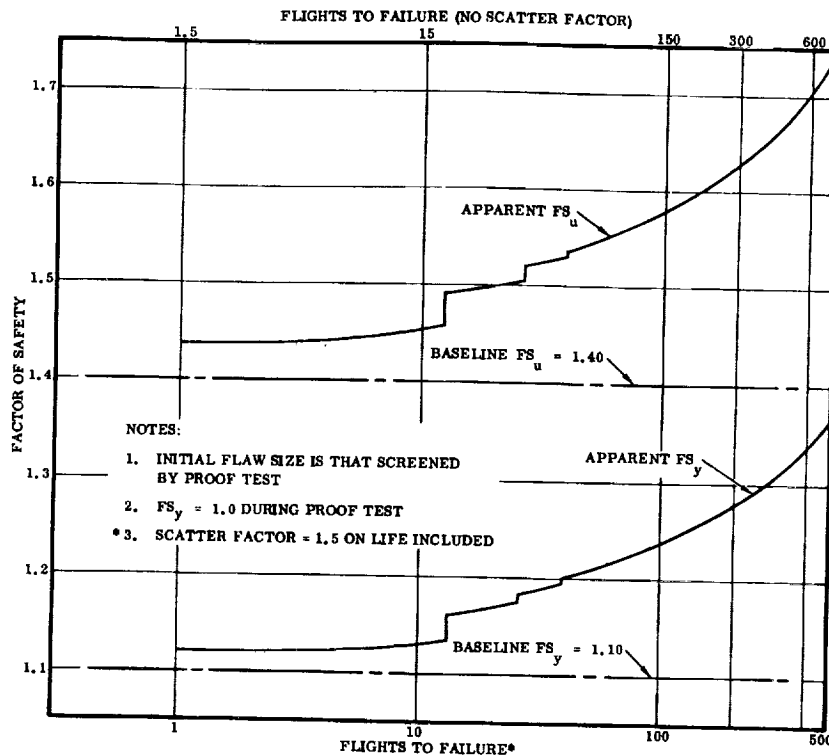


Figure 5-14.  $LO_2$  Tank Safe-Life Versus Factor of Safety

under the influence of the applied pressure loading spectrum. The  $LO_2$  tank wall was assumed to be at  $-320^\circ F$  and to have the following material properties.

Property/Temperature	$-320^\circ F$
$F_{tu}$ (ksi)	78.0
$F_{ty}$ (ksi)	61.0
$K_{I_c}$ (ksi $\sqrt{in.}$ )	35.5

The curves of stress intensity ratio versus flights to failure were converted to apparent ultimate and yield factors of safety through the following relationships:

$$K_{I_i} / K_{I_c} = 1/\alpha$$

$$F_{limit} = F_{ty} / \alpha \text{ (based on } FS_y = 1.0 \text{ during proof test)}$$

$$FS_u(\text{apparent}) = F_{tu}/f_{\text{limit}} = \frac{(F_{tu}/F_{ty})}{(K_{I1}/K_{Ic})}$$

$$FS_y(\text{apparent}) = F_{ty}/f_{\text{limit}} = \frac{1}{(K_{I1}/K_{Ic})}$$

The sensitivity of the safe-life of the baseline LO<sub>2</sub> tank to flaw growth variations is presented in Figure 5-15. The figure reveals that the safe-life decreases very rapidly as the scatter factor is increased above the baseline value of 1.5.

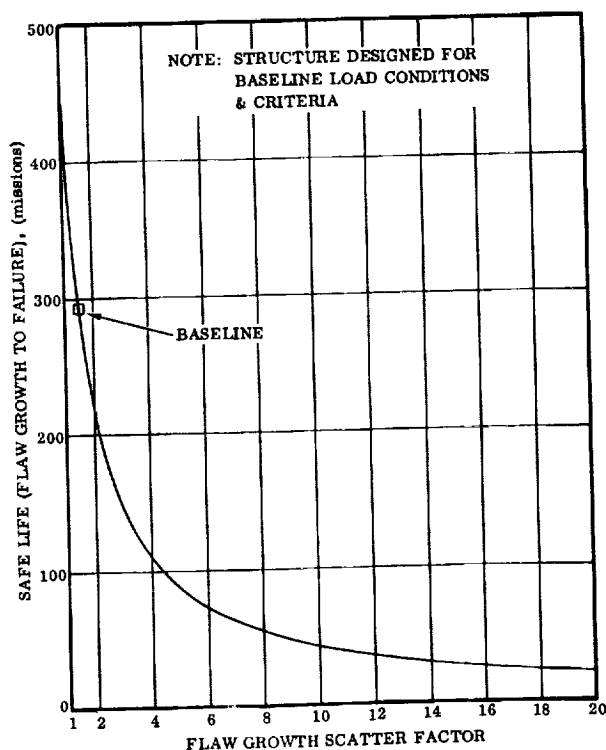


Figure 5-15. LO<sub>2</sub> Tank Safe-Life (Flaw Growth to Failure) Versus Scatter Factor

### 5.3 LIQUID HYDROGEN TANK

**5.3.1 LH<sub>2</sub> TANK SAFE-LIFE ANALYSIS.** The LH<sub>2</sub> propellant tank is assumed to contain two distinct types of flaws. These are an elliptical surface flaw and a through crack, for which the initial size of each is developed in this section. These flaws are propagated to a specified failure criterion under the influence of the applied pressure spectrum loading. The critical crack lengths for both types of flaws are also developed here.

The applied pressure loading spectrum for the LH<sub>2</sub> tank was developed from the curve of Figure 2-35. Only those portions of the complete loading spectrum that could contribute to the growth of the flaws were included in the spectrum for the tank. The pressures used in developing the final spectrum are:



### LH<sub>2</sub> Tank Upper Dome Equator Pressures

Pressure (psi)	Time at Pressure (minutes)	Description
15.0	2.5	Tank lockup pressure
22.3	3.5	Nominal ullage pressure
16.0	6.0	Vent after staging pressure
23.8	3.5	Pressure regulator Malfunction pressure — assumed to occur once every 20 flights

Stresses in the tank at the upper dome equator were developed from these pressures through the use of the formula

$$\sigma = \frac{pR}{t} = \frac{p (198)}{0.116}$$

where

p = pressure (psi)

R = 198 inches = tank radius

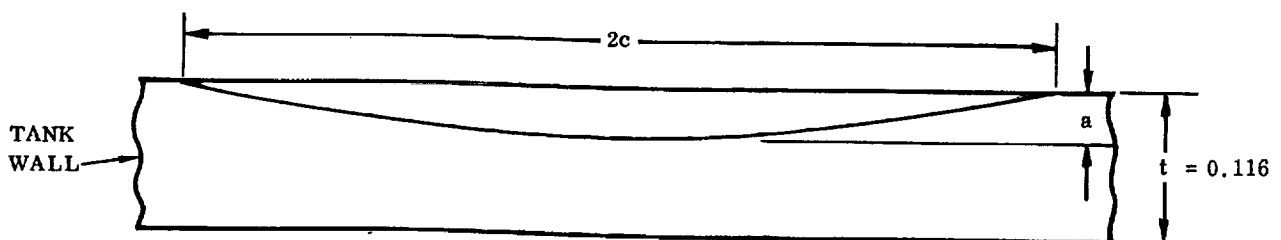
t = 0.116 inch = tank thickness at the upper dome equator

The calculated stresses and the final form of the pressure loading spectrum is shown below.

Minimum Stress (ksi)	Maximum Stress (ksi)	Cycles per Flight	Time per Flight (minutes)
0.000	25.6	1	2.5
0.000	38.1*		3.5
0.000	38.1*		6.0
0.000	27.3		

\*Every 20 flights, this stress is replaced with the pressure regulator malfunction stress, which is 40.6 ksi.

The elliptical surface flaw is assumed to initially have aspect ratios,  $a/2c$ , of 0.1 and 0.4 (see sketch below).



The initial flaw size for each of these aspect ratios is calculated here, based on the maximum flaw size that would be screened by the proof test, using a minimum value for the material toughness parameter  $K_{Ic}$  for consistency with the crack growth analysis.

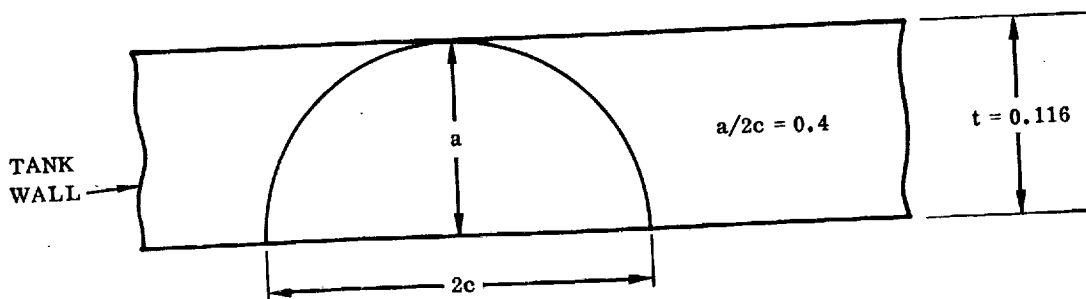
For 2219-T87 aluminum base metal at room temperature the minimum value of the material toughness parameter,  $K_{Ic}$ , is 32.0 ksi  $\sqrt{\text{inch}}$  (Reference 6, Figure 52, lower curve). Using this value of  $K_{Ic}$  in the equation for the stress intensity factor, and substituting  $\sigma = \sigma_Y$  for the proof test stress, the equation becomes

$$32.0 = \frac{1.1 (51.0) \sqrt{\pi} \sqrt{a} (M_K)}{\sqrt{\phi^2 - 0.212 (51.0/51.0)^2}}$$

This equation can now be solved for 'a', which is the maximum flaw size that would be screened by a proof test. It should be noted that  $M_K$  is dependent upon the value of 'a' so that a trial and error solution is necessary. This equation was solved for both aspect ratios of 0.1 and 0.4, and the results follow.

For  $a/2c = 0.1$ , the flaw screened by a proof test,  $a = 0.06195$  inch. This value becomes the initial flaw size,  $a_i$ , for the flaw propagation studies.

For  $a/2c = 0.4$ , the flaw that would be screened by a proof test turned out to be greater than the thickness of the tank wall,  $t = 0.116$  inch. An equivalent through crack with an area equal to the area of a surface flaw of aspect ratio,  $a/2c = 0.4$  on the verge of leakage is calculated here.



$$\text{Area of flaw} = \frac{\pi a c}{2} \quad a = 0.116 \text{ inch} \quad \text{Area} = 0.02642 \text{ in}^2$$

The equation for the stress intensity factor  $K_I$ , for the elliptical surface flaw, is as follows:

$$K_I = \frac{1.1 \sigma \sqrt{\pi} \sqrt{a} (M_K)}{\sqrt{\phi^2 - 0.212 (\sigma/\sigma_Y)^2}}$$

(Reference 10, Equation IX-8)

$\sigma$  = applied stress (ksi)

$\sigma_Y$  = tensile yield stress = 51 ksi

$a$  = flaw size (inch)

$\phi^2$  = is a function which depends on the value of  $a/2c$

For

$$a/2c = 0.1, \quad \phi^2 = 1.10355$$

$$a/2c = 0.4, \quad \phi^2 = 2.01096$$

$M_K$  is a function which depends on both the value of  $a/2c$  and  $a/t$  and is obtained from Reference 18, Page 135.

An equivalent through crack would have an area of  $(2c) \times t$

$$(2c) \times t = 0.02642 \text{ in}^2 \quad 2c = 0.2278 \text{ inch}$$

This value becomes the initial size of the through crack in the flaw propagation studies.

The critical flaw size of the elliptical surface flaw of aspect ratio  $a/2c = 0.1$  is calculated in a manner similar to that in which the initial flaw size was calculated. Obtaining the minimum value of the material toughness parameter,  $K_{Ic}$ , from the minimum curve of Figure 52 of Reference 14,  $K_{Ic} = 32.0 \text{ ksi } \sqrt{\text{inch}}$  and the applied stress becomes the maximum stress from the applied pressure loads spectrum ( $\sigma = 40.6 \text{ ksi}$ ). The stress intensity factor equation then becomes

$$32.0 = \frac{1.1 (40.112) \sqrt{\pi} \sqrt{a_{cr}} (M_K)}{\sqrt{\phi^2 - 0.212 (40.112/51.0)^2}}$$

Solving for  $a_{cr}$ , we find  $a_{cr} = 0.08053 \text{ inch}$ . The critical flaw size for the through flaw is found by using the same minimum  $K_{Ic}$  value of  $32.0 \text{ ksi } \sqrt{\text{inch}}$  and the same applied stress of  $40.6 \text{ ksi}$ . However, the equation for the through crack now becomes

$$K_I = \frac{\sigma \sqrt{\pi} \sqrt{(2c)_{cr}}}{\sqrt{2 - (\sigma/\sigma_Y)^2}}$$

or

$$32.0 = \frac{40.6 \sqrt{\pi} \sqrt{(2c)_{cr}}}{\sqrt{2 - (40.6/51.0)^2}}$$

Solving this equation for  $(2c)_{cr}$ , we find  $(2c)_{cr} = 0.2798$  inch.

Results of flaw growth calculations:

Elliptical Surface Flaw,  $a/2c = 0.1$  (see Figure 5-16).

Starting with  $a_i = 0.06195$  inch, it took 626 flights for the flaw to grow to  $a_{cr} = 0.08053$  inch (scatter factor of 1.5 used on flights) as shown in Figure 5-16.

Through Flaw (see Figure 5-17).

Starting with  $2c_i = 0.2278$  inch, it took 160 flights for the flaw to grow to  $(2c)_{cr} = 0.2798$  inch (scatter factor of 1.5 used on flights).

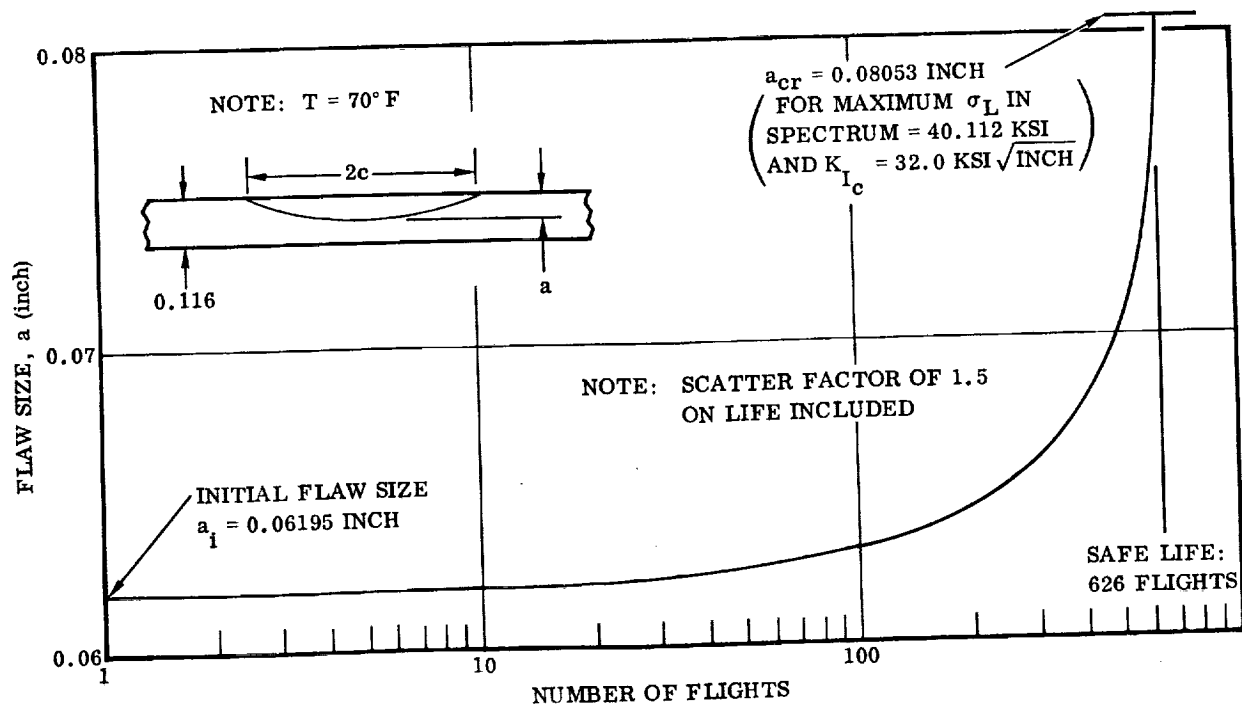


Figure 5-16. Crack Growth in  $LH_2$  Tank for Pressure Load Spectrum (Surface Flaw,  $a/2c = 0.1$ )

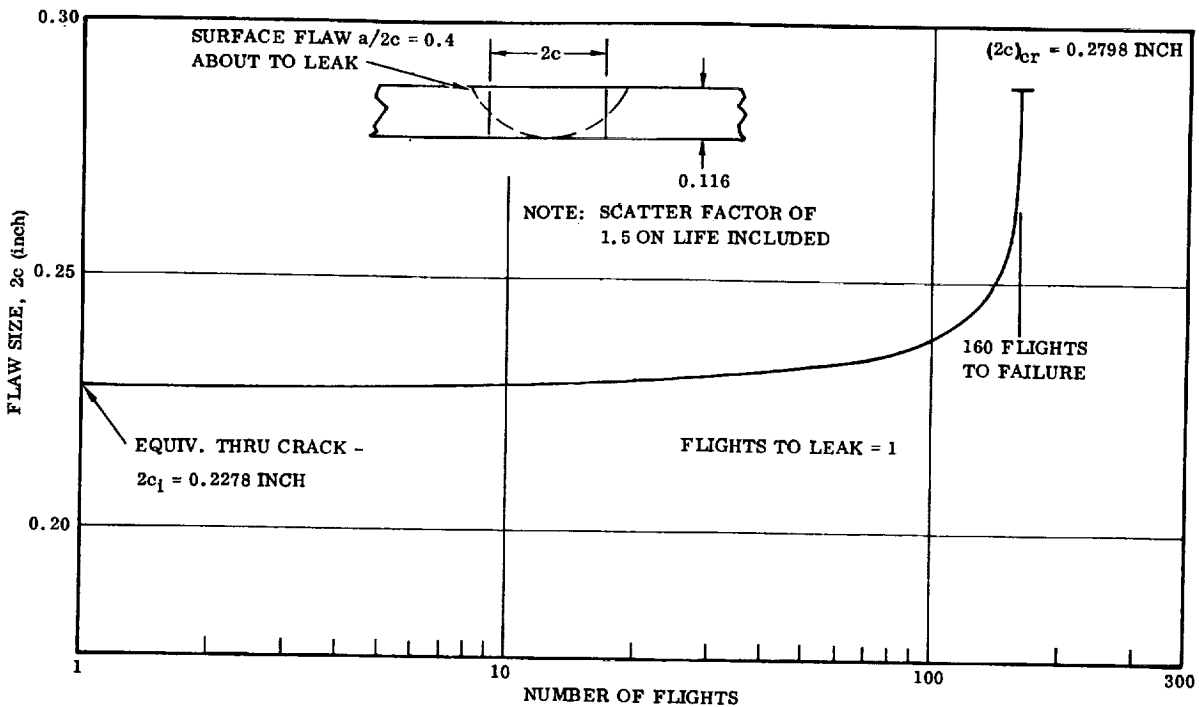


Figure 5-17. Crack Growth in LH<sub>2</sub> Tank for Pressure Load Spectrum (Surface Flaw,  $a/2c = 0.4$  and Equivalent Through Crack)

5.3.2 LH<sub>2</sub> TANK PROOF FACTOR AND APPARENT FACTORS OF SAFETY. For final verification of the structural integrity of the main Space Shuttle booster LH<sub>2</sub> tank, primary reliance is placed in a pressure proof test of each tank prior to assembly into the booster vehicle.

The proof test logic is explained in detail in Reference 19, Fracture Control of Metallic Pressure Vessels, NASA SP8040. The proof test consists of loading the tanks to a stress level greater than the maximum stress level expected in service. In addition the proof test should be conducted at a temperature consistent with the operating temperature. If the proof test is completed successfully, the proof test provides assurance that all existing flaws or defects are less than the critical size required for fracture at the proof stress level. In addition, the safe-life of the tank at the operating stress level can be determined by fracture mechanics analysis where the safe-life ensured by the proof test is the time required to grow the smaller "proof stress flaw" to the larger critical size associated with the maximum service operating stress. The task consists of developing a  $K_{I1}/K_{IC}$  versus number of flight curve by integrating the combined cyclic and sustained load flaw growth over arbitrarily selected flight increments using the flight pressure load spectrum and the flaw growth data. The final curve for the LH<sub>2</sub> tank is presented in Figure 5-18.

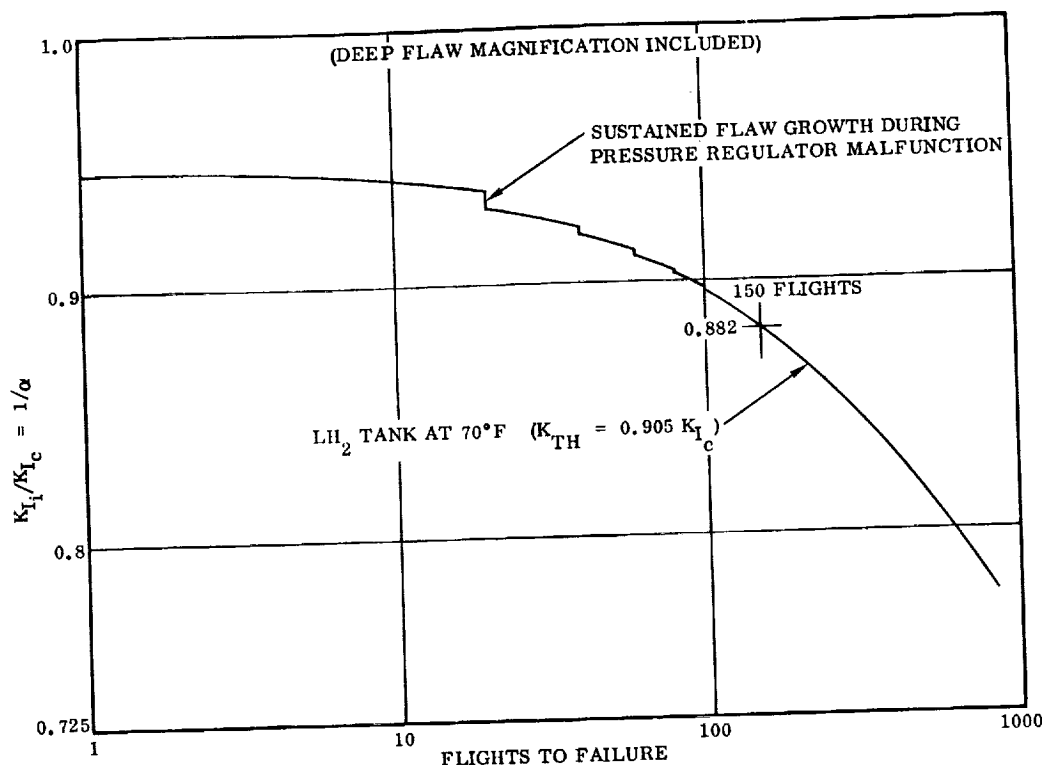


Figure 5-18. LH<sub>2</sub> Tank Stress Intensity Ratio Versus Flights to Failure

The method for obtaining  $\alpha$  from this plot is to read  $K_{Ii}/K_{Ic}$  for the desired number of flights to failure. In this case, for the baseline, the flights to failure were 150; that is, the scatter factor of 1.5 multiplied by the design service life of 100 flights\*. Then,

$$\alpha = \frac{1}{K_{Ii}/K_{Ic}} = \frac{1}{0.882} = 1.13$$

\*Comparison of the number of flights to failure computed in Section 5.3.1 reveals a difference between the actual computed value of safe-life, 160 flights, and the number of flights to failure used to determine the proof factor above. The primary reasons for the difference in the lives calculated are the differences in assumptions and data used to generate the  $K_{Ii}/K_{Ic}$  versus flights to failure curve in Figure 5-18, and the LH<sub>2</sub> tank safe-life analysis of Section 5.3.1. Although deep flaw magnification for both analysis was used, each analysis assumes different skin thicknesses and load spectra, and also utilizes different flaw growth data. Therefore close consistency between the results of the safe-life analysis and the 100 missions used to determine the proof factor should not be expected.

The LH<sub>2</sub> tank is proof tested as illustrated in Figure 2-18. For the LH<sub>2</sub> tank, a one-stage proof test using void reducing plastic balls and room temperature dry air at 29.8 psi pressure is selected. Due to other design conditions, the one-stage proof test results in a small but acceptable weight penalty in the forward portion of the tank where the proof pressure exceeds that required.

Due to the reduced limit design stresses required by the proof test for the safe-life of the tank, there is an apparent ultimate factor of safety that results, and it is given by the expression:

$$FS_u \text{ (apparent)} = \frac{F_{ult}}{f_{limit}}$$

The apparent ultimate factors of safety for the LH<sub>2</sub> tank areas designed by proof pressure are:

Upper Dome. Since the upper dome is designed by proof pressure, the apparent ultimate factor of safety is calculated to compare to the nominal ultimate safety factor of 1.4.

$$F_{tu} = 63,000 \text{ psi (2219-T87 at RT)}$$

$$f \text{ (limiting operating)} = 39,900 \text{ psi}$$

$$FS_u \text{ (apparent)} = \frac{63,000}{39,900} = 1.58$$

Skins. At the forward end of the cylindrical section of the tank near the bottom centerline, the skin thickness is designed by proof pressure. In this area,

$$F_{tu} = 63,000 \text{ psi (2219-T87 at RT)}$$

$$f \text{ (limit operating)} = \frac{pR}{t} = \frac{22.3(198)}{0.116} = 38,200 \text{ psi}$$

$$FS_u \text{ (apparent)} = \frac{63,000}{38,200} = 1.65$$

In both cases the apparent  $FS_u$  is greater than the nominal baseline  $FS_u$  of 1.4.

**5.3.3 LH<sub>2</sub> TANK WEIGHT SENSITIVITY TO FLAW GROWTH SCATTER FACTOR PERTURBATIONS.** The forward LH<sub>2</sub> tank dome is designed by proof pressure, and its weight is therefore sensitive to perturbations of the flaw growth scatter factor. The procedure for determining the weight of the dome for the various scatter factors is presented in Section 5.2.2. Although the lower LH<sub>2</sub> dome is not designed by proof

pressure for the baseline, the lower dome could become proof design critical if the  $FS_u$  were low enough. Therefore the weight sensitivity of both the  $LH_2$  tank end domes to flaw growth scatter factor perturbations is presented in Figure 5-19.

**5.3.4  $LH_2$  TANK SAFE-LIFE SENSITIVITY TO FACTOR OF SAFETY AND FLAW GROWTH SCATTER FACTOR.** Figure 5-20 presents the effect of ultimate and yield factor of safety on the propellant tank safe-life with a yield factor of safety during proof test maintained at a constant value of 1.0, (i.e.,  $FS_y = 1.0$  during proof test). These curves were developed from the stress intensity ratio versus number of flight curves (see Figure 5-18) for the  $LH_2$  tank. These curves were generated assuming a semi-elliptical surface flaw in the tank walls and that the flaws propagated to failure under the influence of the applied pressure loading spectrum. The  $LH_2$  tank wall was assumed to be at 70°F and to have the following material properties.

<u>Property/Temperature</u>	<u>70°F</u>
$F_{tu}$ (ksi)	63.0
$F_{ty}$ (ksi)	51.0
$K_{Ic}$ (ksi $\sqrt{in.}$ )	32.0

The curves of stress intensity ratio versus flights to failure were converted to apparent ultimate and yield factors of safety through the following relationships:

$$K_{Ii}/K_{Ic} = 1/\alpha$$

$$F_{limit} = F_{ty}/\alpha \text{ (based on } FS_y = 1.0 \text{ during proof test)}$$

$$FS_u \text{ (apparent)} = F_{tu}/f_{limit} = \frac{(F_{tu}/F_{ty})}{(K_{Ii}/K_{Ic})}$$

$$FS_y \text{ (apparent)} = F_{ty}/f_{limit} = \frac{1}{(K_{Ii}/K_{Ic})}$$

The sensitivity of the safe-life of the baseline  $LH_2$  tank to flaw growth scatter factor variations is presented in Figure 5-21. The figure reveals that the safe-life decreases very rapidly as the scatter factor is increased above the baseline value 1.5.



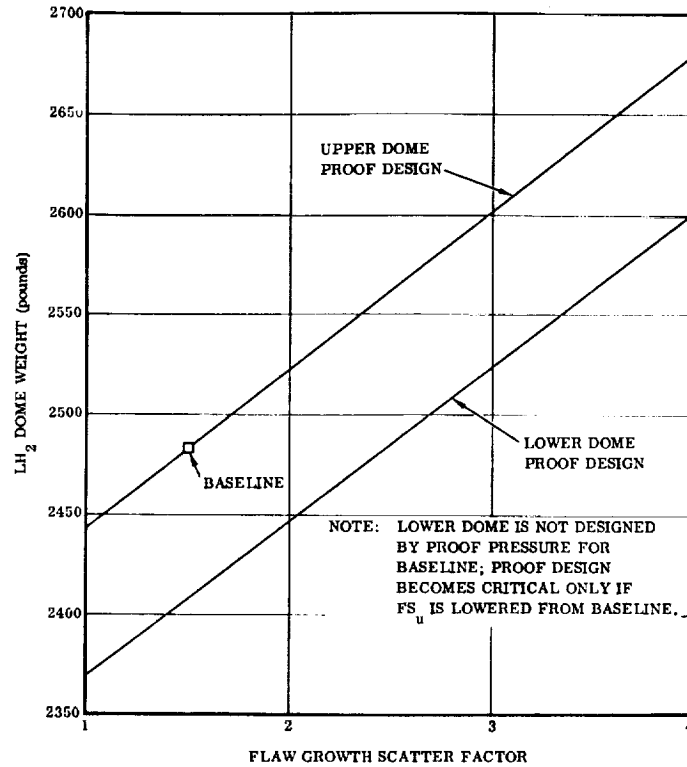


Figure 5-19. Upper and Lower LH<sub>2</sub> Tank Dome Assembly Weight Sensitivity to Flaw Growth Scatter Factor

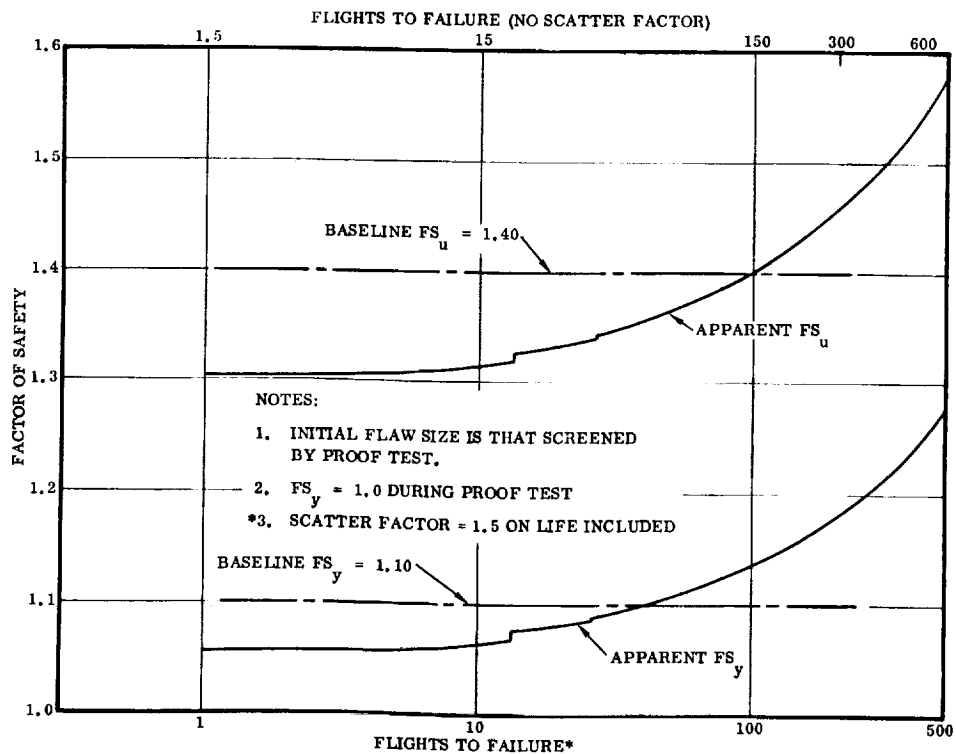


Figure 5-20. LH<sub>2</sub> Tank Safe-Life Versus Factor of Safety

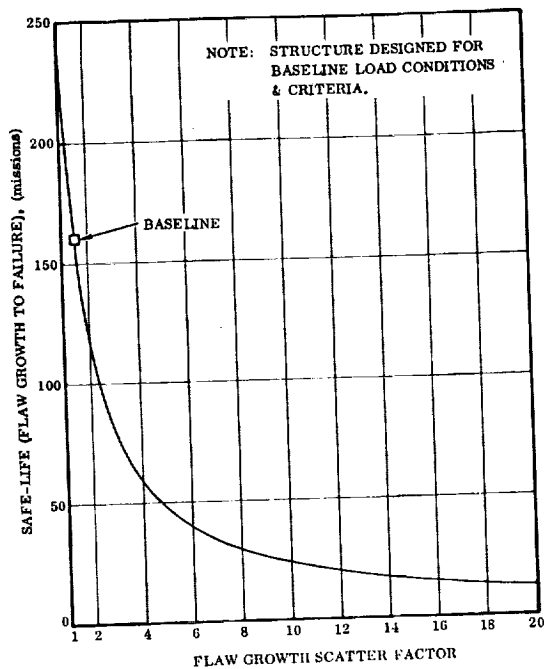


Figure 5-21. LH<sub>2</sub> Tank Safe-Life (Flaw Growth to Failure) Versus Scatter Factor

## 5.4 AFT ORBITER SUPPORT FRAME

**5.4.1 AFT ORBITER SUPPORT FRAME SAFE-LIFE ANALYSIS.** In the analysis of the aft orbiter support frame, one of the frame flanges was assumed to contain a corner crack of an initial size of 0.1 inch, or a crack having a length of 0.1 inch emanating from a hole. This initial size was chosen based on a judgment of the capability of nondestructive evaluation.

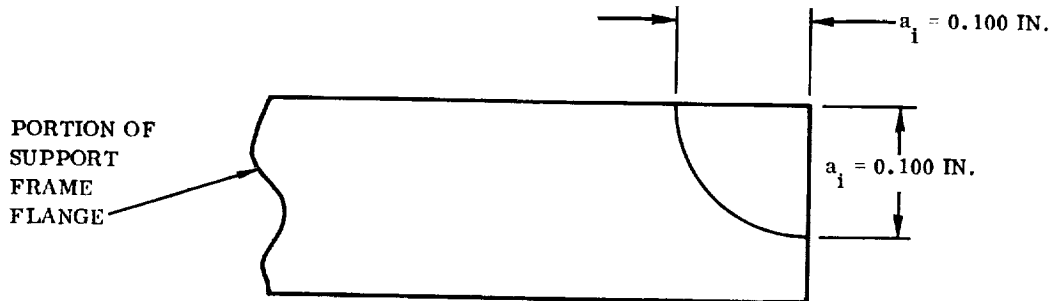
The aft orbiter attachment frame loading spectrum experienced by this flaw configuration is essentially the same spectrum that was used in the safe-life determination for fatigue crack initiation listed in Table 4-4. The only change made was to convert the spectrum, which is for 100 missions, to a spectrum for only one mission. The results of this modification and the final aft orbiter support frame loading spectrum are listed in Table 5-1.

Table 5-1. Aft Orbiter Support Frame Loading Spectrum

Mean Stress (ksi)	Alternating Stress (ksi)	Cycles per Flight (Unless Otherwise Noted)
12.000 ↑         ↓ 12.000	1.000	900
	2.000	90
	2.000	9
	4.000	1
	6.000	1 cycle every 10 flights
	3.000	900
	5.000	90
	9.000	9
	14.000	1
	20.000	1 cycle every 10 flights

The crack growth studies were done on the aft orbiter support frame assuming the structure was maintained at room temperature. Thus room temperature properties were assumed and crack growth rate curves for 2219-T87 aluminum base metal at room temperature were used in the flaw propagation computer program

#### 5.4.1.1 Corner Crack



The equation for the maximum stress intensity factor for a corner crack is

$$K_I = \frac{\sigma \sqrt{\pi a} (0.705)}{\sqrt{1 - 0.177 (\sigma/\sigma_y)^2}}$$

(Reference 10, Equation VII-7 modified to account for the plastic zone correction)

$\sigma$  = applied stress

$\sigma_y$  = tensile yield stress

$a$  = flaw size

The critical value of the material toughness parameter,  $K_{Ic}$ , used here for the 2219-T87 aluminum base metal at room temperature was  $K_{Ic} = 32.0 \text{ ksi } \sqrt{\text{inch}}$  (Reference 14, Figure 52, lower curve). The tensile yield stress used was  $\sigma_y = 51.0 \text{ ksi}$ . The maximum operating stress occurring in the support frame can be found from the spectrum to be  $\sigma = 32.000 \text{ ksi}$ .

Substituting all these values into the stress intensity factor equation results in

$$32.0 = \frac{32.000 \sqrt{\pi a_{cr}} (0.705)}{\sqrt{1 - 0.177 (32.000/51.000)^2}}$$

This equation can be solved for the critical value of 'a', which turns out to be  $a_{cr} = 0.5958 \text{ inch}$ .

Under the influence of the applied loading spectrum, the initial flaw of size  $a = 0.100 \text{ inch}$  grew only  $0.00004 \text{ inch}$  in 4000 flights. Consequently, the safe-life of this structural component can be considered to be extremely large.

5.4.1.2 Crack Emanating from Hole. The loading spectrum, material properties, and maximum operating stress will be the same as those used in the crack growth analysis of a corner crack, above. Substituting the appropriate values into the equation for the stress intensity factor for a crack emanating from a hole results in the following expression:

$$32.0 = \frac{32.0 \sqrt{\pi} \sqrt{a_{cr}}}{\sqrt{1 - 0.177 (32.0/51.0)^2}} \left[ 1.0 + 2.0 e^{(-18.42 a_{cr})} \right]$$

This expression is solved by a trial and error method for the critical value of 'a', which turns out to be  $a_{cr} = 0.29063$  inch.

Under the influence of the applied loading spectrum, the initial flaw ( $a_i = 0.100$  inch) grew 0.01815 inch to  $a = 0.11815$  inch in 2667 flights, using a scatter factor of 1.5 on the number of flights to failure.

Since the initial flaw of size 0.100 inch grew only 0.01815 inch in 2667 flights, and since the critical flaw size for this structural component has been shown to be  $a_{cr} = 0.29063$  inch, the safe-life of this structural component can be considered to be extremely large.

5.4.2 AFT ORBITER SUPPORT FRAME SAFE-LIFE SENSITIVITY TO FACTOR OF SAFETY. The type of flaw assumed to be present in the structure for this analysis is a through crack emanating from a hole. This situation is most critical due to the stress concentration gradient in the vicinity of the hole. The equation for the stress intensity factor for this type of flaw is

$$K_I = \frac{\sigma \sqrt{\pi a}}{\sqrt{1 - 0.177 (\sigma / \sigma_{ys})^2}} \text{ (GKT)}$$

where

GKT = factor to account for the stress concentration in the vicinity of the hole.

The initial flaw size is assumed to be 0.100 inches. This is based upon an estimate of NDE capability. The flaw is propagated to failure under the influence of the applied loading spectrum for the aft orbiter support bulkhead. The loading spectrum, with a maximum applied stress level of 32.0 ksi, is equivalent to a factor of safety of 1.4. Factor of safety can be related to the maximum stress level in the spectrum according to the equation

$$FS_u = 1.4 \left( \frac{32.0}{\sigma_{max}} \right)$$

Therefore by varying the maximum stress level in the applied loading spectrum, the factor of safety can also be varied. Figure 5-22 is a plot of the applied stress level versus the critical flaw size. The effect on the safe-life of the bulkhead of varying the factor of safety is presented in Figure 5-23. The load spectrum for aft orbiter support bulkhead for  $FS_u = 1.4$  is shown in Table 5-1.

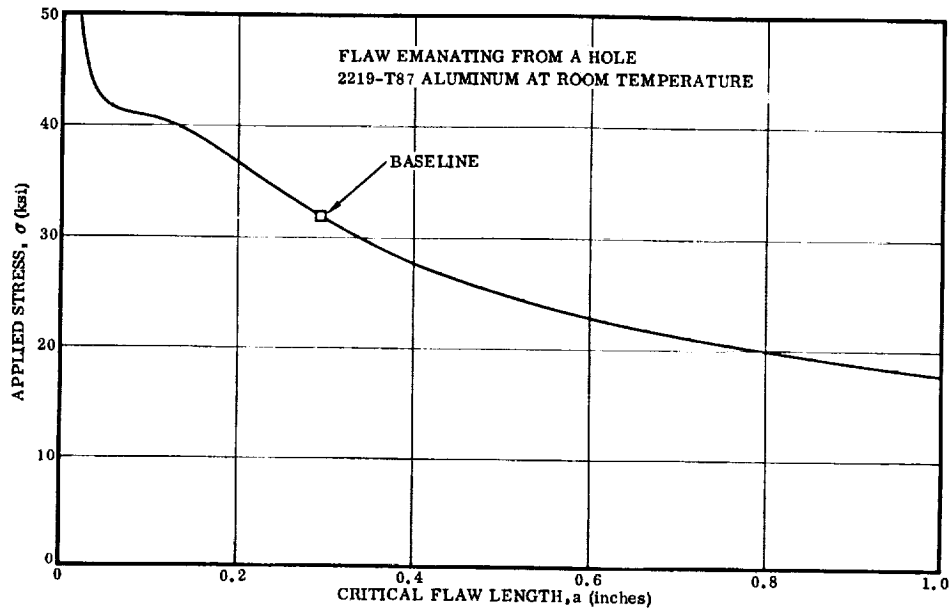


Figure 5-22. Aft Orbiter Support Frame Critical Flaw Size Versus Applied Stress

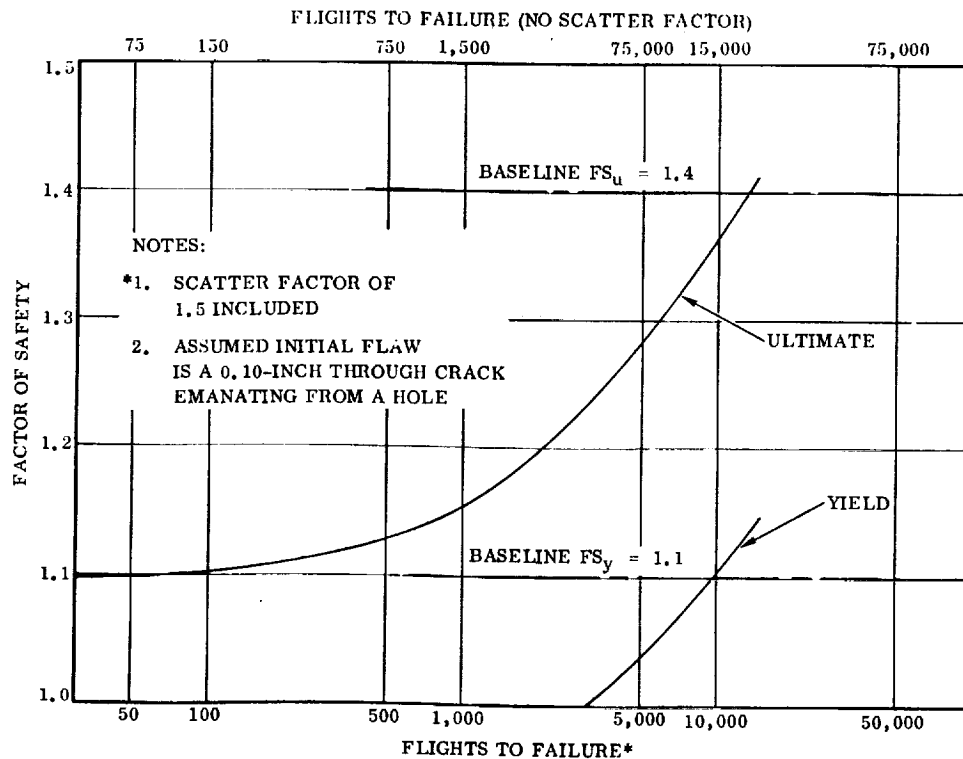


Figure 5-23. Aft Orbiter Support Frame Safe-Life Versus Factor of Safety

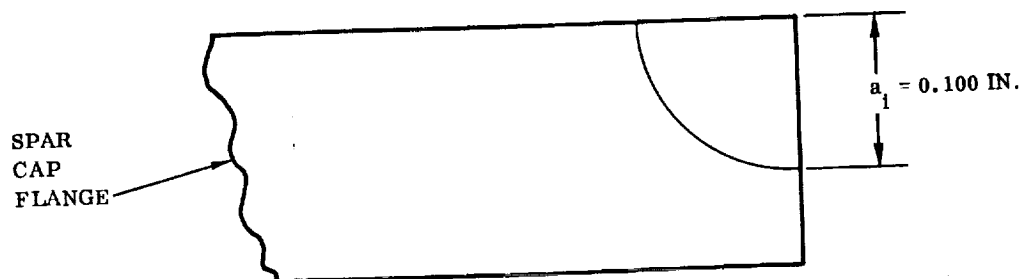
## 5.5 WING BOX

**5.5.1 WING SPAR CAPS SAFE-LIFE ANALYSIS.** In the analysis of the wing spar caps, these members were assumed to contain two types of flaws: a corner crack of an initial size of 0.1 inch (see sketch below), and a crack of 0.1 inch initial length emanating from a fastener hole. The initial size of the cracks was chosen based on judgment of the capabilities of nondestructive evaluation.

The wing loading spectrum experienced by the flaws described above is essentially the same spectrum as was used in the wing fatigue analysis and found in Table 4-6. Certain necessary modifications were made, however, to use this spectrum in the crack growth study. These included the addition of some sustained load, which while not necessary for fatigue analysis can be of great significance in crack growth analysis, and the reduction of the spectrum, which is for 100 missions, to a spectrum for only one mission. The results of these modifications and the final wing loading spectrum can be found in Table 5-2. This spectrum is a very severe loading spectrum, much more so than experienced by any of the other components being analyzed in this study.

The crack growth studies were done on the wing assuming the spar caps were maintained at room temperature. Thus room temperature properties were assumed and crack growth rate curves for Ti-6Al-4V annealed titanium base metal at room temperature were used in the flaw propagation computer program.

**5.5.1.1 Corner Crack.** The configuration of the corner crack assumed for the flaw growth analysis was as shown in the sketch.



The maximum stress intensity factor equation for a corner crack is

$$K_I = \frac{\sigma \sqrt{\pi} \sqrt{a} (0.705)}{\sqrt{1 - 0.177 (\sigma/\sigma_Y)^2}}$$

where

$\sigma$  = applied tensile stress

$\sigma_Y$  = tensile yield stress

$a$  = flaw size

Table 5-2. Wing Spar Cap Loading Spectrum

Flight Phase	$\sigma_{\text{Mean}}$ (ksi)	$\sigma_{\text{Alt}}$ (ksi)	Cycles per Flight (Unless Otherwise Noted)
<div> <div>Ascent</div> <div>↑</div> <div>↓</div> <div>Ascent Entry</div> <div>↑</div> <div>↓</div> <div>Entry Cruise/ Landing</div> <div>↑</div> <div>↓</div> <div>Cruise/ Landing</div> </div>	0.000	1.368	900
		2.280	90
		3.192	9
		4.104	1
	0.000	5.016	1 cycle every 10 flights
	13.680	3.192	900
		4.560	90
		5.928	9
		7.296	1
	13.680	8.208	1 cycle every 10 flights
	0.000	5.016	900
		8.208	90
		11.400	9
		14.136	1
	0.000	16.872	1 cycle every 10 flights
	36.480	7.296	900
		13.224	90
		19.152	9
		24.624	1
	36.480	30.096	1 cycle every 10 flights
	9.120	9.576	900
		16.872	90
		27.360	9
		41.040	1
	9.120	55.176	1 cycle every 10 flights
	13.680	12.312	900
		18.240	90
		33.744	9
		55.632	1
	13.680	72.960	1 cycle every 10 flights
	6.840	6.840	900
	12.312	12.312	90
	16.872	16.872	5
	20.976	20.976	2.5
	33.744	33.744	1.5
	42.864	42.864	1
	42.864	42.864	1 minute sustained load per flight
	45.600	45.600	1 cycle every 10 flights
	45.600	45.600	1 minute sustained load every 10 flights
	18.240	19.152	1800
		23.712	180
		29.184	18
		34.656	2
	18.240	40.128	2 cycles every 10 flights

The critical value of the material toughness parameter,  $K_{Ic}$ , used here for the Ti-6Al-4V annealed titanium base metal as room temperature was  $K_{Ic} = 78.0 \text{ ksi } \sqrt{\text{inch}}$  (Reference 16, Figure 35, Page 89). The tensile yield stress used was  $\sigma_Y = 120.0 \text{ ksi}$ . The maximum operating stress occurring in the spar cap can be found from the spectrum to be  $\sigma = 91.2 \text{ ksi}$ . Substituting all these values into the stress intensity factor equation results in

$$78.0 = \frac{(91.2) \sqrt{\pi} \sqrt{a_{cr}} (0.705)}{\sqrt{1 - 0.177 (91.2/120.0)^2}}$$

This expression can be solved for the critical value of 'a', which turns out to be  $a_{cr} = 0.42057 \text{ inch}$ .

Results of flaw growth calculations:

Under the influence of the applied loading spectrum, it took 31 flights for the initial flaw size of  $a_i = 0.100 \text{ inch}$  to grow to the critical flaw  $a_{cr} = 0.42057 \text{ inch}$ . The reason for the very small number of flights to failure is undoubtedly the very severe loading spectrum experienced by the spar cap. It differs from the other components in this study in that it experiences extreme loads during the entry and cruise/landing flight phases as well as the ascent phase. The flaw growth is shown in Figure 5-24.

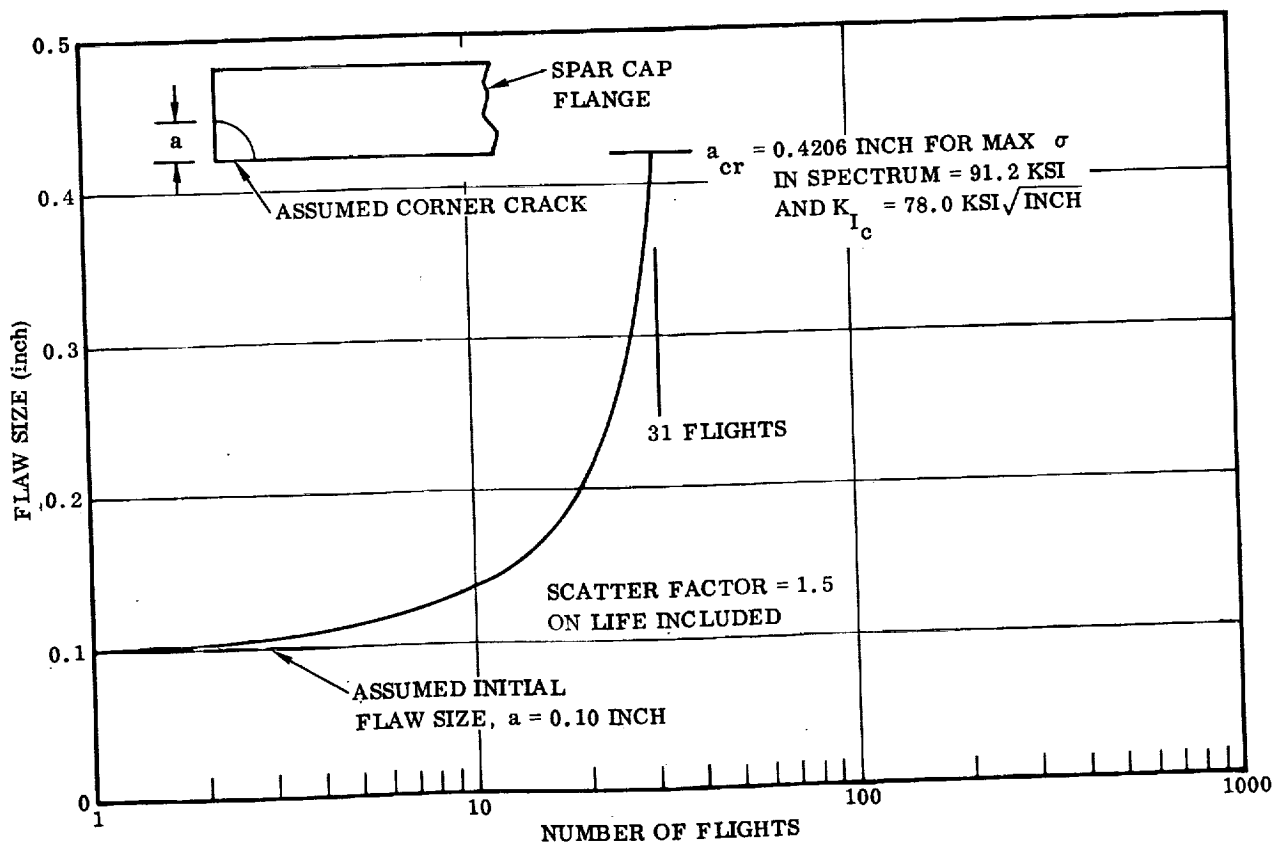


Figure 5-24. Crack Growth in Titanium Wing Spar Caps



5.5.1.2 Crack Emanating from Hole. The flaw configuration investigated in this section is as shown in the sketch. The length of the flaw is specified by 'a', the diameter of the hole is 'D', and the applied tensile stress is ' $\sigma$ '.

The equation for the stress intensity factor at the tip of the crack is

$$K_I = \frac{\sigma \sqrt{\pi a} \text{ (GKT)}}{\sqrt{1 - 0.177 \left(\frac{\sigma}{\sigma_y}\right)^2}}$$

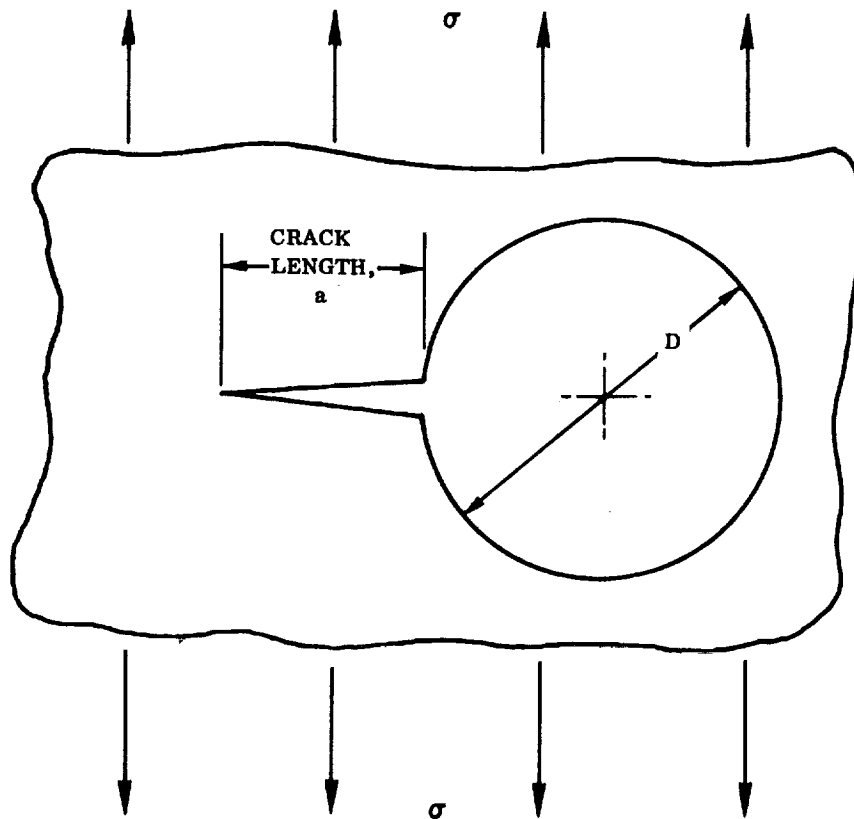
(Reference 10, Equation VII-10 modified to account for the plastic zone correction)

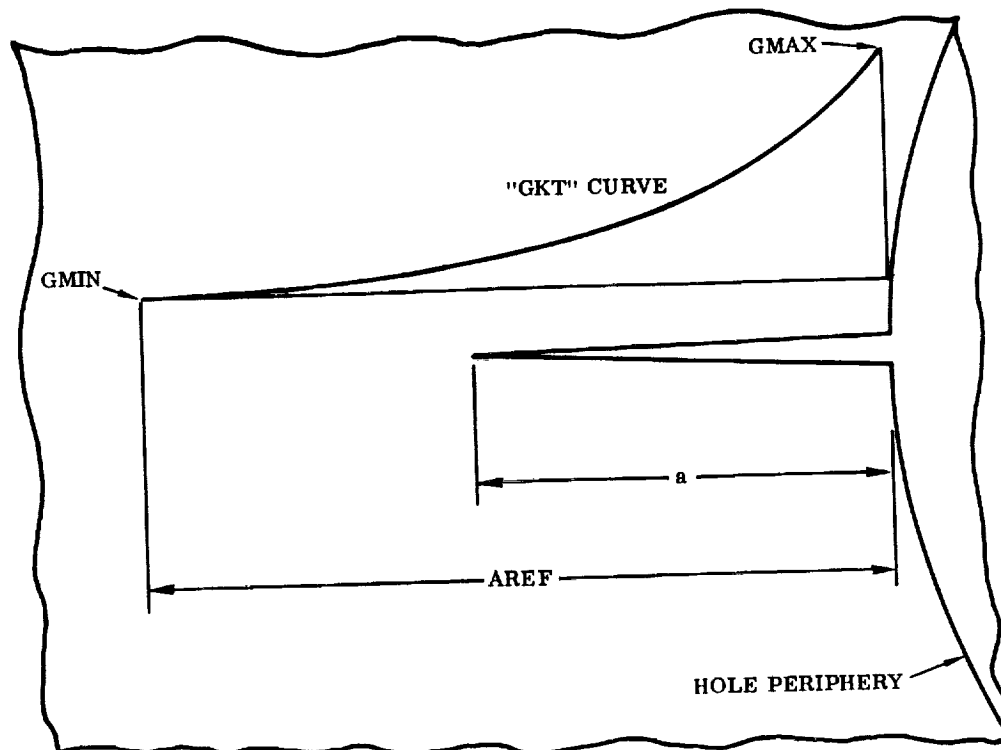
$\sigma$  = applied tensile stress (ksi)

$\sigma_y$  = tensile yield stress (ksi)

a = crack length (inches)

The quantity GKT in the equation is a factor included to account for the stress gradient due to the introduction of the hole into the uniform stress field. It can be thought of as a stress concentration factor. The quantity GKT has a maximum value (GMAX) at the periphery of the hole and decays exponentially to a minimum value (GMIN) at some specified distance (AREF) from the edge of the hole (see sketch on next page).





The curve for GKT is defined by the equation

$$GKT = GMIN + (GMAX - GMIN) e^{\left( \frac{-4.605 a}{AREF} \right)}$$

From the equation, it can be seen that AREF is actually the length at which 99% of the difference between GMAX and GMIN is reached. In other words, if

$$a = AREF, \text{ then } GKT = GMIN + 0.01 (GMAX - GMIN).$$

With GKT defined as shown, the equation for the stress intensity factor becomes

$$K_I = \frac{\sigma \sqrt{\pi a}}{\sqrt{1 - 0.177 \left( \frac{\sigma}{\sigma_y} \right)^2}} \left[ GMIN + (GMAX - GMIN) e^{\left( \frac{-4.605 a}{AREF} \right)} \right]$$

For this portion of the study a value of 3.0 was used for GMAX, 1.0 was used for GMIN, and AREF was taken to be 0.250 inch (one hole diameter). Figure 5-25 is a plot of GKT versus  $a/AREF$  for GMAX = 3.0 and GMIN = 1.0. With the specified values for GMAX, GMIN, and AREF, the equation for the stress intensity factor becomes

$$K_I = \frac{\sigma \sqrt{\pi a}}{\sqrt{1 - 0.177 (\sigma/\sigma_y)^2}} \left[ 1.0 + 2.0 e^{(-18.42 a)} \right]$$

This is the final form of the stress intensity factor used in this portion of the study. By substituting values for the maximum operating stress in the spectrum ( $\sigma$ ), the tensile yield stress ( $\sigma_y$ ), and the critical value of  $K_I$  ( $K_{I_c}$  was used here), the critical crack length ( $a_{cr}$ ) can be found from this equation using a trial and error method.

The wing material is taken to be Ti-6Al-4V annealed titanium maintained at room temperature. Therefore, the following material properties are used:

$$K_{I_c} = 78.0 \text{ ksi } \sqrt{\text{inch}} \text{ (Reference 16, Figure 35, Page 89)}$$

$$\sigma_y = 120.0 \text{ ksi}$$

Again using the wing loading spectrum of Table 5-2, the maximum operating stress is found from the applied loading spectrum to be  $\sigma = 91.2$  ksi. Substituting this stress and the appropriate material properties into the equation for the stress intensity factor for a crack emanating from a hole results in the following expression:

$$78.0 = \frac{91.2 \sqrt{\pi} \sqrt{a_{cr}}}{\sqrt{1 - 0.177 (91.2/120.0)^2}} \left[ 1.0 + 2.0 e^{(-18.42 a_{cr})} \right]$$

This expression is solved by a trial and error method for the critical value of 'a', which turns out to be  $a_{cr} = 0.18308$  inch.

Under the influence of the applied loading spectrum, it took three flights for the initial flaw ( $a_i = 0.100$  inch) to grow to the critical flaw size ( $a_{cr} = 0.18308$  inch), including a scatter factor of 1.5 on the number of flights to failure.

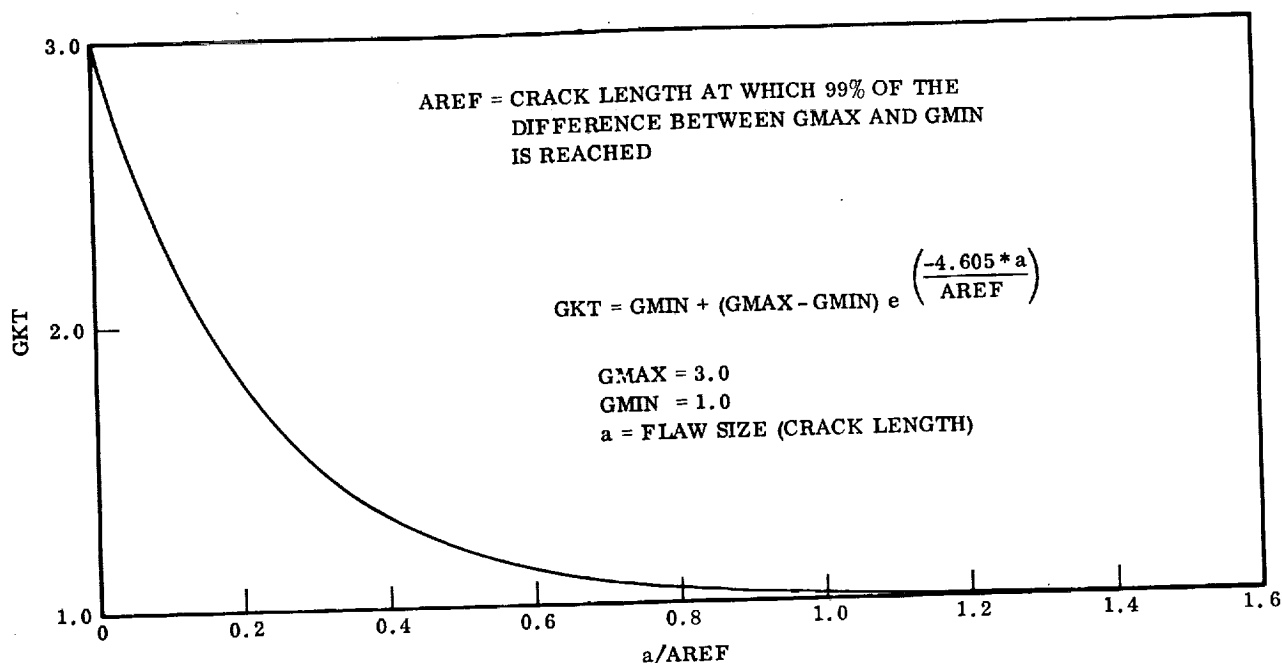


Figure 5-25. Stress Intensity Factor ( $\Delta K_I$ ) Multiple for a Crack Initiating at a Fastener Hole

The small number of flights to failure can be attributed to two things. First is the fact that the loading spectrum experienced by the wing spar cap is an extremely severe spectrum in that it incorporates high magnitude loads during the entry and cruise/landing flight phases as well as the ascent phase. Secondly, the flaw configuration being investigated here is a very critical configuration, especially since a stress gradient multiplication factor is being used on the stress intensity factor to account for the stress concentration around the hole. Consequently, the critical flaw size is not much greater than the initial flaw size, meaning the flaw does not have to grow very much to reach the critical size.

**5.5.1.3 Determination of Acceptable Safe-Life Stress Level for Spar Caps.** In the analysis of the wing for a crack emanating from a hole, the results show that the initial crack ( $a_i = 0.100$  inch) grows to the critical size ( $a_{cr} = 0.18308$  inch) in just three flights. Due to the fact that the number of flights to failure is so small, a study was undertaken to determine the allowable maximum limit stress level that would result in an acceptable safe-life of 100 missions.

The loading spectrum used in the initial analysis of a crack emanating from a hole in the wing spar cap is based on a maximum limit operating stress level of  $\sigma_{MAX} = 91.2$  ksi (see Table 5-2). The procedure used here consists of reducing this maximum limit stress level by some percentage, calculating a new critical flaw size based on



the new maximum stress level, and then propagating an initial flaw size  $a_i = 0.100$  inch to failure using a reduced applied loading spectrum based on the reduced maximum stress level. The critical flaw sizes ( $a_{cr}$ ) were found using the following expression:

$$78.0 = \frac{\sigma \sqrt{\pi} \sqrt{a_{cr}}}{\sqrt{1 - 0.177 (\sigma / 120.0)^2}} \left[ 1.0 + 2.0 e^{(-18.42 a_{cr})} \right]$$

By substituting values of the stress level ( $\sigma$ ) into this equation, the critical flaw size ( $a_{cr}$ ) can be found for the stress level by using a trial and error method. Figure 5-26 is a plot of stress level versus critical flaw size for a crack emanating from a hole in the wing spar cap.

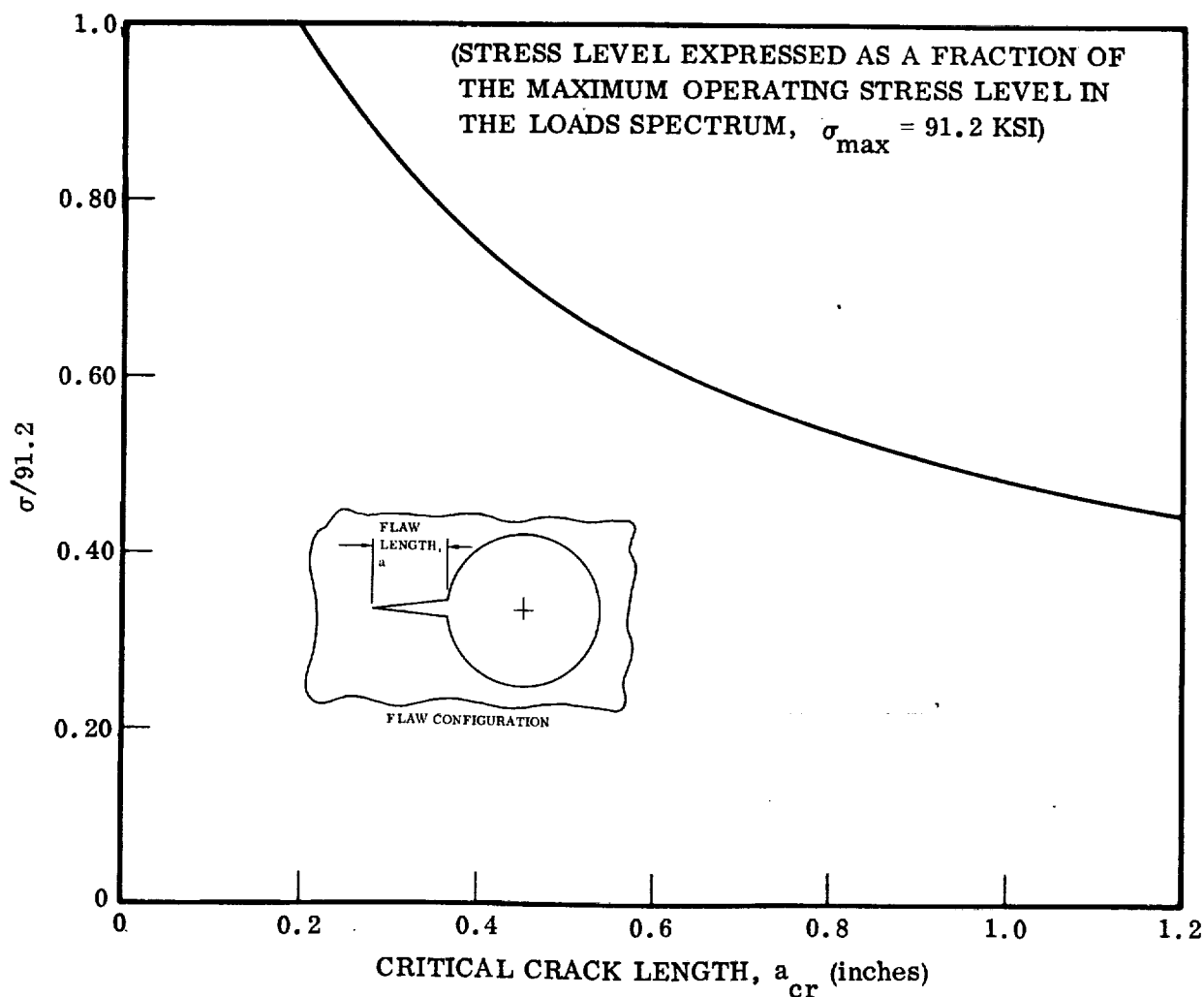


Figure 5-26. Stress Level Versus Critical Flaw Size for the Titanium Wing Spar Caps

After determining the critical flaw size for various maximum stress levels, an initial flaw of size  $a_i = 0.100$  inch was propagated to failure for the various levels and the curve of Figure 5-27 was obtained. From this curve it can be seen that to obtain a safe-life of 100 missions, the maximum allowable operating stress level must be reduced to 50% of the original maximum stress level. In other words, all load levels in the applied loading spectrum must be reduced by 50% so that an initial crack of size  $a_i = 0.100$  inch emanating from a hole will reach criticality in 100 missions, using a scatter factor of 1.5 on the number of missions.

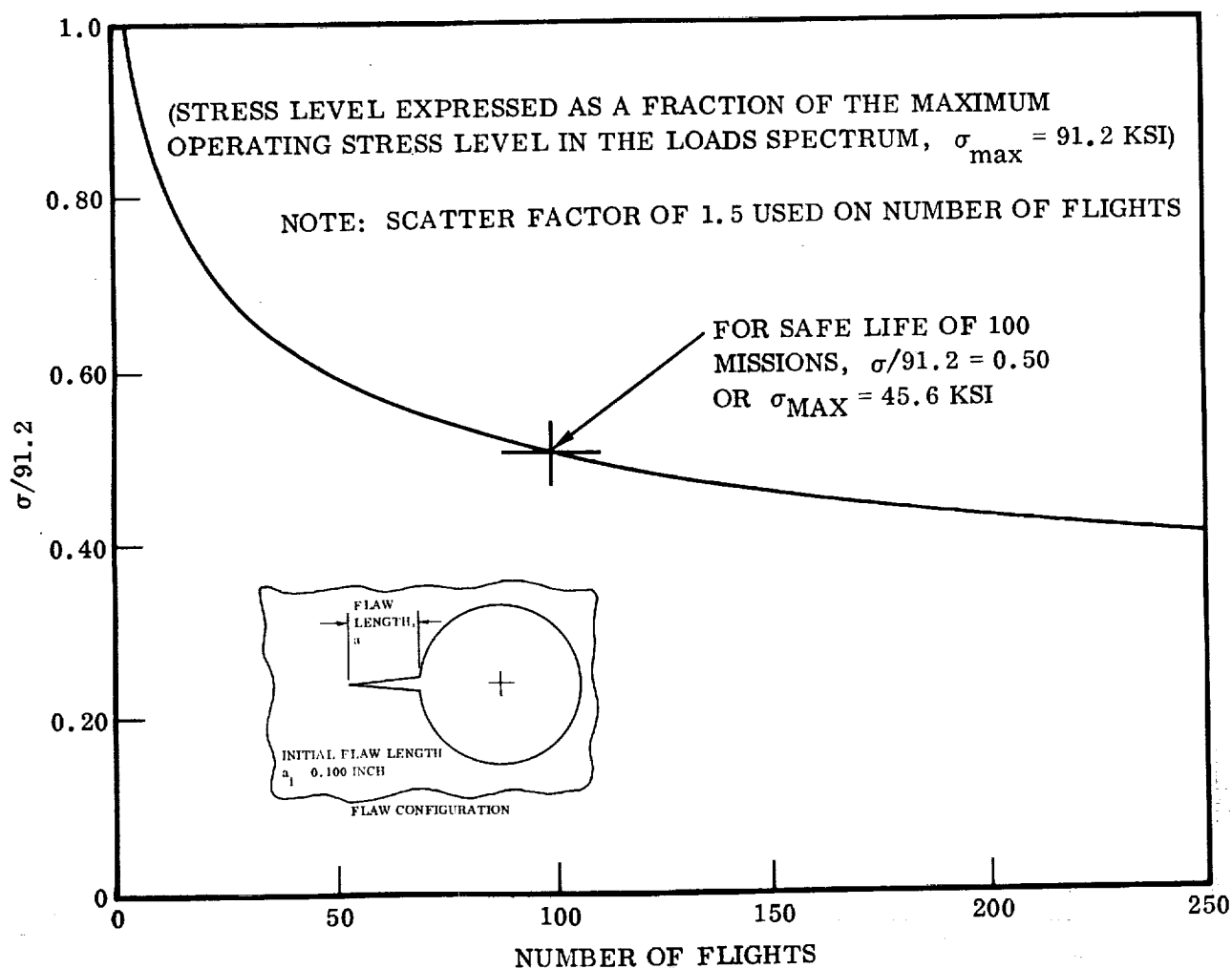


Figure 5-27. Allowable Maximum Operating Stress Level Versus the Number of Flights to Failure (Safe-Life) for the Titanium Wing Spar Caps

**5.5.2 WING SPAR CAPS SAFE-LIFE SENSITIVITY TO FACTOR OF SAFETY AND FLAW GROWTH SCATTER FACTOR.** The type of flaw assumed to be present in the structure for this analysis is a through-crack emanating from a hole. This configuration is most critical due to the stress concentration gradient in the vicinity of the hole. The equation for the stress intensity factor for this type of flaw is

$$K_I = \frac{\sigma \sqrt{\pi} \sqrt{a}}{\sqrt{1 - 0.177 (\sigma / \sigma_{ys})^2}} \text{ (GKT)}$$

where GKT, the factor to account the stress concentration in the vicinity of the hole, is derived in Section 5.5.1.2. The initial flaw size ( $a_i$ ) is assumed to be 0.100 inch. This is based on an estimate of NDE capability. The flaw is propagated to failure under the influence of the applied loading spectrum for the wing. The loading spectrum, with a maximum applied stress level of 91.2 ksi, is equivalent to a factor of safety of 1.4. Factor of safety can be related to the maximum stress level in the spectrum according to the equation

$$FS_u = 1.4 \left( \frac{91.2}{\sigma_{\max}} \right)$$

The effect on the safe-life of the wing of varying the factor of safety and the associated maximum stress level is presented in Figure 5-28. The sensitivity of the safe-life of the baseline wing spar caps to flaw growth scatter factor variations is presented in Figure 5-29. The figure shows that the safe-life of the baseline wing spar caps is inadequate regardless of the scatter factor.

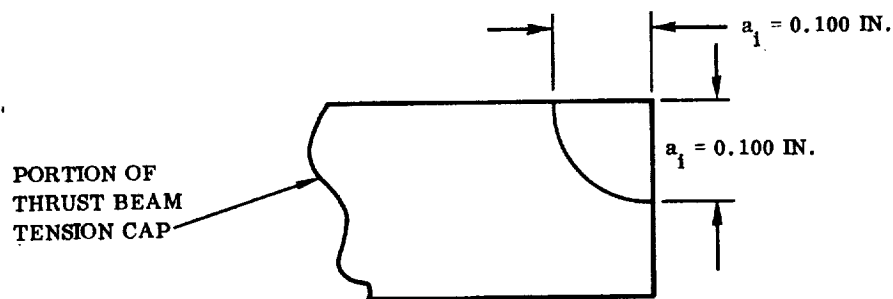
## 5.6 THRUST STRUCTURE

**5.6.1 THRUST BEAM CAP SAFE-LIFE ANALYSIS.** For the thrust structure beams, as for the wing spar caps, a safe-life analysis was carried out using two types of initial flaws: a corner crack, and a crack emanating from a fastener hole.

The thrust structure loading spectrum used in the safe-life analysis is the same as that used in the fatigue life determination and shown in Table 4-5.

**5.6.1.1 Corner Crack.** In the analysis of the thrust structure, one of the thrust beam tension caps was assumed to contain a corner crack of an initial size of 0.1 inch (see sketch on following page). This initial size was chosen based on a judgment of the capability of nondestructive evaluation.





The crack growth studies were done on the thrust structure assuming it was maintained at room temperature. Thus room temperature properties were assumed, and crack growth rate curves for Ti-6Al-4V annealed titanium base metal at room temperature were used in the flaw propagation computer program.

The equation for the maximum stress intensity factor for a corner crack is

$$K_I = \frac{\sigma \sqrt{\pi a} (0.705)}{\sqrt{1 - 0.177 (\sigma/\sigma_Y)^2}}$$

This is Equation VII-7 from Reference 10 modified to account for the plastic zone correction.

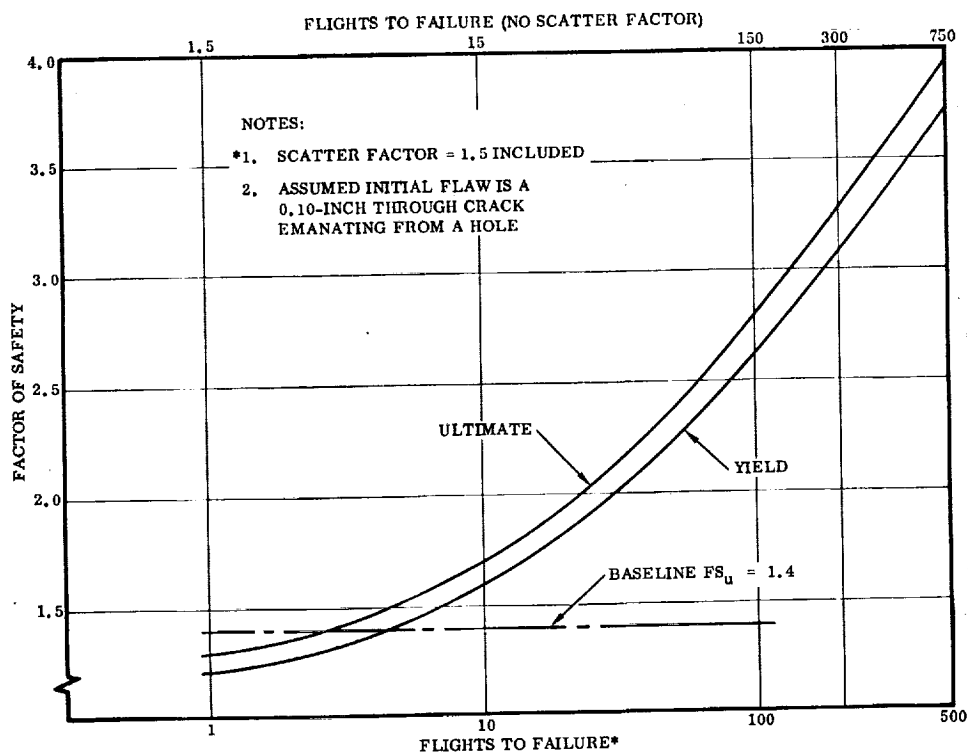


Figure 5-28. Wing Spar Caps Factor of Safety Versus Safe-Life

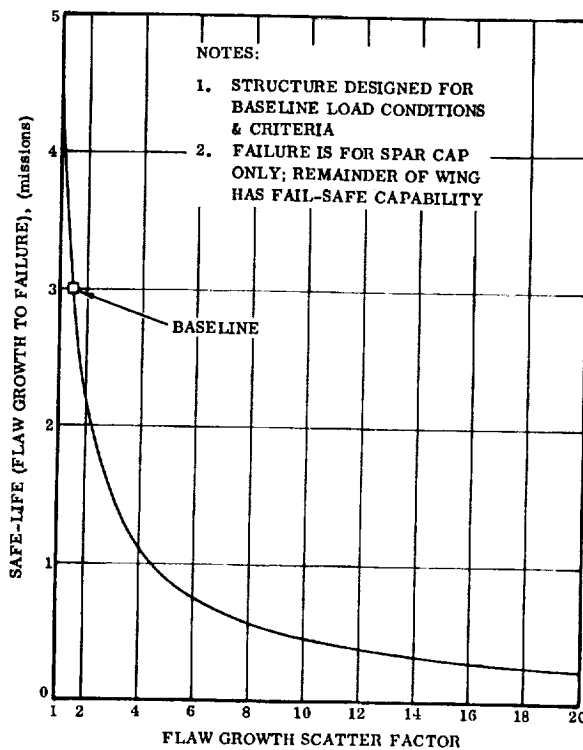


Figure 5-29. Wing Spar Caps Safe-Life (Flaw Growth to Failure) Versus Scatter Factor

$\sigma$  = applied stress

$\sigma_Y$  = yield stress

$a$  = flaw size

The critical value of the material toughness parameter,  $K_{Ic}$ , used here for the Ti-6Al-4V annealed titanium base metal at room temperature was  $K_{Ic} = 78.0 \text{ ksi } \sqrt{\text{inch}}$  (Reference 16, Figure 35, Page 89). The tensile yield stress used was  $\sigma_Y = 120.0 \text{ ksi}$ . The maximum operating stress occurring in the thrust beam cap can be found from the spectrum to be = 92.9 ksi. Substituting all these values into the stress intensity factor equation results in

$$78.0 = \frac{92.9 \sqrt{\pi a_{cr}} (0.705)}{\sqrt{1 - 0.177 (92.9/120.0)^2}}$$

This equation can be solved for the critical value of 'a,' which turns out to be  $a_{cr} = 0.4036 \text{ inch}$ .

Under the influence of the applied loading spectrum, it took 1555 flights for the initial flaw of size  $a_i = 0.100 \text{ inch}$  to grow to the critical flaw size of  $a_{cr} = 0.4036 \text{ inch}$ . Figure 5-30 is a plot of flaw size versus flights. A scatter factor of 1.5 was used on the number of flights to failure.

**5.6.1.2 Crack Emanating From Hole.** The flaw configuration and method of analysis for determining the growth of a crack emanating from a hole is the same as was used in the wing spar cap safe-life analysis and shown in Section 5.5.1.2.

The maximum operating stress is found from the applied loading spectrum to be  $\sigma = 92.9 \text{ ksi}$ . Substituting this stress and the appropriate material properties into the equation for the stress intensity factor for a crack emanating from a hole results in the following expression:

$$78.0 = \frac{(92.9) \sqrt{\pi} \sqrt{a_{cr}}}{\sqrt{1 - 0.177 (92.9/120.0)^2}} \left[ 1.0 + 2.0 e^{(-18.42 a_{cr})} \right]$$

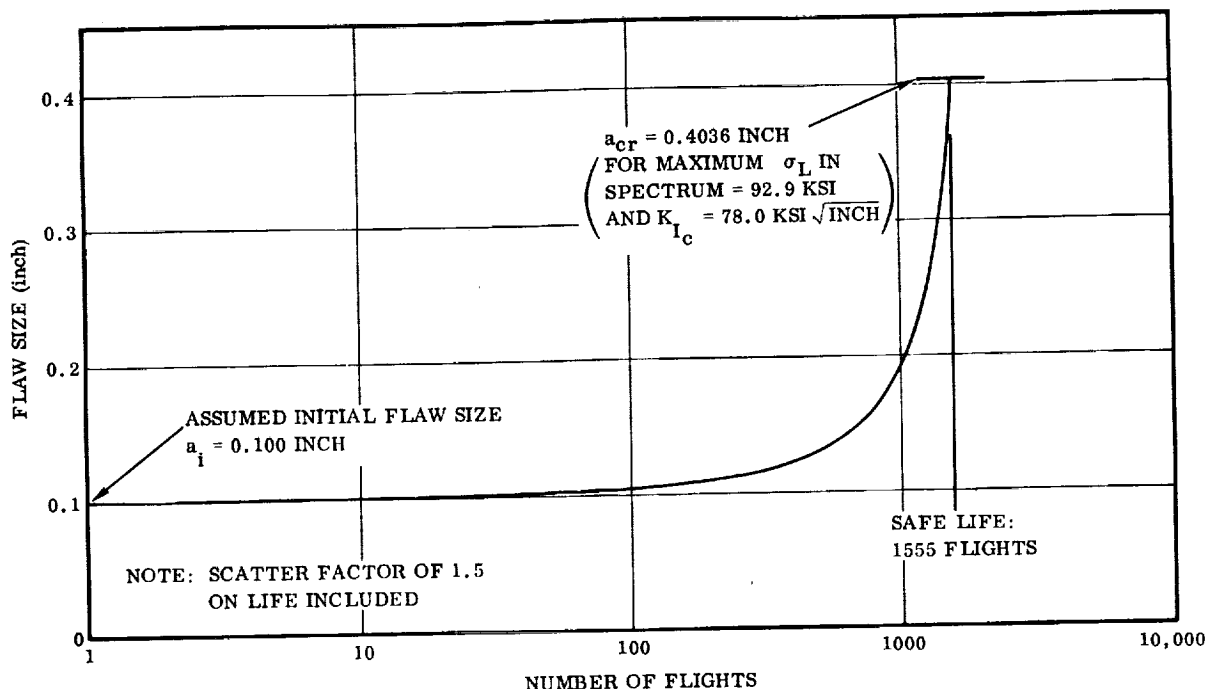


Figure 5-30. Crack Growth in the Titanium Thrust Beam Caps (Flaw Configuration - Corner Crack)

This expression is solved by a trial and error method for the critical value of 'a,' which turns out to be  $a_{cr} = 0.1694$  inch.

Under the influence of the applied loading spectrum, it took 101 flights for the initial flaw ( $a_i = 0.100$  inch) to grow to the critical flaw size ( $a_{cr} = 0.1694$  inch). Note here that a scatter factor of 1.5 was used on the number of flights to failure. Figure 5-31 is a plot of flaw size versus flights.

**5.6.2 THRUST BEAM CAP SAFE-LIFE SENSITIVITY TO FACTOR OF SAFETY AND FLAW GROWTH SCATTER FACTOR.** The type of flaw assumed to be present in the structure for this analysis is a through-crack emanating from a hole. This configuration is most critical due to the stress concentration gradient in the vicinity of the hole. The method of analysis for this configuration was presented in Section 5.5. The initial flaw size is assumed to be 0.10 inch based on a judgment of NDE capability. The factor of safety can be related to the maximum stress level in the spectrum according to the equation

$$FS_u = 1.4 \left( \frac{91.2}{\sigma_{max}} \right)$$

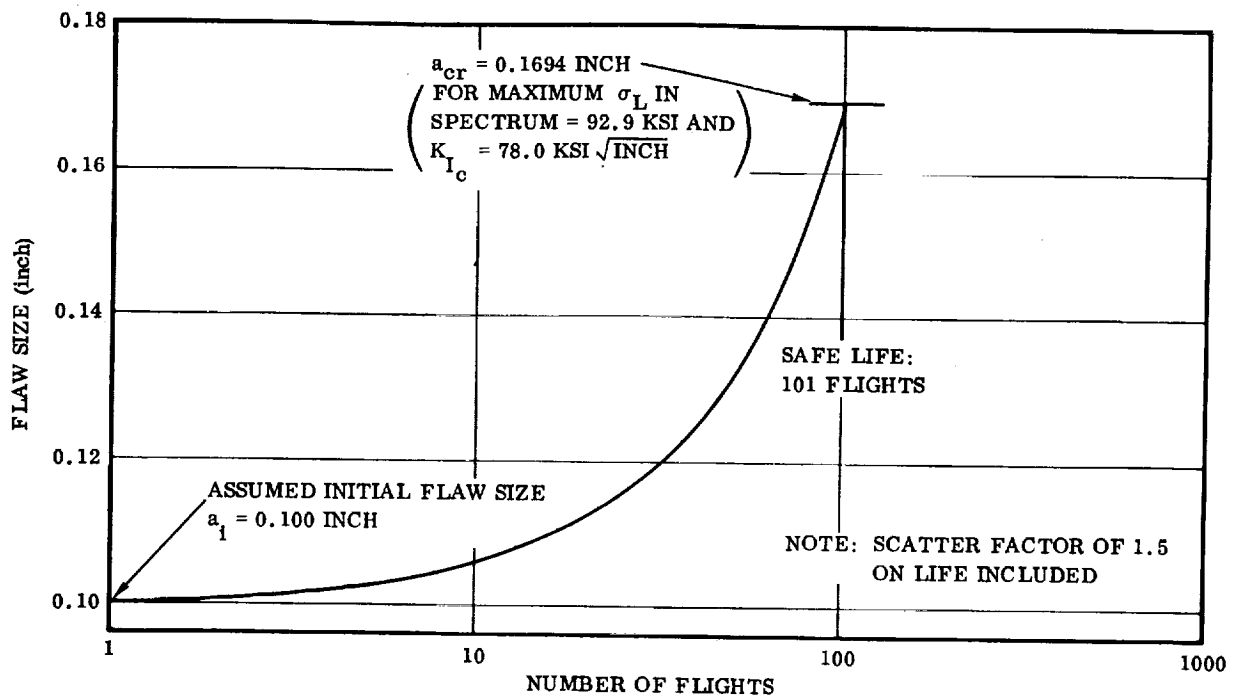


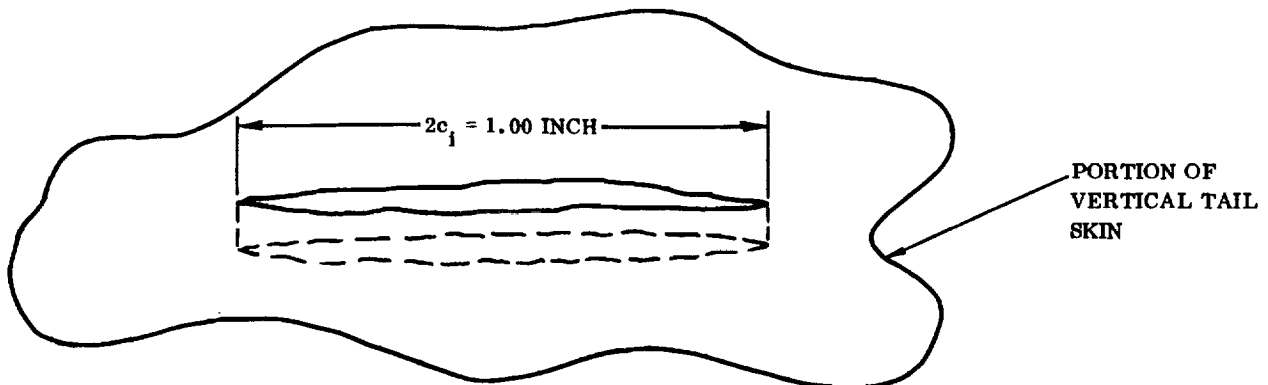
Figure 5-31. Crack Growth in the Titanium Thrust Beam Caps (Flaw Configuration — Crack Emanating from a Hole)

Therefore, by varying the maximum stress level in the applied loading spectrum the factor of safety can also be varied. The effect of varying the factor of safety and corresponding stress levels on the critical flaw size and the number of flights to failure can be found in Figures 5-32 and 5-33 respectively.

The sensitivity of the safe-life of the baseline thrust beam caps to flaw growth scatter factor variations is presented in Figure 5-34. The figure shows that any increase of the scatter factor above the baseline value of 1.5 will reduce the safe-life of the thrust beam caps below the acceptable level of 100 missions.

## 5.7 VERTICAL TAIL

**5.7.1 VERTICAL TAIL SAFE-LIFE ANALYSIS.** The flaw growth analysis of the vertical tail was done assuming that there was an initial through crack in the skin of length  $(2c)_i = 1.00$  inch (see sketch below). This initial size was chosen based on a judgment of the capability of nondestructive evaluation.



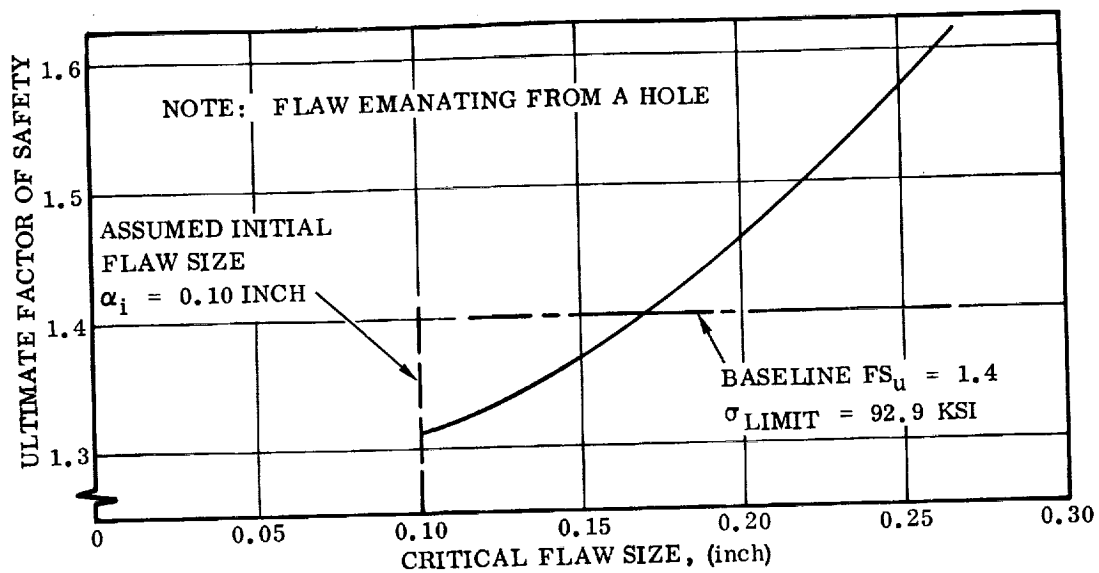


Figure 5-32. Thrust Structure Ultimate Factor of Safety Versus Critical Flaw Size

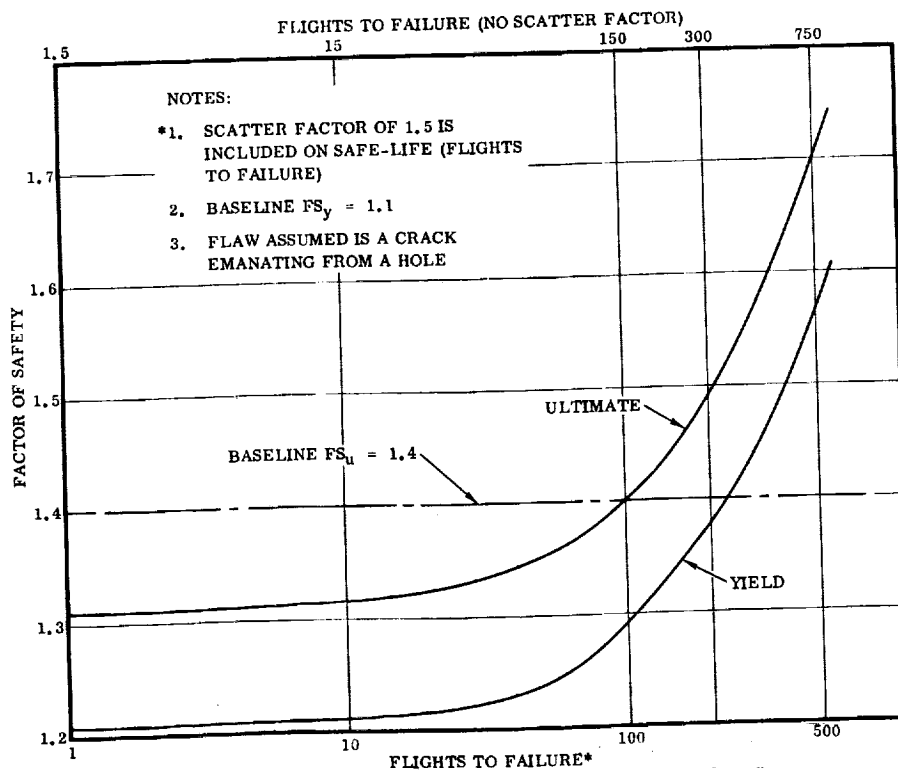


Figure 5-33. Thrust Structure Factor of Safety Versus Safe-Life

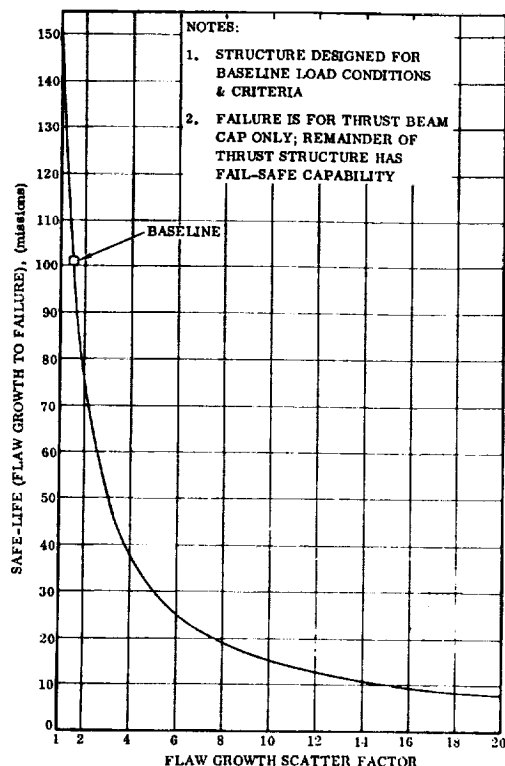


Figure 5-34. Thrust Beam Caps Safe-Life (Flaw Growth to Failure) Versus Scatter Factor

The vertical tail loading spectrum experienced by the flap configuration shown in the sketch is essentially the same spectrum that was used in the fatigue life determination.

The crack growth studies were done on the vertical tail assuming the structure was maintained at room temperature. Thus room temperature properties were assumed and crack growth rate curves for Ti-6Al-4V annealed titanium base metal at room temperature were used in the flaw propagation computer program.

The equation for the maximum stress intensity factor for a through crack of length  $2c$  is:

$$K_I = \frac{\sigma \sqrt{\pi} \sqrt{2c}}{\sqrt{2 - (\sigma/\sigma_y)^2}} \quad \text{(Reference 18, Page 28)}$$

where

$\sigma$  = applied stress

$\sigma_y$  = tensile yield stress

The critical value of the material toughness parameter,  $K_{Ic}$ , used here for the Ti-6Al-4V annealed titanium base metal at room temperature was  $K_{Ic} = 78.0 \text{ ksi } \sqrt{\text{inch}}$ . (Reference 16, Figure 35, Page 89). The tensile yield stress was  $\sigma_y = 120.0 \text{ ksi}$ . The maximum operating stress in the vertical tail can be found from the spectrum to be  $\sigma = 30.940 \text{ ksi}$ . Substituting all these values into the stress intensity factor equation results in:

$$78.0 = \frac{30.940 \sqrt{\pi} \sqrt{(2c)_{cr}}}{\sqrt{2 - (30.940/120.0)^2}}$$

This equation can be solved for the critical value of  $2c$ , which turns out to be  $(2c)_{cr} = 3.9115 \text{ inches}$ .

Under the influence of the applied loading spectrum, it took 534 flights for the initial flaw of size  $(2c)_i = 1.00 \text{ inch}$  to grow to the critical flaw size of  $(2c)_{cr} = 3.9115 \text{ inches}$ . Note here that a scatter factor of 1.5 has been used on the number of flights to failure. A plot of flaw size versus flights to failure can be found in Figure 5-35.

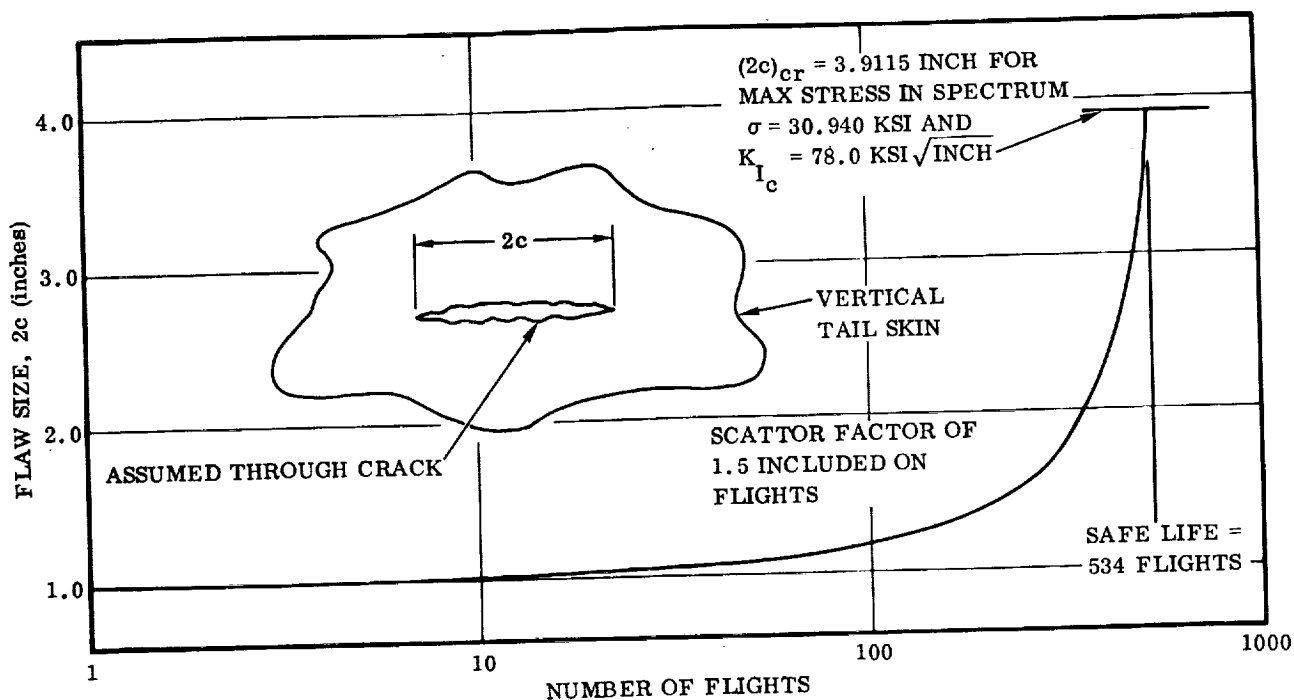


Figure 5-35. Crack Growth in the Vertical Tail Skin

**5.7.2 VERTICAL TAIL SAFE-LIFE SENSITIVITY TO FACTOR OF SAFETY AND FLAW GROWTH SCATTER FACTOR.** The type of flaw assumed to be present in the structure for this analysis is a through-crack of 1.00 inch length, based on an estimate of NDE capability. The equation for the stress intensity factor for this type of flaw is

$$K_I = \frac{\sigma \sqrt{2c\pi}}{\sqrt{2 - (\sigma/\sigma_{ys})^2}}$$

where

$$2c = \text{flaw size}$$

The basic applied loading spectrum for the vertical tail is shown in Table 4-7. The stresses in this spectrum correspond to an ultimate factor of safety of 1.4. Figure 5-36 is a plot of applied stress versus flaw size for a through-crack under the influence of the basic applied load spectrum. The ultimate factor of safety can be related to the limit stress level in the spectrum according to the equation

$$FS_u = 1.4 \left( \frac{34.0}{\sigma_{\text{limit}}} \right)$$

Therefore by varying the limit stress, the factor of safety can also be varied. The effect of varying the factor of safety and corresponding stress levels on the number of flights to failure is presented in Figure 5-37.

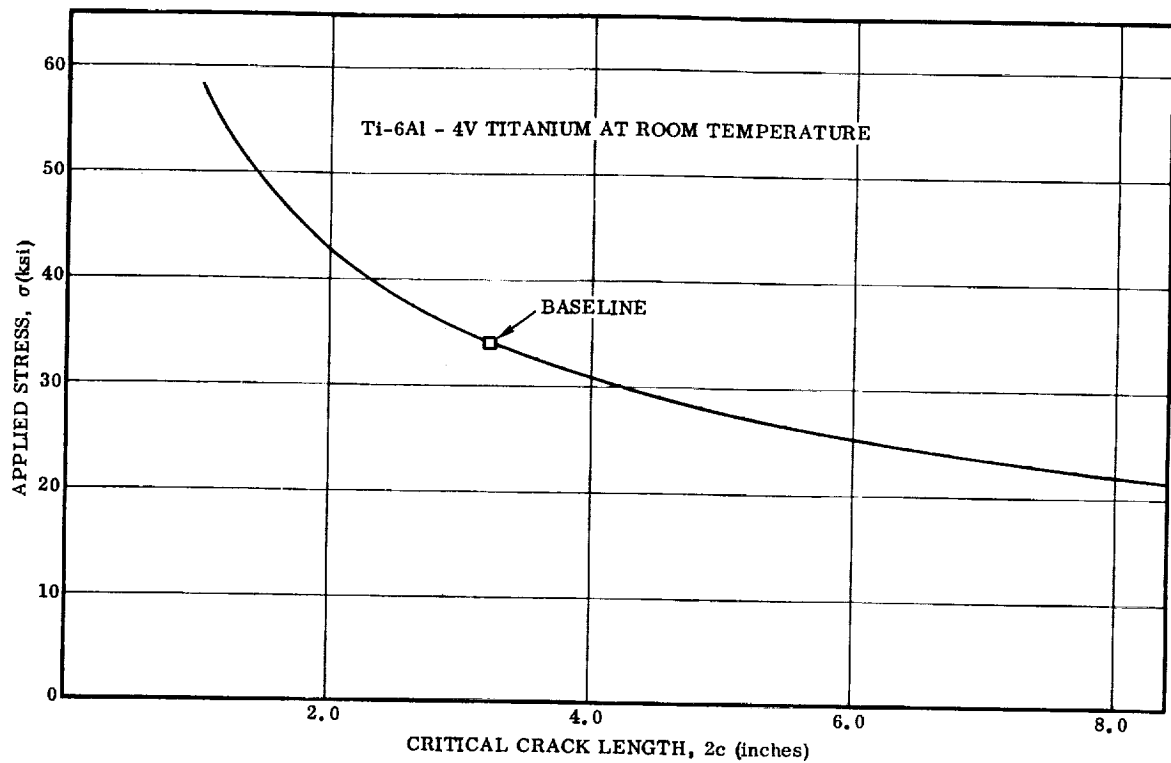


Figure 5-36. Applied Stress Versus Critical Crack Length for a Through-Crack

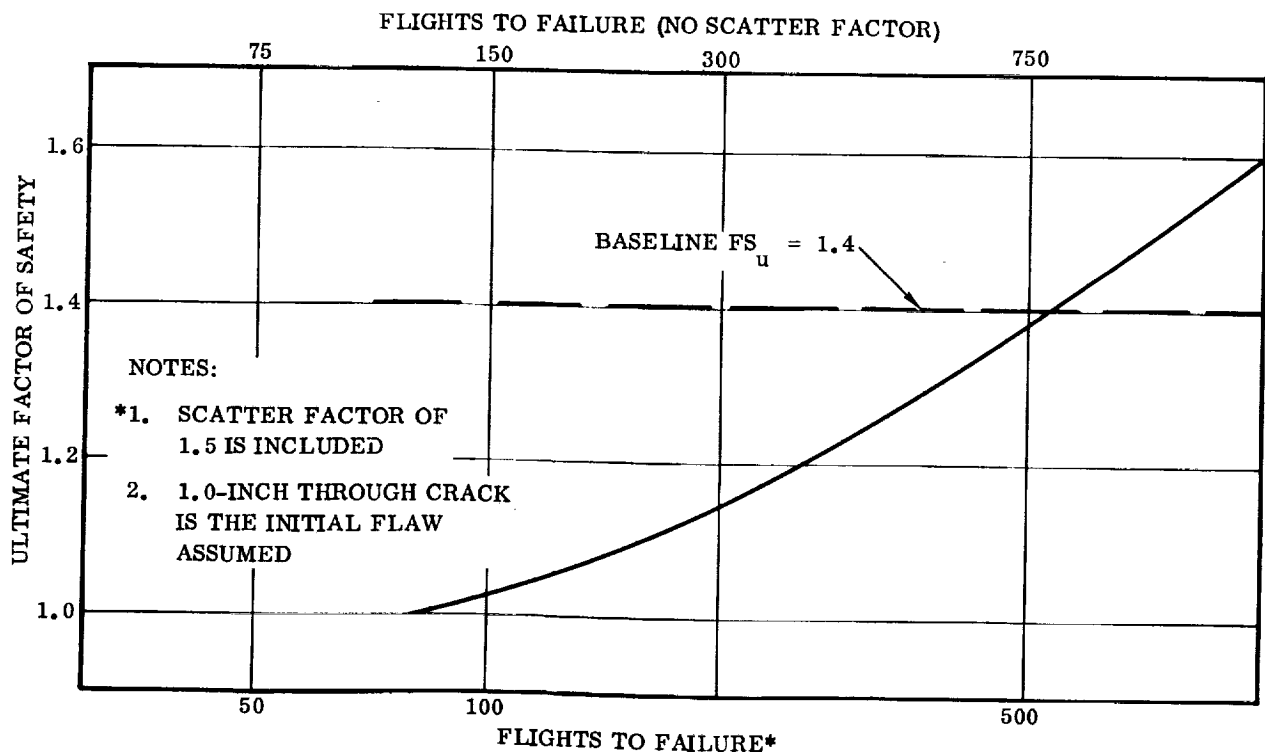


Figure 5-37. Vertical Tail Ultimate Factor of Safety Versus Safe-Life



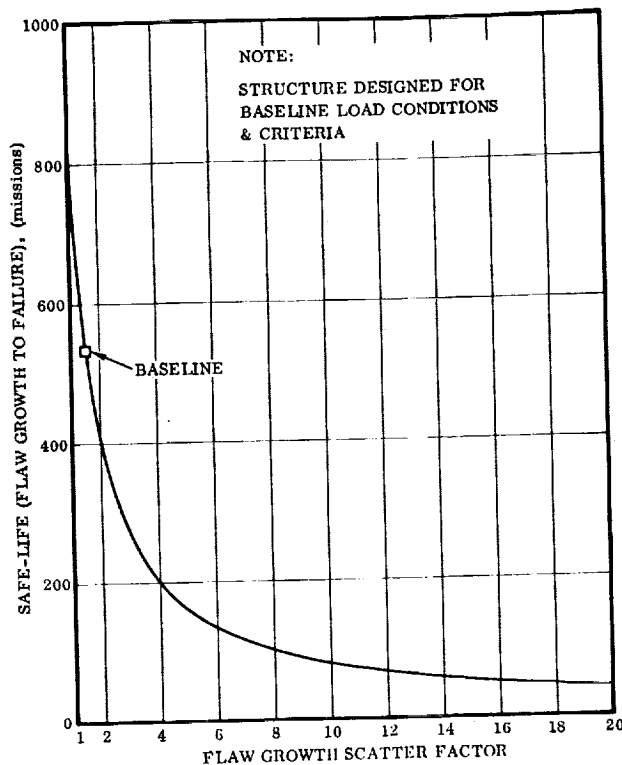


Figure 5-38. Vertical Tail Safe-Life (Flaw Growth to Failure) Versus Scatter Factor

The sensitivity of the safe-life of the baseline vertical tail to flaw growth scatter factor variations is presented in Figure 5-38. The figure shows that although safe-life drops rapidly for increases of the scatter factor from the baseline value of 1.5, the safe-life of the vertical tail remains at an adequate level for scatter factors as high as 8.

## 5.8 CREW MODULE

This section presents the safe-life analysis of the crew module. Since the critical flaw size is greater than the thickness of the crew module skin, the type of flaw assumed to be present in the structure for this analysis is a through-crack. Various size initial cracks were assumed.

The basic applied loading spectrum for the crew module is

$\sigma_{\min}$ (ksi)	$\sigma_{\max}$ (ksi)	Cycles per Flight	Time per Flight (minutes)
0	15.0	1	10
0	8.5	1	90

The stresses in this spectrum correspond to an apparent ultimate factor of safety of 4.2. The high apparent factor of safety was dictated by the requirement that the crew module be fail-safe. Figure 5-39 is a plot of applied stress versus critical crack length for a through-crack under the influence of the applied load spectrum. The ultimate factor of safety can be related to the maximum stress level in the spectrum according to the equation

$$FS_u = 4.2 \left( \frac{15.0}{\sigma_{\max}} \right)$$

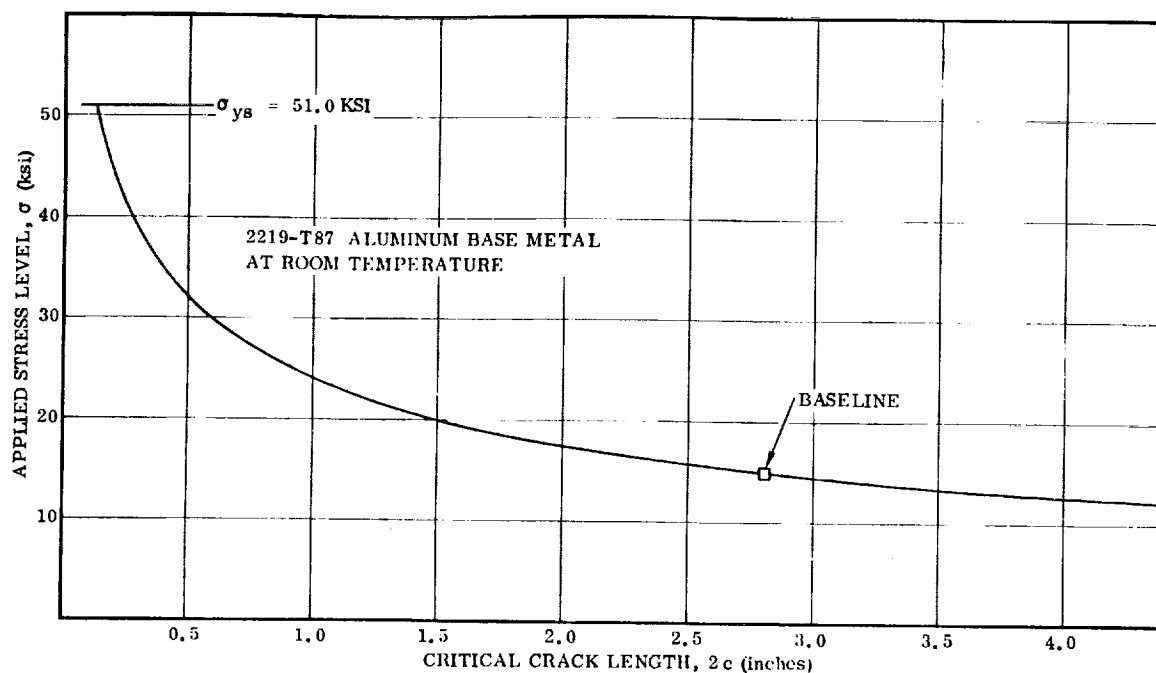
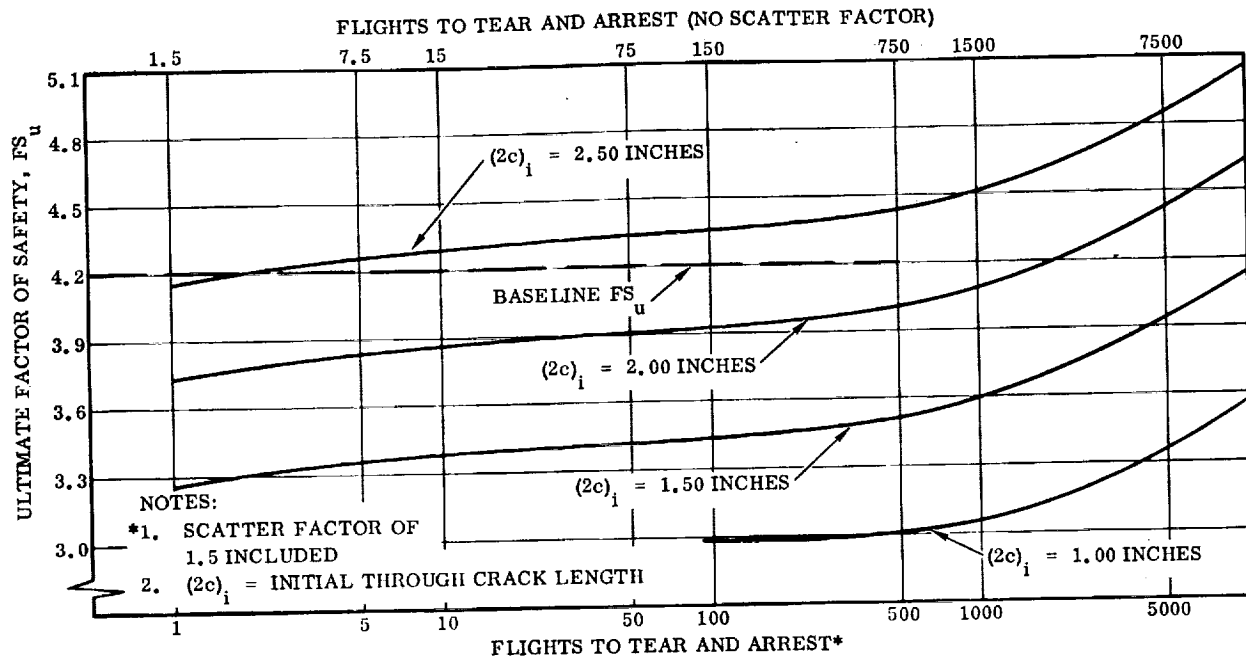


Figure 5-39. Crew Module Applied Stress for a Through-Crack Versus Critical Crack Length

Therefore by varying the maximum stress, the factor of safety can also be varied. The effect of varying the ultimate factor of safety and corresponding stress levels on the number of flights to failure for various initial crack lengths is shown in Figure 5-40. Investigation of the curves reveals that for an initial crack length of 2.00 inches and the baseline apparent factor of safety of 4.2 the safe-life is 1928 missions, which far exceeds the design service of 100 missions. Similarly for an initial flaw size of 1.00 inch and the required 100 mission life, a factor of safety of 2.98 is required. This indicates that the fail-safe design of the crew module gives that structure a safe-life well in excess of what would have been necessary had the safe-life design philosophy been applied. Figure 5-41 presents the sensitivity of the baseline crew module safe-life to flaw growth scatter factor for various initial crack lengths. The figure shows that the crew module has adequate safe-life except for large initial crack sizes and large scatter factors.

It should be noted that for the crew module, safe-life is only the period to the initiation of rapid flaw growth. Arrest of this rapid flaw growth occurs due to the fail-safe capability of the module.



**Figure 5-40. Crew Module Ultimate Factor of Safety Versus Flights to Tear and Arrest**

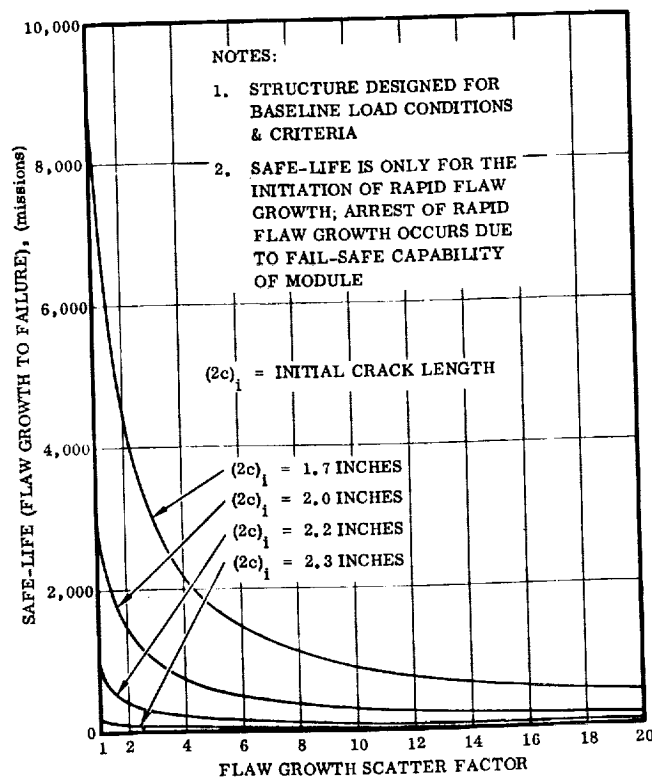


**Figure 5-41. Crew Module Safe-Life (Flaw Growth to Failure) Versus Scatter Factor**

## SECTION 6

### FAIL-SAFE ANALYSIS

The damage tolerance of each of the selected components is analytically determined below, as a measure of its fail-safe capability. Two criteria are used in judging adequacy of fail-safe design:

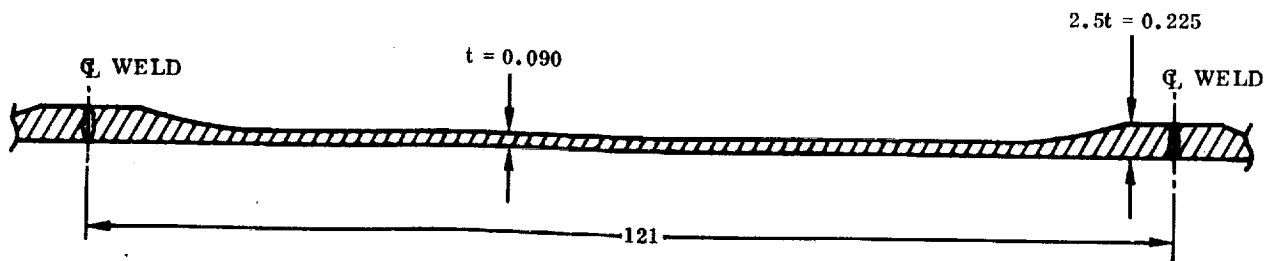
- a. In structure composed of a number of discrete elements (e.g., the wing box), a crack can proceed to the point of complete failure of one principal member. The remaining structure must possess a residual strength capability of carrying critical limit design load without failure.
- b. In monolithic structures (e.g., the integrally stiffened vertical tail box and propellant tanks with crack stoppers), fail-safe can be provided by fracture arrest of a rapidly propagating crack at crack stoppers such as stiffeners, straps, and doublers. The crack stoppers must be of sufficient size to arrest the crack under critical limit load conditions, and the arrested crack must be sufficient size to make detection certain prior to the next flight by normal preflight inspections. Monolithic structures are also considered fail-safe when the critical crack size for onset of rapid fracture is so large as to ensure detection prior to reaching critical size.

The baseline aft orbiter support frame does not possess fail-safe capability because of its monolithic construction. Therefore, it does not appear in this section of the report.

Since the baseline crew module is designed to be fail-safe, the fail-safe analysis of the crew module is presented in Section 3.7, which gives the baseline analysis of the component.

#### 6.1 LIQUID OXYGEN TANK

**6.1.1 FAIL-SAFE ANALYSIS —  $\text{LO}_2$  TANK SKIN UNDER INTERNAL PRESSURE.** A longitudinal section through the tank skin was taken at the upper centerline just aft of the forward dome equator, for analysis of fail-safe capability.



An initial flaw was assumed in the form of a through crack in the center of the panel. Since the weld and frame lands are so widely spaced, the tank skin panel was assumed to be of infinite width. Other assumptions were:

- a. Material is 2219-T87.
- b. Temperature is room temperature.
- c. Gross hoop stress is 42.8 ksi, resulting from maximum relief valve pressure (see Table 4-1).

Determination of Critical Hoop Stress for the Onset of Crack Instability:

$$\sigma_c = \frac{K_c}{\sqrt{\pi a_o + \frac{K_c^2}{2\sigma_{yB}} \left(1 + C \frac{a_o}{R}\right)}} \quad \text{(Equation IX-14 of Reference 10)}$$

where

$a_o$  = initial crack half length

$K_c$  = critical stress intensity factor, assumed as  $2 K_{Ic} = 64 \text{ ksi } \sqrt{\text{inch}}$

$C$  = bulge correction, shown as 9.5 for 2024-T3 in Table XVI of Reference 10. This value is used here for 2219-T87.

$R$  = radius of curvature = 198 inches

$\sigma_{yB}$  = material yield strength in a 2:1 biaxial stress field, assumed to be  $1.25 F_{ty}$  or 64 ksi

Solution of the equation for a range of values of  $a_o$  gives values of  $\sigma_c$  that are plotted as  $\sigma$  versus  $2a$  in Figure 6-1. They indicate a critical initial crack length of slightly less than one inch at a hoop stress of 42.8 ksi.

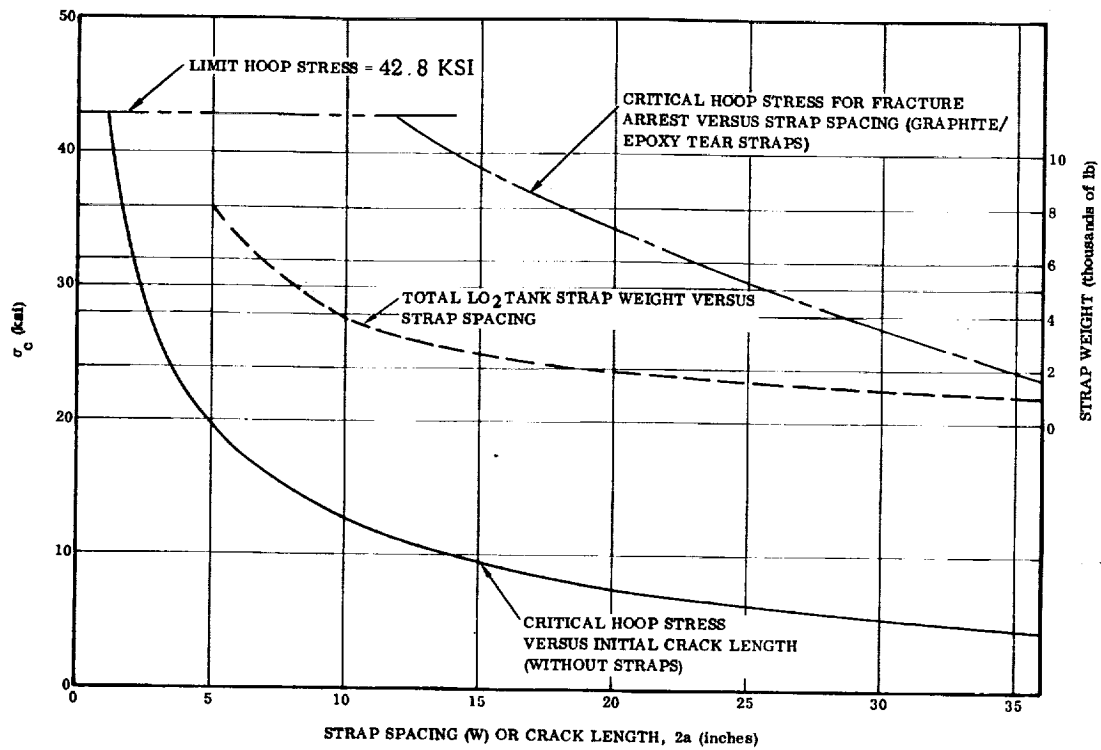


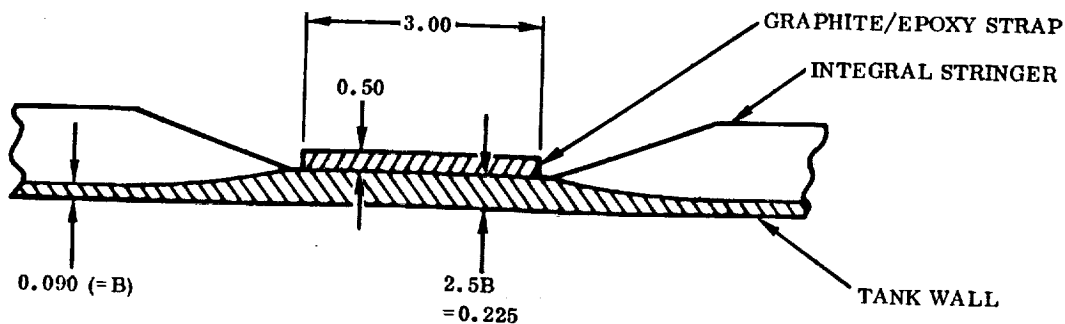
Figure 6-1. LO<sub>2</sub> Tank Crack Arrest Effectiveness of Graphite/Epoxy Tear Straps

In an effort to increase the critical crack length at this gross stress and to evaluate fail-safe tank concepts, crack arresters in the form of graphite/epoxy straps were tried. The straps were assumed to have a 0.50 by 3.00-inch section of HT-S/X904 unidirectional graphite/epoxy with the following properties:

$$F_{tu} = 168 \text{ ksi}$$

$$E = 20 \text{ ksi} \times 10^3$$

Section at Strap:



Determination of the effectiveness of the Graphite/Epoxy tear straps to arrest unstable crack is evaluated by the following method for various strap spacings and hoop stress levels. The method is:

- a. The applied stress intensity for a centrally located crack of variable length between the straps is determined by the method of Reference 18 which accounts for the presence of straps where:

$$K = C \sigma \sqrt{\pi a}$$

C = stress intensity correction factor

A typical plot of applied stress intensity versus crack size is presented in Figure 6-2.

- b. It is hypothesized that the stress level or strap spacing which causes the applied stress intensity curve to fall below the critical stress intensity factor ( $K_{IC}$ ) of the skin panel (i.e., fracture toughness) will cause dynamic fracture arrest and a fail-safe structural arrangement. This condition is illustrated in Figure 6-2. The values of strap spacings and stress levels which satisfy this fracture arrest hypothesis are plotted in Figure 6-1.

Also plotted in Figure 6-1 is the total weight of straps on the LO<sub>2</sub> tank for the strap spacings shown. The curve shows that the weight penalty required to provide fracture arrest at a hoop design stress of 42.8 ksi is 3300 pounds. Since this is an 18% weight penalty on the LO<sub>2</sub> tank, it is considered impractical to use these crack arrest straps.

**6.1.2 SENSITIVITY OF LO<sub>2</sub> TANK FAIL-SAFE CAPABILITY TO FACTOR OF SAFETY PERTURBATIONS.** An initial crack in the longitudinal direction in the form of a through-crack in the center of a panel was assumed. The crack is loaded transversely by hoop tension due to internal tank pressure. The crack location is on the upper centerline just aft of the forward dome equator. The material is 2219-T87 aluminum at room temperature. For the baseline, the gross limit hoop stress is 42.8 ksi. Figure 6-3 presents the critical initial flaw size,  $2a_0$ , versus the ultimate factor of safety for the liquid oxygen tank. To obtain the critical initial flaw size,  $2a_0$ , for a particular factor of safety, the following procedure was used. The limit stress for a factor of safety was determined by use of the equations

$$\sigma_{\text{limit}} = \frac{1.4 (42.8)}{FS_u} \quad \text{or} \quad \sigma_{\text{limit}} = \frac{51}{FS_y}$$

depending on whether ultimate factor of safety or yield factor of safety is critical. Then taking  $\sigma_{\text{limit}} = \sigma_c$ , the equation

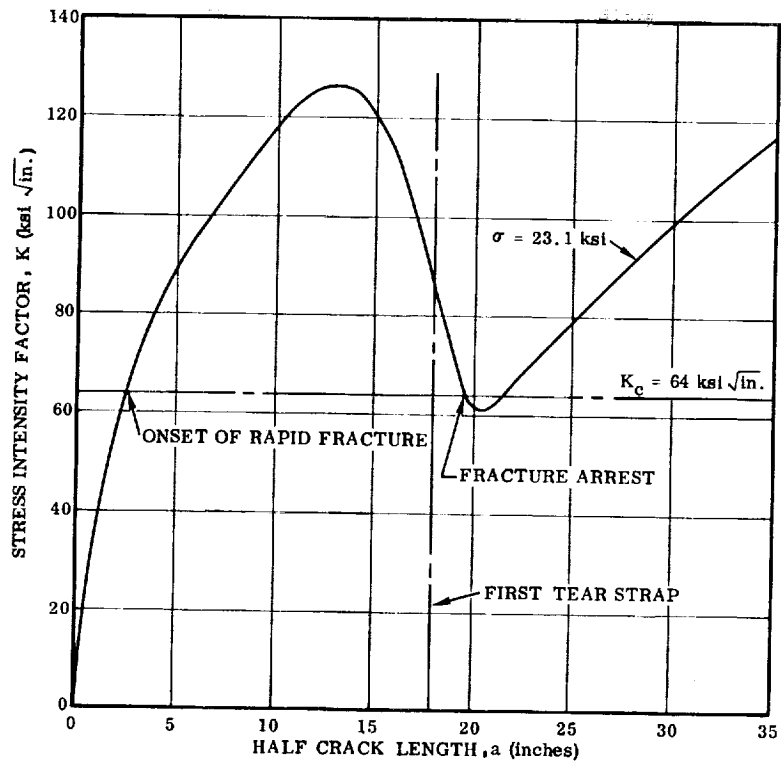


Figure 6-2.  $\text{LO}_2$  Tank Crack Arrest Effectiveness of Graphite/Epoxy Tear Straps, 36-Inch Strap Spacing

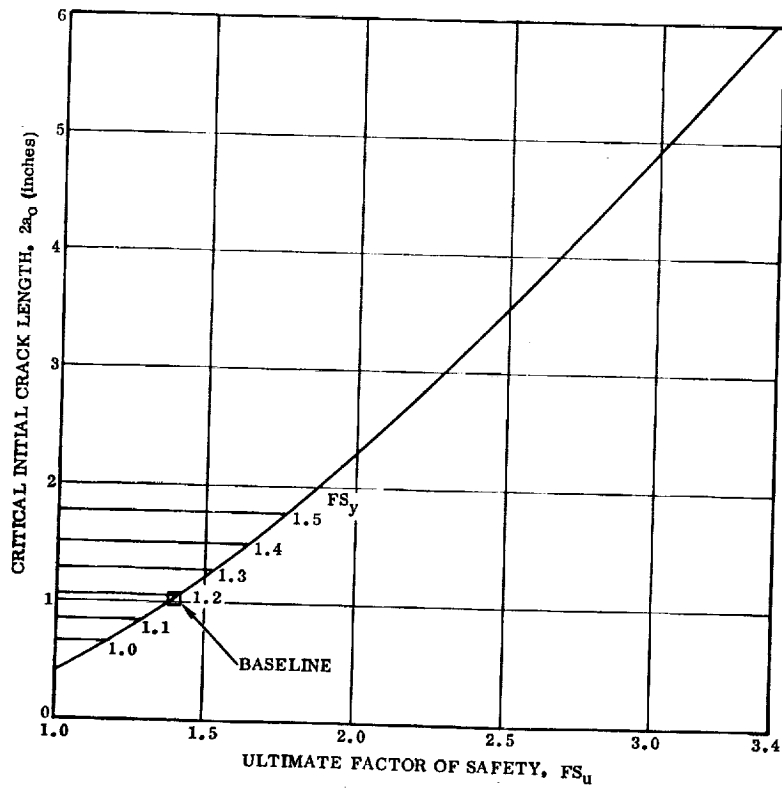


Figure 6-3.  $\text{LO}_2$  Tank Critical Initial Crack Length Versus Ultimate Factor of Safety



$$\sigma_c = \frac{K_c}{\left( \pi a_o + \frac{K_c^2}{2 \sigma_{yB}} \right)^{1/2} \left( 1 + \frac{Ca_o}{R} \right)}$$

is solved for  $a_o$ .

The  $LO_2$  tank, practically speaking, has no fail-safe capability for internal pressure loads. Decreases in factor of safety decrease what little residual strength a flawed tank has. Even large increases in the factor of safety don't appreciably increase the fail-safe capability of the tank. The figure shows that for all factors of safety investigated, the critical initial crack length is much less than the frame spacing, and thus fail-safe capability can be obtained only by use of intermediate crack stoppers between the frames. This solution, however, imposes an inordinate weight penalty, and therefore fail-safe capability is not practical even for increased safety factors.

## 6.2 LIQUID HYDROGEN TANK

### 6.2.1 FAIL-SAFE ANALYSIS — $LH_2$ TANK SKIN UNDER INTERNAL PRESSURE.

The general constructional features of the  $LH_2$  tank are similar to those of the  $LO_2$  tank. The assumptions for the fail-safe analysis were the same except for the gross hoop stress, which is 40.6 psi per Table 4-2, and the skin thickness, which is 0.116 inch with 0.290 inch land thickness.

For the tank without tear straps, the critical hoop stress is the same as for the  $LO_2$  tank for a given initial crack length. If tear straps were added similar to those shown for the  $LO_2$  tank, the results would be similar to the  $LO_2$  tank. A check was therefore made on increasing the size of the straps from 1/2 by 3 inches to 1 by 3 inches.

The critical hoop stresses for dynamic fracture arrest for various tear strap spacings were calculated using the same method as for the  $LO_2$  tank, and the resulting curve of crack arrest effectiveness of the 1 by 3 inch graphite/epoxy straps is shown in Figure 6-4. A plot of strap weight versus spacing is also shown. It can be seen by comparing the upper curve of Figure 6-1 for the  $LO_2$  tank with the equivalent curve of Figure 6-4 that the effectiveness of the graphite/epoxy tear straps was not significantly enhanced by a doubling of the cross-sectional area of the straps. It can also be seen from the strap weight curve that the straps are extremely heavy; at the strap spacing required for the limit stress of 40.6 ksi, the weight penalty would be over 20,000 pounds.

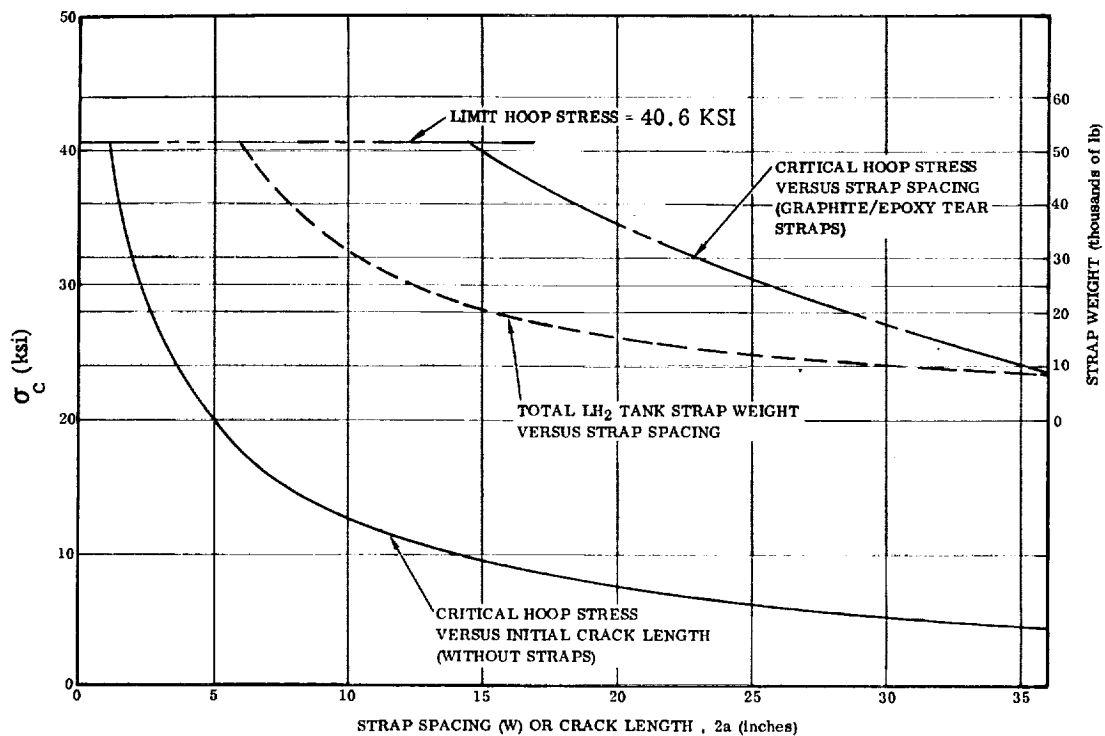
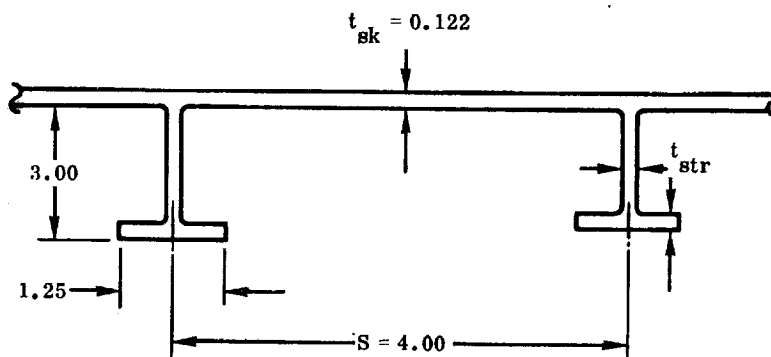


Figure 6-4. LH<sub>2</sub> Tank Crack Arrest Effectiveness of Graphite/Epoxy Tear Straps

#### 6.2.2 FAIL-SAFE ANALYSIS — LH<sub>2</sub> TANK SKIN UNDER LONGITUDINAL LOADS.

Taking a transverse section through the integrally stiffened tank skin in the region of the bottom centerline at Station 2600, the following configuration is obtained.



Using the method given in Reference 20:

$$\begin{aligned}\text{Percent stiffening} &= \frac{100}{1 + \frac{A_{sk}}{A_{str}}} \\ &= \frac{100}{1 + \frac{0.488}{0.264}} = 35.1\%\end{aligned}$$

Values of the stress intensity factor,  $K$ , are computed by use of the formula

$$K = C \sigma \sqrt{\pi a}$$

where

$C$  = stress intensity correction factor

$\sigma$  = gross stress level

$a$  = crack half length

and  $C$  is from Reference 20. The resulting values of  $K$  are plotted versus crack length in Figure 6-5. For this curve it is assumed that the stringer is not completely severed until the crack tip in the sheet has advanced a distance equal to the height of the stringer past the centerline of the stringer. Between the edge of the stringer and the point at which the stringer is assumed to be completely severed,  $K$  is assumed to increase linearly with the crack length,  $a$ , as shown.

Figure 6-5 shows that once rapid fracture has begun for a transverse crack under longitudinal loading the stress intensity doesn't go below the critical value,  $K_c$ , again. Therefore, once rapid fracture begins, it progresses to complete failure and the  $LH_2$  tank therefore has no fail-safe capability for transverse cracks under longitudinal loads.

**6.2.3  $LH_2$  TANK UNDER INTERNAL PRESSURE — FACTOR OF SAFETY PERTURBATIONS FOR FAIL-SAFE.** The method of analysis for the  $LH_2$  tank under internal pressure is the same as for the  $LO_2$  tank as presented in Section 6.1.2 except that the baseline gross limit hoop stress is 40.6 ksi. Figure 6-6 presents the critical initial flaw size,  $2a_o$ , versus the ultimate factor of safety,  $FS_u$ . For the range of safety factors investigated, the  $LH_2$  tank has no fail-safe capability for internal pressure. Decreases in factor of safety decrease what little residual strength a flawed tank has. Even large increases in the factor of safety don't appreciably increase the fail-safe capability of the tank. The figure shows that for all factors of safety investigated, the critical initial crack length is much less than the frame spacing, and therefore fail-safe can be obtained only by use of intermediate crack stoppers between the

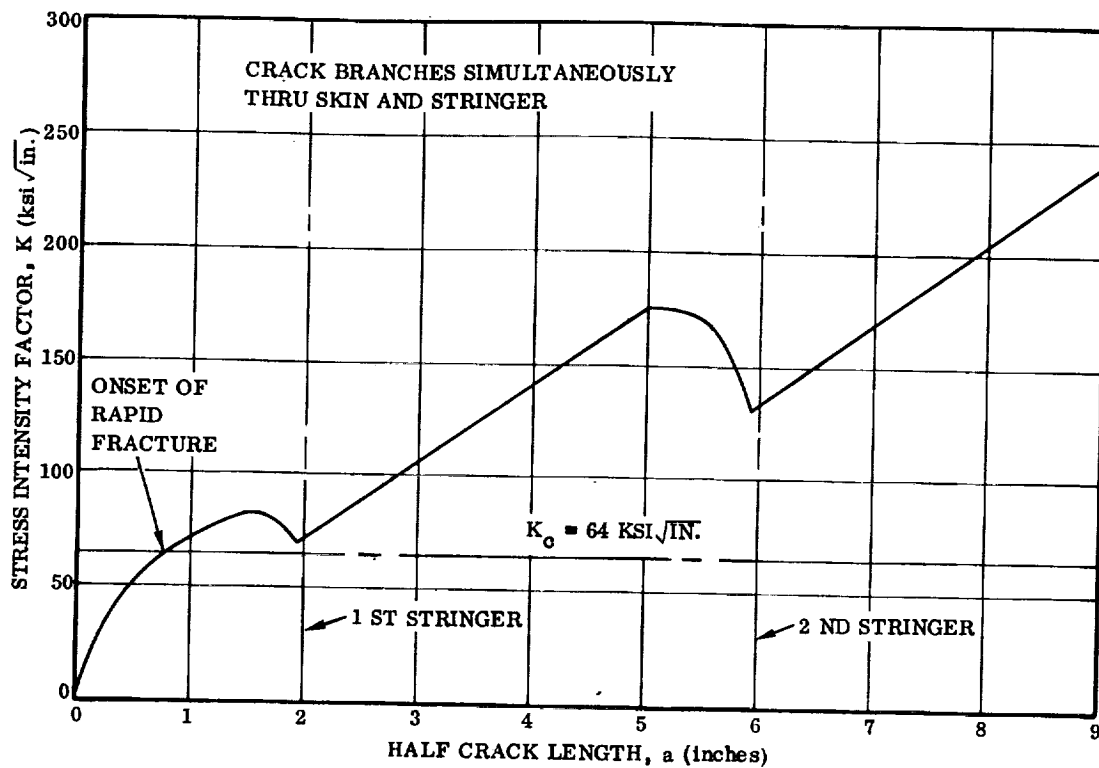


Figure 6-5.  $\text{LH}_2$  Crack Arrestment by Integral Stringers for Longitudinal Loading

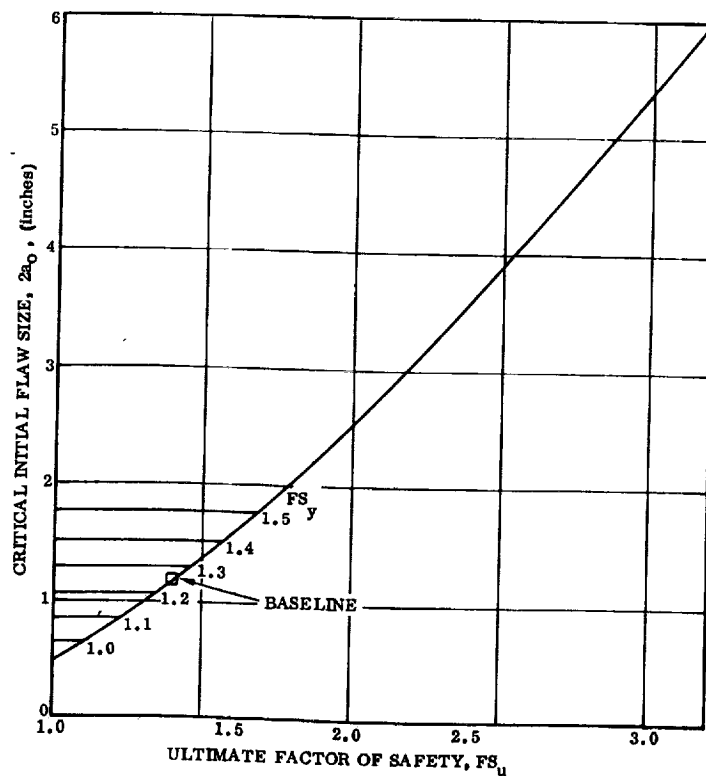


Figure 6-6.  $\text{LH}_2$  Tank Critical Initial Crack Length Versus Ultimate Factor of Safety for Internal Pressure

frames. This solution, however, imposes an inordinate weight penalty and therefore fail-safe is practical for internal pressure loading even for increased safety factors.

**6.2.4 LH<sub>2</sub> TANK UNDER LONGITUDINAL LOADS — FACTOR OF SAFETY PERTURBATIONS FOR FAIL-SAFE.** An initial crack in the transverse direction and centrally located between stringers is assumed at Station 2600 bottom centerline. The stringers are integral with the skin, and the skin-stringer combination is machined from three-inch-thick 2219-T87 aluminum plate. The crack is loaded transversely due to body bending and axial loads. Analysis for the stress intensity factor was performed by the method of Reference 20. The stress intensity factor is computed by use of the formula

$$K = C\sigma \sqrt{\pi a}$$

where

K = stress intensity factor

C = stress intensity correction factor from Figure 9, Reference 20

$\sigma$  = gross stress level

a = half crack length

A gross limit axial stress of 41.1 ksi for the baseline ultimate factor of safety of 1.4 was used for the calculations. Limit stresses for other ultimate safety factors were determined by the same means as for the liquid oxygen tank. The values of K for various ultimate factors of safety and crack lengths are plotted in Figure 6-7. The curves assume that the stringer is not completely severed until the crack tip in the sheet has advanced a distance equal to the height of the stringer past the centerline of the stringer. Between the edge of the stringer and the point at which the stringer is assumed to be completely severed, K is assumed to increase linearly with the crack length, a. This is represented by the straight sections of the curves.

Inspection of Figure 6-7 reveals that once rapid flaw growth has begun, there is no crack arrest except for a very short distance before the first stringer for  $FS_u = 1.6$ . The LH<sub>2</sub> tank therefore has virtually no fail-safe capability for longitudinal loads even at high ultimate factors of safety.

### 6.3 WING BOX

**6.3.1 WING BOX FAIL-SAFE ANALYSIS.** Fail-safe strength of the B-9U wing was evaluated analytically with the aid of a finite element computer program. The idealized structural model used in the fail-safe analysis is the same as that used in the sizing calculations and shown in Figure 3-21. Major tension or tension/shear members of the model were analytically "failed," one at a time, and limit design loads were applied to the weakened structure. Considerable beef-up was required to make

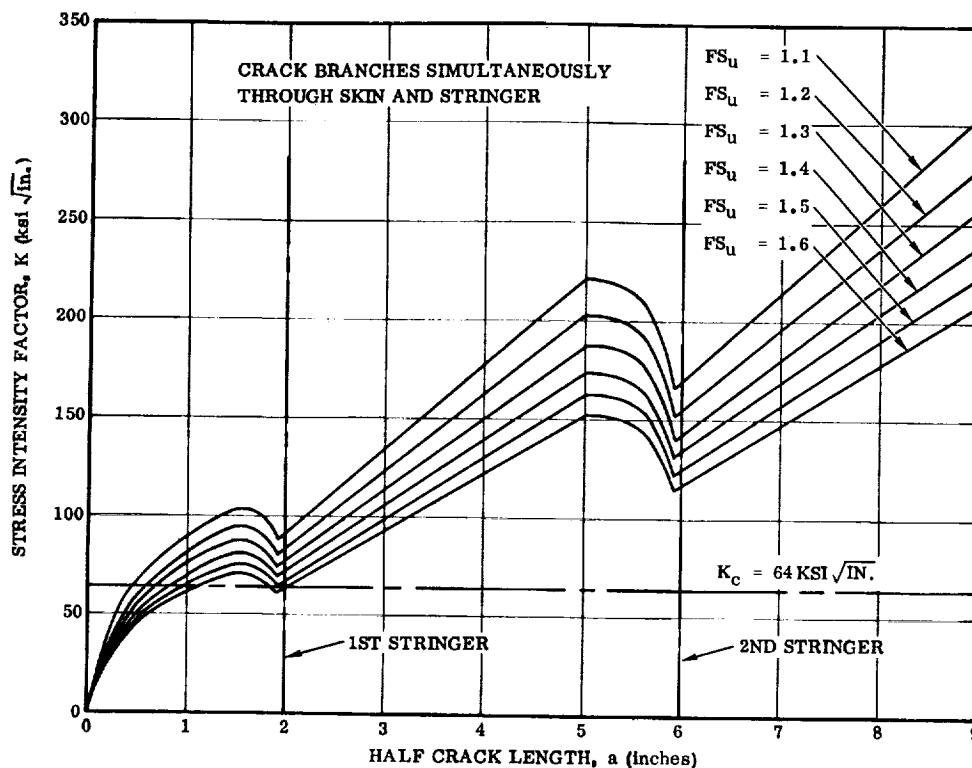


Figure 6-7. LH<sub>2</sub> Tank Longitudinal Loading Crack Arrestment by Integral Stringers for Various Factors of Safety

the structure adequate for design limit load. Total added weight was 534 pounds or 2.16% of the total ultimate strength model weight of 24,660 pounds. This corresponds to a 932-pound penalty of the actual wing box, which weighs 43,104 pounds.

The ascent loading condition W-1 (maximum  $\alpha$   $q$  with headwinds) that produces maximum tension in the lower surface was used for the fail-safe analysis.

Structural members "failed," one at a time, were: 1) spar lower cap between Stations 207 and 267 of Spars 2, 3, 4 and 5; 2) the spar shear diagonal between Stations 207 and 267 of Spar 3; 3) the spar lower cap and web between Stations 267 and 327 of Spars 3 and 4; and 4) the spar lower cap and web of Spar 4 between Stations 447 and 507. In the engine area, where spar shear is carried by webs welded to upper and lower caps, a lower cap/web failure was treated as a single failure with a weld crack assumed to propagate in two directions (i.e., through the tension cap and through the shear web). Note that this type failure appeared only slightly more critical than a simple lower cap failure inboard of the engine area.

Results of the fail-safe analysis are listed in Tables 6-1 and 6-2. Table 6-1 compares wing internal load distribution for ultimate load with the load distribution for limit load with a major tension member failed. The comparison is confined to that part of the

Table 6-1. Wing Box Ultimate and Fail-Safe Internal Loads

Member		Member Loads					
		Ultimate (lb)	Failed Element <sup>(1)</sup> 102-112 (lb)	Failed Element <sup>(1)</sup> 104-114 (lb)	Fail-Safe Failed Elements <sup>(2)</sup> 90-102 & 89-90- 102-101 (lb)	Failed Elements <sup>(2)</sup> 92-104 & 91-92- 104-103 (lb)	Failed Elements <sup>(2)</sup> 58-68 & 57- 58-68-67 (lb)
63-73	Spar 2	-354,199	-281,238	-273,932	-278,766	-271,280	-276,710
73-87		-497,417	-413,813	-376,286	-416,028	-373,735	-380,104
87-99		-628,314	-524,138	-476,391	-544,319	-478,988	-467,626
99-109		-774,735	-580,767	-594,141	-603,342	-588,782	-562,813
109-119		-769,428	-562,900	-588,978	-579,983	-584,184	-556,712
64-74	Spar 2	344,726	382,984	279,594	<u>405,867</u>	283,011	266,205
74-88		473,172	557,997	386,942	<u>599,488</u>	390,504	360,845
88-100		580,829	734,527	494,338	<u>766,134</u>	481,679	434,472
100-110		680,139	<u>893,780</u>	564,003	849,089	554,615	501,286
110-120		746,986	<u>856,912</u>	612,343	765,105	601,494	544,571
63-74	Spar 2	77,987	104,763	43,457	<u>112,634</u>	44,223	61,353
73-88		98,715	130,333	59,082	<u>152,653</u>	61,161	72,975
87-100		110,340	127,462	63,901	<u>176,297</u>	69,903	78,130
99-110		162,279	62,027	125,919	86,582	111,255	108,811
109-120		50,668	21,085	40,882	22,966	40,799	36,594
43-55	Spar 3	-528,592	-370,866	-417,546	-381,026	-418,886	-399,785
55-65		-641,513	-465,418	-497,600	-482,734	-496,145	-495,060
65-75		-842,087	-587,695	-674,859	-609,472	-665,296	-643,451
75-89		-1,046,631	-682,779	-865,611	-698,986	-842,755	-764,095
89-101		-1,256,888	-765,161	-1,050,835	-750,035	-1,026,506	-887,269
101-111	Cap	-1,590,023	-995,483	-1,275,347	-944,438	-1,279,230	-1,096,750
111-121		-1,537,001	-993,688	-1,210,439	-953,750	-1,215,727	-1,061,835
44-56	Spar 3	488,278	276,724	450,650	280,787	466,883	417,658
56-66		683,280	318,786	655,159	316,922	675,788	603,218
66-76		731,348	249,463	713,915	233,734	733,795	637,414
76-90		817,553	165,112	812,416	122,890	835,242	677,512

(1) Lower spar cap.

(2) Lower spar cap and web.

Table 6-1. Wing Box Ultimate and Fail-Safe Internal Loads, Contd

Member		Member Loads					
		Ultimate (lb)	Failed Element 102-112 (lb)	Failed Element 104-114 (lb)	Fail-Safe Failed Elements 90-102 & 89-90- 102-101 (lb)	Failed Elements 92-104 & 91-92- 104-103 (lb)	Failed Elements 58-68 & 57- 58-68-67 (lb)
90-102	Spar 3	913,936	63,198	903,960	0	950,683	725,665
102-112	Lower	984,374	0	994,711	39,481	965,102	761,635
112-122	Cap	1,179,282	212,045	1,087,060	323,493	1,004,734	869,468
43-56~	Diag	173,274	90,455	167,025	89,083	167,676	143,874
55-56-66-65	Spar	3,199(1)	1,414(1)	3,267(1)	1,329(1)	3,240(1)	2,866(1)
65-66-76-75		3,471(1)	1,122(1)	3,816(1)	907(1)	3,772(1)	2,108(1)
75-76-90-89		3,540(1)	814(1)	4,003(1)	328(1)	3,953(1)	2,002(1)
89-90-102-101		3,625(1)	996(1)	3,769(1)	0(1)	3,847(1)	2,132(1)
101-112	Truss	338,957	259,118	224,912	227,263	257,611	214,704
111-122	Diag	66,842	73,865	35,034	71,509	38,038	45,605
45-57	Spar 4	-546,210	-383,012	-376,980	-376,685	-386,762	-366,689
57-67		-615,093	-420,090	-446,691	-409,497	-464,523	-386,686
67-77		-750,268	-519,456	-515,431	-502,112	-529,526	-449,000
77-91		-904,096	-642,663	-562,341	-623,832	-557,866	-578,471
91-103	Cap	-1,083,289	-789,176	-593,802	-790,184	-587,508	-723,816
103-113	Cap	-1,375,423	-1,003,112	-812,022	-1,030,636	-802,961	-947,346
113-123		-1,365,959	-981,314	-851,983	-1,005,879	-840,493	-939,664
46-58	Spar 4	247,467	225,522	6,333	217,837	-33,114	-16,146
58-68		399,349	365,110	-28,338	353,887	-99,125	0
68-78		687,190	576,154	53,305	569,783	-45,874	200,502
78-92		993,679	808,765	85,586	816,134	-44,716	474,391
92-104	Cap	1,318,270	1,056,206	84,617	1,096,882	0	752,421
104-114	Cap	1,457,074	1,177,657	0	1,188,325	164,581	889,401
114-124		1,487,248	1,186,034	159,092	1,161,699	450,694	956,022

(1) Designated values are shear flows in pounds per inch.



Table 6-1. Wing Box Ultimate and Fail-Safe Internal Loads, Contd

Member	Member Loads					
	Ultimate (lb)	Failed Element 102-112 (lb)	Failed Element 104-114 (lb)	Fail-Safe Failed Elements 90-102 & 89-90- 102-101 (lb)	Failed Elements 92-104 & 91-92- 104-103 (lb)	Failed Elements 58-68 & 57- 58-68-67 (lb)
45-58 ~ Diag	87,227	80,842	-2,533	75,425	-14,733	4,458
57-58-68-67	2,327(1)	2,061(1)	284(1)	1,980(1)	31(1)	0
67-68-78-77 } Spar	2,536(1)	2,448(1)	211(1)	2,438(1)	587(1)	1,972(1)
77-78-92-91 } Web	2,743(1)	2,752(1)	572(1)	2,938(1)	1,032(1)	2,388(1)
91-92-104-103	3,093(1)	2,906(1)	134(1)	3,634(1)	0	2,562(1)
103-114 } Truss	232,114	162,798	225,701	176,894	198,845	181,784
113-124 } Diag's	69,298	29,374	80,214	30,741	67,574	50,663
69-79	-367,143	-270,251	-157,854	-268,718	-183,944	-238,428
79-93 } Spar 5	-467,591	-333,448	-264,572	-336,875	-332,019	289,319
93-105 } Upper	-548,177	-383,219	-401,533	-394,563	-413,497	345,348
105-115 } Cap	-659,747	-460,291	-412,639	-472,492	-408,899	435,002
115-125	-498,804	-336,421	-244,786	-346,210	-259,481	326,626
70-80	287,356	223,990	326,206	218,433	396,204	334,084
80-94 } Spar 5	320,662	269,254	451,116	260,559	558,924	301,793
94-106 } Lower	354,609	314,838	644,392	305,804	735,727	288,105
106-116 } Cap	417,071	361,265	877,784	364,091	758,517	307,480
116-126	570,641	483,167	904,873	489,670	698,942	418,741
69-80	199,153	130,920	212,179	136,625	251,173	118,345
79-94 } Spar 5	204,001	133,985	255,727	138,656	301,802	125,575
93-106 } Truss	189,357	126,113	269,086	125,014	212,948	126,414
105-116 } Diag's	255,098	185,261	118,626	179,028	120,140	184,415
115-126	-120,755	-93,957	-152,446	-95,340	-120,351	-84,573

(1) Designated values are shear flows in pounds per inch.

Table 6-1. Wing Box Ultimate and Fail-Safe Internal Loads, Contd

Member	Member Loads					
	Ultimate (lb/in)	Failed Element 102-112 (lb/in)	Failed Element 104-114 (lb/in)	Fail-Safe Failed Elements 90-102 & 89-90- 102-101 (lb/in)	Failed Elements 92-104 & 91-92- 104-103 (lb/in)	Failed Elements 58-68 & 57- 58-68-67 (lb/in)
<b>Skins</b>						
73-87-89-75	1,659	1,008	1,518	817	1,546	1,159
74-88-90-76	2,029	2,370	2,315	<u>2,416</u>	2,171	1,309
87-99-101-89	1,481	978	1,428	679	<u>1,503</u>	1,001
88-100-102-90	2,095	<u>2,648</u>	2,567	1,782	1,987	1,303
99-109-111-101	1,148	533	981	327	924	734
100-110-112-102	1,017	<u>1,248</u>	494	836	1,100	651
75-89-91-77	1,347	1,457	559	<u>1,543</u>	392	996
110-120-122-112	24	<u>1,576</u>	659	1,371	368	55
89-101-103-91	1,257	<u>1,318</u>	456	1,237	651	914
101-111-113-103	1,091	983	516	1,093	460	758
102-112-114-104	1,700	912	2,138	2,165	294	953
65-75-77-67	1,348	1,435	630	<u>1,539</u>	460	1,027
112-122-124-114	570	1,094	<u>1,451</u>	989	965	239
77-91-93-79	1,260	885	<u>1,720</u>	827	1,570	839
78-92-94-80	2,320	1,128	733	1,258	751	2,080
91-103-105-93	1,154	848	992	623	<u>1,438</u>	701
92-104-106-94	2,071	1,009	57	1,017	1,690	1,731
103-113-115-105	1,897	1,494	1,726	1,529	1,822	1,217
104-114-116-106	917	824	317	412	<u>3,174</u>	977

Table 6-1. Wing Box Ultimate and Fail-Safe Internal Loads, Contd

Member		Member Loads					
		Ultimate (lb)	Failed Element 102-112 (lb)	Failed Element 104-114 (lb)	Fail-Safe Failed Elements 90-102 & 89-90- 102-101 (lb)	Failed Elements 92-104 & 91-92- 104-103 (lb)	Failed Elements 58-68 & 57- 58-68-67 (lb)
<u>Skins</u>							
55-65-67-57		1,393 <sup>(1)</sup>	1,390 <sup>(1)</sup>	745 <sup>(1)</sup>	<u>1,489<sup>(1)</sup></u>	637 <sup>(1)</sup>	1,103 <sup>(1)</sup>
114-124-126-116		755 <sup>(1)</sup>	675 <sup>(1)</sup>	<u>2,027<sup>(1)</sup></u>	497 <sup>(1)</sup>	1,392 <sup>(1)</sup>	340 <sup>(1)</sup>
43-55-57-45		1,995 <sup>(1)</sup>	1,590 <sup>(1)</sup>	1,432 <sup>(1)</sup>	1,666 <sup>(1)</sup>	1,400 <sup>(1)</sup>	1,485 <sup>(1)</sup>
44-56-58-46		2,775 <sup>(1)</sup>	1,499 <sup>(1)</sup>	2,852 <sup>(1)</sup>	1,531 <sup>(1)</sup>	<u>2,989<sup>(1)</sup></u>	2,623 <sup>(1)</sup>
67-77-79-69		1,003 <sup>(1)</sup>	690 <sup>(1)</sup>	1,731 <sup>(1)</sup>	714 <sup>(1)</sup>	<u>1,794<sup>(1)</sup></u>	904 <sup>(1)</sup>
68-78-80-70		2,059 <sup>(1)</sup>	1,001 <sup>(1)</sup>	1,068 <sup>(1)</sup>	1,129 <sup>(1)</sup>	904 <sup>(1)</sup>	<u>2,191<sup>(1)</sup></u>
57-67-69-59		1,135 <sup>(1)</sup>	758 <sup>(1)</sup>	1,738 <sup>(1)</sup>	815 <sup>(1)</sup>	<u>1,908<sup>(1)</sup></u>	1,218 <sup>(1)</sup>
58-68-70-60		2,149 <sup>(1)</sup>	1,141 <sup>(1)</sup>	1,433 <sup>(1)</sup>	1,257 <sup>(1)</sup>	1,330 <sup>(1)</sup>	<u>2,156<sup>(1)</sup></u>
59-69	Spar 5	-263,923	-203,747	-85,067	-199,860	-85,133	-203,680
60-70	Caps	260,917	186,214	258,689	184,229	<u>300,192</u>	296,265
59-70 ~	Diag	181,866	120,609	167,789	125,253	191,049	<u>199,963</u>
47-59	Spar 5	-207,683	-164,768	-67,596	-160,649	-58,932	-131,085
48-60	Caps	223,745	150,512	204,146	151,286	227,955	<u>240,001</u>

Member		Member Loads			
		Ultimate (lb)	Failed Element (3) 100-110 (lb)	Fail-Safe Failed Element (3) 106-116 (lb)	Failed Element (4) 101-112 (lb)
99-110	Truss	162,279	Not	-	<u>246,200</u>
103-114		232,114	Critical	-	<u>259,200</u>
78-92-94-80	Skin	2,320 <sup>(1)</sup>		<u>2,461<sup>(1)</sup></u>	-
92-104-106-94		2,071 <sup>(1)</sup>		<u>2,463<sup>(1)</sup></u>	-

Notes:

- (1) Designated values are shear flows in pounds per inch.
- (2) Underlined values are maximum fail safe load of all cases considered.
- (3) Lower spar cap.
- (4) Diagonal.

Table 6-2. Margins of Safety for Baseline Structure, and Area Increases for Fail-Safe Design, Wing Box Area

Member	Spar Caps			Spar Diagonals			Spar Webs			Skins		
	M. S.	Added Area (in <sup>2</sup> )	Added Weight (lb)	M. S.	Added Area (in <sup>2</sup> )	Added Weight (lb)	M. S.	Added Thick-ness (inch)	Added Weight (lb)	M. S.	Added Thick-ness (inch)	Added Weight (lb)
64-74	-0.15	0.51	5.19									
74-88	-0.21	1.05	10.67									
88-100	-0.24	1.55	15.74									
100-110	-0.24	1.78	18.22									
110-120	-0.13	0.92	6.40									
90-102	-0.04	0.31	3.15									
102-112	-0.01	0.30	3.07									
48-60	-0.07	0.13	1.30									
60-70	-0.13	0.33	3.30									
70-80	-0.17	0.90	9.00									
80-94	-0.43	1.98	19.80									
94-106	-0.52	3.18	31.80									
106-116	-0.53	3.83	38.60									
116-126	-0.35	2.62	18.29									
63-74				-0.31	0.29	3.86						
73-88				-0.35	0.45	6.32						
87-100				-0.37	0.55	8.07						
111-122				-0.07	0.04	0.53						
113-124				-0.14	0.09	1.06						
59-70				-0.04	0.07	0.81						
69-80				-0.17	0.35	4.09						
79-94				-0.29	0.73	8.70						
93-106				-0.26	0.58	7.05						
115-126				-0.17	0.21	2.22						
55-56-66-65							-0.01	0.001	0.68			
65-66-76-75							-0.09	0.004	2.96			
75-76-90-89							-0.11	0.005	3.95			
89-90-102-101							-0.05	0.003	2.50			
77-78-92-91							-0.08	0.003	1.98			
91-92-104-103							-0.16	0.007	4.81			
74-88-90-76										+0.40	0	0
87-99-101-89										+1.26	0	0
88-100-102-90										+0.28	0	0
100-110-112-102										+1.72	0	0
75-89-91-77										+1.20	0	0
110-120-122-112										-0.14	.003	2.98
89-101-103-91										+1.57	0	0
102-112-114-104										+0.56	0	0
65-75-77-67										+1.20	0	0
112-122-124-114										-0.07	.001	0.76
55-65-67-57										+1.28	0	0
44-56-58-46										+0.13	0	0
57-67-69-59										+0.78	0	0
58-68-70-60										+0.57	0	0
67-77-79-69										+0.89	0	0
68-78-80-70										+0.55	0	0
77-91-93-79										+0.97	0	0
91-103-105-93										+1.36	0	0
104-114-116-106										+0.07	0	0
114-124-126-116										-0.37	.008	6.86
78-92-94-80										+0.38	0	0
92-104-106-94										+0.38	0	0
99-110				-0.34	0.70	10.68						
103-114				-0.06	0.13	1.80						
Σ Weight		184.53				55.19			16.88			10.60

Total added weight for fail-safe = 2 (184.53 + 55.19 + 16.88 + 10.60) = 534 lb/booster.

wing where the redistribution of limit load due to a single member failure results in loads higher than those experienced by ultimate load on an intact wing. Table 6-2 lists: 1) margins of safety due to fail-safe redistribution of limit load on a structure sized for ultimate load, 2) required increase of bar area (or plate thickness) for zero margins of safety on members under fail-safe limit load redistribution, and 3) weight increases associated with the added material.

Table 6-2 shows a total weight increase of 534 pounds for the requirements that the wing carry limit design load with any reasonable in-service structural failure. Of the 534 pounds, 69% is in spar caps, 21% in spar diagonals, 6% in spar webs, and 4% in skins. All skins requiring beef-up (three per side) were originally 0.016 gage for ultimate requirements. This gage is probably unrealistically thin when handling, sonic fatigue, and thermal stress requirements are considered. Maximum gage increase was 0.009 for a total gage of  $0.016 + 0.009 = 0.025$  inch; therefore, it is doubtful that any skin beef-up would be needed for fail-safe primary loading requirements.

**6.3.2 WING BOX FACTOR OF SAFETY PERTURBATIONS FOR FAIL-SAFE.** The method of fail-safe weight analysis for the wing box is described in the previous section. In order to extend that analysis to other factors of safety, the following procedure was used. First a new ultimate member load was calculated by use of the formula

$$P'_{ult} = \frac{FS_u (P_{ult})}{1.4}$$

where

$P'_{ult}$  = ultimate member load at  $FS_u$

$P_{ult}$  = baseline ultimate member load for  $FS_u = 1.4$

Then a new weight penalty was calculated using

$$WT = \frac{\Delta P}{F} \rho l$$

where

$$\Delta P = P_{fail-safe} - P'_{ult}, P_{fail-safe} > P'_{ult}$$

$$\rho = 0.16 \text{ lb/in}^3 \text{ for annealed Ti-6Al-4V}$$

$$l = \text{length of member}$$

$$F = \text{allowable stress}$$

Figure 6-8 gives the weight penalty for fail-safe design over design for static strength for various ultimate factors of safety in both pounds and percent. It should be noted that the penalties plotted are the penalties that fail-safe design imposes above the weight required for static strength design for a given ultimate factor of safety. Weight penalties are not therefore related directly to the baseline wing box weight. The total wing box weight penalty is also broken down into separate curves for the lower spar caps and other wing box structure in the same figure. Inspection of Figure 6-8 reveals that a wing box designed for static strength at an  $FS_u$  of 1.4 requires local beef-up of 932 pounds to give the box full fail-safe capability for 100% of limit load. To obtain a fail-safe capability of 100% of limit load simply by raising  $FS_u$  for the whole wing box structure, it would be necessary to increase  $FS_u$  to 2.95 and therefore impose a weight penalty of many thousands of pounds. Thus the only efficient way to obtain fail-safe capability for the wing is by judicious local beef-up. The baseline wing box designed for static strength with  $FS_u = 1.4$  has a fail-safe capability of 47% limit-load for the initial failures assumed in Section 6.3.1.

## 6.4 THRUST STRUCTURE

**6.4.1 THRUST STRUCTURE FAIL-SAFE ANALYSIS.** Fail-safe strength of the thrust structure was evaluated analytically with the aid of a finite element computer program. The idealized structural model used for the fail-safe analysis is the same as that described in Figure 3-17. Two major tension members of the model were analytically "failed," one at a time, and limit design loads were applied to the weakened structure. Five members required some beef-up because of the redistribution of loads. Total added weight was 76 pounds or 0.34% of the total weight of 22,450-pound computer model. This is equivalent of 85 pounds for the actual 25,067-pound weight of the structure.

Loading conditions considered were: one hour ground sidewinds, maximum  $\alpha q$  headwinds, and 3g maximum thrust.

Two major tension members were "failed," one at a time. The members were truss elements from one of the four thrust beams (Figure 3-17) and were selected, first, because they were tension members, and second, because they carried very large loads in the unfailed configuration. Engineering judgment indicated that these were the critical members to be considered in fail-safe analysis.

Results of the fail-safe analysis are listed in Table 6-3. Note that, although the analysis was run for a 360-degree model with a single failed member, the results listed refer to the 45-degree model shown in Figure 3-18. The results are, therefore, maxima for the entire structure. Table 6-3 shows that one element (eight on the complete structure) of the aft thrust bulkhead and four elements of the forward thrust bulkhead have negative margins of safety if fail-safe loading is assumed equal to design limit loading. Four elements are truss members; one is a web stiffener.

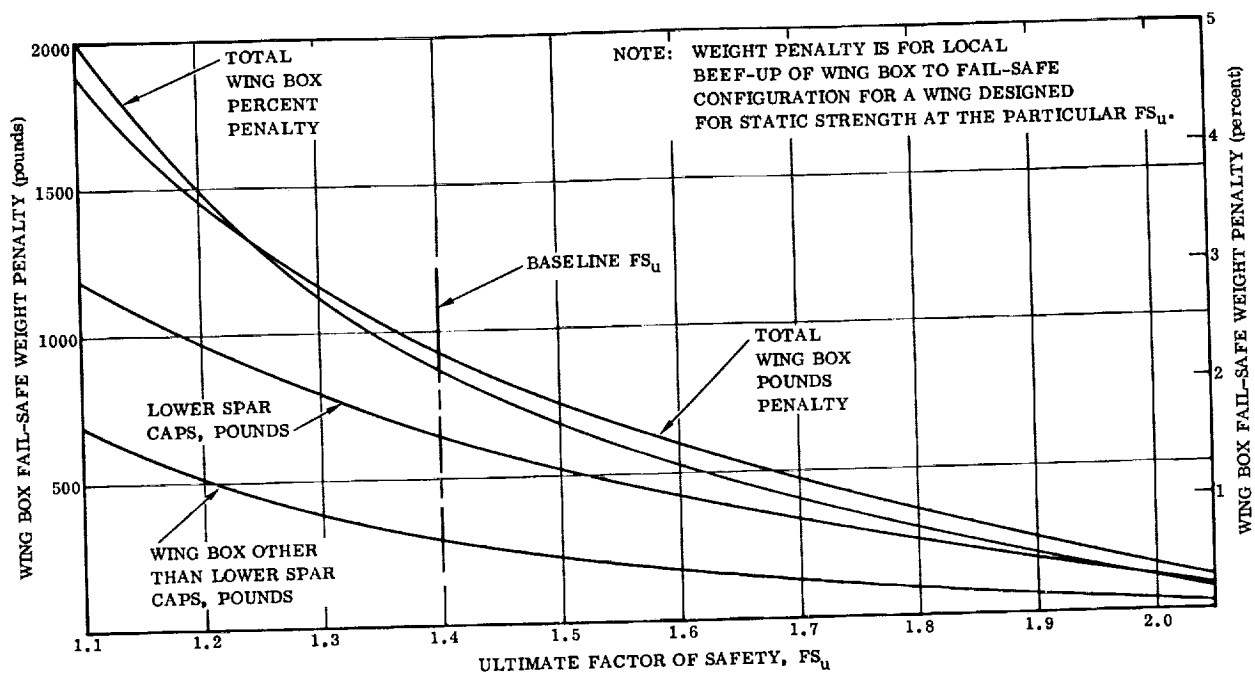


Figure 6-8. Wing Box Weight Penalty for Fail-Safe Versus Ultimate Factor of Safety

Margins of safety vary from a low of -4% on the aft bulkhead to a -37% on the forward bulkhead. It is doubtful that any rational fail-safe criterion could eliminate beef-up of the forward bulkhead with the existing geometric configuration. A slightly different geometry might be less critical for fail-safe loading.

**6.4.2 THRUST STRUCTURE FACTOR OF SAFETY PERTURBATIONS FOR FAIL-SAFE.** The method of fail-safe weight analysis for the thrust structure is described in Section 6.4.1. The procedure used to analyze the thrust structure for other factors of safety is the same as that used for the wing box and previously described in Section 6.3.2. Figure 6-9 gives the weight penalty for fail-safe design over design for static strength for various ultimate factors of safety in both pounds and percent. Once again it should be noted that penalties are at a particular safety factor and are not directly related to the baseline thrust structure weight. Inspection of Figure 6-9 reveals that a thrust structure designed for static strength at an  $FS_u$  of 1.4 requires local beef-up of 85 pounds to give the structure full fail-safe capability for 100% of limit load. To obtain a fail-safe capability of 100% of limit load simply by raising  $FS_u$  for the whole thrust structure, it would be necessary to increase  $FS_u$  to 2.22 and therefore impose a weight penalty of several thousand pounds. Thus, the only efficient way to obtain fail-safe capability for the wing is by judicious local beef-up. The baseline thrust structure designed for static strength with  $FS_u = 1.4$  has a fail-safe capability of 63% of limit load for the initial failures assumed in Section 6.4.1.

Table 6-3. Thrust Structure Fail-Safe Analysis

Name	Element	P (lb) or q (in/lb)	A (in <sup>2</sup> ) or t (in.)	Stress (psi)			Added for Fail Safe		Margins of Safety		Weight (lb.)		
				Critical	Applied	Allow	Area	Thick- ness	Before Beef-up	After Beef-up	Elem	Sub Total	Added
Thrust Beams	1	-762000	10.31	Compr.	-73900	99000	0	0	+.34		114.2	Aft Flg	0
	2	-895000	10.19	Compr.	-87900	99000			+.13		710.9		
	3	-213800	3.44	Compr.	-62100	79000			+.27		240.0		
	4	-175700	2.34	Compr.	-75000	88500			+.18		80.4	1750	
	5	680000	6.10	Tens.	111400	130000			+.17	Same	425.5	Fwd Flg	
	6	458500	3.71	Tens.	123700	130000			+.05	as	596.0		
	7	-104000	3.71	Compr.	-28000	130000			+3.65	Before	49.2	1071	
	8	-259700	4.48	Compr.	-57900	89500			+.54		564.6	Diag &	
	9	669000	6.32	Tens.	105700	130000			+.23		796.5	Web	
	10	-737000	10.23	Compr.	-71300	90600			+.27		1420.3		
	(11)	(14810)	(.300)	Shear	49400	58700			+.19		585.6	3367	
	12	-578000	14.14	Compr.	-40800	119000			+1.92		742.1	Posts	
	13	-1341000	144.0	Bending	+41900	159000			+2.80				
		-578000	14.14	Compr.	-40800	58700			+.44		1050.3	1792	
		-1341000	144.0	Bending	+41900	159000	0	0	+2.80				0
Thrust Beams Total Weight Added Weight for Fail Safe											7980		0



Table 6-3. Thrust Structure Fail-Safe Analysis (Cont'd)

Name	Element	P (lb) or q (in./lb)	A (in <sup>2</sup> ) or t (in.)	Stress (psi)			Added for Fail Safe		Margins of Safety		Weight (lb.)		
				Critical	Applied	Allow	Area	Thick- ness	Before Beef-up	After Beef-up	Elem	Sub Total	Added
Aft Thrust Blkh'd	14	-24040	.701	Compr.	-34350	40000	0	-	+ .16	+ .16	34.6	Braces	3.6
	15	-73100	.995	Compr.	-73500	73500	.038	-	- .04	0.0	98.0	↓	
	16	-47700	.957	Compr.	-49900	73500	0	-	+ .47	Same	94.4	227	
	17	-256100	2.54	Compr.	-101000	126000	0	-	+ .25	as	177.2	Inner Flg	
	18	-186100	2.83	Compr.	-65700	126000	0	-	+ .92	Before	135.6	↓	
	19	-213800	2.04	Compr.	-104900	126000	0	-	+ .20		117.0	430	
	20	(2880)	(.077)	Shear	37400	58700	-	0	+ .57		164.8	Webs	
	21	(9340)	(.211)	Shear	44200	58700	-	0	+ .33		259.8	↓	
	22	(2150)	(.060)	Shear	35900	58700	-	0	+ .64		79.3	504	
	23	-324000	2.62	Compr.	-123700	126000	0	-	+ .02		184.5	Outer Flg	
	24	-354000	3.28	Compr.	-108000	126000	0	-	+ .17		210.0	↓	
	25	-107700	2.62	Compr.	-41100	126000	0	-	+2.06		167.7	562	
	26	26800	.50	Ten.	53600	130000	0	-	+1.42		11.0	Stiffners	
	27	-144800	2.33	Compr.	62100	100000	0	-	+ .61		57.1	↓	
	28	20180	.50	Ten.	40360	100000	0	-	+1.48		8.0	76	
Aft Thrust Bulkhead Total Weight Added Weight for Fail Safe											1799		4

Table 6-3. Thrust Structure Fail-Safe Analysis (Cont'd)

Name	Element	P (lb) or q(in/lb)	A(in. <sup>2</sup> ) or t (in.)	Stress (psi)			Added for Fail Safe		Margins of Safety		Weight (lb.)		
				Critical	Applied	Allow	Area	Thick- ness	Before Beef-up	After Beef-up	Elem	Sub Total	Added
Fwd Thrust Blkh'd	29	109800	0.845	Ten.	130000	130000	.311	-	-.37	0.0	41.6	Braces	15.3
	30	101000	0.777	Ten.	130000	130000	.242	-	-.31	0.0	136.1	↓	42.4
	31	-102600	1.653	Compr.	-62000	62000	.189	-	-.11	0.0	93.9	272	10.8
	32	217500	1.90	Ten.	114400	130000	0	-	+.14	Same	132.5	Inner Flg	0
	33	301000	2.72	Ten.	110800	130000	0	-	+.17	↑	159.5	↓	0
	34	343200	3.14	Ten.	109300	130000	0	-	+.19	↑	172.5	465	0
	(35)	(3590)	(.063)	Shear	57000	58700	-	0	+.03	↑	62.3	Webs	0
	(36)	(3260)	(.061)	Shear	53400	58700	-	0	+.10	↑	64.8	↓	0
	(37)	(698)	(.060)	Shear	11620	58700	-	0	+4.05	↑	104.0	231	0
	38	314000	2.72	Ten.	115400	130000	0	-	+.13	↑	191.6	Outer Flg	0
	39	324000	2.64	Ten.	122700	130000	0	-	+.06	↑	169.0	↓	0
	40	141000	2.00	Ten.	70500	130000	0	-	+.84	↑	128.0	489	0
	41	-7090	.50	Compr.	-14180	100000	0	-	+6.05	↑	5.8	Stiff.	0
	42	10990	.50	Ten.	21980	100000	0	-	+3.55	Same	17.1	↓	0
	43	-87700	.88	Compr.	99600	100000	.150	-	-.17	+.01	18.1	41	3.1
Forward Thrust Bulkhead Total Weight											1498		
Added Weight for Fail Safe											72		

Table 6-3. Thrust Structure Fail-Safe Analysis (Cont'd)

Name	Element	P (lb) or q (in./lb)	A (in <sup>2</sup> ) or t (in.)	Stress (psi)			Added for Fail Safe		Margins of Safety		Weight (lb.)		
				Critical	Applied	Allow	Area	Thick- ness	Before Beef-up	After Beef-up	Elem	Sub Total	Added
Backup Frame	44	-38000	.489	Compr.	-77700	115000	0	0	+ .50	Same	30.1	Inner Flg	0
	45	16820	.468	Ten.	36000	130000			+2.61	as	26.2		
	46	39500	.450	Ten.	87900	130000			+ .48	Before	25.2	81	
	47	(398)	.040	Shear	9950	58700			+4.90		65.4	Webs	
	48	(882)	.040	Shear	22050	58700			+1.66		59.5		
	49	(665)	.040	Shear	16620	58700			+2.53		59.5	185	
	50	-19520	.342	Compr.	-57100	84500			+ .48		24.1	Outer Flg	
	51	-14190	.316	Compr.	-44900	80000			+ .78		20.2		
	52	25600	.291	Ten.	88000	130000			+ .48		18.6	63	
	53	6950	.500	Ten.	13900	100000			+6.20		48.0	48	0
Backup Frame Total Weight												377	0
Added Weight for Fail Safe													
Hold Down	54	-1289000	15.21	Compr.	-84600	126000	0	0	+ .49	+ .49	798.2		
	55	-749000	8.84	Compr.	-84800	126000	0	0	+ .49	+ .49	424.3	1223	0
Holddown Fittings Total Weight												1223	0
Added Weight for Fail Safe													

Table 6-3. Thrust Structure Fail-Safe Analysis (Cont'd)

Name	Element	N <sub>x</sub> (lb/in) or q(in/lb)	A(in <sup>2</sup> ) or t(in.)	Stress (psi)			Added for Fail Safe		Margins of Safety		Weight (lb.)		
				Critical	Applied	Allow	Area	Thick- ness	Before Beef-up	After Beef-up	Elem	Sub Total	Added
↑  Skin Panels  ↓	56	-13680 (5030)	.302 (.160)	Compr.	-45200	108870	0	0	+.74	Same as Before	1586.2	Aft Bay	0
	57	-4120 (2050)	.182 (.120)	Compr.	-22700	63270	0	0	+1.39	↓	956.1	3363 Ctr. Bay	
	58	-3840 (2462)	.142 (.080)	Compr.	-27050	55540	0	0	+.61		820.7		
	59	-9310 (2620)	.222 (.160)	Compr.	-42000	71370	0	0	+.60		1066.4		
	60	-8030 (2620)	.222 (.160)	Compr.	-36200	71370	0	0	+.83		1066.6		
	61	-7620 (1196)	.202 (.140)	Compr.	-37800	67300	0	0	+.75		1067.6		
	62	-7840 (912)	.202 (.140)	Compr.	-38800	67300	0	0	+.57		970.4		
	63	-8490 (226)	.202 (.140)	Compr.	-42000	67300	0	0	+.59		970.6		
	64	-7950 (788)	.202 (.140)	Compr.	-39400	67300	0	0	+.70		1067.7		
					Shear	5625	80000	0	0				
Skin Panels Total Weight											9573	0	
Thrust Structure Total Weight											22450	0	
Total Added Weight for Fail-Safe												76	

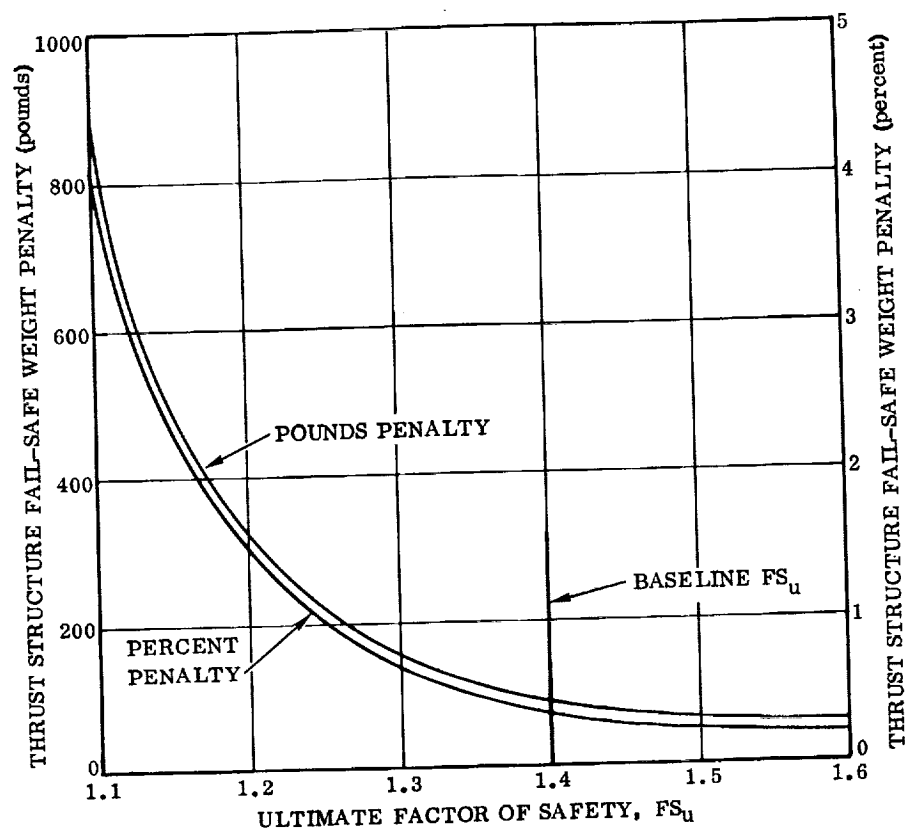
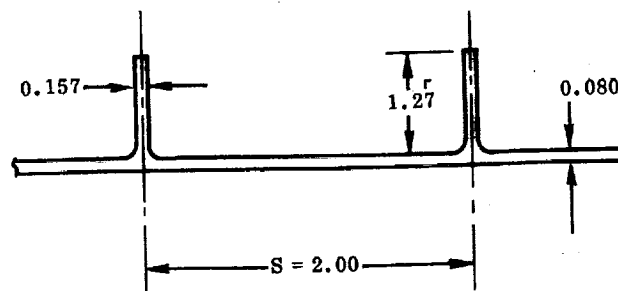


Figure 6-9. Thrust Structure Sensitivity of Weight to Ultimate Factor of Safety for Fail-Safe

## 6.5 VERTICAL TAIL BOX

6.5.1 VERTICAL TAIL FAIL-SAFE ANALYSIS. At Section (A) - (A) (Figure 3-24), the plate-stringer configuration is as shown below.



The material is annealed titanium alloy Ti-6Al-4V, having an ultimate tensile strength of 130 ksi. As in previous examples,  $K_c$  will be taken as  $2 K_{IC}$ , or 156 ksi  $\sqrt{\text{inch}}$ .

Using Poe's method (Reference 20)

$$\text{Percent stiffening} = \frac{100}{1 + \frac{A_{sk}}{A_{str}}} = \frac{100}{1 + \frac{2.00(0.080)}{1.27(0.157)}} = 55.5$$

$$\text{Stress intensity } K = C \sigma \sqrt{\pi a}$$

Values of  $K$  are calculated by the substitution in this expression of values of the stress intensity correction factor  $C$  from Reference 20, and the design limit stress level of 34 ksi from Table 4-7. The resulting values of  $K$  are plotted versus crack length in Figure 6-10, which shows that over the range of crack lengths considered (up to eight inches),  $K$  for the integrally stiffened panel does not approach the critical stress intensity level of 156 ksi  $\sqrt{\text{inch}}$ .

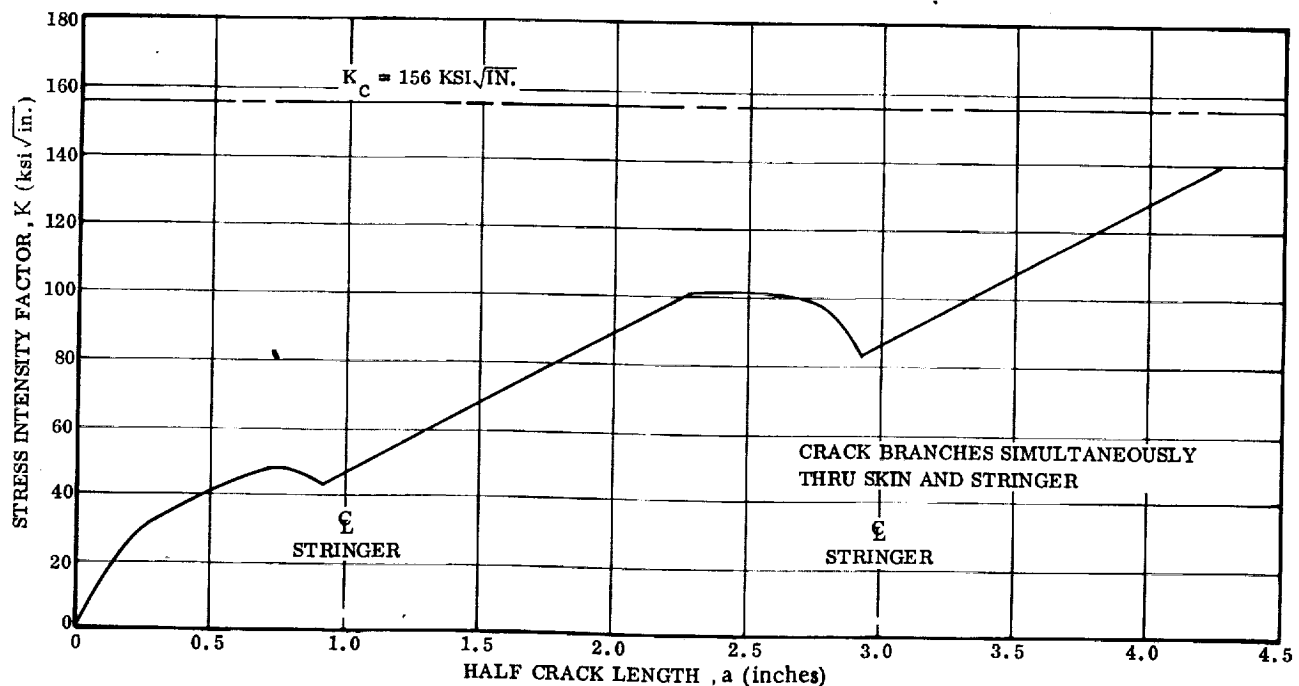


Figure 6-10. Vertical Box Stress Intensity Factor Versus Crack Length

One conclusion to be drawn is that the vertical tail box possesses a high degree of fail-safe capability, even though of monolithic construction. The principal reason is that the stiffened covers of the box are designed for compression, which results in low tensile stresses.

#### 6.5.2 VERTICAL FAIL FACTOR OF SAFETY PERTURBATIONS FOR FAIL-SAFE.

The method of analysis used is the same as that used previously for the liquid hydrogen tank under longitudinal loads in Section 6.2.4.

Figure 6-11 presents the applied stress intensity factor,  $K$ , versus the half crack length,  $a$ , for ultimate factors of safety ranging from 1.1 to 1.6. It will be noted that even for the low ultimate factor of safety of 1.1 rapid flaw growth does not commence until a total flaw length,  $2a$ , of 7.6 inches is reached. Even so, fracture arrest will occur somewhere before the third stringer from the crack center, and slow flow growth will continue until sometime after the fracture of the third stringer. Thus flow growth is slow for cracks exceeding 10 inches in length even for low factors of safety. Therefore, the vertical tail has a good degree of fail-safe capability since a crack of considerably smaller size than 10 inches can easily be detected by visual inspection techniques.

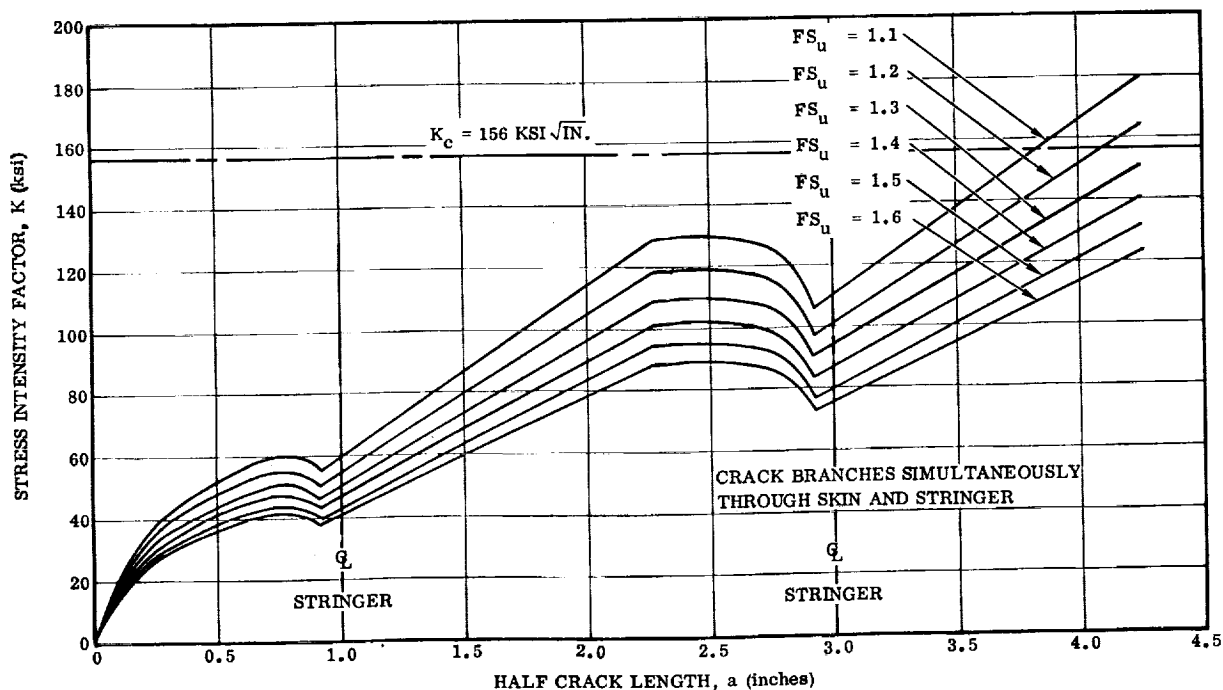


Figure 6-11. Vertical Tail Box Stress Intensity Factor Versus Crack Length for Various Ultimate Factors of Safety

## SECTION 7

### RELIABILITY ANALYSIS

The traditional static strength analysis compares an applied stress with an allowable strength by means of a factor of safety. If the factor of safety multiplied by the applied stress does not exceed the allowable strength, then the object under analysis is considered to be structurally adequate. In actuality, however, loads and strengths are probabilistic in nature. The structural reliability analysis, therefore, quantitatively analyzes the relationship of the statistical distribution of loads to the statistical distribution of strength to determine the survival probability of a loaded part. The static strength analysis deals with load and strength magnitudes only, whereas the reliability analysis deals with the two basic parameters of both load and strength, which are the arithmetic mean, (i. e. , a measure of magnitude) and the standard deviation (i. e. , a measure of variation). Reliability is dependent on the degree to which the mean strength is greater than the mean load and the respective variances. Quantitatively

$$R = P(S \geq L)$$

The general relationship between the factor of safety and structural reliability when the strength and load distribution curves are superimposed as in Figure 1-3 is discussed in Section 1.2.3. The detailed derivation of the method for relating structural reliability and factor of safety is presented in Section 7.1, and the sensitivities of structural reliability to factor of safety perturbations for the B-9U components selected for study are presented in Section 7.2.

The structural reliability requirements selected for the baseline vehicle are 0.999 for yield and 0.9999 for ultimate.

#### 7.1 METHOD OF ANALYSIS

In practice, applied loads and material strengths can be considered to be values randomly taken from the respective probability distributions of loads and strengths appropriate to the missions and materials. Structural reliability is defined as the probability that, during a specified mission, the structural strength exceeds the maximum applied load.

To determine structural reliability, distributions of loads and component strengths must be developed. It is customary to use normal distributions for this type of analysis. Experience has shown that structural loads have normal distributions to a good approximation. In generating tables of material strengths in terms of ultimate or yield stresses at some probability, normal distributions of material strengths are usually assumed. Tables of A and B values of strength for various materials, given



in Reference 9, are examples. If the normal is not a good approximation of the true distributions, the accuracy of values of structural reliability will be significantly affected. Insufficient evidence is available to assure the validity of the normal distribution of material strengths, particularly in the region of the lower tail. However, the results of structural reliability analysis based on the assumption of normal distributions are useful for evaluating relative adequacy of reliability and sensitivities.

A factor of safety is applied in structural design to ensure that structural strength will exceed applied loads. Regardless of how large this factor is made, there is always an overlap of distribution of loads and strengths; that is, there is some slight probability of failure. That probability depends on the difference between the means, or other predetermined distribution points, of the distributions of loads and strengths and their respective scatters, as usually measured by their variances.

Where  $L$  and  $S$  are variables in their respective normal distributions with  $\ell^2$  and  $s^2$  as the respective variances, the difference  $D = S - L$  is also a random variable with normal distribution. The mean of this distribution is  $\bar{D} = \bar{S} - \bar{L}$  and the variance is  $d^2 = s^2 + \ell^2$ . This distribution of the differences is a consequence of the reproductive property of the normal distribution. Letting  $L$  = applied load and  $S$  = component strength, when their difference  $D$  is negative, structural failure occurs. Therefore, structural reliability can be expressed:

$$R = P(D \geq 0) = P(S \geq L)$$

The density function for  $D$  is the normal density

$$f(D) = \frac{1}{d\sqrt{2\pi}} e^{-1/2 \left( \frac{D - \bar{D}}{d} \right)^2}$$

The reliability can be found as

$$R = P(D \geq 0) = \frac{1}{d\sqrt{2\pi}} \int_0^{\infty} e^{-1/2 \left( \frac{D - \bar{D}}{d} \right)^2} dD$$

This expression can be simplified by setting

$$Z = \frac{D - \bar{D}}{d} \text{ and } \frac{\bar{D}}{d} = z$$

Then

$$R = \frac{1}{\sqrt{2\pi}} \int_{-z}^{\infty} e^{(-1/2 Z)^2} dZ$$

R is evaluated by the usual means from a normal probability table, using the computed value of z, the number of standard deviations, as the argument. Conversely,

$$z = \frac{\bar{D}}{d} = \frac{\bar{S} - \bar{L}}{\sqrt{s^2 + \ell^2}}$$

can be found from the tables for particular values of reliability. In this manner the required strength parameter values can be determined.

Before the expression given for reliability can be used, it is necessary to have a means of determining  $\bar{L}$ ,  $\ell^2$ ,  $\bar{S}$ , and  $s$ .  $L$  and  $\ell^2$  will be determined from the range of critical loads developed for the structural component for a typical mission. This range is taken as  $\bar{L} \pm 3\ell$ , so that the  $\bar{L}$ ,  $\ell$ , and  $\ell^2$  are readily found. The maximum or design load,  $L + 3\ell$ , is the value to which the critical (ultimate or yield) safety factor, FS, is applied to determine the allowable strength. Allowable strength is related to applied load as follows:

$$\bar{S} - z_p s = FS (\bar{L} + 3\ell)$$

where  $z_p$  is the number of standard deviations, with  $s$  corresponding to the given probability that the component will withstand the established ultimate or yield stress. Some common  $z_p$  values are:

$$\begin{aligned} z_p &= 2.326 \text{ for probability of } 0.99 \\ &= 2.576 \text{ for probability of } 0.995 \end{aligned}$$

If  $s$  is known,  $\bar{S}$  can be readily found from the previously stated relationship between stress and strength. More commonly, the 0.99 and 0.995 probable material strengths are given in ksi. For example, many of the tables of stresses for various materials in Reference 9 are given for both probabilities at a confidence of 0.95. Mean material strength in ksi and the standard deviation can be found by solving the two simultaneous equations:

$$\bar{x} - K_1 \sigma = F_A, \quad \bar{x} - K_2 \sigma = F_B$$

where  $\bar{x}$  and  $\sigma$  are mean and standard deviation for material strength.  $F_A$  and  $F_B$  are values of ultimate or yield stress, as applicable, at two different probabilities from sources such as columns A and B of Reference 9. If point values are stated for  $F_A$  and  $F_B$ ,  $K$  is merely the  $z$ - values corresponding to the given probabilities. If  $F_A$  and  $F_B$  are tolerance limits for a given confidence level,

$$K = \frac{z_p + \sqrt{z_p^2 - ab}}{a},$$

where

$$a = 1 - \frac{z_\gamma^2}{2(n-1)}$$

$$b = z_p^2 - \frac{z_\gamma^2}{n}$$

$z_\gamma$  =  $z$ - value for given confidence level = 1.645 for 95% confidence, and  $n$  = test sample size. Using  $F_A$  and  $F_B$  tolerance limits, limiting values for  $\bar{x}$  and  $\sigma$  can be determined at one end by setting  $K = z_p$  and at the other by using the expression for  $K$  with  $n = 100$ , the usual minimum test sample size. Values of  $\bar{x}$  and  $\sigma$  in ksi can be converted to  $\bar{S}$  and  $s$  in kips by using the ratio:

$$FS (\bar{L} + 3\ell) / F_A \quad \text{or} \quad FS (\bar{L} + 3\ell) / F_B$$

depending on which probability is used for the allowable strength.

In summary, structural reliability was found by multiplying the design load by the safety factor, finding  $\bar{x}$  and  $\sigma$  for the material, converting those parameters to  $\bar{S}$  and  $s$ , and determining the probability that  $S - L$  was non-negative. Conversely, a given value of reliability was used to derive the corresponding factor of safety. Values of  $\bar{x}$  and  $\sigma$  for the material were computed to determine a ratio

$$r = \frac{\sigma}{\bar{x}} = \frac{s}{\bar{S}}$$

The value of  $z$  for the given  $R$  was defined to be:

$$z = \frac{\bar{S} - \bar{L}}{\sqrt{s^2 + \ell^2}}$$

From above,  $s = r \bar{S}$ .

Therefore,  $z^2 (r^2 \bar{S}^2 + \ell^2) = (\bar{S} - \bar{L})^2$ , which is solved for  $\bar{S}$ , using the quadratic formula:

$$\bar{S} = \frac{\bar{L} + z \sqrt{r^2 \bar{L}^2 - z^2 \ell^2 r^2 + \ell^2}}{1 - z^2 r^2}$$

The plus sign is used for the radical because of the constraint  $\bar{S} > \bar{L}$ . Now  $s$  is found, so that allowable strength can be determined and the factor of safety established.

## 7.2 RELIABILITY ANALYSIS AND SENSITIVITY TO FACTORS OF SAFETY

**7.2.1 RELIABILITY ANALYSIS OF WING SPAR CAPS.** This section presents the results of structural reliability analysis of the wing lower spar caps, critical in the tension failure mode. Reliability factors,  $R$ , are calculated by the method of Section 7.1 for the load variability that occurs during ascent and entry load conditions and the material strength variability exhibited by several structural materials, including René 41 and 7075-T6 aluminum in addition to the baseline Ti-6Al-4V material.

Load variability on the wing structure is presented schematically in Figure 7-1 and is based on engineering experience and judgement only. The distribution of entry condition loads was developed considering the combined effects of sensors, control system, aerodynamic load distribution, and avionics. The distribution on ascent load distribution considered the additional effects of winds, turbulence, and guidance system. As can be seen, the entry condition has low load variability while the ascent condition has high load variability.

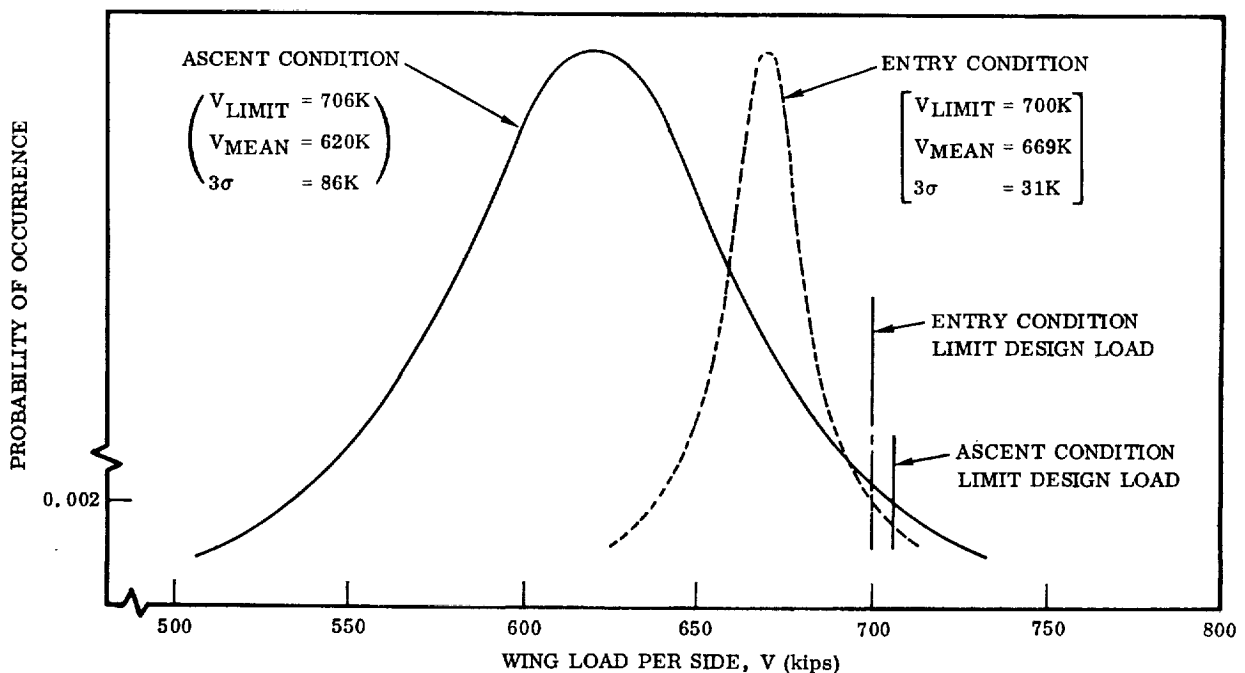


Figure 7-1. Estimate of B-9U Wing Load Distribution

Data on material strength variability were obtained from References 7, 8, and 9 and are presented in Figures 7-2 and 7-3. The  $z_p$  value used in the following structural reliability analysis is 2.326. This value is the ninety-ninth percentile corresponding to the tabulated A values of  $F_{tu}$  and  $F_{ty}$ , the design allowable ultimate and yield stresses, respectively. Since no allowance is made for the sample size used to obtain the A values, the value used for  $z_p$  provides an upper limit for s, resulting in conservative values for reliability as a function of factor of safety.

A preliminary stress analysis for the wing during ascent and entry provides a coefficient of variability of stress,  $C_{VL}$ , of 0.0462 for ascent and 0.0165 for entry.  $C_{VL}$  is the ratio of standard deviation to the mean of the distribution of possible stresses applied during the mission, computed for the time at which the stress is maximum. The design limit stress is established from the design allowable stress and safety factor and is the mean stress plus three standard deviations, assuming a normal distribution of stresses.

A comparison is shown in Figures 7-4 and 7-5 between the reliability of wing spar caps made from aluminum 7075-T6 and annealed Ti-6Al-4V over the indicated range of factor of safety. These values of reliability are based on the maximum stress conditions during ascent at or near room temperature. Ascent is the critical phase for these members. The data for the aluminum alloy is computed from Reference 7, using a hole-out factor of 1.05, while that for the titanium alloy is similarly computed from Reference 8.  $C_{VS}$  is the coefficient of variability of strength similar to  $C_{VL}$  for stress.

If a reliability of 0.999 is considered adequate for yield, a yield factor of safety of 0.97 would be adequate for both materials. The design limit stress is then

$$62.9/0.97 = 64.8 \text{ ksi for 7075-T6 aluminum}$$

and

$$120/0.97 = 123.7 \text{ ksi for Ti-6Al-4V annealed}$$

References 7 and 8 give values of  $F_{tu}$  and corresponding  $C_{VS}$  for 7075-T6 and Ti-6Al-4V, respectively, to which the hole-out factor was applied.  $F_{tu}$  for 7075-T6 is 73.3 ksi, with  $C_{VS}$  of 0.04, and for Ti-6Al-4V is 127.6, with  $C_{VS}$  of 0.0216. Thus, the ultimate factors of safety corresponding to a yield reliability of 0.999 are

$$73.3/64.8 = 1.13 \text{ for 7075-T6 aluminum}$$

and

$$127.6/123.7 = 1.03 \text{ for Ti-6Al-4V annealed}$$

These factors of safety result in ultimate structural reliability of 0.999999995 for the aluminum and 0.9999954 for the titanium.

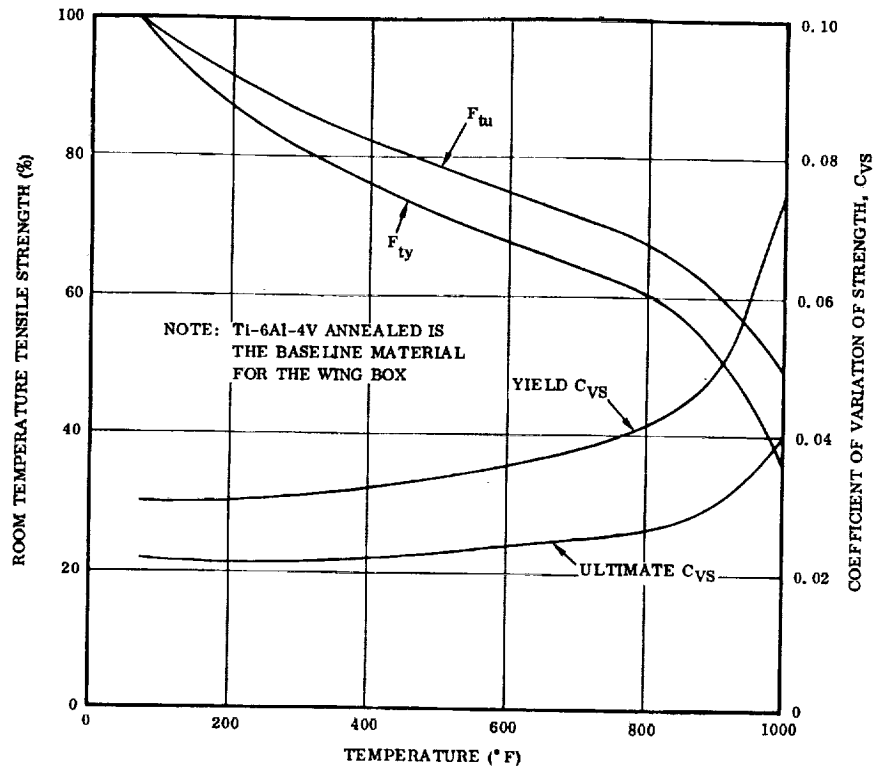


Figure 7-2. Percent of Room Temperature Tensile Strength and Coefficient of Variation Strength Versus Temperature for Ti-6Al-4V Annealed

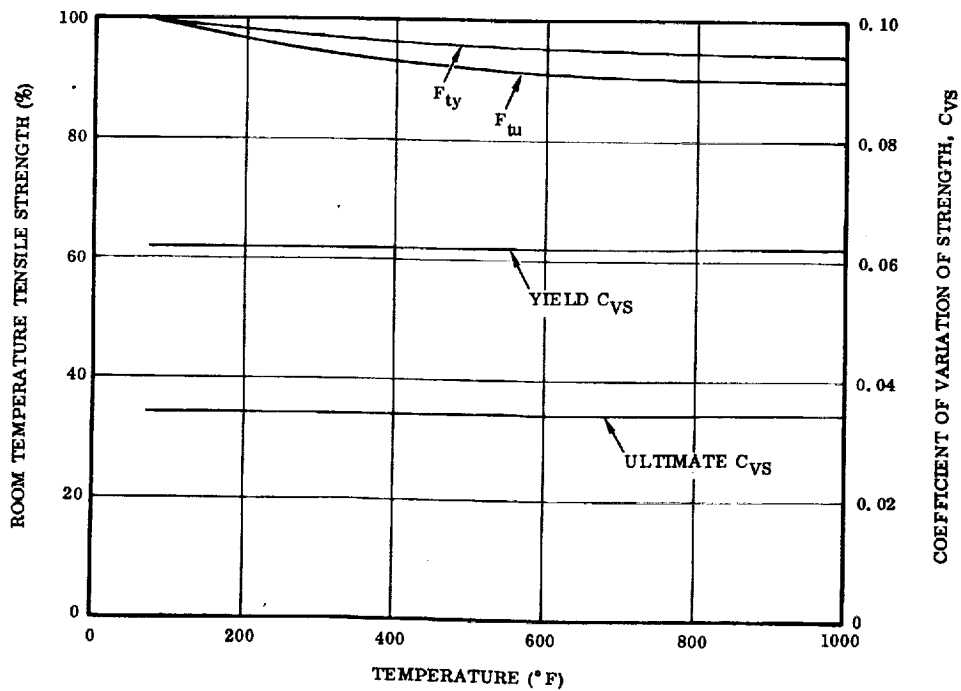


Figure 7-3. Percent of Room Temperature Tensile Strength and Coefficient of Variation Strength Versus Temperature for René 41

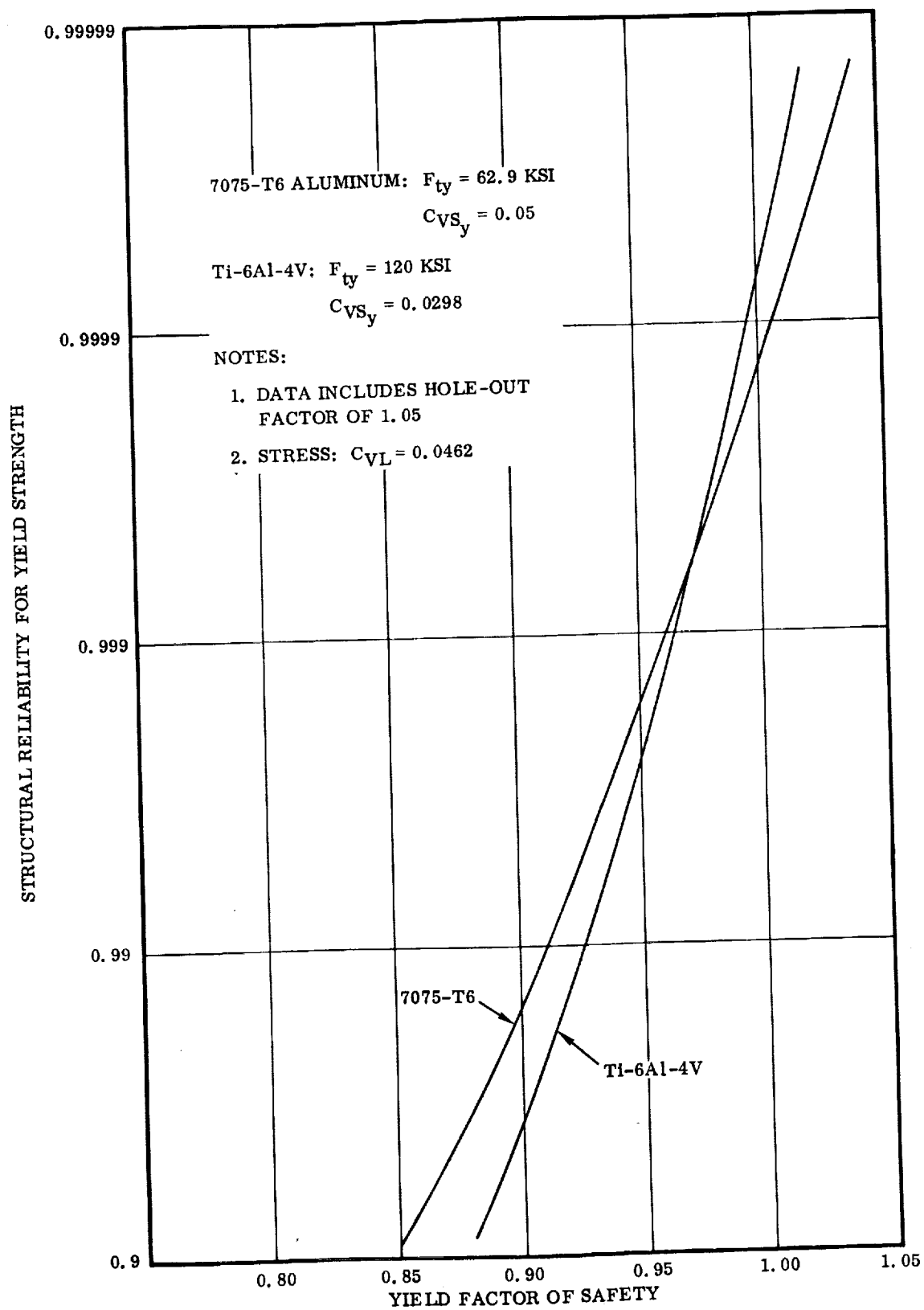


Figure 7-4. Wing Yield Reliability Versus Factor of Safety at Room Temperature

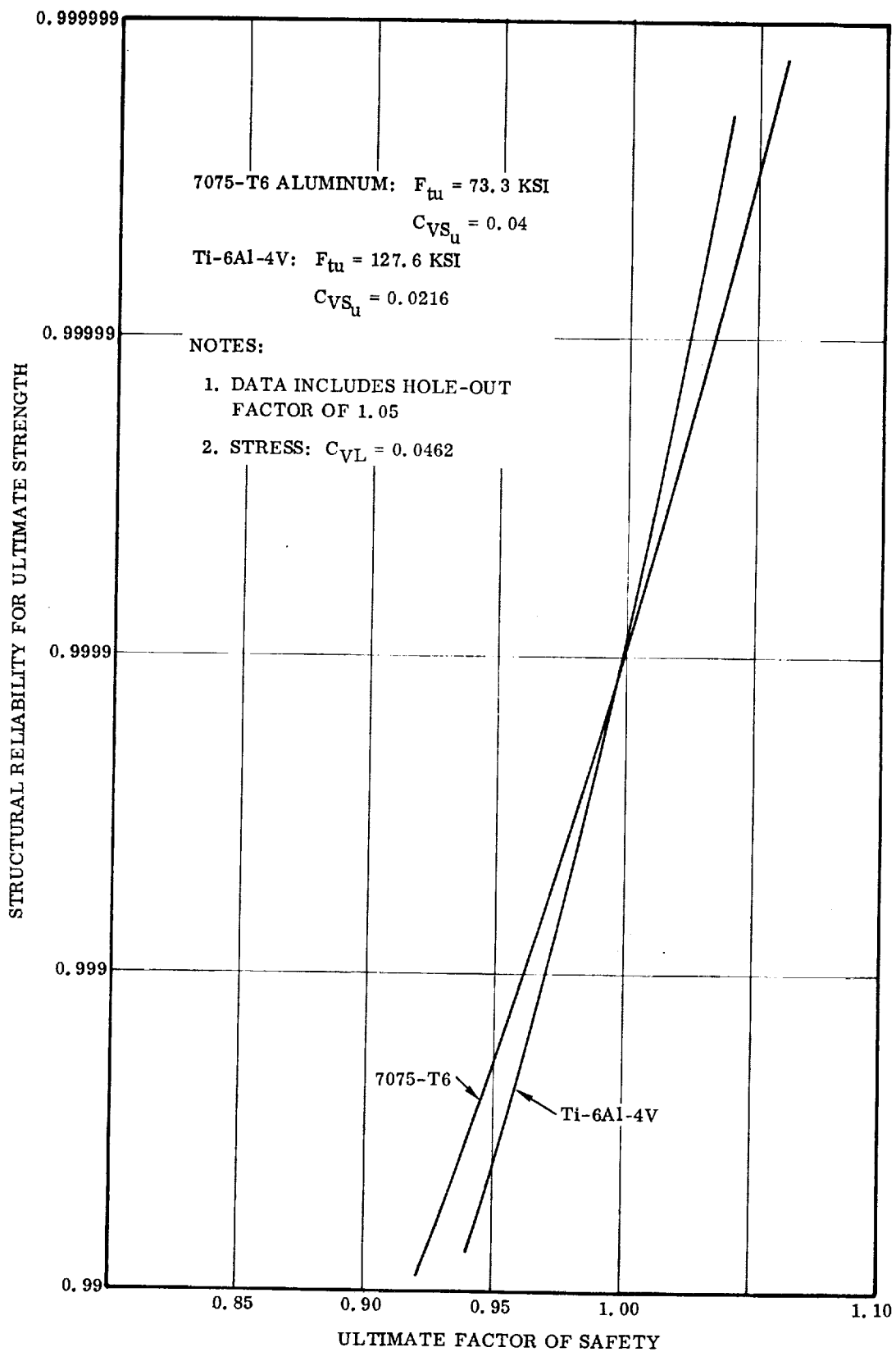


Figure 7-5. Wing Ultimate Strength Reliability Versus Factor of Safety at Room Temperature



For wing elements subjected to high temperatures, entry phase is critical because of aerodynamic heating and resultant loss of tensile strength. Reference 9 gives curves showing the reduction in  $F_{tu}$  and  $F_{ty}$  due to temperature, for various materials. In Reference 7 is a similar curve for 7075-T6 aluminum, along with a curve showing the increase in  $C_{VS}$  with temperature. It does not appear that this material would be a good candidate assuming heating during reentry to 650°F. Ti-6Al-4V and René 41 appear to be more suitable. Since curves of  $C_{VS}$  versus temperature are not readily available, they were constructed, assuming the same variation of  $C_{VS}$  with allowable tensile strength as for the aluminum. The curves show  $C_{VS}$  for Ti-6Al-4V, yield and ultimate in Figure 7-2 and  $C_{VS}$  for René 41, yield and ultimate, in Figure 7-3. The coefficient of variation for René 41 does not vary appreciably over the range shown, if the assumption of behavior similar to that of aluminum is valid. The values of  $C_{VS}$  were obtained from Reference 8. The  $F_{tu}$  and  $F_{ty}$  for René 41 were computed from the Reference 9 A values. Figures 7-6 and 7-7 are plots of reliability versus factor of safety for titanium and René 41. Again, the greater variability of René 41 is reflected in the shallower curve.

If the yield criterion is again a reliability in excess of 0.999, Figure 7-6 indicates a yield safety factor of 0.99 for Ti-6Al-4V and 1.02 for René 41. The ultimate factors of safety corresponding to a yield reliability of 0.999 are

$$147.3/94.9 = 1.55 \text{ for René 41}$$

and

$$93.8/80.6 = 1.16 \text{ for Ti-6Al-4V}$$

These factors of safety produce structural reliability of virtually 1.0 for both materials in ultimate tensile strength.

As a result of this study, it can be concluded for the wing that the selection of a yield factor of safety that fulfills the 0.999 structural reliability requirement establishes an ultimate factor of safety that produces a structural reliability that far exceeds the 0.9999 reliability requirement for ultimate strength.

**7.2.2 RELIABILITY ANALYSIS OF OTHER B-9U COMPONENTS.** Curves of structural reliability versus factor of safety (Figures 7-8 and 7-9) have been computed and drawn for the following components:

- a. Crew module.
- b. Liquid hydrogen tank.
- c. Liquid oxygen tank.
- d. Thrust structure.
- e. Aft orbiter support frame.
- f. Vertical tail.

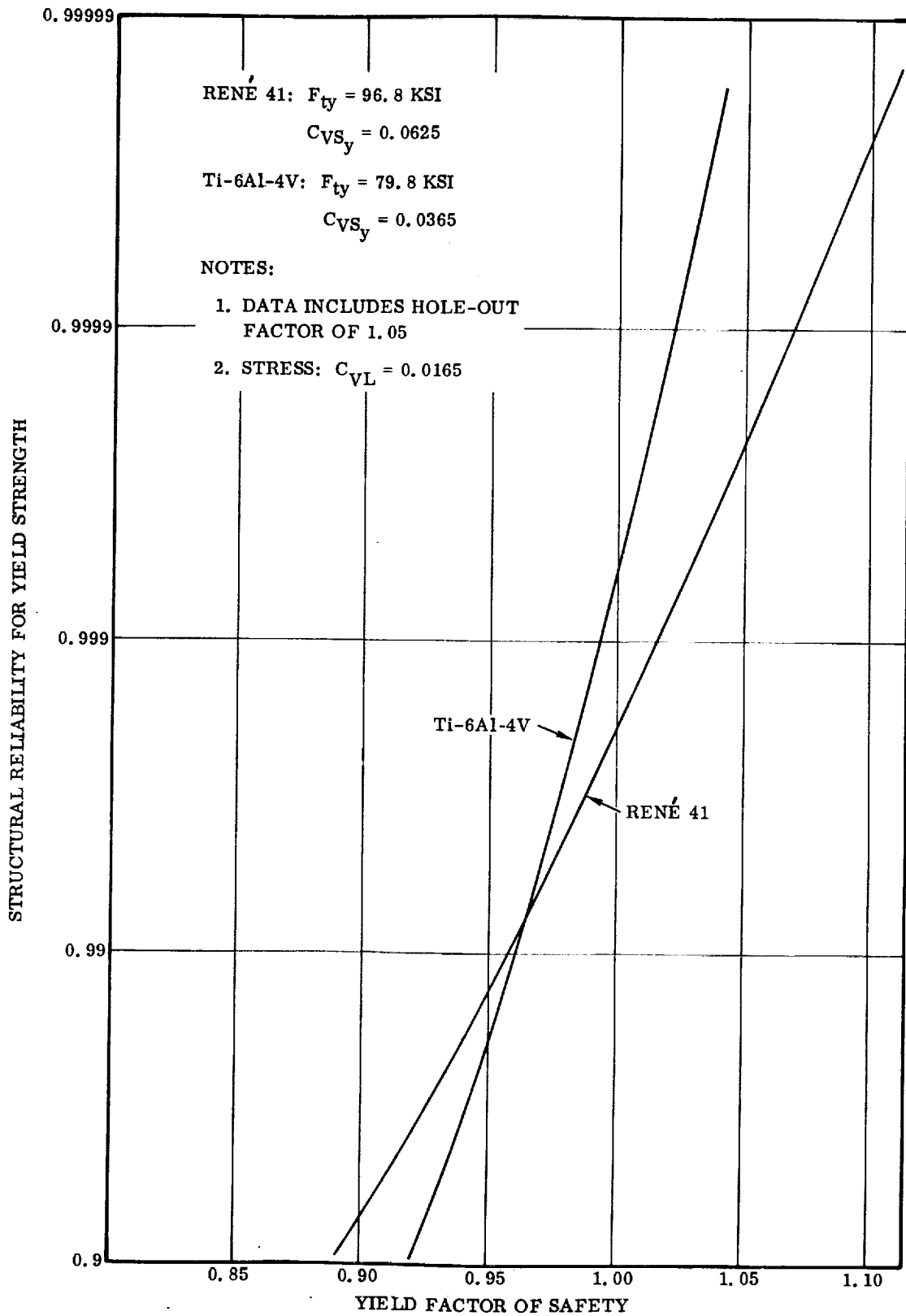


Figure 7-6. Wing Yield Reliability Versus Factor of Safety at 650° F

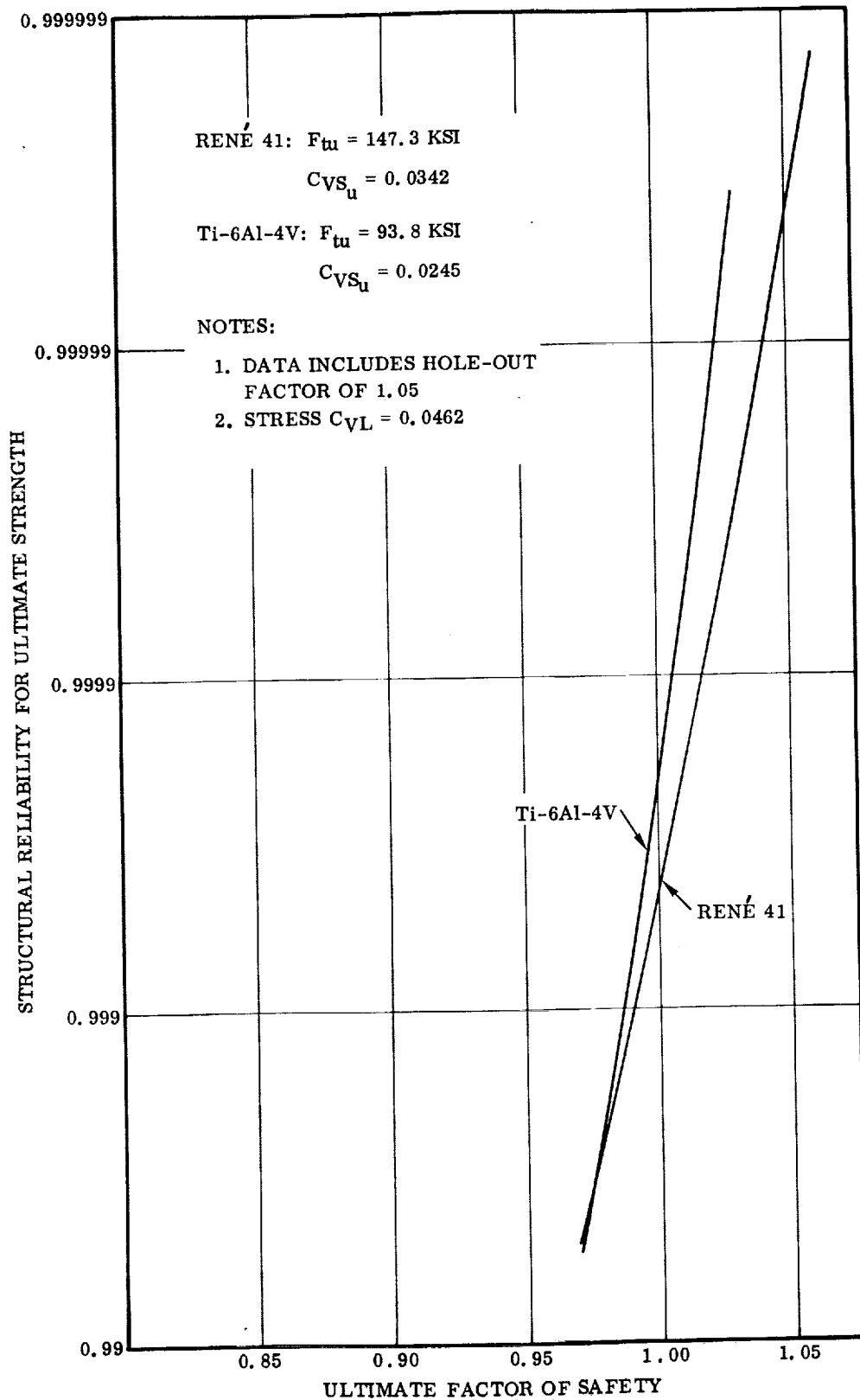


Figure 7-7. Wing Ultimate Strength Reliability Versus Factor of Safety at 650° F

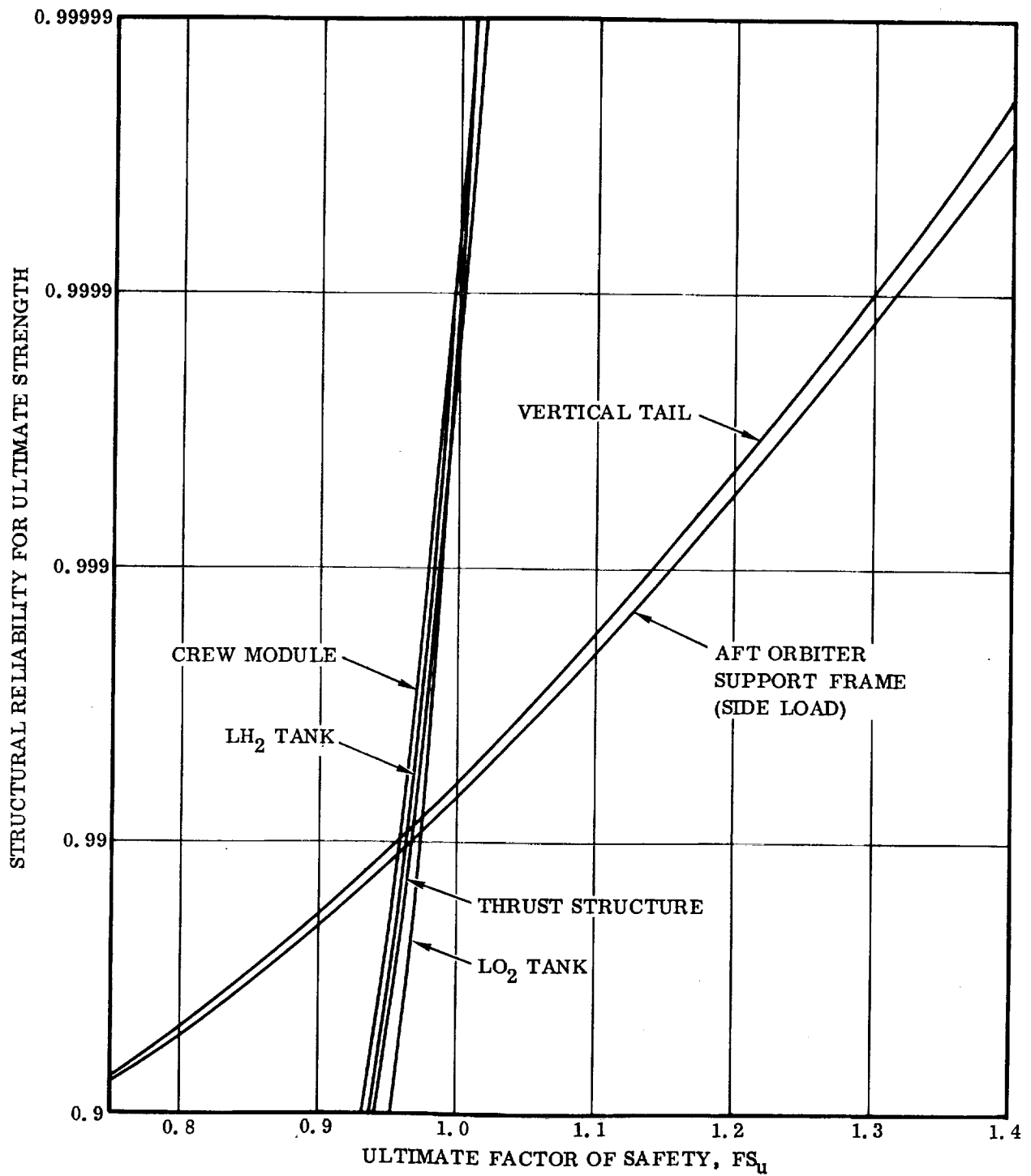


Figure 7-8. Structural Reliability at Ultimate Strength for Several B-9U Components Versus Factor of Safety

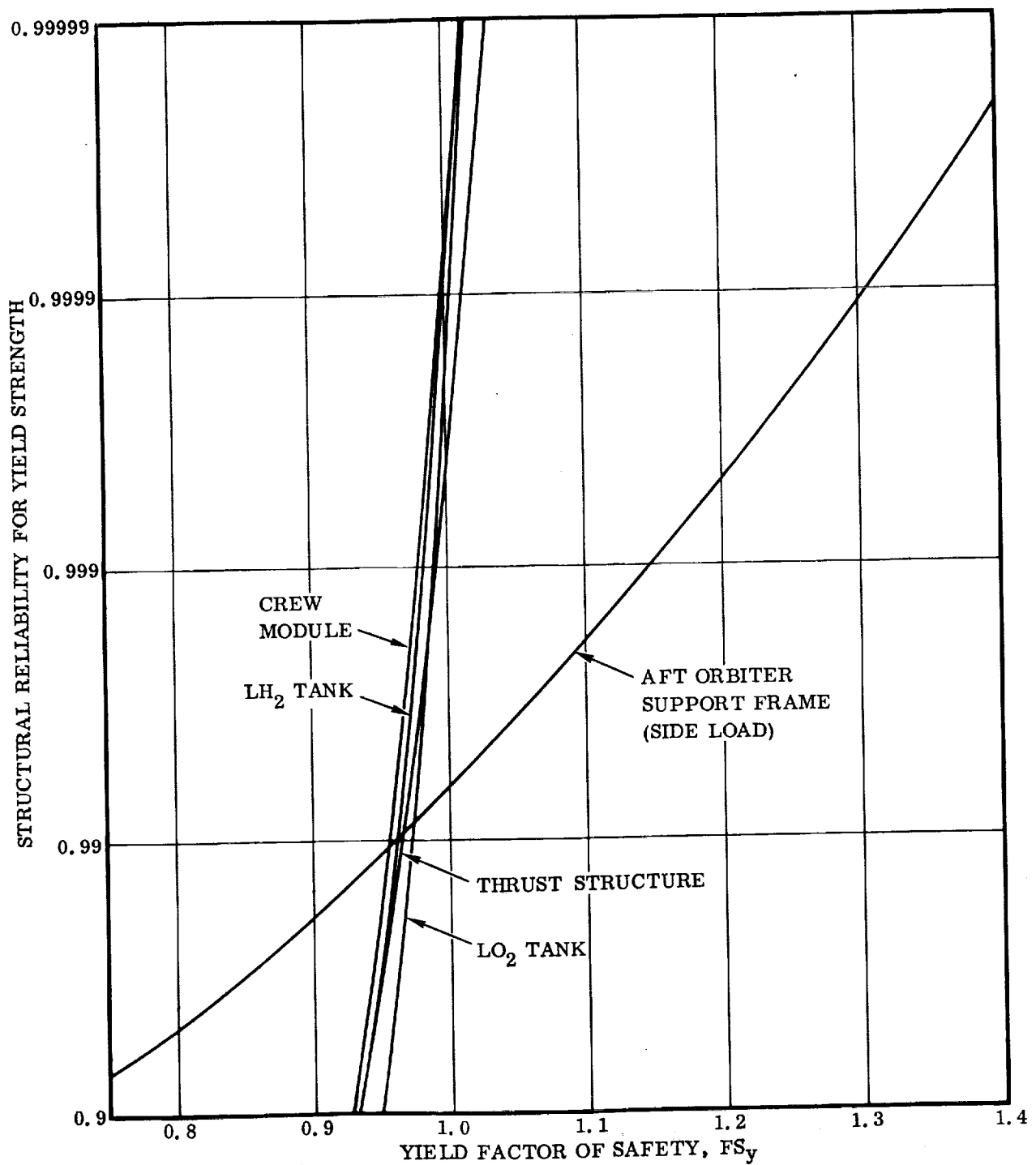


Figure 7-9. Structural Reliability at Yield Strength for Several B-9U Components Versus Factor of Safety

The computations utilized data giving load variability furnished by analysis of vehicle flight dynamics and strength and variability of strength data from Reference 9. This data is listed in Table 7-1.

Table 7-1. Component Materials, Strength Values, and Coefficients of Variation

Component	Material	Temperature* (° F)	Ultimate Strength			Yield Strength		
			F <sub>tu</sub> ** (ksi)	C <sub>VS</sub>	C <sub>VL</sub>	F <sub>ty</sub> ** (ksi)	C <sub>VS</sub>	C <sub>VL</sub>
LH <sub>2</sub> Tank	2219-T87	RT	61	0.0158	0.0200	49	0.0195	0.0200
LO <sub>2</sub> Tank	2219-T87	-297	73	0.0158	0.0125	57	0.0195	0.0125
Crew Module	2219-T87	RT	61	0.0158	0.0240	49	0.0195	0.0240
Aft Orbiter Support Frame	2219-T87	RT	61	0.0158		49	0.0195	
Thrust Structure	Ti-6Al-4V	RT	130	0.0216	0.0143	120	0.0298	0.0143
Vertical Tail	Ti-6Al-4V	RT	130	0.0216		120	0.0298	

\* RT indicates room temperature.

\*\* Mechanical properties listed as "A" basis.

For each of the listed components, a pair of curves is shown. One curve for each component is plotted for yield tensile strength, the other for ultimate. For yield strength, reliability signifies the probability of no gross yielding, while for ultimate it means the probability of no static failure. It is assumed that all critical flight stresses are tensile.

The curves for items a through d are based on calculations as described in Sections 7.1 and 7.2.1. In these cases the value of the critical stress during the mission varies about a non-zero mean value. Also, it is seen that, with assumed component reliability requirements of 0.999 and 0.9999 for yield and ultimate, respectively, the yield requirement is critical. However, items e and f represent cases in which the critical stress can be applied in either direction on a symmetrically designed structure. The distribution of stresses is assumed to be symmetrical about zero. In other words, mean wind and mean dynamic loading are assumed to be along the vehicle's longitudinal axis. At a given time in flight, when  $\beta q$  is maximum, in the cases of items e and f, the distribution of stresses is approximately normal, with mean of zero and a large value of standard deviation. The design stress, on which factor of safety is based, is established at the  $3\sigma$  (three times standard deviation) value.

However, the distribution described has a maximum likelihood value of stress equal to zero, which is really not the critical value. At various times during the flight, the applied tensile stress in one or both directions is bound to be non-zero. These stresses

are obviously more critical than zero. It is reasonable to assume that the most critical of these stresses will occur at a time near that at which  $\beta q$  is maximum. To determine structural reliability under these loading conditions, the distribution of these critical stresses in each direction must be established. With the assumption of load symmetry about zero load, the two distributions will have equal moments, and their means will be located equally distant from and on either side of zero.

These distributions could be determined from a fairly exact flight simulation of the Space Shuttle mission. This sort of analysis is beyond the scope of the present study. However, by assuming finite duration stress maxima that are critical stresses that occur in each direction during the maximum  $\beta q$  period, noise theory can be applied to establish the required distribution. Since stress fluctuates in a completely random manner, it has the property of noise. If the root-mean-square (rms) value of the noise amplitude were constant over a given frequency spectrum and constant as a function of time, the noise maxima would be normally distributed. The mean would be approximately 0.91 of the rms value and standard deviation about 0.82 rms (Reference 27, Figure 2, p. 80). All of these assumptions are inexact representations of reality. Therefore, the distribution described can only approximate the true situation, but this distribution is the best obtainable within the scope of the present study.

The rms value of noise is, by definition, the standard deviation of instantaneous amplitude. The  $3\sigma$  (equal to three times rms) point of the overall stress distribution was used as the reference for factor of safety. However, the  $3\sigma$  point of noise maxima, assumed to be critical stresses, is 1.122 times the value of the factor of safety reference. Also, the variance of critical stresses is much greater than for items a through d. Finally, in the case of symmetrical stress distributions due to side loading of a symmetrically designed structure, the structure has to withstand critical stresses in both directions. Two sets of supports or two tail skins, each having its own random value of tensile strength drawn from common distributions, must each withstand critical stress for mission success. Therefore, the reliability calculated for one support or skin must be squared to obtain component structural reliability, assuming independence of strengths of the two supports or skins.

The consequences of these considerations are a reduced rate of change of reliability with respect to factor of safety and required higher factor of safety to achieve an acceptable level of reliability. As a result, ultimate strength reliability becomes more critical than yield as a design parameter under the previously stated assumed component requirements of 0.999 for yield and 0.9999 for ultimate.

## SECTION 8

### SYSTEM SAFETY ANALYSIS

The fundamental goal of system safety engineering is the elimination or lessening of all hazards as a result of equipment operation. System safety engineering involves a systematic application of analytical techniques, scientific data and derived criteria, evaluation methods, experience retention devices, and management ability. Because it emphasizes prevention rather than correction of problems, particular emphasis is placed on early engineering design and procedural analysis. It is conceivable to take into consideration all aspects of the planning, design, development, fabrication, test, installation, maintenance, operation, and system evaluation of complex man-machine systems. System safety analysis methods that can be used to ensure the attainment of the appropriate design safety levels are the design review, the catastrophic failure analysis, and the design hazard analysis.

#### 8.1 RELIABILITY AND CREW SAFETY

In most cases the safety of the vehicles and crews is consistent with structural reliability. Certainly any catastrophic structural failure after launch causing premature termination of mission is likely to result also in loss of vehicle and crew. Therefore, any measure taken to increase reliability will also increase crew safety. Conversely, crew safety as influenced by the structure has little effect on probability of mission success. Except for the very early mission phases for the orbiter, noncatastrophic structural failures do not require abort to increase crew safety. Only leak failures in orbiter components such as in propellant tanks or crew or passenger cabin would require immediate mission termination that could be chargeable as a mission failure.

As previously stated, any catastrophic structural failure at any time during the mission after launch would probably cause loss of vehicle and crew. The degree of hazard of any lesser structural failure in the booster would depend on the failure mode, to be discussed later, and the remaining mission time. No abort procedure for the baseline booster has been found that would reduce the hazard of structural failure, except for landing at the closest possible site. Meantime, the measures available to the crew to control the effects of the failure are limited, so that the effects would tend to be cumulative with time. The same is true of the orbiter, even though it has abort capability. After the failure and initiation of abort, the orbiter flight is at least as complex as that of the booster, if not more so.

#### 8.2 SAFETY OF COMPONENTS

The following is a list of generalized failure modes of structural components, with their causes.



<u>Mode</u>	<u>Cause</u>
Deformation	Stress exceeds yield strength (inadequate factor of safety)
Tensile (compressive, shear) failure	Stress exceeds ultimate strength (inadequate factor of safety)
Fatigue	Insufficient fatigue life (design deficiencies or stress level too high)
Brittle fracture	Insufficient safe-life (inadequate proof test or poor choice of material and processes)
Leak	Flaw growth through wall

For components stressed primarily by internal pressure (propellant tanks and crew compartment) all the above modes apply. However, flaw growth leading to brittle fracture is a more significant factor in pressure component failure than fatigue. Also, in pressure components, most deformation tends to be local in nature, except in cases of severe tank overpressure or flight overloads. The local yielding tends to relieve local overstresses and is not failure from a safety point of view. The other modes do represent either catastrophic events or safety hazards. Failures due to both overstress conditions, either local or general, and brittle fractures occurring within elastic limits usually lead to total rupture of the pressure component. This kind of failure would prove catastrophic to the crew because of the destructive release of energy, if a sizeable volume of gas is involved, or loss of essential propellants or gases. A leak through a crew cabin wall could be fatal to the crew due to cabin decompression. A propellant leak is not likely to be immediately catastrophic, but would pose a potential hazard of fire or explosion.

Members that primarily bear flight loads, including aerodynamic surfaces, intertank adapters, thrust structure, and orbiter-booster attachments, are subject to all the listed structural failure modes except leaking. Partial or total deformation or failure of any structural member in these components results in a redistribution of loads, resulting in increased stress in the remaining members. If this stress redistribution results in exceeding ultimate or elastic limits or in rapidly accelerated crack growth, structural failure of the component will ensue. It is readily apparent that such structural failure would be catastrophic to the crew of one or both vehicles.

### 8.3 CREW SAFETY AND DESIGN CRITERIA

Design criteria affecting crew safety include factors of safety, proof factors, protective and warning devices, and ability of the crew to react to a possible impending failure.

The relationship of crew safety to factor of safety is similar to that between reliability and factor of safety. In general, a higher factor of safety means greater crew safety for a particular mission profile and a particular material. When considering different materials, different temperatures, or different stress distributions, the distributions of possible strengths at each of various temperatures and stresses for each of the different situations, along with factor of safety, affect probability of failure. Therefore, these distributions also affect crew safety in a manner similar to the effects on reliability (Section 7). A similar but somewhat more complex situation exists for the relationship of crew safety with proof factor. Involved are the distributions of material toughness, initial flaw size, loads inducing flaw growth, and the variability of the presence of influencing environments. The factor of safety or proofing factor, as applicable, required for a given degree of crew safety depends on the variability in the relevant material properties and mission conditions. For reasonable levels of safety the factor must be increased if variability is greater.

With structures there are a few protective devices that can guard against the occurrence of unusually excessive loads or undetected significant material flaws. One device is the provision of extra members to provide structural redundancy. In this way, if a member should fail or if the structure should be subjected to excessive load, the resulting load distribution remains within the strength of the structure. A device applied to pressure vessels is a relief valve, to assure that the vessel remains within the stress limits established. For greater safety these valves should be redundant, with isolation provided in the event that one of the relief valves should fail open. Another device that might be considered is a self-sealing liner inside a tank. This liner might be used to prevent accumulation of an explosive mixture or to hold pressure. This device has several disadvantages. A potential safety problem is the possibility that the liner could conceal a flaw that could grow to critical size with catastrophic results. If a leak of a fluid that is potentially flammable or explosive occurs in a confined area, the hazard is usually better controlled by a device that dispenses a material displacing the fluid through vents to prevent buildup of a explosive mixture.

Possible structural warning devices include strain gages, break wires, leak detectors, and cabin pressure gages. The strain gages or break wires can detect excessive strains or failures of individual members when placed at key locations. Leak detectors are usually incorporated where there is danger of a leak causing an explosive mixture of any sort to be formed. A cabin pressure gage and warning device will be used to monitor the air-tight integrity of the crew compartment.

If the crew is aware of the development of a structural hazard, there may be certain measures taken by the crew to eliminate or reduce the hazard. For example, a moderate leak in the cabin bulkhead can be filled with a sealing material. If a leak or fire detector indicates a leak from a tank, the crew can use manual backup controls as necessary to assure that the proper material dispensing (i.e., foam) and vent devices are activated. Excessive strains in members of components bearing flight loads can, in most cases, be controlled by maneuvering to reduce the loading on those members.

For the crew to perform reliably under these circumstances, training will be required for the crew members to know when and how to override automatic controls so as to relieve affected members without inducing dangerous control disturbances.

#### 8.4 DESIGN FOR CREW SAFETY

Consideration of crew safety requires that the design provides for reduction of probability of structural failure and to control the effects of failure where possible. Design measures for providing increased crew safety include redundancy, leak-before-rupture, allowance for thermal and other environmental effects, provisions for inspection, protective and warning devices, and emergency override controls, in addition to the selection of safety and proof factors appropriate to the materials and stress distributions. These measures should receive full consideration in design trade studies.

If a tank wall can be made sufficiently thin, considering the tank proof factor, the critical flaw size can exceed the tank thickness. In this way, the tank will leak before it ruptures. Leaking is the preferable failure mode, since tank rupture is certain to be catastrophic for the crew. The drawback to leak-before-rupture is that the proof test does not automatically guarantee freedom from leak failures during tank life. It merely assures that no flaw has an initial size that would result in growth to critical size. A proper selection of tank thickness, proof pressure, and nondestructive inspection might overcome this difficulty. The selection would provide assurance that critical flaw size at proof pressure is not greater than the initial flaw size necessary for wall penetration during vehicle life under operational use. If this is not feasible and it is necessary to avoid leaks, then wall thickness greater than critical flaw size and greater proof factors are required for an adequate safe-life.

Material strength and toughness characteristics are sensitive to elevated temperature. Therefore, each structural part must be designed for the maximum temperature to which it will be exposed. In other words, the factor of safety must be based on material strength or fracture toughness at maximum operating temperature. Also, fracture toughness is greatly influenced by aggressive environments such as salt air and moisture. Pressure components potentially exposed to such environments must have flaw growth rates calculated for those conditions.

Access to normally hidden structural members should be provided, especially for areas subject to stress corrosion, fatigue, flaw growth, or deformation. Turnaround maintenance procedures should provide for inspection of such members, including nondestructive evaluation (NDE) in critical areas.

#### 8.5 CREW SAFETY AND WEIGHT

Effects on vehicle weight of design measures to increase crew safety are listed on the opposite page:

<u>Measure</u>	<u>Weight Effect</u>
Redundancy	Increase
Leak-before-rupture or Increased proof factor	Increase
Increased proof factor	Increase
Allowance for worst case environment	Increase
Inspection provisions	Negligible
Protective devices	Negligible to moderate increase
Warning devices	Negligible
Emergency manual overrides	Negligible



## SECTION 9

### OPTIMUM FACTORS OF SAFETY IDENTIFICATION

In the past, factors of safety for aerospace structures have been chosen arbitrarily, and have been quite difficult to justify on a rational basis. Usually, justification for their use was made on the basis that they led to successful structures. This method, however, is risky because of increasingly complex environmental and loading conditions and more advanced and complex materials. Factors now in use are based upon successful use in aircraft and non-reusable spacecraft programs. The reusable space shuttle system, however, represents a major advancement in structural technology. The system embodies the characteristics of aircraft, spacecraft, and launch vehicles with their associated severe environments and loads, long mission life, high reliability requirement, and considerations for low cost and weight. Therefore, the arbitrary selection of factors of safety, as has been practiced in the past, cannot be used with as high a degree of confidence for the Space Shuttle, because of the unknown effects of its environments and loads. It therefore becomes highly desirable to have a rational method for determination of structural factors of safety for the Space Shuttle structure, and, as an extension of this concept, this method or procedure should also be adaptable to other types of aerospace vehicles.

#### 9.1 METHOD OF FACTOR OF SAFETY SELECTION AND ASSOCIATED WEIGHT CHANGE

The primary objective of the information in the preceding sections of this report is to provide the background material necessary to make rational selections of ultimate and yield factors of safety for the seven primary B-9U booster structural components selected for study. The following items (a through e) present the method for selecting the safety factors:

- a. Determine the type of failure modes, design considerations, and design philosophy (requirements or criteria) that are deemed to be critical to the vehicle design.
- b. Determine the sensitivity curves of these criteria or requirements to factors of safety.
- c. Select numerical values for the design criteria or requirements and establish the design philosophy that is to be applied to the particular vehicle or vehicle component.
- d. Determine the required factor of safety for each design criterion or requirement from the sensitivity curves determined in step b.
- e. The optimum factor of safety is then the maximum of the factors of safety determined for each of the design parameters in Item d.

The procedure can be applied to an aerospace structure in any degree of detail desired. It may be applied once for the whole vehicle and thus a single  $FS_u$  and a single  $FS_y$  would be obtained, or, the procedure may be applied to every structural element of a vehicle and an individual pair of  $FS_u$ 's and  $FS_y$ 's may be obtained for a very large number of structural members. The optimum depth of analysis lies somewhere in between, and it is a matter of judgement as to the extent to which the procedure should be applied. Strong influences in such a decision would be the availability of money, time, manpower, and the necessary data to perform the required analyses.

Once the optimum factors have been determined, the weight change can be determined from curves that have been developed to show the sensitivity of structural weight to the factor of safety.

## 9.2 SAMPLE FACTOR OF SAFETY SELECTION AND WEIGHT CHANGE DETERMINATION

This section presents an example of the application of the method used in determining the factor of safety described in Section 9.1. All of the sample analyses in this section refer to Table 9-2, Fail-Safe Design Requirements.

9.2.1 ESTABLISHMENT OF CRITICAL TYPES OF DESIGN REQUIREMENTS. The following design criteria or requirements were deemed critical for the B-9U components selected for this study:

- a. Design philosophy
- b. Service life (missions)
- c. Safe inspection interval (missions)
- d. Safe-life (scatter factor)
- e. Fatigue (scatter factor)
- f. Reliability

The safe-life scatter factor is one that is applied to the desired vehicle service life to obtain the number of missions (in this case,  $1.5 \times 100 = 150$  missions) for which it must be shown by fracture mechanics that a structure with an assumed initial flaw will not fail. The fatigue scatter factor is one that is applied to the desired service life of the vehicle (in this case,  $4.0 \times 100 = 400$  missions) for which it must be shown by fatigue analysis that fatigue cracks will not initiate in an unflawed structure.

The previously mentioned criteria or requirements are the principal factors considered when selecting factors of safety for design purposes. It stands to reason that when calculations show excess life capability and excess reliability, the factors of safety criteria can be reduced to a more optimum value. Conversely, when large

service lives are required or loads and strength show large variability, larger factors of safety criteria may be required.

The sensitivity of these design requirements to the factor of safety, as required by Item b of Section 9.1, were determined in the preceding sections of this report.

**9.2.2 SELECTION OF CRITICAL DESIGN REQUIREMENT VALUES AND PHILOSOPHY.** The baseline values of parameters that were used for the example in Table 9-2 are: 1) service life, 100 missions; 2) safe inspection intervals, 100 missions; and 3) safe-life scatter factor of 1.5 (not applicable for fail-safe components). The design philosophies selected for the components are also baseline (i.e., crew module is fail-safe, and the LO<sub>2</sub> tank, LH<sub>2</sub> tank, and aft orbiter support frame are safe-life designed) with the exception of the thrust structure and wing box, which were selected to be fail-safe for this example. In addition, reliability factors of 0.9999 for ultimate strength and 0.999 for yield strength were selected for all components in the study.

**9.2.3 DETERMINATION OF FACTORS OF SAFETY NECESSARY TO FULFILL DESIGN REQUIREMENTS.** In accordance with Item d of Section 9.1, factors of safety necessary to fulfill the design requirements determined in Sections 9.2.1 and 9.2.2 are selected. In Table 9-2, the example case, this involves the filling in of the four columns labeled "Factors of Safety to Meet Requirements." The factors of safety which must be determined are those necessary to fulfill fatigue, safe-life, reliability, and fail-safe requirements.

**9.2.3.1 Crew Module.** First the required factor of safety to meet the fatigue requirement is determined. Fatigue life versus FS is presented in Figure 4-16. The fatigue life of the crew module is so high due to its fail-safe design that the curve does not present the FS<sub>u</sub> and FS<sub>y</sub> for a 100-mission life. Therefore, for fatigue FS<sub>u</sub> < 1.2 and FS<sub>y</sub> < 1.0, which are the minimum values shown in the graph, are entered in Table 9-2.

Factors of safety are not selected for the safe-life requirement since this requirement is not applicable due to the fact that the fail-safe design philosophy was selected for the crew module.

For reliability, the factors of safety are selected from Figures 7-8 and 7-9 for ultimate strength and yield strength, respectively. From Figure 7-8, for an ultimate strength reliability of 0.9999, FS<sub>u</sub> = 0.99 is required; from Figure 7-9, for a yield strength reliability of 0.999, FS<sub>y</sub> = 0.98 is required.

For fail-safe, reference is made to the baseline analysis of Section 3.7.2 where it was determined that the apparent factors of safety for fail-safe are FS<sub>u</sub> = 4.2 and FS<sub>y</sub> = 3.4. These values are entered in Table 9-2.

**9.2.3.2 Liquid Oxygen Tank.** The procedure for the liquid oxygen tank is much the same as for the crew module, except that the safe-life design philosophy is used in this case instead of the fail-safe philosophy, which was used for the crew module.



The factors of safety for fatigue are presented in Figure 4-4.  $FS_u = 1.1$  and  $FS_y = 1.0$  are the minimum FS plotted and both give a fatigue life larger than the 100-mission service life. Therefore,  $FS_u < 1.1$  and  $FS_y < 1.0$  are entered in Table 9-2.

The factors of safety for safe-life are obtained from Figure 5-14. For the baseline of 100 missions with a scatter factor of 1.5, the required factors of safety are  $FS_u = 1.58$  or  $FS_y = 1.23$ . It should be noted that use of both of these factors of safety is not required, but that the use of either one of them will give the limit operating stress necessary to produce the desired safe-life.

Figure 7-8 and 7-9 are used for selection of the factors of safety required to insure reliability. From Figure 7-9 an  $FS_u$  of 1.00 is required for 0.9999 ultimate strength reliability, and from Figure 7-9 an  $FS_y$  of 0.99 is required for a yield strength reliability of 0.999.

Since the safe-life design philosophy was used for this component, it is not necessary to select factors of safety for fail-safe.

**9.2.3.3 Liquid Hydrogen Tank.** The procedure for selection of the factors of safety to meet the requirement is the same for the  $LH_2$  tank as for the  $LO_2$  tank. For fatigue, the FS are selected from Figure 4-6. For the 100-mission service life, the figure gives  $FS_u < 1.1$  and  $FS_y < 1.0$ . For safe-life, the FS are obtained from Figure 5-20. This figure yields, for the 100-mission life and a scatter factor of 1.5,  $FS_u = 1.40$  or  $FS_y = 1.14$ . As for the  $LO_2$  tank, either of these factors may be used, but the use of both is not necessary to meet the safe-life requirement. The factors of safety for reliability are determined from Figures 7-8 and 7-9. These figures give  $FS_u = 1.00$  and  $FS_y = 0.98$  for ultimate reliability of 0.9999 and yield reliability of 0.999, respectively. Since the  $LH_2$  tank is safe-life designed, it is not necessary to determine factors of safety for fail-safe.

**9.2.3.4 Aft Orbiter Support Frame.** The sensitivity of fatigue life to factor of safety is presented in Figure 4-8. The figure reveals that the fatigue life of the frame far exceeds the 100-mission requirement for all factors of safety investigated. Therefore,  $FS_u < 1.1$  and  $FS_y < 1.0$  are entered in Table 9-2. The factors of safety required for safe-life are given in Figure 5-23. For the required 100-mission service life and 1.5 scatter factor,  $FS_u = 1.1$  and  $FS_y < 1.0$  since the curve for  $FS_y$  goes below 1.0 at slightly over 3000 flights. For reliability, the factors of safety are once again obtained from Figures 7-8 and 7-9. These figures give  $FS_u = 1.32$  and  $FS_y = 1.15$  for ultimate reliability of 0.9999 and yield reliability of 0.999, respectively. No factors of safety are determined for fail-safe since the frame is designed for safe-life.

**9.2.3.5 Thrust Structure.** The sensitivity of fatigue life to factor of safety is presented in Figure 4-10. The fatigue life in that figure is greater than the 100-mission requirement for all factors of safety investigated. Therefore, the entries in the table

are  $FS_u < 1.1$  and  $FS_y < 1.0$ . Entries are not made in the safe-life column of the table since the fail-safe design philosophy has been selected for this component. For reliability, the factors of safety are obtained from Figures 7-8 and 7-9. They show that  $FS_u = 1.00$  and  $FS_y = 0.99$  are required for 0.9999 ultimate strength reliability and 0.999 yield strength reliability, respectively. For a fail-safe capability of 100% of limit load,  $FS_u = 2.22$  is required, as is stated in Section 6.4.2.

**9.2.3.6 Wing Box.** The sensitivity of wing box fatigue life to factors of safety is presented in Figure 4-12. From this figure, the 100-mission service indicates that  $FS_u = 1.26$  or  $FS_y = 1.19$  are required. It is not necessary to use both of these safety factors simultaneously – they both give the same limit operating stress, the use of one of the factors is sufficient. Factors of safety are not determined for safe-life for the wing box since fail-safe design is employed. Figures 7-4 and 7-5 are used for selection of factors of safety required for wing spar cap reliability. From Figure 7-4,  $FS_y = 0.97$  for 0.999 yield strength reliability and  $FS_u = 1.00$  is required for 0.9999 ultimate strength reliability. For a fail-safe capability of 100% of limit load,  $FS_u = 2.95$  is required, as is stated in Section 6.3.2.

**9.2.3.7 Vertical Tail Box.** Yield design is not a consideration for the vertical tail box due to low operating stresses from compression strength design and therefore only ultimate factors of safety are given for the vertical tail. The sensitivity of the vertical tail fatigue life to  $FS_u$  is given in Figure 4-14. Since the fatigue life of the vertical tail box far exceeds the 100-mission requirement for all  $FS_u$  investigated,  $FS_u < 1.1$  is entered in Table 9-2.  $FS_u$  for safe-life is found in Figure 5-37 and is required to be 1.02 for the 100-mission life with a 1.5 scatter factor. For reliability,  $FS_u$  is obtained from Figure 7-8 and is required to 1.30 for 0.9999 reliability. Section 6.5.2 indicates that the vertical fail box has fail-safe capability for  $FS_u < 1.1$ .

**9.2.4 COMPONENT FACTOR OF SAFETY SELECTION.** Optimum factors of safety for the individual components are selected for the sample analysis of Table 9-2 on the basis of Section 9.2.3 and the analysis of Sections 3 through 8. These selections correspond to the column labeled "FS Apparent or Recommended" in Table 9-2.

**9.2.4.1 Crew Module.** The factors of safety selected are  $FS_u = 4.2$  or  $FS_y = 3.4$ , which are the apparent factors of safety that fulfill the fail-safe requirement. The use of either of these FS is sufficient to meet the fail-safe requirement, since either one of the FS will, of necessity, restrict the limit operating stress to a level that provides the required fail-safe capability.

**9.2.4.2 Liquid Oxygen Tank.** For the liquid oxygen tank skin and ellipsoidal end domes, which are critical for tension,  $FS_u = 1.58$  or  $FS_y = 1.23$  are the apparent factors of safety that fulfill the safe-life requirement of 100 missions with a scatter factor of 1.5. The use of either of these FS is sufficient to meet the safe-life requirement, since either one of the FS will, of necessity, restrict the limit operating stress to a level that provides the required safe-life.

The compression critical stringers are not critical for safe-life and therefore the FS for the tension structure are not appropriate. The stringers are designed by the lift-off plus ground winds load conditions. Since the thrust loads at liftoff are deterministic in nature,  $FS_u = 1.25$  is recommended on the thrust portion of the loading. For the more variable wind portion of the loading,  $FS_u = 1.4$  is recommended since the aircraft type loading conditions ( $FS_u = 1.5$ ) are not critical for the stringers.  $FS_y = 1.0$  is recommended for yield.

9.2.4.3 Liquid Hydrogen Tank. For the liquid hydrogen tank skin and end domes which are critical for tension,  $FS_u = 1.40$  or  $FS_y = 1.14$  are the apparent factors of safety that fulfill the safe-life requirement of 100 missions with a scatter factor of 1.5. The use of either of these FS is sufficient to meet the safe-life requirement, since either one of the FS will, of necessity, restrict the limit operating stress to a level that provides the required safe-life.

The stringers and belt frames are critical for compression loads and therefore the FS for the tension structure are not appropriate. Since the 3g maximum thrust loading condition produces maximum compression in many areas of the tank,  $FS_u = 1.25$  and  $FS_y = 1.00$  are recommended for use on this condition because the loads are due to thrust, which is deterministic in nature. For other load conditions,  $FS_u = 1.4$  is recommended since the aircraft type loading conditions ( $FS_u = 1.5$ ) are not critical. For yield,  $FS_y = 1.0$  is recommended.

9.2.4.4 Aft Orbiter Support Frame. For the support frame, structural reliability produces the required factors of safety. Yield strength reliability requires  $FS_y = 1.15$ . The material strengths used for the aluminum frame were  $F_{tu} = 50$  ksi and  $F_{ty} = 40$  ksi. These reduced values were used to account for the effect of strength reducers (i.e., fastener holes, welds, etc.). The limit stress is then:

$$f_{\text{limit}} = \frac{40}{1.15} = 34.8 \text{ ksi}$$

$$FS_u = \frac{F_{tu}}{f_{\text{limit}}} = \frac{50}{34.8} = 1.43$$

Thus,  $FS_u = 1.43$  is the ultimate factor of safety that produces the required yield strength reliability of 0.999. Figure 7-8 shows that  $FS_u = 1.43$  gives an ultimate strength reliability greater than the required value of 0.9999. The use of either  $FS_u = 1.43$  or  $FS_y = 1.15$  is therefore sufficient to fulfill the reliability requirement.

9.2.4.5 Thrust Structure. Table 9-2 indicates that  $FS_u = 2.22$  is required for a fail-safe capability of 100% of limit load. It is inefficient to design the whole structure to this  $FS_u$ , however, when other criteria require low  $FS_u$ s and fail-safe can be obtained at these lower  $FS_u$ s by judicious local beef-up. Since large portions of the thrust

structure are designed by thrust loads that have high predictability,  $FS_u = 1.25$  is recommended for loads along with local beef-up to obtain fail-safe capability. Since design requirements all require an  $FS_y < 1.0$ , and the use of such a low factor is not considered to be an acceptable design practice,  $FS_y = 1.0$  is selected.

9.2.4.6 Wing Box. Table 9-2 shows that  $FS_u = 2.95$  is required to provide a fail-safe capability of 100% limit load for the wing lower spar caps. Just as for the thrust structure, it is inefficient to obtain fail-safe capability by designing large amounts of structure to a high factor of safety when other criteria require lower  $FS_u$ s and fail-safe can be obtained at these lower  $FS_u$ s by judicious local beef-up. Therefore,  $FS_u = 1.26$  or  $FS_y = 1.19$ , the factors which fulfill the fatigue requirement, are selected and the spar caps are beefed up locally to obtain the fail-safe capability. Use of either one of these factors of safety reduces the limit operating stress to a value low enough to meet the fatigue requirements. For other wing box structure, the baseline values of  $FS_u = 1.4$  and  $FS_y = 1.1$  for the launch vehicle type conditions are recommended since the aircraft type loading conditions ( $FS_u = 1.5$ ) are not critical (see Figure 3-23). This structure must also be evaluated for fail-safe.

9.2.4.7 Vertical Tail Box. The structural reliability requirement for 0.9999 ultimate strength reliability controls the selection of the factor of safety.  $FS_u = 1.30$  is necessary to meet this requirement. Since yield design is not critical for the vertical tail box,  $FS_y = 1.0$  is selected.

9.2.5 COMPONENT WEIGHT CHANGE DETERMINATION. This section presents the determination of the weight changes which result as a consequence of the new factors of safety that were determined for the structural components in Section 9.2.4. Again, the weights refer to the sample case of Table 9-2. The calculated weights refer in particular to the column in that table labeled " $\Delta Wt.$ "

9.2.5.1 Crew Module. The crew module weight does not change from the baseline. However, if a change of requirements were to cause a factor of safety change, then the new weight would be found in Figure 3-28.

9.2.5.2 Liquid Oxygen Tank. The weight changes for the liquid oxygen tank are determined from Figures 3-2 through 3-5. The weight changes are determined in the following table:

Element	New $FS_u$	New Weight (lb)	Baseline Weight (lb)	$\Delta$ Weight (lb)
Upper Dome	1.58	1812	1715	+97
Skin	1.58	5616	5616	0
Lower Dome	1.58	3180	2998	+182
Stringers	1.25	1275	1473	-198
				+81

Since proof test pressures design the skin and end domes, it would appear at first that no weight changes should occur for the end domes. The reason there is a weight increase for the domes is that the new  $FS_u$  was determined by analysis of the skin. If the domes were designed for their actual proof pressures, as could properly be done, there would be no weight increase for the domes. Inspection of Figure 3-4, at first, makes it appear that there could be a weight reduction for the skin due to  $FS_u = 1.58$ , as determined by the proof test requirement. This would be true if a perfect proof test could be devised for which the proof pressure was exactly equal to the proof factor multiplied by the maximum operating pressure at all points along the tank. In reality, a three-stage proof test is the most practical and the minimum weight for the skin is 5616 pounds for the 100-mission service life with a scatter factor of 1.5.

9.2.5.3 Liquid Hydrogen Tank. The  $LH_2$  tank weight changes are from the analysis of Section 3.2.2 and are presented in the following table:

<u>Element</u>	<u>New <math>FS_u</math></u>	<u><math>\Delta</math>Weight (lb)</u>
Upper Dome	1.40*	0
Skin	1.40*	0
Lower Dome	1.40*	0
Stringers	1.25 3g thrust	-168
Belt Frames	1.4 other	-254
		<u>-422</u>

\* Unchanged from baseline

The weight of the domes and skin do not change because the factor of safety is determined by the baseline requirement for proof test with a proof factor of 1.13. The weight change for the belt frames was determined by the Curve 3 maximum thrust at  $FS_u = 1.25$  in Figure 3-10. For  $FS_u = 1.25$ , the frame weight is 3999 pounds, or a 168 pound decrease from the baseline weight of 4167 pounds. The change in stringer weight is determined from Figure 3-11, which gives the weight sensitivity of skin and stringer to factor of safety. First, the weight change is determined from the 3g maximum curve at  $FS_u = 1.25$  for the combined skin and stringer. This change gives a decrease of 782 pounds from the baseline weight of 52,486 pounds to 51,704 pounds. Since the stringers constitute 32.5% of the skin stringer weight, the weight change for the stringers alone is 0.325 (782) or a decrease of 254 pounds.

9.2.5.4 Aft Orbiter Support Frame. For the support frame, the weight sensitivity to factor of safety is given in Figure 3-16. For the new  $FS_u$  of 1.43, the figure indicates a weight increase 100 pounds over the baseline weight of 2400 pounds.

9.2.5.5 Thrust Structure. The weight sensitivity of the thrust structure to factor of safety is given in Figure 3-19. For the new  $FS_u$  of 1.25, the weight decreases from the baseline of 25,067 pounds to 23,050 pounds, or a decrease of 2017 pounds. In

order to make the structure fail-safe, Figure 6-9 shows that 217 pounds of local beef-up is required at  $FS_u = 1.25$ ; thus, there is a net weight decrease in the thrust structure of 1800 pounds.

**9.2.5.6 Wing Box.** The factor of safety for the lower spar caps has been reduced to  $FS_u = 1.26$ . This produces an 11% increase in allowable spar cap stress level. The baseline weight of the lower spar caps is 5685 pounds (reference Table 2-4). Thus, the weight savings in the spar caps due to decrease in  $FS_u$  is equal to  $(0.11)(5685)$  or 625 pounds. From Figure 6-8, the local lower spar cap beef-up, which is necessary to make them fail-safe at  $FS_u = 1.26$ , is 858 pounds. The same figure shows that the beef-up of other structure, which is designed to  $FS_u = 1.4$ , requires 288 pounds of material. The net increase for the wing box, therefore, is 521 pounds.

**9.2.5.7 Vertical Tail Box.** The weight sensitivity of the vertical tail box to  $FS_u$  is given in Figure 3-25. For  $FS_u = 1.3$ , the weight decreases 420 pounds from the baseline value of 8775 pounds to 8355 pounds.

### 9.3 OPTIMUM FACTORS OF SAFETY FOR VARIOUS SETS OF DESIGN REQUIREMENTS

In this section, four basic sets of design requirements are analyzed to determine the optimum factors of safety and the associated weight changes. These four basic sets of requirements are analyzed in Tables 9-1 through 9-4. A sample of the analytical procedure used to fill in these tables is presented in Section 9.2. The required data to perform the four analyses are presented in Sections 3 through 8. The baseline set of design requirements selected for analysis are presented in the following table. These requirements are analyzed in Section 9.3.1.

Component	Baseline Design, Life and Reliability Requirements					
	Design Philosophy	Service Life (Missions)	Safe Inspection Interval (Missions)	Safe-Life Scatter Factor	Fatigue Scatter Factor	Reliability Factor
Crew Module	Fail-Safe	100	100	N/A	4.0	0.9999 ULT 0.999 YLD
LO <sub>2</sub> Tank	Safe-Life	100	100	1.5	4.0	0.9999 ULT 0.999 YLD
LH <sub>2</sub> Tank	Safe-Life	100	100	1.5	4.0	0.9999 ULT 0.999 YLD
Aft Orbiter Support Frame	Safe-Life	100	100	1.5	4.0	0.9999 ULT 0.999 YLD
Thrust Structure	Safe-Life	100	100	1.5	4.0	0.9999 ULT 0.999 YLD
Wing Box	Safe-Life	100	25	1.5	4.0	0.9999 ULT 0.999 YLD
Vertical Tail Box	Fail-Safe Safe-Life	100	100	1.5	4.0	0.999 ULT 0.999 YLD

The three other sets of design requirements that were selected for analysis vary from the baseline set in a logical manner and encompass what are thought to be possible design alternatives. The variations of these three sets of requirements from the baseline set presented in the preceding table are presented in the following table.

Component	Requirement Change from Baseline			
	Fail-Safe Design Approach	Extended Service Life		Increased Safe-Life Scatter Factor
		and Inspection Interval, Missions	Inspection Interval	
Crew Module	-	500	500	-
LO <sub>2</sub> Tank	-	500	500	4.0 Safe-Life Scatter Factor
LH <sub>2</sub> Tank	-	500	500	4.0 Safe-Life Scatter Factor
Aft Orbiter Support Frame	-	500	500	4.0 Safe-Life Scatter Factor
Thrust Structure	Fail-Safe*	500	-	4.0 Safe-Life Scatter Factor
Wing Box	Fail-Safe*	500	50	4.0 Safe-Life Scatter Factor
Vertical Tail Box	-	500	500	4.0 Safe-Life Scatter Factor

\*Inspection for gross failure every flight required; safe-life scatter factor not applicable.

The "Fail-Safe Design Approach" is analyzed in Section 9.3.2; the "Extended Service-Life and Inspection Interval" is analyzed in Section 9.3.3; and the "Increased Safe-Life Scatter Factor" is analyzed in Section 9.3.4.

### 9.3.1 BASELINE DESIGN REQUIREMENTS ANALYSIS WITH SAFE-LIFE APPROACH.

The analysis of the baseline design requirements is presented in Table 9-1, with the addition of the requirement of 0.9999 structural reliability for ultimate strength and 0.999 structural reliability for yield strength. The analysis results in structural components with a weight increase of 1044 pounds over their baseline B-9U counterparts. This increase is due primarily to the inadequacy of the baseline wing with respect to safe-life requirements. Even with 1705 pounds of beef-up in the lower spar caps, an inspection for flaw growth is required every 25 flights. To increase the inspection interval to a full 100 missions, it would be necessary to decrease the limit to 50% of the baseline value (reference Figure 5-27). Since this would impose an unacceptable weight penalty, a reduction to 70% of the baseline operating stress level and the corresponding 25-mission inspection interval was settled upon.

The remaining six components analyzed in this table are the same as in Table 9-2, except for the thrust structure. Therefore, since Table 9-2 was used as the example of the analysis procedure in Section 9.2, the analysis of those five components can be found in detail there. The remaining component, the thrust structure, was found to require no changes from the baseline.

9.3.2 FAIL-SAFE DESIGN REQUIREMENTS ANALYSIS. The analysis of the seven selected structural components for fail-safe design requirements is presented in Table 9-2. The rationale behind this analysis was to use the fail-safe design philosophy

Table 9-1. Optimum Factor of Safety Identification -

Component and Elements	Design, Life, and Reliability Requirements						Type of Loading		Material	Factors of Safety	
	Design Philosophy	Service Life (Missions)	Safe Inspection Interval (Missions)	Safe-Life Scatter Factor	Fatigue Scatter Factor	Reliability Factor	Load Source	Type of Stress		FS Fatigue	FS
I. Crew Module - Skin, Frames and Ellipsoidal Dome (Bulkhead)	Fail-Safe	100	100	NA	4.0	0.9999 Ult 0.999 Yld	Internal Pressure	Tension	2219-T87 Aluminum	<1.2 Ult <1.0 Yld	
II. LO <sub>2</sub> Tank	Safe-Life	100	100	1.5	4.0	0.9999 Ult 0.999 Yld	Internal Pressure	Tension	2219-T87 Aluminum	<1.1 Ult <1.0 Yld	
a. Skin and Ellipsoidal Domes (Bulkheads)							Flight	Compr			
b. Stringers											
III. LH <sub>2</sub> Tank	Safe-Life	100	100	1.5	4.0	0.9999 Ult 0.999 Yld	Internal Pressure	Tension	2219-T87 Aluminum	<1.1 Ult <1.0 Yld	
a. Ellipsoidal Domes (Bulkheads) and Skin							Flight	Compr			
b. Stringers and Belt Frames											
IV. Aft Orbiter Support Frame Sta. 2666	Safe-Life	100	100	1.5	4.0	0.9999 Ult 0.999 Yld	Flight	Tension	2219-T87 Aluminum	<1.1 Ult <1.0 Yld	
V. Thrust Structure	Safe-Life	100	100	1.5	4.0	0.9999 Ult 0.999 Yld	Flight	Tension	Ti-6Al-4V Annealed Titanium	<1.1 Ult <1.0 Yld	
VI. Wing Box	Safe-Life	100	25	1.5	4.0	0.9999 Ult 0.999 Yld	Flight	Tension	Ti-6Al-4V Annealed Titanium	1.26 Ult or 1.19 Yld	
a. Lower Spar Caps							Flight	Shear & Compr			
b. Other Structure											
VII. Vertical Tail Box	Fail-Safe Safe-Life	100	100	1.5	4.0	0.9999 Ult 0.999 Yld	Flight	Tension	Ti-6Al-4V Annealed Titanium	<1.1 Ult	

Notes: 1.  $FS_u = x.xx$  or  $FS_y = y.yy$  indicates that the use of either  $FS_u$  or  $FS_y$  is sufficient to fulfill the design requirement, but that the use of the other is not.  
2. NA = Not Applicable  
3. Apparent Factor of Safety  
4. Recommended Factor of Safety





# Baseline Design Requirements (Safe-Life Approach)

Safety to Meet Requirements			FS Apparent or Recommended	FS Baseline Criteria	Remarks	$\Delta$ Weight (lb)
FS Safe-Life	FS Reliability	FS Fail-Safe				
NA	0.99 Ult 0.98 Yld	4.2 Ult or 3.4 Yld	4.2 Ult or 3.4 Yld <sup>3</sup>	2.0 Ult 1.5 Yld	Factor of safety determined by fail-safe requirement. Proof test, $\alpha = 1.5$ , required.	0
1.58 Ult or 1.23 Yld	1.00 Ult 0.99 Yld	NA	1.58 Ult or 1.23 Yld <sup>3</sup>	1.4 Ult 1.1 Yld	Factor of Safety determined by safe-life requirement. Proof test, $\alpha = 1.23$ , required.	+279
			1.25 Ult on liftoff thrust + 1.4 Ult on winds 1.0 Yld <sup>4</sup>	1.4 and 1.5 Ult 1.1 Yld	Stringers are critical in compression; therefore, safe-life does not control FS. Since stringers are designed by liftoff + ground winds, the reduced $FS_u = 1.25$ and $FS_y = 1.0$ (estimated) are used on the thrust loads, which are deterministic in nature. Aircraft-type load conditions ( $FS_u = 1.5$ for baseline) are not critical.	-198
1.40 Ult or 1.13 Yld	1.00 Ult 0.98 Yld	NA	1.40 Ult or 1.13 Yld <sup>3</sup>	1.4 and 1.5 Ult 1.1 Yld	Factor of safety determined by safe-life requirement. Proof test, $\alpha = 1.13$ required. Aircraft-type load conditions not critical.	0
			1.25 Ult on 3g max thrust + 1.4 Ult on other cond 1.0 Yld <sup>4</sup>	1.4 and 1.5 Ult 1.1 Yld	Stringers are critical in compression; therefore, safe-life does not control FS. Since 3g maximum thrust produces maximum compression in many areas of the tank, $FS_u = 1.25$ and $FS_y = 1.0$ (estimated) are used on the 3g thrust loads, which are deterministic in nature. Aircraft-type load conditions ( $FS_u = 1.5$ for baseline) are not critical.	-422
1.1 Ult 1.0 Yld	1.32 Ult 1.15 Yld	NA	1.43 Ult or 1.15 Yld <sup>3</sup>	1.4 Ult 1.1 Yld	Factor of safety determined by reliability requirement for yield. $FS_u = 1.43$ gives 0.999 yield reliability and an ultimate reliability of $> 0.9999$ .	+100
1.40 Ult or 1.29 Yld	1.00 Ult 0.99 Yld	NA	1.40 Ult or 1.29 Yld <sup>3</sup>	1.4 Ult 1.1 Yld	Factor of safety determined by safe-life requirement.	0
2.05 Ult or 1.93 Yld	1.00 Ult 0.97 Yld	NA	2.05 Ult or 1.93 Yld <sup>3</sup>	1.4 and 1.5 Ult 1.1 Yld	Factor of safety determined by safe-life (inspection interval). Aircraft conditions not critical.	+1705
			1.4 Ult 1.1 Yld <sup>4</sup>	1.4 and 1.5 Ult 1.1 Yld	Only tension critical structure is flaw growth critical. Therefore, use the baseline factors of safety (estimated) due to the high wind load variability of the critical max $\alpha q$ condition.	0
1.02 Ult	1.30 Ult	<1.1 Ult	1.30 Ult 1.0 Yld <sup>3</sup>	1.4 and 1.5 Ult 1.1 Yld	Factor of safety determined by reliability requirement for ultimate. Yield design is not critical due to low design ult stresses which remain within the elastic range of the material. Aircraft conditions are not critical.	-420
$\Sigma(\Delta W)$						+1044

of both is not necessary.



Table 9-2. Optimum Factor of Safety Ident

Component and Elements	Design, Life, and Reliability Requirements						Type of Loading		Material	Factors of Safety	
	Design Philosophy	Service Life (Missions)	Safe Inspection Interval (Missions)	Safe-Life Scatter Factor	Fatigue Scatter Factor	Reliability Factor	Load Source	Type of Stress		FS Fatigue	Safety Factor
I. Crew Module — Skin, Frames and Ellipsoidal Dome (Bulkhead)	Fail-Safe	100	100	NA	4.0	0.9999 Ult 0.999 Yld	Internal Pressure	Tension	2219-T87 Aluminum	<1.2 Ult <1.0 Yld	NA
II. LO <sub>2</sub> Tank	Safe-Life	100	100	1.5	4.0	0.9999 Ult 0.999 Yld	Internal Pressure	Tension	2219-T87 Aluminum	<1.1 Ult <1.0 Yld	1.1 or 1.1
a. Skin and Ellipsoidal Domes (Bulkheads)							Flight	Compr			
b. Stringers											
III. LH <sub>2</sub> Tank	Safe-Life	100	100	1.5	4.0	0.9999 Ult 0.999 Yld	Internal Pressure	Tension	2219-T87 Aluminum	<1.1 Ult <1.0 Yld	1.1 or 1.1
a. Ellipsoidal Domes (Bulkheads) and Skin							Flight	Compr			
b. Stringers and Belt Frames											
IV. Aft Orbiter Support Frame Sta. 2666	Safe-Life	100	100	1.5	4.0	0.9999 Ult 0.999 Yld	Flight	Tension	2219-T87 Aluminum	<1.1 Ult <1.0 Yld	1.1 or <1.1
V. Thrust Structure	Fail-Safe	100	Note 5	NA	4.0	0.9999 Ult 0.999 Yld	Flight	Tension	Ti-6Al-4V Annealed Titanium	<1.1 Ult <1.0 Yld	NA
VI. Wing Box	Fail-Safe	100	Note 5	NA	4.0	0.9999 Ult 0.999 Yld	Flight	Tension	Ti-6Al-4V Annealed Titanium	1.26 Ult or 1.19 Yld	NA
a. Lower Spar Caps							Flight	Shear & Compr			
b. Other Structure											
VII. Vertical Tail Box	Fail-Safe Safe-Life	100	100	1.5	4.0	0.9999 Ult 0.999 Yld	Flight	Tension	Ti-6Al-4V Annealed Titanium	<1.1 Ult	1.0

- Notes: 1. FS<sub>u</sub> = x.xx or FS<sub>y</sub> = y.yy indicates that the use of either FS<sub>u</sub> or FS<sub>y</sub> is sufficient to fulfill the design requirement, but that the use of both is recommended.
2. NA = Not Applicable
3. Apparent Factor of Safety
4. Recommended Factor of Safety
5. Inspection for cracks, which could grow to failure, is not required because of fail-safe capability; however, a visual inspection for gross damage is required.

